

Sediment transport and sedimentation dynamics in  
small mountainous, dry-summer river systems

By

ANDREW GRAY  
B.S. (The University of Chicago) 2001

DISSERTATION

Submitted in partial satisfaction of the requirement for the degree of

DOCTOR OF PHILOSOPHY

in

Hydrologic Sciences

in the

OFFICE OF GRADUATE STUDIES

of the

UNIVERSITY OF CALIFORNIA

DAVIS

Approved:

---

Dr. Gregory Pasternack, Chair

---

Dr. Elizabeth Watson

---

Dr. Dawn Sumner

Committee in Charge

2014

UMI Number: 3637835

All rights reserved

INFORMATION TO ALL USERS

The quality of this reproduction is dependent upon the quality of the copy submitted.

In the unlikely event that the author did not send a complete manuscript and there are missing pages, these will be noted. Also, if material had to be removed, a note will indicate the deletion.



UMI 3637835

Published by ProQuest LLC (2014). Copyright in the Dissertation held by the Author.

Microform Edition © ProQuest LLC.

All rights reserved. This work is protected against unauthorized copying under Title 17, United States Code



ProQuest LLC.  
789 East Eisenhower Parkway  
P.O. Box 1346  
Ann Arbor, MI 48106 - 1346

## **Für Sonja**

Einander  
gefunden  
zu haben,  
war  
der Anfang  
meines groessten  
Abenteurs.

Die Verwirklichung  
mein groesstes  
Traumes  
ist  
immer noch  
unsere Welt  
zu erschaffen.

Zusammen.

## ABSTRACT

Fluvial suspended sediment is a master variable affecting a wide range of fluvial and coastal environmental processes, and dominating the terrestrial mass flux to the oceans. Although it has long been recognized that relationships between suspended sediment concentration and discharge are not stationary in small, mountainous rivers over time scales from hours to decades, most studies continue to assume stationarity. This collection of studies directly addresses the issue of non-stationarity in the suspended sediment –discharge relationship of the Salinas River, central California, and examines the progression of abandoned channel fill sequences in the Eel River Estuary of northern California.

Preceding these studies is a methodological analysis of the pretreatment of fluvial and marsh sediments for particle size analysis. Pretreatment of sediment with hydrogen peroxide to remove organic constituents and aid deflocculation is a common component of particle size analyses of terrestrial and marine sediments. The first chapter presents the quantitatively determined effect of a range of treatment levels on particle size distribution among four sediment types representing a range of mineral/organic particle size distributions, organic content and particle characterization (charcoal or detrital plant material).

The following three chapters examine the effects of antecedent basin conditions on the suspended sediment – discharge relationship in the Salinas River. In chapter two, forty-five years of suspended sediment data from the lower Salinas and 80 years of hydrologic data were used to construct hydrologic descriptors of basin preconditioning and test the effects of these preconditions on suspended sediment behavior. Fine (diameter ( $D$ ) < 63  $\mu\text{m}$ ) and sand sized ( $D$  > 63  $\mu\text{m}$ ) sediment were found to respond differently to antecedent hydrologic conditions. Fine sediment was most sensitive to flushing flows of moderate discharge (10 – 20x mean discharge ( $Q_{mean}$ )) that led to lower subsequent fine sediment concentrations, while sand concentrations were generally decreased by periods of drought and longer elapsed time since a wide range of discharges acting as maintenance flows.

Chapter three examines the interannual to decadal scale persistence of suspended sediment – discharge relationship states in the lower Salinas River, assesses the role of antecedent hydrologic conditions in controlling these patterns, and addresses their relationship to El Niño Southern Oscillation

(ENSO) climatic states. The decadal scale variability in suspended sediment behavior was influenced by interannual to decadal scale fluctuations in hydrologic characteristics, including: elapsed time since small ( $\sim 0.1 \times Q_{\text{mean}}$ ), and moderate ( $\sim 10 \times Q_{\text{mean}}$ ) threshold discharge values, the number of preceding days that low/no flow occurred, and annual water yield. El Niño climatic activity was found to have little effect on decadal-scale fluctuations in the fine suspended sediment – discharge relationship due to low or no effect on the frequency of moderate to low discharge magnitudes, annual precipitation, and water yield. However, sand concentrations generally increased in El Niño years due to the increased frequency of moderate to high magnitude discharge events, which generally increase sand supply.

Chapter four brings to bear the decadal scale persistence of suspended sediment – discharge behavior, the effects of antecedent hydrologic conditions, and ENSO influences on the estimation of inter-decadal scale sediment flux from the Salinas River. The longer sampling records employed in this study and incorporation of decadal scale behavior or antecedent hydrologic conditions resulted in average annual load estimates of 2.1 or 2.4 Mt, in comparison to earlier estimates of  $\sim 3.3$  Mt by previous researchers. El Niño years dominated the sediment budget by producing on average ten times more sediment than non-El Niño years.

Chapter five proposes a modification of the current generic model for abandoned channel fill stratigraphy produced in unidirectional flow river reaches to incorporate seasonal tidal deposition. This work was based on evidence from two consecutive abandoned channel fill sequences in Ropers Slough of the lower Eel River Estuary. Planform geomorphic characteristics derived from these images were used in conjunction with sub-cm resolution stratigraphic analyses to describe the depositional environment processes and their resultant sedimentary deposits. The abandoned channel fill sequences appeared to differ due to the topographic steering of bed sediment transport and deposition previously identified in rivers experiencing only unidirectional flow, while also expressing the seasonal dichotomy of fluvial and tidal deposits.

## TABLE OF CONTENTS

<u>Chapter</u>		<u>Page</u>
<b>1</b>	<b>Hydrogen peroxide treatment effects on the particle size distribution of alluvial and marsh sediments.....</b>	<b>1</b>
<b>1.1</b>	<b>Introduction.....</b>	<b>2</b>
<b>1.2</b>	<b>Methods.....</b>	<b>4</b>
1.2.1	<i>Test sediments.....</i>	4
1.2.2	<i>Treatments.....</i>	6
1.2.3	<i>Grain size analysis.....</i>	6
1.2.4	<i>Data analysis.....</i>	7
1.2.5	<i>1.2.5 Organic content, particle size and characterization.....</i>	8
<b>1.3</b>	<b>Results.....</b>	<b>9</b>
1.3.1.	<i>Internal Texture Ratios, Mean Values and Organic Content.....</i>	9
1.3.2	<i>S1- Salinas River Lagoon.....</i>	10
1.3.3	<i>S2 - Navarro River Floodplain.....</i>	13
1.3.4	<i>S4 - Suisun Marsh.....</i>	14
1.3.5	<i>S4 – Cosumnes Riverbank.....</i>	15
<b>1.4</b>	<b>Discussion.....</b>	<b>16</b>

1.5	Conclusions.....	20
1.6	References.....	21
2	<b>Suspended sediment behavior in a coastal dry-summer subtropical catchment: Effects of hydrologic preconditions.....</b>	<b>23</b>
2.1	Introduction.....	24
2.2	Study region characteristics.....	26
2.3	Data.....	30
2.3.1	<i>Experimental design.....</i>	30
2.3.2	<i>Hydrologic data.....</i>	31
2.3.3	<i>Precipitation data.....</i>	34
2.3.4	<i>Bias analysis.....</i>	34
2.4	<b>Suspended sediment rating curves and residuals.....</b>	<b>34</b>
2.5	<b>Antecedent hydrologic conditions.....</b>	<b>37</b>
2.5.1	<i>Hydrologic variable effects on <math>C_{SS}</math>-Q residuals.....</i>	37
2.5.2	<i>Hydrologic variable test results.....</i>	39
2.6	<b>Effects of hydrographic position and flow regime.....</b>	<b>40</b>
2.6.1	<i>Rating curve subgroup comparison with ANCOVA.....</i>	40
2.6.2	<i>Rating curve subgroup ANCOVA results.....</i>	44
2.7	<b>Suspended sediment hysteresis.....</b>	<b>47</b>

2.7.1	<i>Hysteresis identification</i> .....	47
2.7.2	<i>Hysteresis results</i> .....	47
<b>2.8</b>	<b>Effects of subbasin water provenance</b> .....	<b>50</b>
2.8.1	<i>Routing analysis</i> .....	50
2.8.2	<i>Routing results</i> .....	51
<b>2.9</b>	<b>The channel bed and suspended sediment</b> .....	<b>51</b>
2.9.1	<i>Channel bed analysis</i> .....	51
2.9.2	<i>Channel bed results</i> .....	53
<b>2.10</b>	<b>Discussion</b> .....	<b>57</b>
2.10.1	<i>Synthesis</i> .....	57
2.10.2	<i>Event characteristics and routing</i> .....	59
2.10.3	<i>Channel mediation</i> .....	61
2.10.4	<i>The power of antecedent conditions</i> .....	63
<b>2.11</b>	<b>Conclusions</b> .....	<b>63</b>
<b>2.12</b>	<b>References</b> .....	<b>65</b>
<b>2.A</b>	<b>Supplemental material</b> .....	<b>72</b>
2.A.i	<i>Bias testing</i> .....	72

2.A.ii	<i>The ANCOVA method of rating curve comparison.....</i>	74
<b>3</b>	<b>Decadal patterns in the suspended sediment behavior of a coastal dry-summer subtropical catchment: The role of hydrologic preconditions.....</b>	<b>76</b>
3.1	<b>Introduction.....</b>	<b>77</b>
3.2	<b>Study region.....</b>	<b>79</b>
3.3	<b>Methods.....</b>	<b>80</b>
3.4	<b>Computation and data analysis.....</b>	<b>84</b>
3.5	<b>Results.....</b>	<b>85</b>
3.6	<b>Discussion.....</b>	<b>98</b>
3.7	<b>Conclusions.....</b>	<b>102</b>
3.8	<b>References.....</b>	<b>103</b>
<b>4</b>	<b>Effects of antecedent hydrologic conditions, time dependence, and climate cycles on the suspended sediment load characteristics of the Salinas River, California.....</b>	<b>110</b>
4.1	<b>Introduction.....</b>	<b>111</b>
4.2	<b>Study region.....</b>	<b>112</b>
4.3	<b>Experimental overview.....</b>	<b>113</b>
4.4	<b>Data.....</b>	<b>115</b>
4.5	<b>Suspended sediment rating curve development.....</b>	<b>115</b>
4.5.1	<i>Linear regression and LOESS rating curves.....</i>	115
4.5.2	<i>Temporally zoned rating curves.....</i>	116
4.5.3	<i>Multiple regression rating curves.....</i>	120

<b>4.6</b>	<b>Suspended sediment load.....</b>	<b>124</b>
4.6.1	<i>Q<sub>SS</sub> estimation methods.....</i>	124
4.6.2	<i>Comparison of suspended sediment load estimations.....</i>	126
4.6.3	<i>Differences in Q<sub>SS</sub> estimation for critical years.....</i>	130
<b>4.7</b>	<b>Magnitude and frequency analysis of Q and Q<sub>SS</sub>.....</b>	<b>137</b>
4.7.1	<i>Methods of magnitude and frequency analysis.....</i>	137
4.7.2	<i>Magnitude/frequency results.....</i>	138
<b>4.8</b>	<b>ENSO controls on flood frequency and sediment discharge.....</b>	<b>144</b>
<b>4.9</b>	<b>Discussion.....</b>	<b>144</b>
4.9.1	<i>Q<sub>SS</sub> magnitude.....</i>	144
4.9.2	<i>Effective discharge of suspended sediment.....</i>	148
4.9.3	<i>The role of ENSO in suspended sediment discharge.....</i>	149
<b>4.10</b>	<b>Conclusions.....</b>	<b>150</b>
<b>4.11</b>	<b>References.....</b>	<b>151</b>
<b>5</b>	<b>Abandoned channel fill sequences in the tidal estuary of a small mountainous, dry- summer river.....</b>	<b>156</b>
<b>5.1</b>	<b>Introduction.....</b>	<b>157</b>
5.1.1	<i>Background.....</i>	157

5.1.2	<i>New conceptual model.....</i>	158
<b>5.2</b>	<b>Study region.....</b>	<b>160</b>
<b>5.3</b>	<b>Materials and methods.....</b>	<b>164</b>
5.3.1	<i>Sedimentology.....</i>	164
5.3.2	<i>Planform geomorphology.....</i>	166
<b>5.4</b>	<b>Data analysis.....</b>	<b>168</b>
<b>5.5</b>	<b>Results.....</b>	<b>171</b>
5.5.1	<i>Stratigraphic zones.....</i>	171
5.5.2	<i>Particle size distribution characteristics of stratigraphic zones.....</i>	174
5.5.3	<i>Stratigraphic units.....</i>	178
5.5.4	<i>Carbon composition by stratigraphic unit.....</i>	178
5.5.5	<i>Chronostratigraphic model.....</i>	182
5.5.6	<i>Depositional environments.....</i>	182
5.5.7	<i>Channel geometry.....</i>	185
5.5.8	<i>Hydro-stratigraphy.....</i>	188
5.5.9	<i>Eel River suspended, bed, and bedload sediment characteristics.....</i>	191
5.5.10	<i>Tanner domains: EDRS and Eel River sediment suite statistics.....</i>	195
<b>5.6</b>	<b>Discussion.....</b>	<b>196</b>

5.6.1	<i>Stratigraphic and geomorphic synthesis.....</i>	196
5.6.2	<i>Sedimentology and discharge magnitude.....</i>	199
5.6.3	<i>Particle size distribution domains and sediment source.....</i>	200
5.6.4	<i>Mechanisms.....</i>	201
5.6.5	<i>Conceptual model evaluation.....</i>	202
<b>5.7</b>	<b>Conclusions.....</b>	<b>203</b>
<b>5.8</b>	<b>References.....</b>	<b>205</b>
	<b>Acknowledgements.....</b>	<b>212</b>

## Chapter 1

### Hydrogen peroxide treatment effects on the particle size distribution of alluvial and marsh sediments

#### Abstract

Pretreatment of sediment with hydrogen peroxide to remove organic constituents and aid deflocculation is a common component of particle size analyses of terrestrial and marine sediments. This study quantitatively determined the effect of a range of treatment levels on particle size distribution among four sediment types representing a range of mineral/organic particle size distributions, organic content and particle characterization (charcoal or detrital plant material). The hypothesis was that complete removal of organic particles would lead to improved repeatability of results for a given sample and treatment level. Repeatability was assessed with a coefficient of variance calculation and a comparison of particle size distribution patterns within and across treatments. The effect of treatment levels on commonly used distribution descriptors (e.g. texture ratios and measures of central tendency) were then examined for each sample. Samples characterized primarily by detrital material responded most readily to treatment, whereas charcoal-dominated samples required higher levels of treatment to achieve increased repeatability and disappearance of large organic particles. Certain distribution descriptors such as modal analysis were found to be more resilient to organic particle presence, although amplitude of the organic distribution and the degree of overlap with the inorganic signal in some cases obscured even this metric. Thus, final treatment recommendations are based on sample characteristics and the types of distribution descriptors used in a study.

## 1.1 Introduction

Paleogeographic studies of alluvial sediments often include some consideration of particle size distribution. Such analyses are now routinely brought to bear on questions involving geomorphic and anthropogenic factors associated with sediment sourcing (Chen et al., 2000; Ghilardi et al., 2008), fluvial processes governing these depositional environments (Visher, 1969; Orton and Reading, 1993), and paleoclimate reconstruction (Tebbens et al., 1998; Allen and Haslett, 2006). Advances in instrumentation now allow many more samples to be run at higher levels of resolution and precision than was possible in the days of the pipette method and contemporaries (Syvitski, 1991), increasing the feasibility of large-scale grain size analysis and the value of this approach. Consequently, preparation and pretreatment of samples for such studies are now required on a larger scale of production, which raises issues of procedural standardization within and between studies.

Alluvial sediments commonly contain significant amounts of co-depositional and extraneous organic matter that in most cases must be removed to analyze the inorganic particle distribution. Extraneous organic matter in this study is considered to be any organic material that became incorporated into the study sediments from local biotic sources, including plant litter and roots which did not experience the transport regime that deposited the inorganic sediments. Co-depositional organic matter was considered to be material transported hydraulically to the sampling site along with the inorganic sediments of interest. Despite the common mode of entry into the sedimentary record, co-depositional organic matter is commonly removed from the inorganic fraction for particle size distribution analysis, as inorganic particles are denser than organic particles, and uniformed particle density is a major assumption implicit to the interpretation of depositing flow characteristics (Lewis, 1984).

While other strong oxidizing agents have been used to digest organics, isolation of the lithic fraction is normally accomplished through treatment with 30% hydrogen peroxide (Robinson, 1922; Kunze, 1982; Lewis, 1984). The long history and widespread use of this treatment has led to a certain complacency that accompanies many such laboratory methods. Indeed, a survey of current literature suggests that most studies where hydrogen peroxide was employed for organic digestion did not report the specific protocol used, with only a few exceptions (Konert and Vandenberghe, 1997). Furthermore,

few recent studies have attempted to determine to what extent different levels of treatment result in measurable differences in grain size distribution (Matthews, 1991; Allen and Thornley, 2004). In fact, most protocols simply propose a qualitative approach. Treatment with hydrogen peroxide is often prescribed, with or without heating, until visible reaction (bubbling) has ceased and/or a desired lightening of color has occurred.

However, qualitative assessment of organic digestion may be complicated by other reactions, such as the rapid decomposition of hydrogen peroxide above 70 °C and interactions with inorganic constituents of sediments such as manganese oxide (Kunze, 1982; Lewis, 1984; Percival, 1997). Both of these reactions can serve to obscure a definitive endpoint of organic digestion. For example, the laboratory experience of the authors has shown that unheated treatments left to react for days often reach an apparently inert state, only to begin liberating gas again with the application of heat. Heated samples may continue to exhibit signs of reaction, assumed to be the presence of organic carbon, with each additional hydrogen peroxide aliquot, even after many treatments. In order to ensure comparability across and within studies, a standardized method for organic removal with hydrogen peroxide that does not rely solely upon such qualitative assessments of the reaction's conclusion should be developed.

This study quantitatively examines whether different levels of hydrogen peroxide treatment for the removal of organic matter result in measurable differences in particle size distribution. To this end, four levels of hydrogen peroxide treatment and an untreated control were tested on four different alluvial sediments. Comparisons of grain size distributions produced from these experiments were used to establish the level of treatment required to obtain the lithic particle signature. Grain size distribution response to hydrogen peroxide treatment was then examined in regard to the proportion of organic material present and the microscopic characterization of coarse organics ( $\geq 150 \mu\text{m}$  sieve class), which classified the samples according to the most prevalent form of organic particles. Conclusions based on these parameters lead to broad treatment suggestions for a range of sediment types and study goals. To further inform these recommendations, changes of internal texture ratios (clay:silt:sand) and modal position between untreated and "fully treated" replicates were evaluated for sensitivity to the presence of organic particles. In light of these findings, the choice of organic treatment and grain size distribution metric for application to the sediment of interest can be more confidently approached.

## 1.2 Methods

### 1.2.1 Test sediments

Selection of sediment was conducted to establish a range of sediment texture ratios and organic content levels that one may commonly encounter when sampling alluvium (Table 1.1, Fig. 1.1). Initial selection was performed on the basis of qualitative assessments of these parameters, which were later quantitatively refined by our laboratory techniques. Final sediment texture characterization as reported here is based on grain size distributions obtained after treatment with five heated 20ml aliquots of hydrogen peroxide, with one anomalous replicate excluded for sample S4 (Cosumnes Riverbank). Four samples were tested and they all were obtained from field sites on low-lying depositional landforms in California, U.S.A. All four sample sediments were collected from approximately 10 to 20 cm depths from structureless sediments. All samples possessed post depositional roots with the exception of S4, Navarro River Floodplain. Three samples were composed of only silt and clay from a lithic perspective, with ratios of about 1:1 silt to clay (S3: Suisun Marsh) and 2:1 (S1: Salinas River Lagoon; S4: Cosumnes Riverbank) and bulk organic contents of 29.4, 8.4, 5.8 and 10.4 % by mass, respectively. One sample primarily composed of sand was used, which contained about 3 times more sand than fines with a 4:1 silt to clay ratio, and only 1.9 % organics (S2, Navarro River Floodplain).

All bulk samples were homogenized within plastic bags by hand due to their moist, clayey nature, except for S2, which was carefully stirred on a plate to avoid grain size partitioning of this sandy sample. Subsampling was conducted with truncated, plastic 2cc syringes to produce 5, ¼ cc replicates for each treatment, which were extruded into 150 ml beakers for treatment with hydrogen peroxide. The untreated control replicates were deposited directly into 20 ml scintillation vials. No attempts were made to manually remove organic particles.

**Table 1.1** Sediment samples

Sample	Provincence	Organics	
		(% mass)*	character
S1	Salinas River Lagoon	8.4	roots
S2	Navarro River Floodplain	1.9	charcoal
S3	Suisun Marsh	29.4	stems
S4	Consumnes Riverbank	5.8	charcoal

\*Estimated from loss on ignition

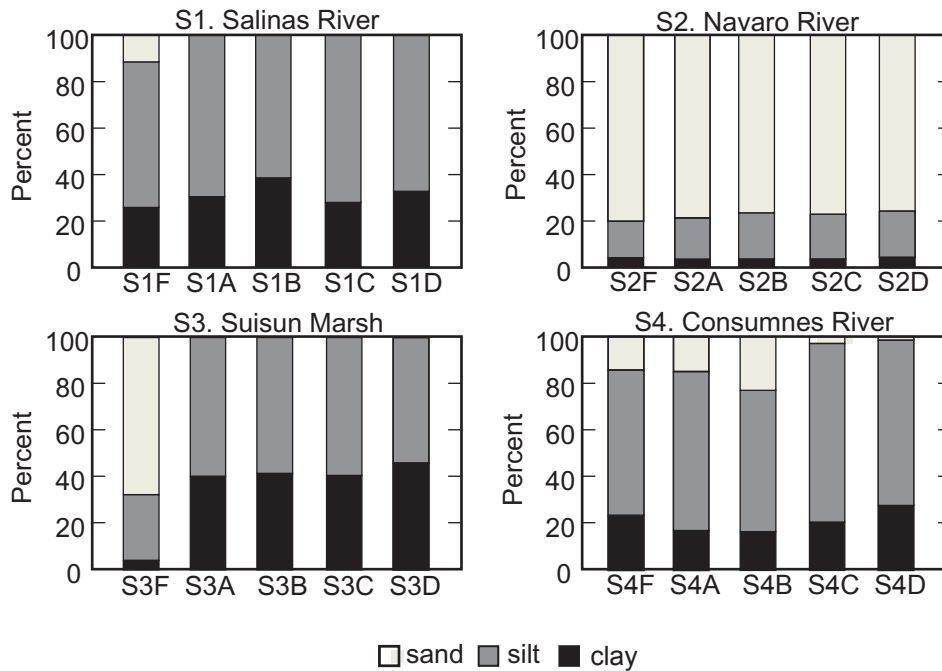


**Figure 1.1** Internal texture ratios for averaged sample treatments. Letters indicates level of treatment (F = no treatment, A = 20 ml unheated H<sub>2</sub>O<sub>2</sub>, B = 20 ml heated H<sub>2</sub>O<sub>2</sub>, C = 2 x 20 ml heated H<sub>2</sub>O<sub>2</sub>, D = 5 x 20 ml heated H<sub>2</sub>O<sub>2</sub>).

### 1.2.2 Treatments

Hydrogen peroxide (30% H<sub>2</sub>O<sub>2</sub>) was used for all treatments except the control (Table 1.2). In treatment A, 20 ml of H<sub>2</sub>O<sub>2</sub> was added to each beaker, then covered with watch glasses and allowed to react for 24 hrs. To dilute the peroxide, 60 ml of de-ionized (DI) water was then added and the samples were allowed to evaporate uncovered at ambient temperature until reaching a volume of about 5 ml, a process that lasted up to a week for some samples. Treatments B, C and D were all heated applications of H<sub>2</sub>O<sub>2</sub> in 20 ml aliquots with one, two and five applications respectively. These treatments were conducted under watch glasses on hotplates at levels adjusted to produce solution temperatures of 70 °C. When bubbling ceased for one H<sub>2</sub>O<sub>2</sub> application, the watch glass was removed to allow the solution to evaporate more readily to 5 ml, otherwise the solution would remain under the watch glass until reaching the aforementioned volume. Upon reaching the reduced volume the next aliquot of peroxide was added and the process of reacting under the watch glass followed by evaporation repeated until the final aliquot was processed to the reduced volume. At this stage 60 ml of DI water was added to dilute the remaining H<sub>2</sub>O<sub>2</sub> in solution and evaporated to ~5 ml.

The sediment and supernatant from completed treatments and the control, untreated subsamples were transferred to 20 ml scintillation vials with 1.00 g of Sodium Metaphosphate (SMP) as a dispersant. These vials were adjusted with DI water to a total volume of ~20 ml to create a solution of approximately 5% SMP. Replicates were mixed momentarily on a test tube vortex to aid initial dissolution of SMP, followed by agitation on a mechanical vibrator for 24 hours.

**Table 1.2** Pre-treatment for grain size analysis

Treatment	Method
A	20 ml unheated H <sub>2</sub> O <sub>2</sub>
B	1 X 20 ml heated H <sub>2</sub> O <sub>2</sub>
C	2 X 20 ml heated H <sub>2</sub> O <sub>2</sub>
D	5 X 20 ml heated H <sub>2</sub> O <sub>2</sub>
F	no treatment

### 1.2.3 Grain size analysis

Particle size analysis was performed with a Beckman-Coulter LS 230 (Beckman Coulter Inc., Fullerton, CA, USA) laser diffraction type granulometer with polarization intensity differential scattering

(PIDS). Each replicate was flushed through the machine in three 90 second runs, while the reservoir was sonicated for 60 s before and during the entirety of each run. The average of the three runs was then used as the grain size distribution for the replicate.

Our initial preference settings lead to volumetric grain size distributions reported with a sensitivity range of 0.375 to 2000  $\mu\text{m}$  in 94 bins. However, due to operator error in setting run preferences, a sensitivity range of 0.0399 to 2000  $\mu\text{m}$  was used for sample treatments D and F, reporting an additional 23 finer bins. An incidental comparison of the two settings was possible for a sample outside of this study, as replicates were run each way. Inclusion of the additional fine bins raised the aggregate percent clay reported, but otherwise did not seem to affect the distribution of the coarser materials' grain size spectra. Thus, for comparisons between treatments, the additional fine bins were removed from D and F spectra and concomitant modification of the remaining distribution by a multiplier to achieve a summed volume of 100% was performed. Multipliers were also used on occasion for comparisons between portions of grain size distributions to eliminate the effect of certain parts of the distribution, as these data were in the form of percent volume. To compare portions of distributions while discounting others, one must correct the remaining array of percent volumes with a multiplier calculated as:

$$M = (100)/(100-D) \quad (1.1)$$

where M is the multiplier and D is the percent volume that has been removed from the population.

#### 1.2.4 Data analysis

The resultant grain size distributions were examined under the hypothesis that effective treatment would produce the same findings between replicates within a given treatment and across further, more extensive treatments. Although the distribution of organic particles in a sample may be uniform across subsamples if homogenization and subsample size were successful and appropriate respectively, it is expected that the process of organic matter digestion with hydrogen peroxide does not progress uniformly. Therefore, incomplete digestion of organic matter was hypothesized to produce a higher level of variance across replicates for a given sample treatment than those sample treatments where all organic matter was removed. Furthermore, invariance of grain size distribution with increased levels of treatment should also indicate complete removal of organics.

Assessment of repeatability of the results was approached by (i) comparing grain size frequency distributions at the replicate level within treatments, (ii) as average sample treatment distributions for inter-treatment comparison and then (iii) cross referencing these results with the mean coefficient of variation value for each sample treatment. By sample treatment, reference is being made to the group of replicates that went through a given treatment for a given sample, for example sample S1 treatment D.

The coefficient of variation ( $v$ ) is a non-dimensional measure of variance that is scaled to the mean value, and is defined as:

$$v = \sigma/\mu \quad (1.2)$$

where  $\sigma$  is the standard deviation of the samples and  $\mu$  is the mean. For a given sample treatment the coefficient of variation was calculated for each grain size bin across replicates. The  $v$  values obtained for all grain size bins within the distribution were then averaged to produce a representation of variation ( $V_{avg}$ ) for the entire sample treatment using the equation:

$$V_{avg} = \sum v/n \quad (1.3)$$

where  $n$  is the number of individual coefficients of variation produced.  $V_{avg}$  values were also calculated for the size classes 0.375-1.83  $\mu\text{m}$  (denoted as  $V_{clay}$ ) to compare the effect of different treatments on clay size particles.

This study does not establish a maximum  $V$  value that is used directly to identify successful organic digestion. Rather,  $V$  is used comparatively between sample treatments as an indicator of effective organic removal, with lower values of  $V$  indicating lower levels of variance between replicates for a given treatment. On the other hand, distribution comparisons between replicates and treatment averages are used to identify the lithic and organic particle size signatures through the disappearance of organic distributions with treatment. The identified lithic signature is then used to differentiate between replicates that are near complete organic removal and those that contain residual organic distributions. The lithic distributions, modified using Eq. (1.1) to represent a complete distribution, are also compared to their respective control distributions to assess the overlap of these two sedimentary constituents.

### *1.2.5 Organic content, particle size and characterization*

Characterization of organic particle size for each sample was approached via two methods. First,

the average grain size distribution of the untreated replicates was compared to the average lithic grain size distribution obtained after effective treatment and the difference plotted. Second, 2.5 cc subsamples were dispersed in 5% SMP for 24 hrs of agitation and then washed through nested 850, 600, 300 and 150  $\mu\text{m}$  sieves. The contents of each sieve were transferred to dissection dishes where the organic particles were characterized qualitatively with the aid of a dissection microscope under magnifications of 10 to 40 times.

Organic content was approximated through the loss-on-ignition method. Three, 1.2-cc subsamples (1/4 teaspoon) were collected from each homogenized alluvium and then dried for 24 hours at 105 °C, weighed, combusted for four hours at 550 °C in a laboratory furnace, and re-weighed. Calculations of organic content are reported as percent of dry weight.

### **1.3 Results**

Large changes, primarily reduction of the coarser portion of the grain size distributions, were evident with hydrogen peroxide treatment for S1, S3 and S4 in comparison to control samples. Examination of sample treatments at the replicate level showed repeated post treatment patterns of complete coarse material loss of a constant range (by sample) for S1, S3 and S4. Sample distributions produced their lowest V values with treatments A and D in general, as these treatments generally produced fewer replicates with persistent coarse distributions.

#### *1.3.1 Internal texture ratios, mean values and organic content*

Sediment response to treatments generally resulted in large changes in texture ratios and mean values in sediments with higher levels of organic content (Table 1.1, Fig. 1.1). S2 experienced very little change between all treatments and the control, while S3 shifted from primarily sand sized particles to a clayey silt ratio that was very similar between all treatments. S1 changed from a clayey, sandy silt to a clayey silt that varied more in clay:silt ratio between treatments, although treatments A and D were very similar. The sand fraction in S4 was present in the control and across all treatments, although it was much reduced in treatments C and D.

### 1.3.2 S1- Salinas River Lagoon

The grain size frequency distribution for the Salinas River Lagoon sample showed a persistent bimodal distribution in the clay to medium silt range across all treatments with hydrogen peroxide (Fig. 1.2a). The primary mode varied in placement from 2.01-3.20  $\mu\text{m}$ , while the secondary, more leptokurtic peak showed up at 15.65  $\mu\text{m}$  for all treatments and 17.18  $\mu\text{m}$  for the control (Table 1.3). Deviations from this consistent pattern appeared in replicates from the untreated control, treatment B and treatment C (Fig. 1.3). The anomalous replicates from the control and Treatment C contained multi or single modal, negatively (coarse) skewed distributions of coarse sand size particles up to a maximum of about 1mm. A single anomalous replicate from treatment B was the only replicate for all treatments of this sample which lacked the bimodal silt distribution, exhibiting a strongly leptokurtic clay peak followed by a secondary fine silt peak. This replicate shared no distributive characteristics in common with others from this sample, and as such was discarded under suspicions of laboratory error. Comparison of  $V_{\text{avg}}$  values showed the largest values calculated for the control and treatment C, reflecting the presence of the coarse particle bearing replicates (Table 1.3). Treatment A produced the lowest value of  $V_{\text{avg}}$  (0.10) in contrast to the heated treatments B and D which had values nearly twice as large.

Examination of the Salinas sample with a dissection microscope after dispersion and sieving revealed organic particles dominated by root pieces from all sieve sizes used; many of those caught by the 850  $\mu\text{m}$  sieve had lengths in excess of 1 mm. Experience during sub-sampling indicated that the longest root pieces often did not make it into  $\frac{1}{4}$  cc subsamples, as evidenced by the fact that these particles showed up in only 2 of 5 control replicates. Plotting the difference in grain size distribution between treatment D and the control revealed a poly modal range of particles from 20.71 to 1142.8  $\mu\text{m}$  with a major mode at 24  $\mu\text{m}$  (Fig. 1.4a).

Amplification of the control distribution to bring the total percent volume up to 100% for the section that overlaps with the treatment D distribution allowed for a comparison of the control with what we will henceforth refer to as the fully treated or "lithic range" (Fig. 1.5a). The distributions over this range were remarkably similar. The control shared the same general curve shape with treatment D, but the primary mode was slightly depressed in intensity and both mode placements shifted one grain size bin coarser, while the notch between the two modes was softer than for the treated sample.

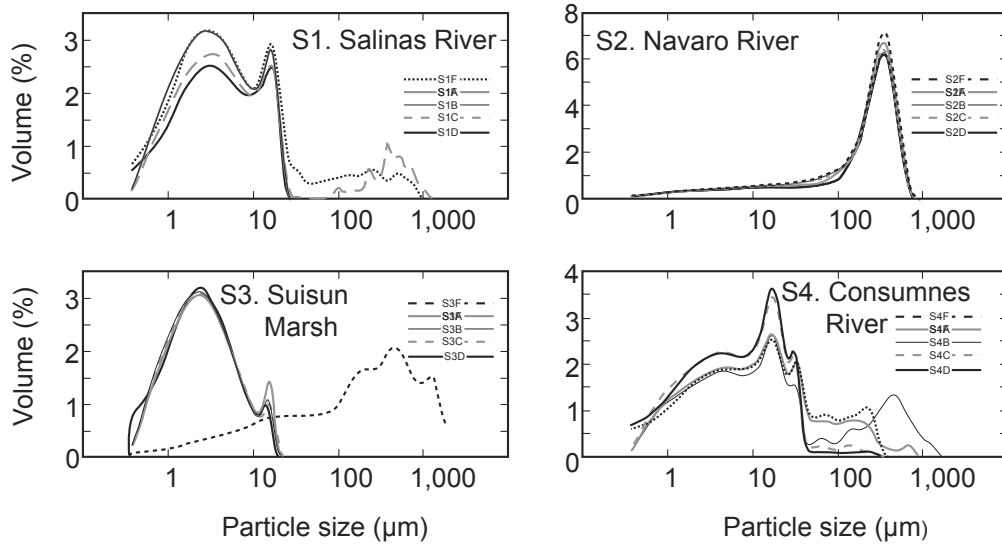


**Figure 1.2** Average grain size distribution for each treatment. Letter indicates level of treatment (F = no treatment, A = 20 ml unheated H<sub>2</sub>O<sub>2</sub>, B = 20 ml heated H<sub>2</sub>O<sub>2</sub>, C = 2 x 20 ml heated H<sub>2</sub>O<sub>2</sub>, D = 5 x 20 ml heated H<sub>2</sub>O<sub>2</sub>).

**Table 1.3** Mean, average primary mode and modal intensity for all sample treatments. Treatment D<sub>mod.</sub> has been modified to remove grain size detectors below 0.375 μm.

Sample	Mean (μm)	Intensity (% vol)	Mode (μm)
S1F	42.11	2.41	3.21
S1A	6.02	3.15	2.92
S1B	5.14	4.20	2.01
S1C	61.12	2.73	3.21
S1D	5.82	3.04	2.92
S1D <sub>mod.</sub>		3.19	2.92
S2F	276.78	7.02	339.9
S2A	262.23	6.63	339.9
S2B	250.14	6.25	339.9
S2C	253.52	6.33	339.9
S2D	244.46	6.14	339.9
S2D <sub>mod.</sub>		6.18	339.9
S3F	368.03	2.63	449.7
S3A	4.00	3.92	2.21
S3B	3.73	3.99	2.21
S3C	3.87	3.96	2.21
S3D	3.36	3.75	2.21
S3D <sub>mod.</sub>		4.07	2.21
S4F	33.10	2.34	17.18
S4A	40.55	2.65	17.18
S4B	112.43	2.62	17.18
S4C	15.03	3.46	17.18
S4D	12.20	3.34	17.18
S4D <sub>mod.</sub>		3.65	17.18

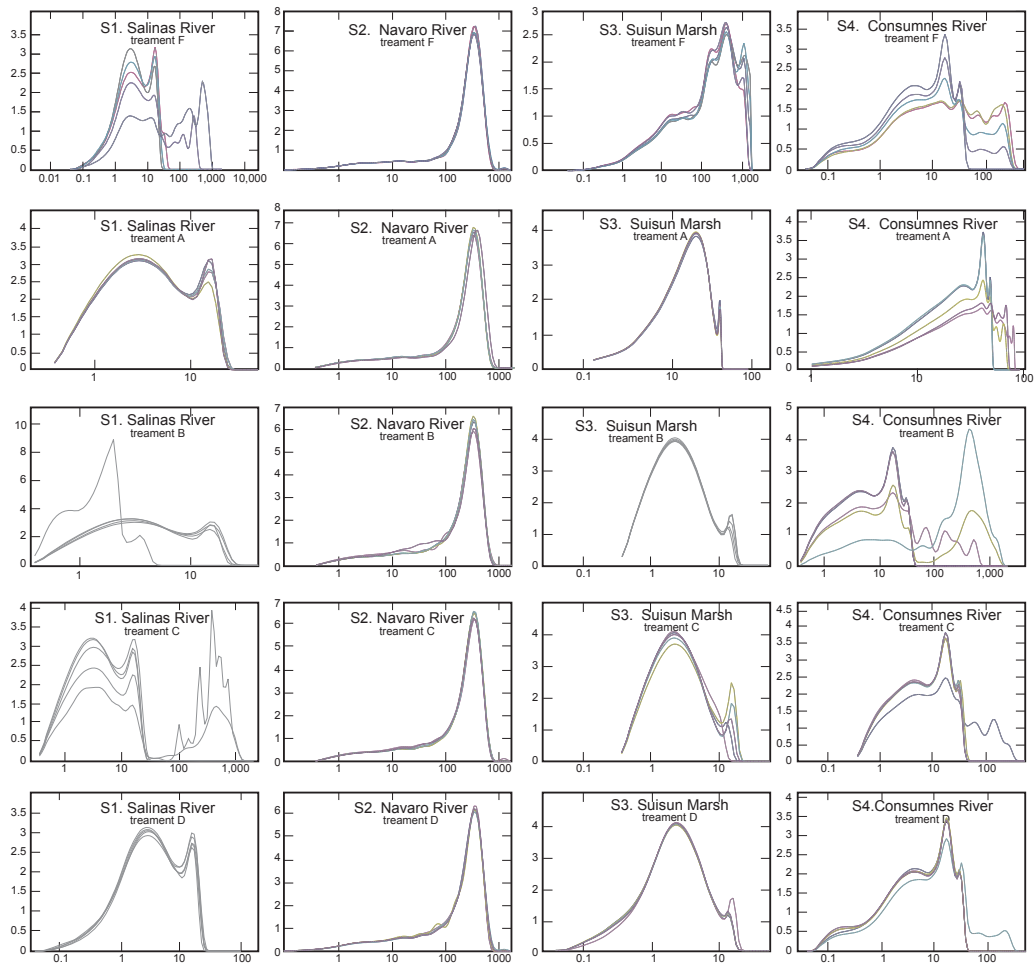


**Figure 1.3** Grain size distribution of all sample treatment replicates.

**Table 1.4** Coefficient of variation for all sample treatments ( $V_{avg}$ ) and grain sizes 0.375 to 2  $\mu\text{m}$  ( $V_{clay}$ ).

Sample	$V_{avg}$	$V_{clay}$
S1A	0.10	0.02
S1B	0.18	0.06
S1C	0.83	0.18
S1D	0.16	0.04
S1F	0.76	0.26
S2A	0.07	0.02
S2B	0.16	0.07
S2C	0.25	0.04
S2D	0.23	0.03
S2F	0.15	0.01
S3A	0.03	0.01
S3B	0.07	0.01
S3C	0.20	0.04
S3D	0.15	0.02
S3F	0.10	0.06
S4A	0.69	0.21
S4B	0.80	0.41
S4C	0.82	0.01
S4D	0.63	0.08
S4F	0.36	0.17
S5A	0.05	0.01
S5B	1.15	0.20
S5C	0.16	0.02
S5D	0.02	0.01
S5F	0.13	0.02

### 1.3.3 S2 - Navarro River Floodplain

Distribution analysis of the Navarro River Floodplain showed a unimodal, leptokurtic distribution negatively skewed toward medium sand with a long platykurtic tail extending through fine sand, silt and clay sizes (Fig. 1.2b). The mode was remarkably consistent at 339.9  $\mu\text{m}$  for 23 of 25 replicates across all treatments (Table 1.3, Fig. 1.3). The control exhibited a small secondary peak (~ 2 orders of magnitude lower than the major mode) at 1254.4  $\mu\text{m}$  for two replicates, which is also evident in a Treatment C replicate and one from treatment D. Heated treatments of these floodplain sediments produced larger average coefficient of variance values than that calculated for the control, while the unheated treatment resulted in a value about half that of the control (Table 1.4). Much of this variance again arose as a result of replicates that contained small amounts of the larger particles that did not show up on the majority of distributions.

The grain size frequency diagram of the average distribution obtained for each treatment

revealed two major zones of variability between treatments: 1) medium silt to fine sand and 2) the major modal sand peak (Fig. 1.2b). Changes in total frequency within these two zones were inversely related between treatments. The strength of the major mode generally decreased through the progression of treatments from the control to treatment A, followed by the heated treatments (B, C, D), while the silt/fine-sand region increased in frequency throughout this progression.

Microscopic characterization revealed that the organic particle assemblage was primarily composed of charcoal. Only a few pieces of plant debris showed up on the 600 and 300  $\mu\text{m}$  sieves. Charcoal abundance increased between the 800, 600 and 300  $\mu\text{m}$  sieves, and then decreased on the 150  $\mu\text{m}$  sieve relative to quartz grains present. This assessment agreed with the difference between the average control distribution and the treatment that differed most from it (treatment D). The plot of this difference showed a range of particle sizes from 213 to 1821  $\mu\text{m}$  with a lepidokuritic mode at 373.13  $\mu\text{m}$ , similar in shape to the grain size distribution obtained for all treatments of this sample (Fig. 1.4b).

#### 1.3.4 S3 - Suisun Marsh

The Suisun Marsh sample showed large difference in grain size distribution between the control and all treatments (Fig. 1.2c). The control distribution was polymodal, bearing a 449.66  $\mu\text{m}$  primary mode, negatively skewed with a platykurtic shoulder in the medium silt to fine sand range and has an extensive fine tail (Table 1.3). Treated subsamples had a broad major modality at 2.2072  $\mu\text{m}$  and a secondary peak at 15.651  $\mu\text{m}$ . Only two replicates (both from treatment D) varied slightly from the major mode, while the minor mode showed more variance in size and placement within and between treatments (Fig. 1.3c). Average treatment mode placement spanned three grain size bins from 13.00 to 15.65  $\mu\text{m}$  and strengths of 1.118 to 1.797 percent volume.

A high level of repeatability ( $V_{\text{avg}} = 0.10$ ) was found for the control replicates (Table 1.3). In fact, there was a high level of repeatability within and between all peroxide treatments, in contrast to the large difference in grain size distribution between treated samples and the control (Table 1.3, Figs. 1.2c, 1.3). The unheated treatment had a very low  $V_{\text{avg}}$  (0.03), while heated treatments experienced higher values with increased treatment.

Organic particles were abundant for all sieve classes. Microscopic characterization revealed a

suite of plant detritus dominated organics composed primarily of stem pieces with only minor amounts of root pieces and seeds and very little charcoal across all sieve sizes. The difference plot between the control and treatment D showed a poly modal distribution of medium silt to sand sized material, ranging from 15.7-1821.9  $\mu\text{m}$  with a primary mode at 449.66  $\mu\text{m}$  (Fig. 1.4c). Comparison of overlapping portions of the distributions for treatment D and the control (corrected for the removed coarse section) showed large differences in the lithic range, as the two distributions did not resemble each other (Fig. 1.5b).

### 1.3.5 S4 – Cosumnes Riverbank

All Cosumnes Riverbank treatments and the control shared the same polymodal characteristics for the fine portion of the grain size distribution (Fig. 1.2d, 1.3). A major, leptokurtic peak at 17.181  $\mu\text{m}$  was flanked by a platykurtic, shoulder- like minor mode around 4.24 to 5.61  $\mu\text{m}$  and a notch at 27.4  $\mu\text{m}$  followed by a small peak 30.1-33.0  $\mu\text{m}$  peak (Table 1.3). More variation was visible in the coarse portion of the spectra across treatments, although there were resilient peaks in this region for the control around 73-80  $\mu\text{m}$  and 213-234  $\mu\text{m}$  (Fig. 1.3). This coherence between distributions led to a lower  $V_{\text{avg}}$  for the control than any treatment; the lowest treatment value was for D at nearly twice that of the control (Table 1.3). Across treatments a reduction in the number of replicates that exhibited the presence of any sand size particles was apparent as one progressed from the control (4 replicates) to treatments A and B (three replicates each), and finally the more extensive heated treatments C and D (one replicate each) (Fig. 1.3).

The bulk of organic particles produced by sieving was charcoal, with some plant debris present in the form of stem and root pieces. Organic material showed up in low amounts relative to S1 and S3 on each sieve. The grain size spectra of sand sized particles were heavily affected by peroxide treatment for this sample. Removal of the one replicate of treatment D that continued to display particles above 43.667  $\mu\text{m}$  was performed for the calculation of the average lithic distribution as it was assumed to bear organics. The plot of the difference in grain size distribution between the control and treatment D showed a broad, multimodal distribution of medium silt to medium sand size particles ranging from 33 to 450  $\mu\text{m}$  (Fig. 1.4d). The modified control and Treatment D lithic range comparison revealed similar distributions, although the control exhibited a depressed mode and elevated % volume on the coarse end of the

distribution relative to treatment D (Fig. 1.5c).

#### **1.4 Discussion**

Reduction of the coarse range of material with H<sub>2</sub>O<sub>2</sub> treatment in S1, S3 and S4 indicates that the abundance of larger particle sizes in these sediments was due to the presence of organics. This finding is supported by the observation of distinct organic particles in the sand sized sieve fractions with microscopy. Changes in grain size distribution due to the removal of organics are also noticeable in S2, though muted due to the lower amount of organics in this sample and the overlapping distribution of the inorganic and primarily co-depositional charcoal particles.

The major modes of all samples, except S3, which also contained the highest level of organics (29.3%), were very resilient to organic particle presence. Although control replicates from these samples also deviated from the mineralogic major mode, the concomitant average distributions either agreed with this mode (S2 and S4) or deviated from it by only one grain size bin (S1). Examination of the control distribution ranges that overlap with treatment D distributions in S1, S3 and S4 shows salient characteristics in S1 and S4 that do not change much with treatment, while sample S3 fines are heavily influenced by organic particles in the control (Fig. 1.5).

The four samples in this study therefore exemplify three different results of organic interference with inorganic particle size determination. In the cases of S1 and S4, the inorganic and organic distributions are disparate to a degree in which the organic distribution primarily has a dampening effect due to the occupation of % volume; reducing the intensity of the inorganic distribution but causing little distortion in its morphology. For such distributions, measurements of central tendency that rely upon summed distribution calculations (mean, median) and internal texture ratios are highly skewed by the presence of organics, while modal analysis may be little affected. The overlap of organic and inorganic particle size distribution in S2 and S3 bore very different results. Low amount of organics present and their nearly identical distribution to that of the inorganic fraction in S2 lead to very little change in texture ratios and central tendency metrics. Conversely, in S3 the overlap of the inorganic clayey silt distribution with the fine tail of the primarily coarse organic distribution served to blot out all of the inorganic

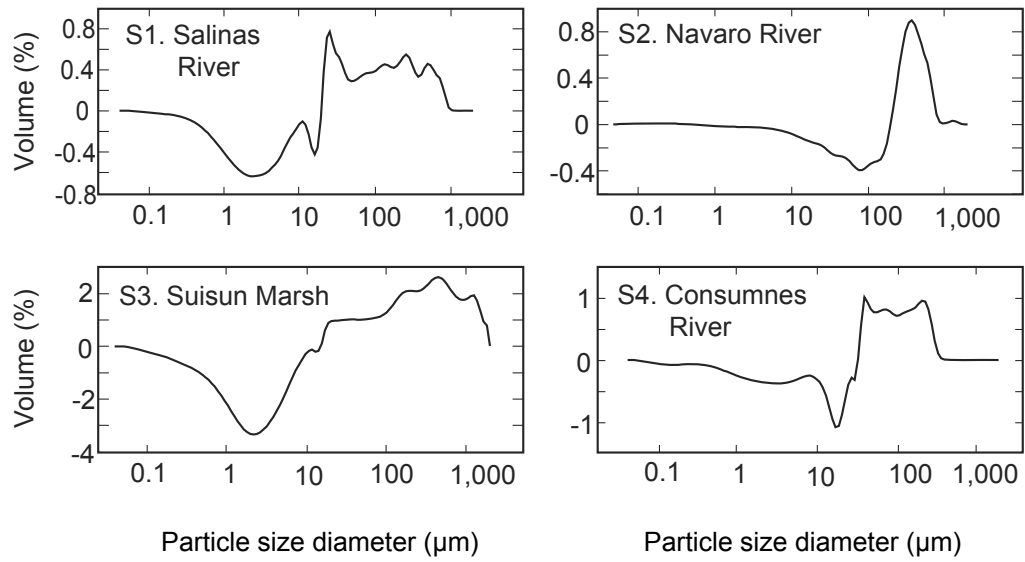


**Figure 1.4** Difference in grain size distribution between the control and treatment with five aliquots of heated peroxide.

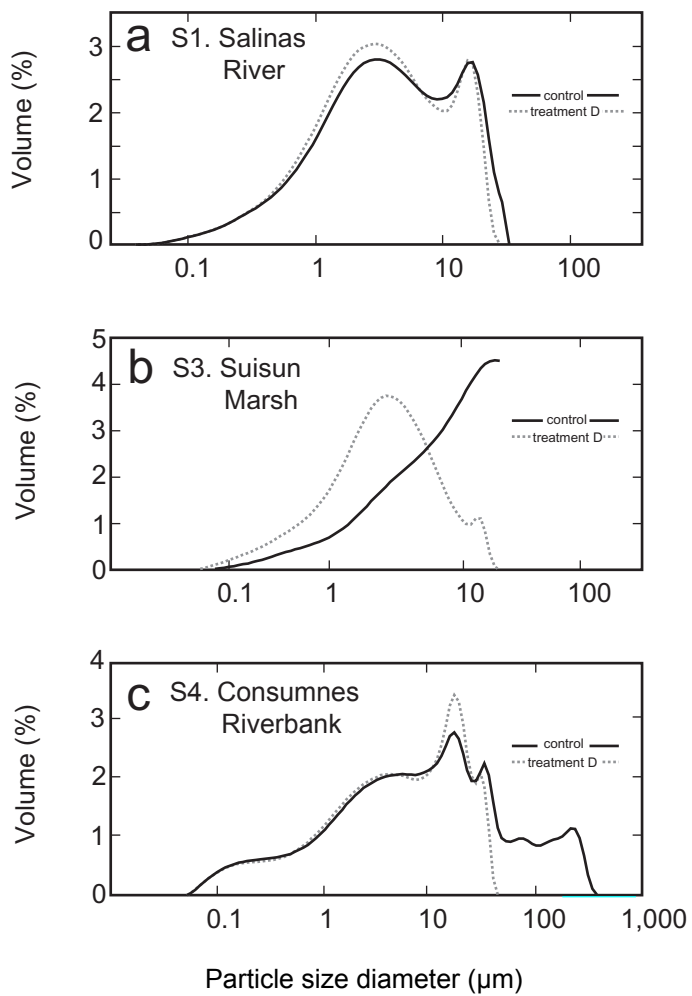


**Figure 1.5** The average grain size distribution over the lithic range of samples 1, 3 and 4 subjected to Treatment D plotted with each respective control rescaled to 100%.

characteristics, destroying any chance to describe this fraction without pretreatment.

Thus, we recommend that all analyses utilizing total distribution metrics such as textural ratios or mean grain size for alluvial sediments take into account sensitivity to the effect of organic particle presence, even at more moderate organic levels such as those found in the S1 and S4 samples (8.35 and 5.80 % respectively). Moreover, modal analyses are not significantly affected by the presence of moderate amounts of organics only in cases where organic and inorganic distributions either do not overlap significantly or overlap almost precisely. Therefore, even when utilizing modal characterization of grain size distribution one must be cautious in the presence of organics. Although analyses focusing solely on modal trends in terms of grain size distribution may simply elect to deflocculate samples rather than pursue treatment for organic removal, which has been suggested for clayey silts with little organic content (Allen and Thornley, 2004), we recommend that hydrogen peroxide treatment should be employed for samples with moderate to large amounts of organics.

Sample response to H<sub>2</sub>O<sub>2</sub> treatment appears to be contingent upon organic particle size and characterization rather than the proportion of organic to lithic particles. Those samples with organic assemblages comprised primarily of plant roots and detritus at moderate and high organic levels (S1 and S3) responded well to all forms of peroxide treatment, with the exception of replicates which are assumed to have contained large residual root fragments. In contrast, samples characterized by charcoal were more recalcitrant in terms of organic digestion. Charcoal pieces in excess of 800 µm were present in very low amounts in S2, and may have persisted when present across all treatments, although the small subsamples required for laser diffraction analysis may have also only occasionally captured the coarsest mineral grains present. Coarse charcoal was present in S4 at higher levels than in S2 and also showed resilience to peroxide digestion, with more complete removal arising from extensive heated treatments.

The large size of the organic particles in S1 and S4 may have led to the inability to homogenize the organics in these samples in regard to our subsampling methods, as evidenced by the lack of these distributions in several control replicates. Homogenization/sub-sampling of the organic constituents was more successful for S3 than all other samples as reflected in the coefficient of variation value for this sample treatment. In such cases where very large particles contribute much of the organic distribution interference, the time and effort necessary to conduct manual removal is probably warranted.

Yet, there may be other options for large organic particle removal. A sample outside of this study was collected near S4 and bore nearly the same lithic distribution and organic characterization (charcoal) with almost twice as much organic content (>10%). However, this copious coarse fraction did not show up on particle size distributions even without treatment. The high occlusion produced by fine lithics and humic/fulvic acids required a large amount of sample dilution within the LS-230 sample chamber before running the sample. It seems that dilution through successive bleeding/filling cycles in the sample chamber may provide a method for drawing off low-density organic material.

In light of the sensitivity of some sediments to degradation due to H<sub>2</sub>O<sub>2</sub> exposure, particularly weathered micas (Drosdoff, 1938), the clay fraction of sample replicates were examined for this effect. Assuming that the breakdown process would not be uniform, one would expect to find increased variability with increased levels of treatment. Comparison of  $V_{\text{clay}}$  between treatments for each sample did not indicate a single treatment that consistently produces the lowest values, nor are there indications of an increase in  $V_{\text{clay}}$  with increased levels of heated treatment (Table 1.3). The control displayed the largest values for S1 and S3, but had the lowest values for S2. Taking only H<sub>2</sub>O<sub>2</sub> treatments into consideration, treatment A resulted in the lowest  $V_{\text{clay}}$  for S1 and S2, however the second lowest value was reported from treatment D for both samples. Also,  $V_{\text{clay}}$  values decreased with increased heated treatment (B-C-D) in both S2 and S4. Thus, this study found no evidence for inorganic particle degradation in regard to alterations in grain size distributions. However, further studies that include the full range of clay size analysis available to the LS-230 would tackle this issue in more depth.

## 1.5 Conclusions

A uniform approach to peroxide treatment that yields complete organic removal is desirable for comparisons between samples that are meant to reflect differences in parameters other than sample pretreatment. When a large range of organic constituents may be encountered, down the length of a sediment core for example, the necessary uniform treatment must be tailored toward the most recalcitrant of samples. Unless in-depth characterization of organic particles is conducted before grain size analysis, one should assume the presence of both large plant material and charcoal. Based on the results from

this study, textural ratios and measures of the central tendency of particle size distributions, including modal analysis, can be heavily impacted by the presence of organic particles. Thus, a protocol for the removal of organic constituents requires the application of long duration, unheated dispersions in 30% H<sub>2</sub>O<sub>2</sub> for a standard amount of time, followed by a fixed amount of further heated aliquots in combination with the removal of large particles by manual methods.

## 1.6 References

- Allen JRL, Haslett SK. 2006. Granulometric characterization and evaluation of annually banded mid-Holocene estuarine silts, Welsh Severn Estuary (UK): coastal change, sea level and climate. *Quaternary Science Reviews* **25**: 1418-1446
- Allen JRL, Thornley DM. 2004. Laser granulometry of Holocene estuarine silts: effects of hydrogen peroxide treatment. *Holocene* **14**: 290-295
- Chen ZY, Stanley DJ, Wright EE. 2000. Selective sorting, storage and progressive dilution of sediment in two tropical deltas, Veracruz, Mexico. *Journal of Coastal Research* **16**: 470-481
- Drosdoff M, Miles EF. 1938. Action of hydrogen peroxide on weathered mica. *Soil Science* **46**: 391-396
- Ghilardi M, Kunesch S, Styllas M, Fouache E. 2008. Reconstruction of Mid-Holocene sedimentary environments in the central part of the Thessaloniki Plain (Greece), based on microfaunal identification, magnetic susceptibility and grain-size analyses. *Geomorphology* **97**: 617-630. DOI: 10.1016/j.geomorph.2007.09.007
- Konert M, Vandenberghe J. 1997. Comparison of laser grain size analysis with pipette and sieve analysis: A solution for the underestimation of the clay fraction. *Sedimentology* **44**: 523-535
- Kunze GW, Dixon, JB. 1982. Pretreatment for Mineralogical Analysis. In *Methods of Soil Analysis, Part 1. Physical and Mineralogical Methods - Agronomy Monograph no. 9*, Klute A (ed). Soil Science Society of America, Inc.: Madison, WI; 91-100.
- Lewis DW. 1984. *Practical Sedimentology*. Hutchinson Ross Publishing Company
- Matthews MD. 1991. The effect of pretreatment on size analysis. In *Principles, Methods, and Application of Particle Size Analysis*, Syvitski JPM (ed). Cambridge University Press: Cambridge; 34-44.

- Orton GJ, Reading HG. 1993. Variability of Deltaic Processes in Terms of Sediment Supply, with Particular Emphasis on Grain-Size. *Sedimentology* **40**: 475-512
- Percival JB, Lindsay, PJ. 1997. Chapter Two: Measurement of physical properties of sediments. In *Manual of Physico-Chemical Analysis of Aquatic Sediments*, Mudroch A, Azcue, J. M., Mudroch, P. (ed). CRC Press, Inc: Boca Raton; 297.
- Robinson GW. 1922. Note on the Mechanical Analysis of Humus Soils. *Journ. of Agric. Sci.* **7**: 287-291
- Syvitski JP, LeBlanc KWG, Asprey KW. 1991. Interlaboratory, interinstrument calibration experiment. In *Principles, Methods and Applications of Particle Size Analysis* Syvitski JP (ed). Cambridge University Press: Cambridge; 174-193.
- Tebbens LA, Veldkamp A, Kroonenberg SB. 1998. The impact of climate change on the bulk and clay geochemistry of fluvial residual channel infillings: the Late Weichselian and Early Holocene River Meuse sediments (The Netherlands). *Journal of Quaternary Science* **13**: 345-356
- Visher GS. 1969. Grain size distributions and depositional processes. *Journal of Sedimentary Petrology* **39**: 1074-1106

## Chapter 2

### Suspended sediment behavior in a coastal dry-summer subtropical catchment: Effects of hydrologic preconditions

#### Abstract

Variation in fluvial suspended sediment–discharge behavior is generally thought to be the product of changes in processes governing the delivery of sediment and water to the channel. The objective of this study was to infer sediment supply dynamics from the response of suspended sediment behavior to antecedent hydrologic factors. The Salinas River (California) is seasonally active, moderately sized, and potentially susceptible to lasting impacts of hydrologic event history because of aridity, high discharge variability, and in-channel terminating flows. Forty-five years of suspended sediment data from the lower Salinas and 80 years of hydrologic data were used to construct hydrologic descriptors of basin preconditioning and test the effects of these preconditions on suspended sediment behavior. Hydrologic precondition factors — including change in mean daily discharge and increasing elapsed time since the last moderate discharge event ( $\sim 10\text{--}20$  times mean discharge ( $Q_{mean}$ )) — were found to have significant positive effects on discharge-corrected, fine suspended-sediment concentrations. Conversely, increased elapsed time since the last low discharge event ( $\sim 0.1\text{--}0.4$  times  $Q_{mean}$ ), and the sum of low flow conditions over interannual time scales were found to cause significant negative trends in fine suspended sediment concentration residuals. Suspended sand concentrations are suppressed by increased elapsed time after threshold discharges of  $\sim 0.1\text{--}2$  and  $5\text{--}100$  times  $Q_{mean}$ , and increased low to no flow days over time scales from 1 to 2000 days. Current and previous year water yield and precipitation magnitudes correlate positively with sand concentration. Addition of fine sediment from lower Salinas hillslope or channel sources on the rising limb of the hydrograph is the major mechanism behind an overall positive hysteretic pattern, which was forensically supported by the annual occurrence of in-channel suspended sediment deposition by early season, channel terminating flows and by the flushing function of moderate hydrologic events found in this study. The importance of hillslope and/or channel fine sediment contributions proximal to the lower Salinas are further highlighted by the lack of control exerted by upper

subbasin water provenance on fine suspended sediment concentration, while sand behavior is differentiated by upper basin water provenance. Investigation of suspension of bed-sized sediment showed that the channel bed could exert significant effects on fine and sand-sized suspended sediment dynamics, but this mediation for fine sediment was most likely small in terms of decadal-scale sediment budgets. The magnitude of the effects of hydrologic variables on sediment dynamics remains uncertain, but the factors identified here may play a significant role in water quality, if not long-term sediment flux to the ocean.

## 2.1 Introduction

Rivers of small to moderate size ( $\sim 10^1$ – $10^4$  km<sup>2</sup>) draining active margins are recognized as transporting the majority of terrestrial sediment to the oceans (Milliman and Syvitski, 1992). Sediment yields from their basins are often highly episodic, caused by rare high discharge floods (Gonzalez-Hidalgo et al., 2010; Wheatcroft et al., 2010). Small rivers in dry-summer subtropical regions, such as coastal California, are particularly prone to episodic hydrologic event control on sediment discharge, as most precipitation occurs during a short winter season that occasionally produces intense storm events (Inman and Jenkins, 1999; Farnsworth and Milliman, 2003; Warrick and Mertes, 2009).

Sediment dynamics in systems with high discharge variability are further impacted by the deposition and/or reorganization of sediment in the channel by flow recession and ephemeral flows that terminate in the channel (López-Tarazón et al., 2011) as well as sediment supply augmentation or suppression associated with large precipitation/hydrologic events and prolonged periods of no precipitation (Lana-Renault et al., 2007). Basin preconditioning — the sequence and temporal proximity of events that impact hillslope and channel sediment supply — and the long-term implications of these events as well as slower, extensive alteration of the land surface and vegetation also play significant roles in altering fluvial sediment production, particularly in episodic systems (Lenzi and Marchi, 2000; Pasternack et al., 2001; Chakrapani, 2005; Gao and Josefson, 2012; Warrick et al., 2013).

Sediment transported in suspension accounts for the majority of particulate matter conveyed by rivers (Meade et al., 1990). Because of the difficulty in collecting suspended sediment data, suspended

sediment transport for most rivers has been estimated through rating curves that relate suspended sediment concentration ( $C_{SS}$ ) to water discharge ( $Q$ ), as the latter is more easily measured and often available in longer time series (Horowitz, 2003). Early investigations into antecedent hydrologic effects on suspended sediment flux were primarily focused either on the association of regional scale patterns in suspended load resulting from long-term precipitation and discharge characteristics (i.e., Langbein and Schumm, 1958) or watershed scale studies of the 'lag effect' during individual hydrologic events, which results from slower moving sediment pulses relative to the transmission of peak water discharge at the event scale (Heidel, 1956; Carson et al., 1973; Shi et al., 1985). Identification of the principal factors affecting suspended sediment behavior has been an active field of study since suspended sediment–discharge rating relationships were found to lack predictive power in smaller catchments (Walling, 1977; Syvitski et al., 2000; Warrick and Rubin, 2007; Sadeghi et al., 2008).

As the amount of suspended sediment moved by a river is generally limited by sediment supply rather than the transport capacity of channelized flow, the residual variability of  $C_{SS}$  beyond that explained by  $Q$  in a given watershed is usually the result of factors that affect erosional processes, the delivery of eroded sediment to the channel, or the trapping efficiency of the channelized system (de Vente et al., 2007). Sediment and water supply to the channel are controlled by the same major factors, namely precipitation distribution and intensity, basin structure (relief, substrate composition), and basin preconditions (moisture levels, vegetation states, disturbance states) (Wischmeier and Smith, 1978; Syvitski et al., 2000; Lana-Renault et al., 2007; Mano et al., 2009). Increased shear stress during floods can erode channel margins, scour away stabilizing structures such as vegetation, and activate landslide snouts adjacent to the channel in upper basin areas, all of which can lead to increased channel bank and hillslope sediment delivery (Kelsey, 1980; Benda and Dunne, 1997; Poesen and Hooke, 1997; Korup, 2012). Conversely, large events can flush the channel system of fine sediment stores deposited by recessional or ephemeral flows and can exhaust intermediate storage of hillslope sediment supplies, which can lead to depressed sediment yields from subsequent discharges (Droppo and Stone, 1994; Walling et al., 1998; Brasington and Richards, 2000; Hudson, 2003; Constantine et al., 2005; Batalla and Vericat, 2009). Thus, the  $C_{SS} \sim Q$  rating curve is an exercise in the use of discharge as a proxy for the master variables controlling sediment delivery to the stream of channelized flow, even though it will not

capture the dynamics of these landscape and channel processes.

The overall goal of this study was to test the hypothesis that antecedent hydrologic conditions significantly control suspended sediment behavior. The specific objectives were to (i) develop variables representing basin preconditions from hydrologic and precipitation time series data and (ii) determine if variability in suspended sediment behavior could be explained using the precondition variables. As the Salinas River flows only intermittently during the year, it was posited that in-channel deposition of sediment from incipient flows, and the eventual reworking of this sediment, would have a significant effect on suspended sediment dynamics. The results of hydrologic precondition analysis were explored to infer the sediment supply processes at play. The most significant aspect of this work is that it provides an approach for incorporating event to interannual scale hydrologic precondition characterization into the process of deciphering sediment supply dynamics at the basin scale.

## **2.2 Study region characteristics**

The ~ 11,000-km<sup>2</sup> Salinas River watershed drains a portion of the Central Coast Ranges of California, USA, flowing from the SE to NW along the Rinconada fault zone between the Sierra de Salinas and Santa Lucia Mountains to the SW and the Diablo and Gabilan Ranges to the NE (Rosenberg and Joseph, 2009) (Fig. 2.1). Maximum relief is ~ 1900 m; average watershed bounding ridge heights are 750 m to the NE and 1200 m in the SW, with ridge crest height generally decreasing toward the mouth of the Salinas (Neagley et al., 1990). Mountainous highlands are mostly composed of Mesozoic-aged sedimentary and metasedimentary rock with some igneous intrusions, while the northern extent of the mainstem valley floor is Tertiary and younger alluvial fill (Nutter, 1901). Land cover in the Salinas watershed largely follows local relief, with steep forested terrain giving way downslope to chaparral/scrub in the wetter western hills and grassland in the drier eastern hills (Farnsworth and Milliman, 2003). Valley bottoms were mostly converted to irrigated agriculture with a small proportion of urbanization (Thompson and Reynolds, 2002).

Climate along California's central coast is dry-summer subtropical with most precipitation delivered by a few winter storms. The largest storms are produced during strong El Niño years

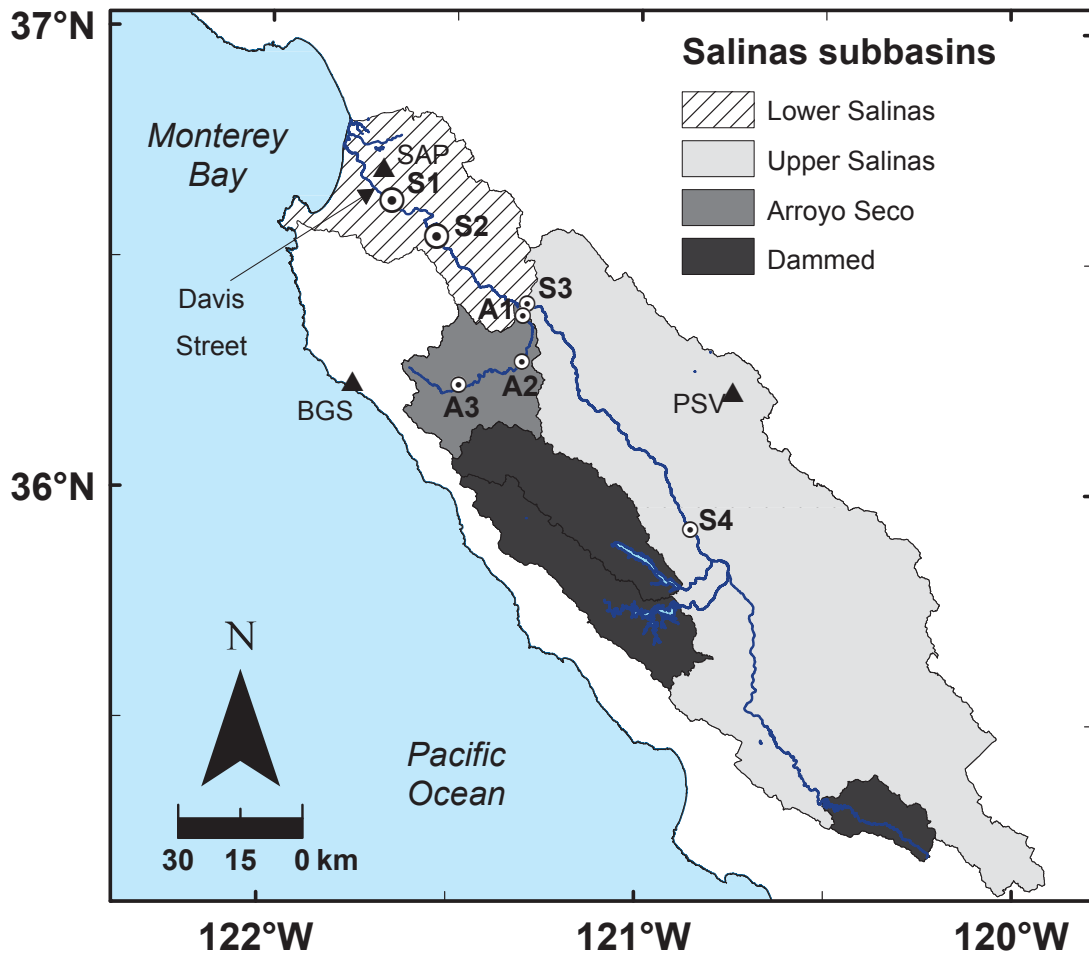


**Figure 2.1** The Salinas River watershed drains a portion of the northern California Coast Ranges into Monterey Bay. Dark gray areas represent the watersheds of the dammed reservoirs (from S to N) Santa Margarita Lake, Lake Nacimiento and Lake San Antonio completed in 1941, 1961, and 1965, respectively. S1–S4 and A1–A3 are USGS hydrologic gaging stations located on the Salinas and Arroyo Seco rivers, respectively (see Table 1 for details). BGS, SAP, and PSV are the NOAA precipitation gages, Big Sur State Park, Salinas No. 2, and Priest Valley, respectively.

(Farnsworth and Milliman, 2003; Andrews et al., 2004). Convection of western tropical moisture through westerly storm tracks generally leads to S–SW impingement of storms (Andrews et al., 2004). Because of the SE to NW orientation of the basin and its small size, such storms can simultaneously deliver precipitation to the entire watershed to produce the largest floods on record. Orographically forced precipitation in the SW mountain ranges coupled with the preponderance of smaller storms and prevailing storm tracks leads to average annual precipitation rates that are much higher (~ 1000 mm/y) than in the NE region (~ 300 mm/y) (Farnsworth and Milliman, 2003).

Average annual suspended sediment load was previously calculated as 1.7–3.3 Mt using monthly and daily Q with log-linear rating curves (Inman and Jenkins, 1999; Farnsworth and Milliman, 2003). Ongoing work in this system by the authors has found that suspended sediment load estimated from daily discharge data using a combination of sand and fine suspended sediment rating curves for temporal domains of distinct suspended sediment behavior resulted in an average annual load of ~ 2.2 Mt.

The Salinas is a losing stream with naturally transient flow and no surface water passing through the lower reaches for much of the summer. The aquifers in the alluvial valley are overdrafted for agriculture, causing saltwater intrusion. Three major dams emplaced from 1941 to 1965 on the San Antonio and Nacimiento tributaries, as well as the upper most reaches of the Salinas, moderate flow from a total of ~ 2100 km<sup>2</sup> of the Salinas watershed, primarily for groundwater recharge purposes (Fig. 2.1). Average sediment trapping efficiency for dams in the central California coastal region have been estimated as ~ 84% by Willis and Griggs (2003) with the simple Brune (1953) method. Estimations of trapping efficiency by the authors based on the methods of Brown (1943) and the improved Brune method from Heinemann (1981, 1984) place the Salinas basin reservoirs in the range of 94–99% for bulk sediment and ~ 90% or greater for fine sediment (clay and silt) trapping efficiency

United States Geological Survey (USGS) daily average Q gauging stations on the mainstem and on the Arroyo Seco tributary date to 1901 (A3, Arroyo Seco near Greenfield) and 1931 (S1, Salinas River near Spreckels), respectively (Table 2.1; Fig. 2.1). The confluence of the Arroyo Seco and the Salinas is located 1.36 and 1.74 river kilometers below the nearest upstream gages on the Salinas (S3, Salinas River near Soledad) and the Arroyo Seco (A1, Arroyo Seco below Reliz Creek near Soledad), respectively. Below the Arroyo Seco/Salinas confluence is referred to as the 'lower Salinas' in this study,

**Table 2.1** Gage stations and Salinas River reaches

ID <sup>a</sup>	USGS gage name	USGS gage #	SS data	Record interval of $Q_d$ (water years)	Drainage area (km <sup>2</sup> )	Reach	Distance <sup>b</sup> (km)
S1	<i>Salinas R. near Spreckels</i>	11152500	yes	1931 - 2011	10,764	S1 to S2	23.51
S2	<i>Salinas R. near Chualar</i>	11152300	yes	1976 - 2011	10,469	S2 to confluence	28.41
S3	<i>Salinas R. at Soledad</i>	11151700	no	1969 - 2011	9,228	Confluence to S3	1.36
S4	<i>Salinas R. near Bradley</i>	11150500	no	1948 - 2011	6,566	S3 to S4	84.69
A1	<i>Arroyo Seco below Reliz Creek</i>	11152050	yes	1994 - 2011	787	Confluence to A1	1.74
A2	<i>Arroyo Seco near Soledad</i>	11152000	no	1962 - 1986	632	A1 to A2	17.28
A3	<i>Arroyo Seco near Greenfield</i>	11151870	yes	1901 - 2011	113	A2 to A3	24.79

<sup>a</sup>Identification code for this study.

<sup>b</sup>River distance measure by following approximate thalweg.

which bears two mainstem gages 28.41 km (S2, Salinas River near Chualar) and 51.92 km (S1, Salinas River near Spreckels) downstream, respectively, both of which have a mean discharge of  $\sim 10 \text{ m}^3\text{s}^{-1}$  with a 2-year return flood of  $100\text{--}200 \text{ m}^3\text{s}^{-1}$ . The 100-year flood is estimated to be  $\sim 3000 \text{ m}^3\text{s}^{-1}$ , as per log-Pearson Type III flood frequency analysis (USGS NWIS). The mouth of the Salinas River is 21.14 km downstream from S1 and remains closed to the Monterey Bay via impounding sand bars, except under conditions of high river discharge and/or strong ocean waves (Watson et al., 2013).

The Arroyo Seco is the only undammed tributary of the Salinas River originating from the wet, mountainous western side of the basin and is also the last major tributary to enter the Salinas. In contrast, the Salinas watershed upstream of the confluence with the Arroyo Seco (referred to hereafter as the ‘upper Salinas’) is generally low gradient and bordered by intensively irrigated agriculture, while the Arroyo Seco is the least developed subbasin in the Salinas system, with  $\sim 95\%$  chaparral/blue oak forest land cover and steep terrain. Most of the Salinas channel is broad and sand-bedded, with complex, braided, base-flow inset channels and low sandy banks with highly variable vegetation coverage. Transition to a primarily gravel bed occurs high in the upper Salinas, below the mainstem dam, while the Arroyo Seco transitions to a sand bed just before its confluence with the Salinas. Sediment export from the Arroyo Seco has been shown to be dominated by the convergence of wildfire and subsequent large precipitation events (Warrick et al., 2012). The flashy nature of discharge in the Arroyo Seco leads to large flows produced rapidly relative to the upper Salinas, which can lead to lower Salinas discharge events that are primarily expressions of Arroyo Seco runoff.

## **2.3 Data**

### *2.3.1 Experimental design*

This study attempted to determine the effect of antecedent hydrologic conditions on  $C_{SS}$  behavior and infer the physical mechanisms behind these effects, with a particular emphasis on the possibility of in-channel mediation. The first phase of this study involved testing the residuals of  $C_{SS}\text{-}Q$  behavior for correlations with variables describing antecedent hydrology and comparing  $C_{SS}\text{-}Q$  behavior between subgroups defined by hydrologic conditions. Physical mechanisms behind these behaviors were

approached by investigating hysteresis, the effects of subbasin water provenance, and analysis of the evolution of suspended sediment particle size distribution in terms of discharge and long profile position.

### 2.3.2 Hydrologic data

This study was based on suspended sediment samples collected by the authors and historical USGS samples. Samples were collected for this study between water years 2008 and 2011 from bridges crossing the Salinas River at Davis Street (3.99 km river distance below S1) and the USGS gauging stations S1 and S2 (Figs. 2.1 and 2.2B; Table 2.1). Water years for this region begin October 1 of the previous calendar year and end on September 30 of the calendar year. Samples were collected as per Warrick et al. (2012), except for the following modifications. In all cases, samples were retrieved from the water surface at cross-channel stations of ~ one-quarter, one-half, and three-quarters wetted channel width. Two 1-L samples from each cross-channel station were collected for (i) total suspended sediment concentration ( $C_{SS}$ ) and (ii) particle size distribution analysis. One event was sampled at high resolution — 250-ml samples every 2–3 hours. All samples were measured volumetrically and then filtered through preweighed, combusted, Whatman GF/A, 0.7  $\mu\text{m}$  glass fiber filters. Filters were dried at 60°C for > 24 h, cooled to room temperature under vacuum in a desiccator, and then weighted to  $\pm 0.0001$  g. Sample sediment mass was obtained by subtracting filter mass from total mass. The  $C_{SS}$  was then calculated by dividing sample sediment mass by water sample total volume.

Particle size distribution analysis began with centrifuging water samples at 3250 g in 500-mL bottles for 10 min. After removing the supernatant, the remaining sediment was transferred to 150-mL beakers and treated with unheated and heated 30%  $\text{H}_2\text{O}_2$  aliquots to remove organic materials, dispersed with sodium metaphosphate solution, and run through a Beckman-Coulter LS 230 (Beckman Coulter Inc., Fullerton, CA, USA) laser diffraction granulometer using polarization intensity differential scattering (PIDS) as per Gray et al. (2010).

Suspended sediment samples were collected from the surface of the river, and for this reason coarse suspended sediment particles were expected to be underrepresented. Simple sediment suspension calculations by particle size based on the characteristics of the highest and lowest flows showed that fine particles in the silt to clay range (diameter ( $D$ ) < 62.5  $\mu\text{m}$ ) should be uniformly distributed

throughout the vertical profile (Rouse, 1937, 1938; Hill et al., 1988). Thus, particle size distribution analysis was restricted to fine particles of  $D < 62.5 \mu\text{m}$ . For all samples containing coarse ( $D > 62.5 \mu\text{m}$ ) sediments, values for fine suspended sediment concentration ( $C_{SSf}$ ) were calculated by multiplying  $C_{SS}$  by the proportion of sediment occurring in the fine fraction:

$$C_{SSf} = \frac{C_{SS} \times (\% \text{ particles} < 62.5 \mu\text{m})}{100} \quad (2.1)$$

The USGS collected flow-integrated  $C_{SS}$  samples from the Salinas River at locations corresponding to S1 and S2 from water years 1969 to 1986 and 1967 to 2010, respectively (USGS NWIS, 2013) (Fig. 2.2a). Bed sediment samples were also collected between 1967 and 1992. The particle size distribution of bed sediments at S1 and S2 was characterized by sieving on nine and six occasions, respectively, between 1967 and 1992.

The USGS suspended sediment data had to uniquely represent a given discharge event and be associated with both instantaneous  $Q$  and particle size data for inclusion in this study. Multiple samples collected during the same event at constant discharge were combined into single samples through simple averaging of  $C_{SS}$ ,  $Q$ , and particle size distribution data. Most USGS suspended sediment samples were processed for particle size distribution by sieving to establish the relative contribution of coarse and fine fractions. The  $C_{SSf}$  for these samples was calculated using Eq. (1), and the concentration of sand-sized suspended sediment ( $C_{SSs}$ ) was obtained by subtracting  $C_{SSf}$  from  $C_{SS}$ . Hereafter, the term  $C_{SS}$  is used as a general term for suspended sediment concentration when referring to tests that were conducted separately on  $C_{SSf}$  and on  $C_{SSs}$ .

All suspended sediment data from the USGS were obtained with associated instantaneous discharge values. New samples collected in this study were assigned discharge values through linear interpolation between the two temporally nearest 15-min discharge data from the appropriate USGS gage. Discharge for Davis Street samples were obtained from the S1 record of 15-min discharge data, by lagging the time by the estimated transit time ( $t_t$ ), where  $t_t$  was equal to the distance between Davis Street and S1 divided by the transit speed ( $\text{m s}^{-1}$ ) of peak flow between S2 and S1 for each discharge event in question. Although transit speeds were found to be highly variable, ranging from  $0.01$  to  $2.38 \text{ m s}^{-1}$ , most

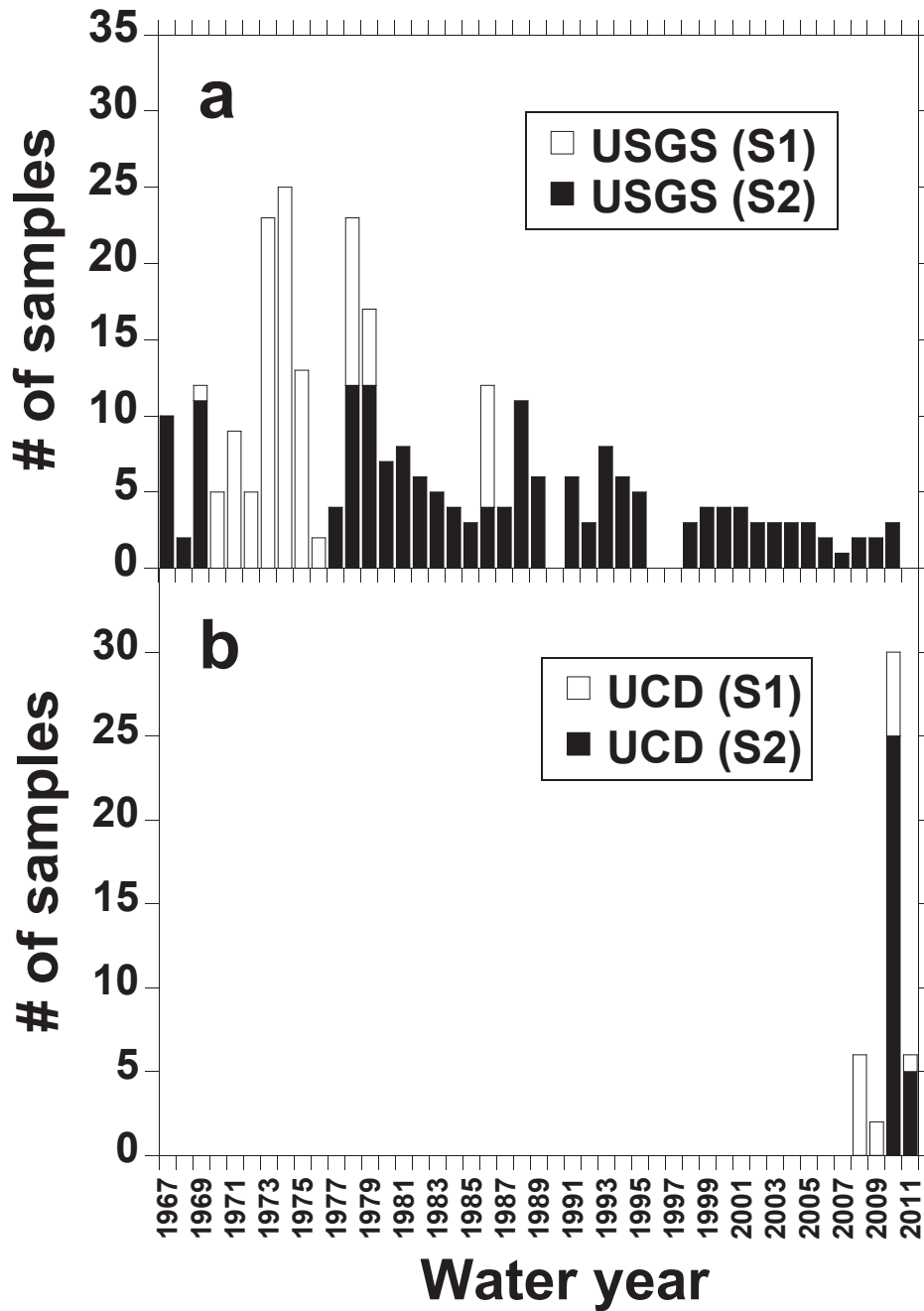


**Figure 2.2** Lower Salinas suspended sediment samples collected by the (A) USGS and (B) the authors (UCD) at stations S1 and S2, which correspond to the USGS gaging stations #11152500 (Salinas Spreckels) and #11152300 (Salinas Chualar), respectively.

values fell between 0.2 and 0.8 m s<sup>-1</sup>. When the resultant lagged time fell between 15-min discharge records, the associated discharge was calculated through linear interpolation.

Field measurements of flow characteristics collected between 1974 and 2012 were used in hydraulic geometry calculations for sites S1, S2, S3, and A1, which were measured for instantaneous discharge, flow area ( $a$ ), flow width ( $w$ ), and average velocity ( $u$ ) by the USGS between 1974 and 2012.

### 2.3.3 *Precipitation data*

Three National Weather Service monthly precipitation records were used in this study, including those from stations at Big Sur State Park (BGS), Priest Valley (PSV), and Salinas no.2 (SAP) (Fig. 2.1). The BGS gage is located outside of the Salinas watershed, just inland from the coast at 36.247° N., 121.811° W.; while PSV sits in the central, western portion of the upper Salinas at 36.183° N., 120.700° W.; and SAP in the lower Salinas at 36.667° N., 121.667° W. The BGS data set contained the fewest gaps. Regression between log-transformed annual precipitation ( $P$ ) and log-transformed annual water yield at S1 fitted by station also showed that more variation in water yield was explained by BGS than the other two precipitation stations, so BGS was used in further analyses. Precipitation data gaps for years 1981, 1982, and 1983 were reconstructed using the inverse of the water yield ~ precipitation rating curve.

### 2.3.4 *Bias analysis*

The effects of the inclusion of two sampling sites and the selection of certain samples for particle size distribution analysis by the USGS were found to not bias the ensuing analyses. For further details see Appendix 2.A.

## 2.4 **Suspended sediment rating curves and residuals**

Available  $C_{SS}$  and associated  $Q$  data were used to model the dependence of  $C_{SS}$  on  $Q$  for the system (hereafter referred to in the form of  $C_{SS} \sim Q$ ). A log-linear sediment rating curve describes this relationship through a linear regression fitted to log-transformed data in the form

$$\log(C_{SS}) = \log(a) + b \log(Q) + \varepsilon \quad (2.2)$$

Log-linear rating curves were constructed for the entire lower Salinas  $C_{SSf}$  and  $C_{SSs}$  data set (USGS and data collected for this study at sites S1 and S2; Figs. 2.3a,b). These rating curves accounted for a moderate proportion of variation in  $C_{SSf}$ , with  $r^2$  values of 0.55 and a standard error of 0.63 log (mg L<sup>-1</sup>) for the linear regression model and an  $r^2$  value of 0.70 with a standard error of 0.60 log (mg L<sup>-1</sup>) for  $C_{SSs}$ .

Rating curve residuals, which are the difference between sample values of  $C_{SS}$  and the value of the rating curve, can be used to reveal systematic departures in sample  $C_{SS}$  behavior from that of the rating curve model (Figs. 2.3c,d). Residual values plotted by discharge for lower Salinas fine suspended sediment show that the log-linear rating curve generally underestimated the lowest ( $q < 1 \text{ m}^3\text{s}^{-1}$ ) and highest ( $q > 800 \text{ m}^3\text{s}^{-1}$ ) discharge range  $C_{SSf}$  (positive rating curve residuals), and slightly overestimated moderate discharge range  $C_{SSf}$  (negative rating curve residuals) (Fig. 2.3c). The concentration of sand in suspension was also consistently underestimated for the lowest discharge range of  $q < 1 \text{ m}^3\text{s}^{-1}$  (Fig. 2.3d). It has been recognized that the  $C_{SS} \sim Q$  relationships of many episodic river systems on the west coast of North America often systematically depart from the log-linear rating curve, particularly at low and high discharge (Farnsworth and Warrick, 2007; Warrick et al., 2013).

To avoid potential bias from the systematically poor fit of log-linear curves, LOESS curves were fitted to the  $C_{SS} \sim Q$  data sets for subsequent residual analysis, as well as particle size distribution estimation, using  $\alpha = 0.75$  and second-degree polynomials (Cleveland, 1979; Cleveland and Devlin, 1988; Helsel and Hirsch, 2002). LOESS curves fit to each of the entire fine and sand data sets produced standard errors of 0.59 and 0.55 log(mg/L), respectively (Figs. 2.3a,b). LOESS residuals for fine sediment appeared to have low structure with discharge (Figs. 2.3e,f). This was confirmed by sequential summation of linear regression and LOESS residuals over the discharge domain, as LOESS rating curves displayed less persistent dependence on discharge than the corresponding linear regression curves (Figs. 2.3g,h). Note that rating curves in this study were not adjusted for log-transform bias (i.e., Ferguson, 1986), as they were used solely for intercurve comparison rather than prediction of  $C_{SS}$  in terms of untransformed units of measure.

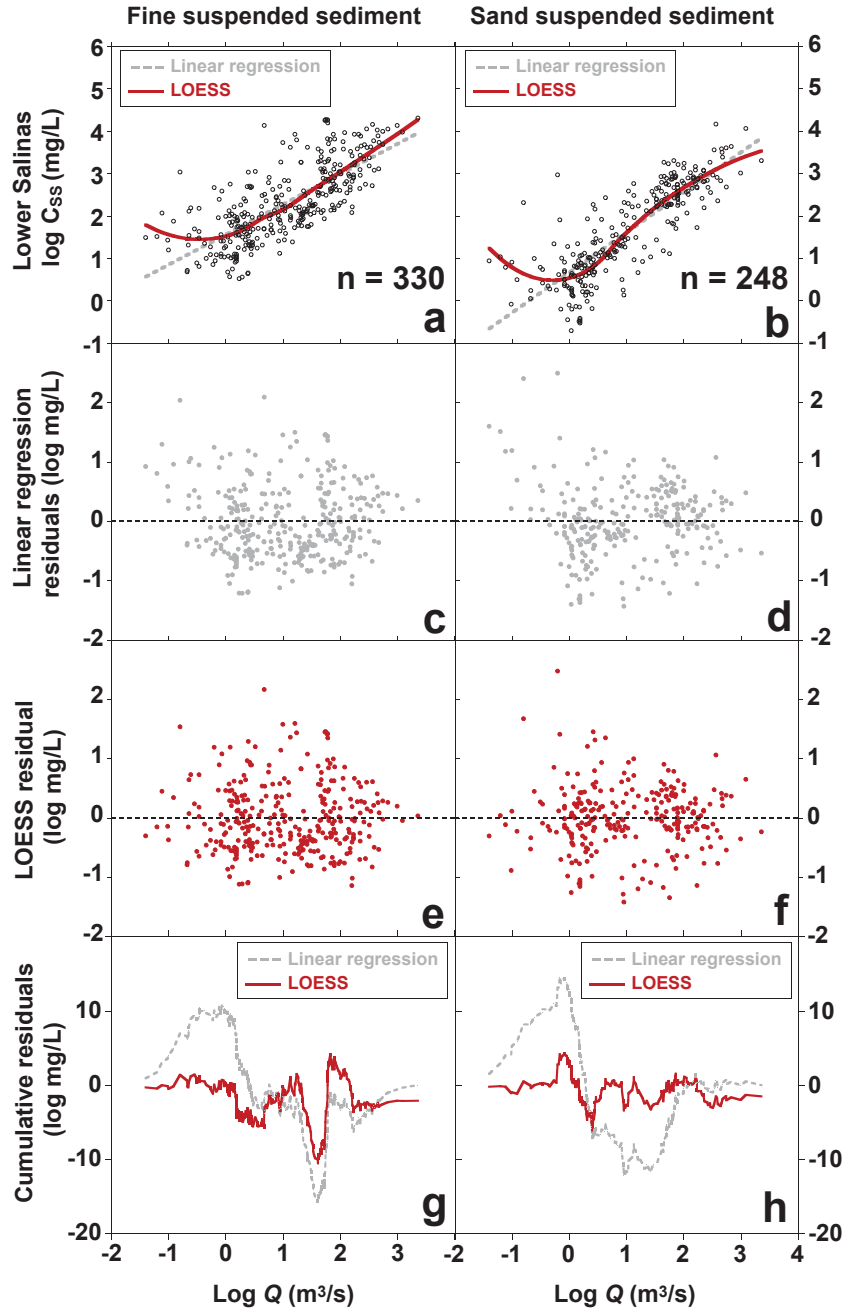


**Figure 2.3** Suspended sediment rating curves and residuals from lower Salinas River samples. Fine suspended sediment concentration (A) and sand suspended sediment concentration (B) plotted with simple linear regression curves in dashed lines and LOESS curves in solid lines. Concomitant linear regression rating curve residuals for (C) fines and (D) sand are followed by LOESS rating curve residuals (E) and (F) for fine and sands respectively, and sequentially summed residuals over the discharge regime (G) and (H).

## 2.5 Antecedent hydrologic conditions

### 2.5.1 Hydrologic variable effects on $C_{SS}$ -Q residuals

Hydrologic variables representing event conditions, basin wetness, seasonality, basin aridity, and hydrologic event history were computed from discharge data to account for variability in suspended sediment concentration not explained by instantaneous discharge (Table 2.2). Event scale hydrology was described using the change in daily discharge ( $\Delta Q_d$ ), calculated as

$$\Delta Q_d = Q_{dts} - Q_{dts-1} \quad (2.3)$$

where  $Q_{dts}$  is the mean daily discharge value for the day of a given  $C_{SS}$  sample, and  $Q_{dts-1}$  is the mean daily discharge value for the day before the sample. Basin wetness was represented by lower Salinas annual water yield computed from mean daily discharge at S1 and annual precipitation at BGS for the current and previous water years. The effects of seasonality and basin aridity were both examined through the set of variables called  $\Sigma Q_{0.1}$ , calculated as the sum of days that satisfied the hydrologic argument of daily average  $Q \leq 0.1 \text{ m}^3\text{s}^{-1}$  in a given  $t_{s-1}$  to  $t_{s-x}$  temporal window, where  $t_s$  is the day that a given  $C_{SS}$  sample was collected and  $x$  is the number of days prescribed by the sampling window. The value of  $0.1 \text{ m}^3\text{s}^{-1}$  was chosen because of the accuracy of the hydrologic gages in the lower Salinas, whereby flows  $\leq 0.1 \text{ m}^3\text{s}^{-1}$  could be considered as ‘no-flow’ conditions. The  $\Sigma Q_{0.1}$  variable set was generated by calculating  $\Sigma Q_{0.1}$  for each suspended sediment sample using sampling windows from 1 to 2000 days, in one-day increments. Shorter sampling windows (~ 10–100 days) tested season-scale effects, as lower Salinas discharge during the summer dry season is often  $< 0.1 \text{ m}^3\text{s}^{-1}$ . Longer sampling windows (200–2000 days) tested the effects of extended low/no flow conditions as well as aridity. Hydrologic event history was represented by the variable  $Q_j \text{ time}$ , which is a measure of the elapsed time between the last daily average  $Q$  value  $\geq$  a given threshold discharge magnitude ( $Q_j$ ) and the date of collection for each  $C_{SS}$  sample. The set of  $Q_j \text{ time}$  variables were created by varying  $Q_j$  from 1 to 1000  $\text{m}^3\text{s}^{-1}$  in  $1\text{-m}^3\text{s}^{-1}$  steps.

**Table 2.2** Hydrologic variables tested for correlation with discharge-corrected suspended sediment concentrations<sup>a</sup>

Hydrologic variables	Unit	Index	Hydrologic argument	Temporal criteria	Temporal window
$\Delta Q_d$	m <sup>3</sup> /s	event conditions	$Q_{dt} - Q_{d(t-1)}$	n/a	1 day
<i>Current annual water yield</i>	10 <sup>5</sup> m <sup>3</sup>	basin wetness	$\Sigma Wy$	year = sampling year	1 water year
<i>Previous annual water yield</i>	10 <sup>5</sup> m <sup>3</sup>	basin wetness	$\Sigma Wy$	year = sampling year -1	1 water year
<i>Current annual precipitaton</i>	cm	basin wetness	n/a	year = sampling year	1 water year
<i>Previous annual precipitaton</i>	cm	basin wetness	n/a	year = sampling year	1 water year
$\Sigma Q_{0.1}$	days	seasonality, basin aridity	$Q_d \leq 0.1 \text{ m}^3/\text{s}$	sum of days	10 to 2000 days
$Q_j \text{ time}$	days	event history	$Q_d \leq Q_j$	elapsed time	1930-2011

<sup>a</sup>Discreet variables:  $\Delta Q_d$  = the difference in  $Q_d$  from the day before sampling to the day of sampling. Collections of variables:  $\Sigma Q_{0.1}$  = sum of days where daily discharge ( $Q_d$ ) is less than or equal to 0.1 m<sup>3</sup>/s, with individual variables defined by days between the last  $Q_d$  of a given magnitude  $j$  and the date of sample, with individual variables defined by values of  $j$  from 1 to 1000 m<sup>3</sup>/s in 1-m<sup>3</sup>/s steps.

The effect of hydrologic variables on ( $C_{SS} \sim Q$ ) LOESS residuals was tested with the nonparametric Mann-Kendall trend analysis using the R package 'Kendall' (McLeod, 2011; R Development Core Team, 2012). Mann-Kendall  $T$  values indicate the strength and direction of monotonic trends, with -1 and 1 representing perfectly negative and positive monotonic trends, respectively, along with  $p$ -values used to assess significance (Helsel and Hirsch, 2002).

### 2.5.2 Hydrologic variable test results

Fine and sand-sized sediment responded differently to antecedent hydrologic conditions. Fine sediment concentration was found to have a weak though significant, positive correlation with  $\Delta Q_d$  (Table 2.3). The set of variables  $\Sigma Q_{0.1}$  produced consistently negative and significant trends for summation windows between  $\sim 1150$  and 2000 days, with slightly stronger (larger  $T$  magnitude) correlations found with increasing summation window size (Fig. 2.4a). This suggests that long-term arid conditions decreased fine sediment supply. The set of hydrologic event history variables ( $Q_j$  time) produced significant negative trends in fine suspended sediment rating curve residuals with increasing elapsed time since the last low flow ( $Q \geq 1, 2, \text{ and } 4 \text{ m}^3\text{s}^{-1}$ ), while moderate events of  $\sim 100$  to  $200 \text{ m}^3\text{s}^{-1}$  produced significant positive trends in residuals with increasing elapsed time (Fig. 2.5a). The former result is evidence that sediment supply is suppressed by prolonged low flow (dry) conditions, while the latter provides some insight into how wetter conditions, resulting in moderately high discharges, may act as flushing functions, decreasing fine sediment supply for a time after the event.

Sand concentration exhibited significant positive correlations with wet conditions, and negative correlations with dry conditions (Table 2.3). Significant negative trends were found for sand-sized suspended sediment residuals and the entire  $\Sigma Q_{0.1}$  variable set, from window sizes 1–2000 d (Fig. 2.4b). Significant negative trends were found in ( $C_{SSs} \sim Q$ ) residuals for the  $Q_j$  time variable set for  $Q_j$  values between 1–20 and 50–1000  $\text{m}^3\text{s}^{-1}$ , which also points to a general decrease in sand-sized sediment supply with less discharge in the lower Salinas (Fig. 2.5b). Larger  $T$  magnitudes— indicating stronger monotonic trends — were found at  $Q_j \approx 400 \text{ m}^3\text{s}^{-1}$  and  $\Sigma Q_{0.1}$  for summations windows of  $\sim 75$ –100 days, suggesting perhaps threshold sediment supply production associated with discharges around  $400 \text{ m}^3\text{s}^{-1}$  and a

Table 2.3

seasonal suppression of sand supply for flows after the summer dry season.

Although Mann-Kendall tests are not as sensitive as linear regression to outliers positioned at the beginning or end of data series, problems with outliers can arise. Furthermore, proper use of the Mann-Kendall test requires that the dependent variable response is monotonic in relation to the independent variable. Values of  $C_{SS} \sim Q$  LOESS rating curve residuals were plotted against  $\Sigma Q_{0.1}$  and  $Q_j$  time values found to be significant (Fig. 2.6). All linear regressions, added for illustrative purposes, were found to be significant, except for fine suspended sediment residuals vs.  $\Sigma Q_{0.1}$  variables, which appeared to be compromised by nonlinear responses (Figs. 2.a,b,c). The other representative scatter plots reveal generally monotonic structures that do not appear to be highly steered by outliers, with the exception of the response of fine sediment to the  $Q_j$  time variable at  $j = 200 \text{ m}^3\text{s}^{-1}$  (Fig. 2.6f), which was highly steered by a few values above 1500 d (results not shown).

Analysis of hydrologic variables showed that the behaviors of fine and sand fractions in the lower Salinas River are affected by hydrologic event history. But which pools of sediment are impacted by these factors: the hillslope, channel banks, or channel bed? The remainder of this study is oriented toward this question.

## **2.6 Effects of hydrographic position and flow regime**

### *2.6.1 Rating curve subgroup comparison with ANCOVA*

The first step toward deciphering process was to test for differences in  $C_{SS}$  behavior resulting from hydrographic position and flow regime. The  $C_{SS}$  data sets were split into subgroups (rising/falling or storm/winter recessional/summer base flow, respectively). Log-linear rating curves were then fitted to each subgroup and tested for differences in behavior. An ANCOVA approach was used to determine if the rating curves were statistically 'coincident' (indistinguishable), and if not, whether they differed in rating curve slope or offset. The homoscedasticity of all hydrologic position subsets was tested using a two sample  $F$ -test statistic (e.g., Larsen, 2003). In all cases the subgroups were found to be homoscedastic unless otherwise noted. For a detailed account of the ANCOVA approach to comparing rating curves, see Appendix 2.A.

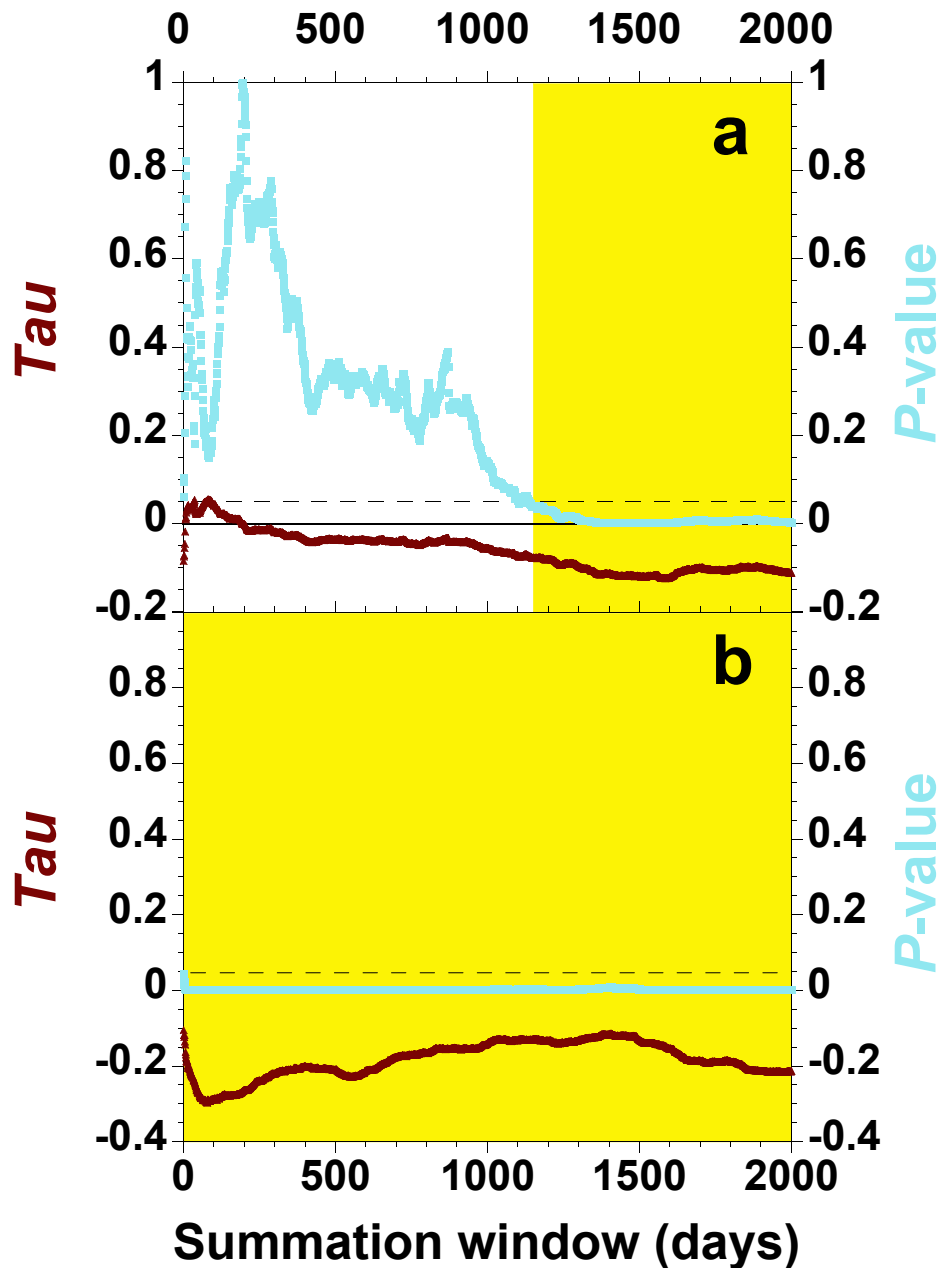


**Figure 2.4** Mann-Kendall analysis of monotonic trends in lower Salinas for (A) fine and (B) sand-sized suspended sediment LOESS rating curve residuals in relation to the sum of days with  $Q_d \leq 0.1$  m<sup>3</sup>/s over summation windows of 1–2000 days. Instability in the response of (A) fine residuals to variables produced from shorter windows was followed by consistently negative trends for all summation windows above ~ 1150 days or ~ 3 years, as indicated by shading. The response of (B) sand residuals was stable and negative across the entire range of summation window lengths.

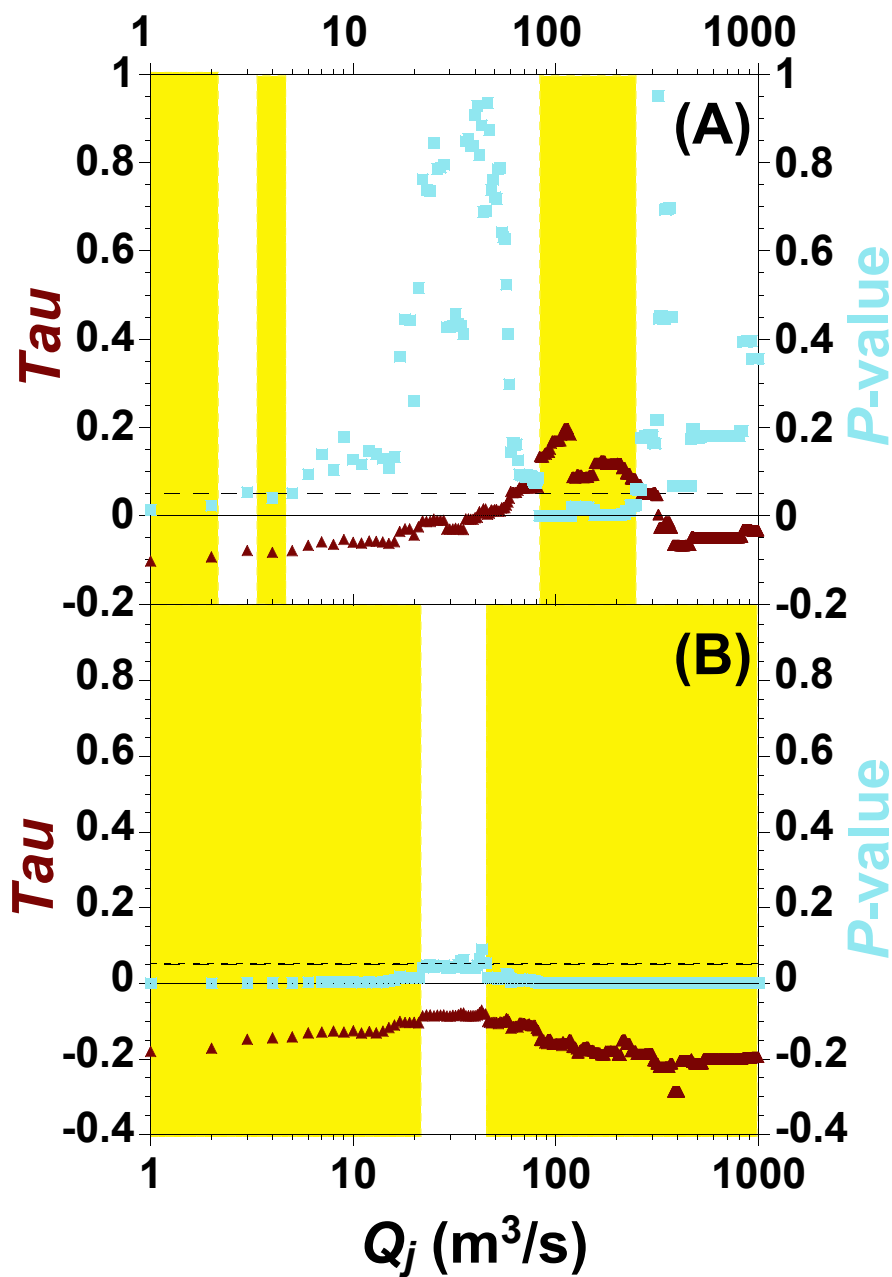


**Figure 2.5** Mann-Kendall analysis test results for monotonic trends in lower Salinas (A) fine, and (B) sand-sized suspended sediment LOESS rating curve residuals in relation to elapsed time since the last hydrologic event of a given size ( $Q_j$ ). Shaded bars indicate intervals of hydrologic event values that yielded significant monotonic trends in the rating curve residuals. (A) Very low and high discharges produced significant, negative trends in fine rating curve residuals with increasing elapsed time between events, while moderately large events affected positive trends as elapsed time increased. Trends in sand-sized rating curve residuals were negative and significant for all magnitudes of  $Q_j$  except for the range of  $\sim 20\text{--}50\text{ m}^3\text{s}^{-1}$ .

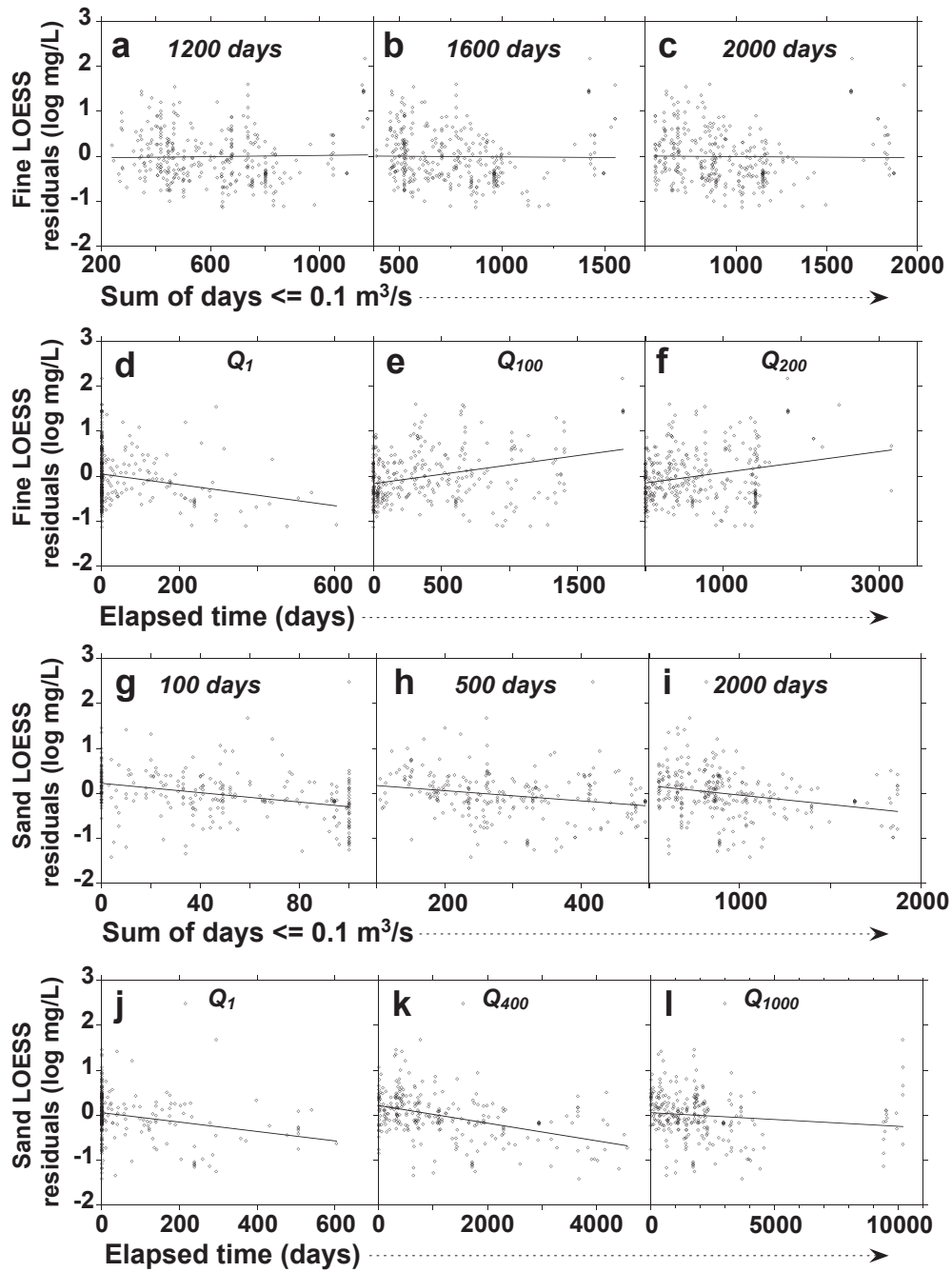


**Figure 2.6** Plots of fine (A–F) and sand (G–L) LOESS rating curve residuals against different variable states for  $\sum Q_{0.1}$  (A–C, G–I) and  $Q_j$  time (D–F, J–L). (A–C) Fine residual response to  $\sum Q_{0.1}$  does not appear to be monotonic for the variables shown, whereas all other plots appear to exhibit monotonic behavior.

Flow regime assignment was determined by examination of the precipitation record at BGS and discharge at S1, S2, and S3. Samples were identified as originating from storm flow if they were collected during the rising or falling limb of a hydrographic event that occurred because of precipitation, with the end of the falling limb identified as a change in concavity. This was visually assessed for those samples that were located far from the concavity change or found by computing the second derivative of a fitted fourth-order polynomial when samples were proximal to the shift. Winter recessional samples were those that were collected during the precipitation season but after the end of a given falling limb. The precipitation season was determined by examination of the monthly precipitation record. Summer base flow samples were those collected after the final falling limb of the winter precipitation season.

### 2.6.2 Rating curve subgroup ANCOVA results

Hydrologic variable correlation analyses indicated significant differences in ( $C_{SSf} \sim Q$ ) behavior with  $\Delta Q_d$ , while previous studies suggested that there may be large differences in suspended sediment behavior between different flow regimes (i.e., storm, winter recessional, and summer base flow) for most rivers (e.g., Walling, 1977; Estrany et al., 2009). A trend in  $C_{SSf}$  dependence on  $\Delta Q_d$  implies that consistent hysteretic patterns in  $C_{SSf}$  behavior based on hydrographic position may occur in the system. Fine sediment from rising limb samples was found to have a greater slope than falling limb samples and a slightly higher offset (Fig. 2.7a), while the sand-sized hydrologic position rating curves were almost identical (Fig. 2.7b). Results of the ANCOVA tests indicated that the rating curves for the fine suspended sediment hydrologic position subgroups could be considered parallel and offset equivalent, but were not coincident; while the rising and falling limbs of sand-sized suspended sediment were statistically coincident (Table 2.4; Fig. 2.7a,b). ANCOVA results for storm, winter recessional, and summer base flow rating curves were not significantly different in terms of parallelism, offset, or total coincidence, nor were the summer and winter recessional flow curves (Table 2.4; Fig. 2.7c,d). Thus a weak hysteretic pattern was evident for fine suspended sediment, but not sand, over the entire sample record; while no evidence was found of flow regime control on suspended sediment concentration.

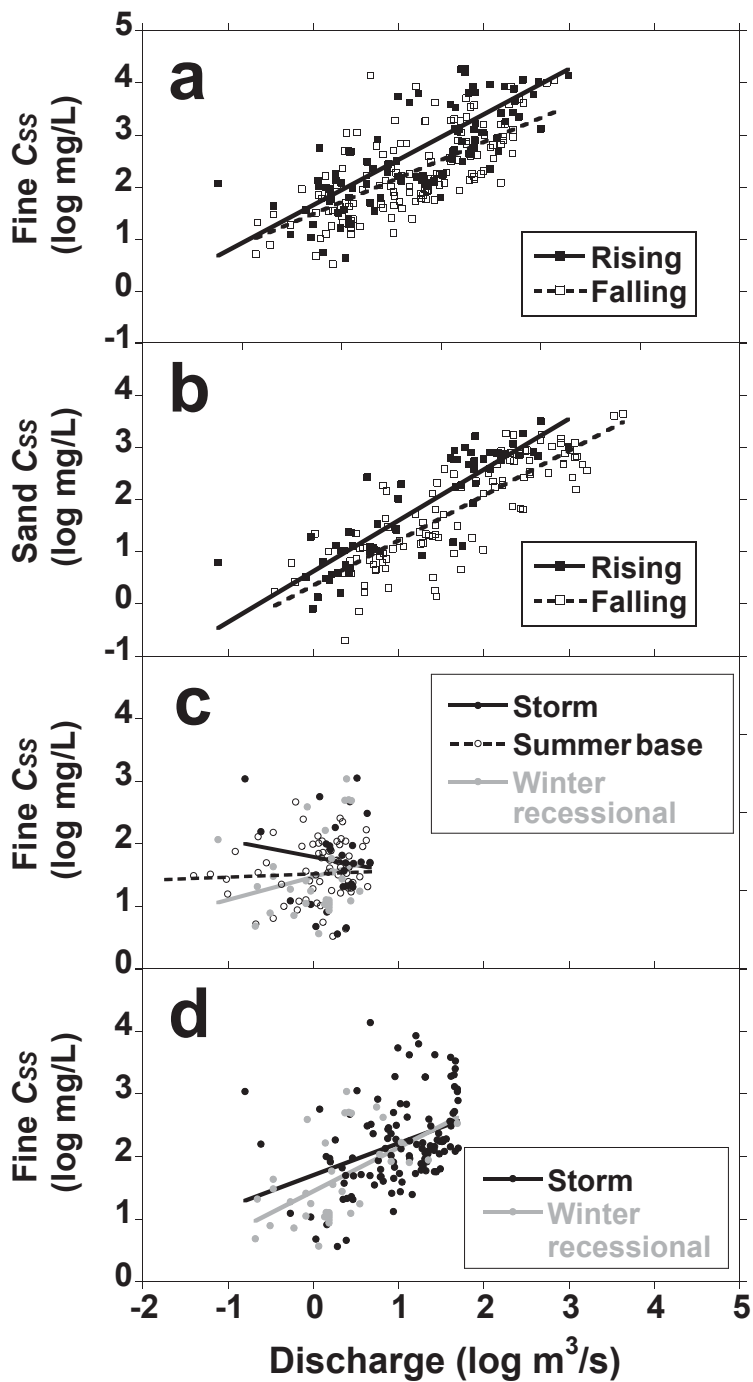


**Figure 2.7** Lower Salinas subgroup sediment rating curves defined by hydrographic and hydrologic criteria: (A) fine, and (B) sand-sized sediment by hydrographic position (samples from rising or falling limbs of the hydrograph), and (C–D) hydrologic modes (storm, winter recessional, and base flow). Discharge ranges are limited to shared ranges for the hydrologic mode rating curves. The difference between (A) fine rising and falling limb samples was significant at the  $p < 0.05$  level. The differences between the (B) sand-sized rising and falling limb samples and (C–D) hydrologic mode subgroups were not significant.

**Table 2.4** ANCOVA results<sup>a</sup>

Regression pair	n	Coincidence	Parallelism	Offset
Rising,falling (fines)	97, 139	***	parallel	equivalent
Rising, falling (sand)	61, 107	coincident	parallel	equivalent
Storm, winter recessional, summer base	27, 31, 69	coincident	parallel	equivalent
Storm, winter recessional	122, 38	coincident	parallel	equivalent
Upper Salinas, Arroyo Seco (fines)	118, 61	coincident	parallel	equivalent
Upper Salinas, Arroyo Seco (sand)	99, 24	*	**	*
S1, S2 (< 2 µm clay)	50/38	coincident	parallel	equivalent
S1, S2 (2 to 4 µm clay)	50/37	coincident	parallel	equivalent
S1, S2 (4 to 8 µm silt)	49/38	coincident	parallel	equivalent
S1, S2 (8 to 16 µm silt)	47/37	coincident	parallel	equivalent
S1, S2 (16 to 31 µm silt)	42/32	coincident	parallel	equivalent
S1, S2 (31 to 62.5 µm sand)	42/33	coincident	parallel	equivalent
S1, S2 (62.5 to 125 µm sand)	76/45	*	parallel	equivalent
S1, S2 (125 to 250 µm sand)	86/51	*	parallel	equivalent
S1, S2 (250 to 500 µm sand)	69/46	coincident	parallel	equivalent
S1, S2 (500 to 1000 µm sand)	18/18	coincident	parallel	equivalent
S1, S2 (125 to 2000 µm sand)	87/51	*	parallel	equivalent

<sup>a</sup>Rising and falling refer to hydrographic position. Storm, winter recessional, and summer base flow are hydrologic regime subgroups. Upper Salinas and Arroyo Seco refer to subgroups defined by dominant subbasin contribution to flow. S1 is the Salinas mainstem gauging station at Spreckels, S2 is the Salinas mainstem gauging station at Chualar. n = number of samples by subgroup. The results of coincident, parallel, and offset equivalent (respectively) are identified as such, and significant results to the contrary are indicated as: \* P-value < 0.05, \*\* P-value < 0.01, \*\*\* P-value < 0.001.

## 2.7 Suspended sediment hysteresis

### 2.7.1 Hysteresis identification

The next step in the investigation of physical processes was to examine event-scale patterns in suspended sediment hysteresis. Six events sampled by the USGS between 1970 and 1978 and two by the authors in 2010 were sampled sufficiently for some degree of fine sediment hysteresis determination. Sampling resolution from the USGS data set was also sufficient to compare fine and sand-sized sediment behavior over the course of seven events. 'Positive' hysteresis occurs when rising limb  $C_{SS}$  values are larger than  $C_{SS}$  values of corresponding discharge magnitude on the falling limb, while 'negative' hysteresis occurs because of the opposite effect (Hudson, 2003). Log-log plots of sequential samples collected over a given discharge event, with  $C_{SS}$  on the ordinate and  $Q$  on the abscissa, were used to assess the presence of hysteresis.

### 2.7.2 Hysteresis results

Only eight hydrologic events were sampled sufficiently for some insight into event scale hysteretic behavior of fine sediment; of these, six were sampled at S1 and two at S2 (see Fig. 2.8). Log-log plots of  $C_{SSf}$  against  $Q$  revealed evidence for positive, negative, and mixed positive/negative hysteretic patterns for five events with low to moderate peak discharges ( $\sim 10\text{--}100\text{ m}^3\text{s}^{-1}$ ; see Figs. 2.8a-e) and evidence of positive hysteresis for three high peak discharge events ( $\sim 250, 450, \text{ and } 1600\text{ m}^3\text{s}^{-1}$ , respectively, which were the peak discharge events for water years 1974, 1973, and 1978, respectively, see Figs. 2.8g,h). Sample density for most of the events with indications of positive or negative behavior was not sufficient to rule out more complex mixed hysteretic behaviors, however, these plots do show that the lower Salinas River fine suspended sediment exhibited positive and negative hysteresis behavior over a wide range of discharges.

Although few events were sampled sufficiently for determination of sand hysteresis, seven were sampled adequately for comparisons of rising/falling limb behavior between the fine and sand fractions of suspended sediment (Fig. 2.9). Three events showed fine and sand-sized sediment behaving very

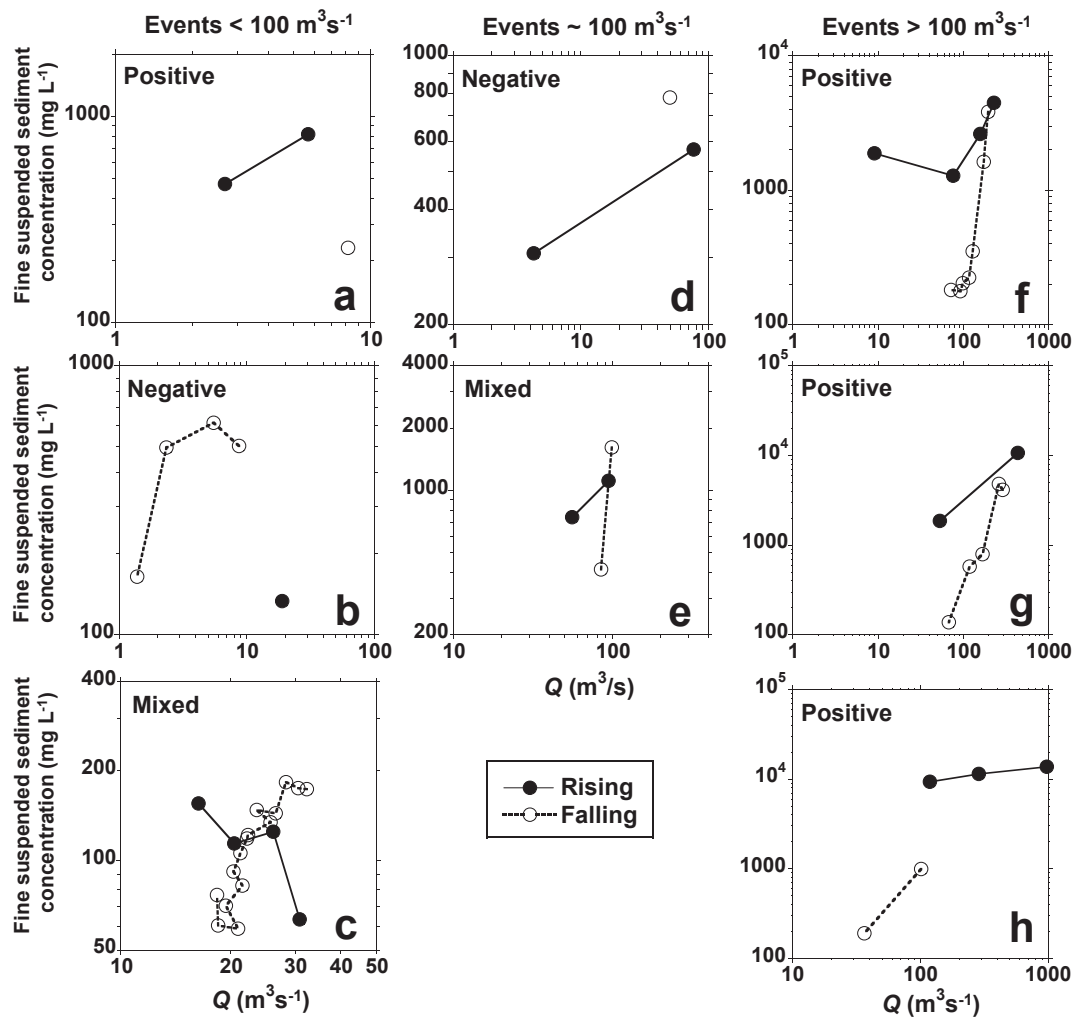


**Figure 2.8** Diagrams of all fine suspended sediment hysteresis events identified from the lower Salinas River USGS and UCD data sets plotted in log-log scale and organized by discharge magnitude of the peak event flow. Rising flows progress in temporal sequence from left to right (low to high discharge), while falling flows progress from right to left (high to low discharge). Positive or clockwise hysteresis occurs when rising limb flows have higher suspended sediment concentrations than falling limb flows. Negative or counter-clockwise hysteresis occurs when falling limb samples have higher suspended sediment concentrations than rising limb flows. Mixed hysteresis events display each of these patterns over different ranges of discharge magnitude. Samples were collected from the lower Salinas at location S1 (USGS Spreckels gage) during events plotted in (A), (B), (D) and (F-H), and at S2 (USGS Chualar gage) for (C) and (E). Samples (C) and (E) were collected by UCD, all others by the USGS. Event date ranges are as follows: (A) 12/10–14/1974, (B) 12/27/1971–1/1/1972, (C) 2/25–26/2010, (D) 1/11–17/1970, (E) 1/20–25/2010, (F) 1/5–25/1974, (G) 2/10–22/1973, (H) 2/8–27/1978.

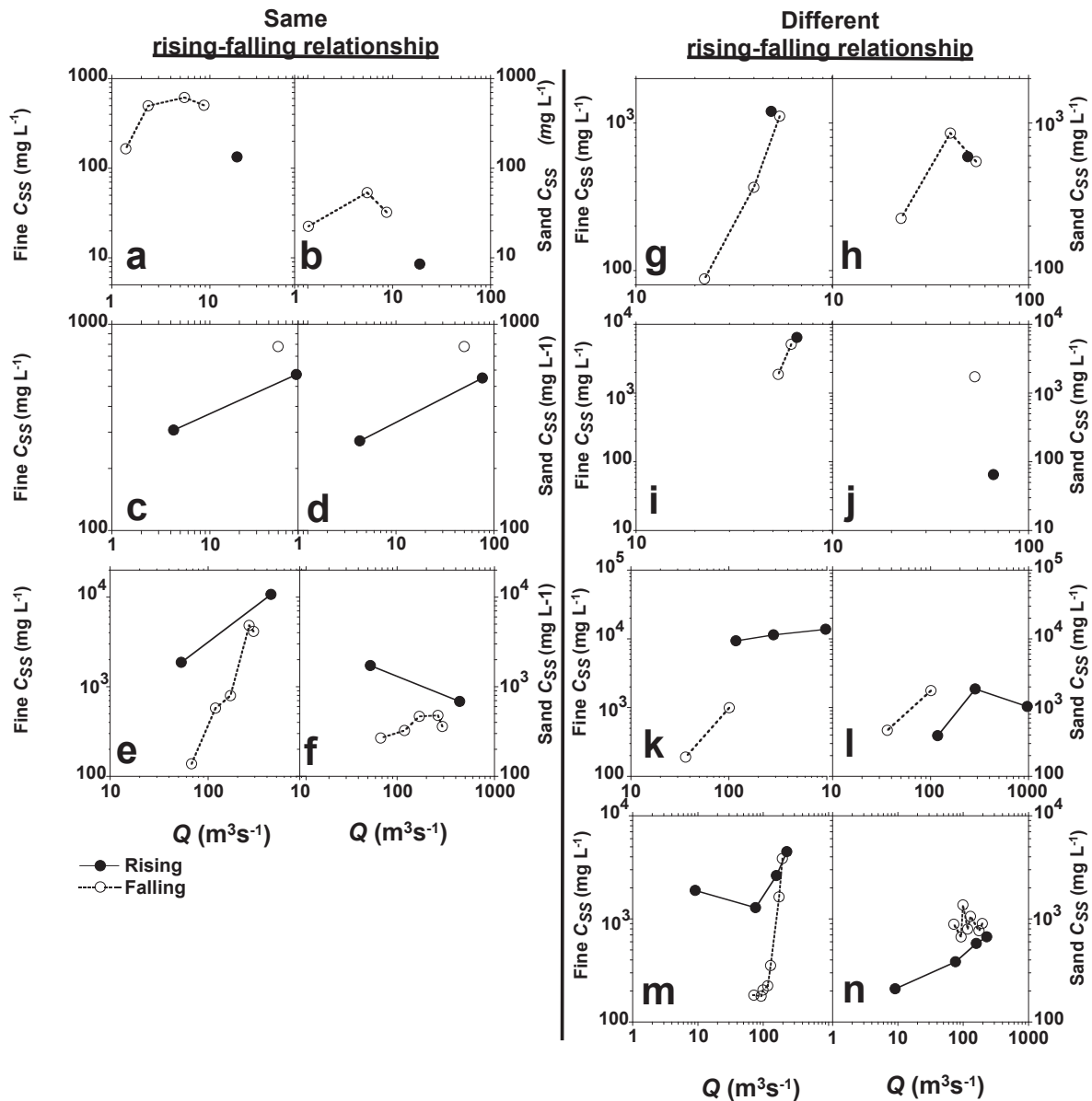


**Figure 2.9** Paired plots of fine and sand-sized CSS behavior over the course of rising and falling  $Q$  magnitudes during lower Salinas hydrologic events. Rising limb samples progress in temporal sequence from left to right (low to high  $Q$ ), and falling limb samples from right to left (high to low  $Q$ ). All samples were collected from the lower Salinas at location S1 (USGS Spreckels gage). Event date ranges are as follows: (a,b) 12/27/1971–1/1/1972, (c,d) 1/11–17/1972, (e,f) 2/10–22/1973, (g,h) 4/2–11/1974, (i,j) 2/8–10/1973, (k,l) 2/8–27/1978, (m,n) 1/5–25/1974.

similarly, with indications of negative (Figs. 2.9a–d) and positive (Figs. 2.9e,f) hysteresis. For those events when the rising/falling limb relationship of fine and sand fraction behavior was found to differ, it consistently manifested as an increase in the concentration magnitude of falling limb samples relative to rising limb samples in the sand fraction (Figs. 2.9g–n). Next, the potential mechanisms associated with hysteretic behavior in the lower Salinas were assessed by examining subbasin routing effects on  $C_{SS}$  behavior (section 2.8) and channel bed contributions to suspended sediment (section 2.9).

## **2.8 Effects of subbasin water provenance**

### *2.8.1 Routing analysis*

Hysteresis in  $C_{SS}$ - $Q$  relationships in rivers of moderate to large size can result from differences in subbasin suspended sediment dynamics (Shi et al., 1985; Asselman, 1999). Examination of the potential for such routing effects on  $C_{SSf}$  in the lower Salinas was motivated by a bifurcation of the Salinas system that occurs 28.4 km upstream from S2, at the confluence of the Salinas and Arroyo Seco (Table 2.1; Fig. 2.1). Because of large differences in subbasin characteristics, differential contribution of the upper Salinas and the Arroyo Seco could be a major driver of hysteretic suspended sediment behavior.

Identification of lower Salinas sampled flows that were dominated by contributions of the upper Salinas or the Arroyo Seco and testing of these subgroups for differences in  $C_{SS}$ - $Q$  behavior allowed for a joint assessment of the potential differences in subbasin suspended sediment behavior and the attenuation of this signal downstream. The entire lower Salinas fine and sand-sized suspended sediment data sets were sorted into those samples grossly dominated by one tributary or the other by following peak flow transmission of daily discharge data from gages throughout the basin. Because of the low temporal resolution of the discharge data (daily average  $Q$ ) that could be used for samples collected before 1989, only 198 of the 330 fine sediment and 123 out of 248 sand-sized sediment sampled discharges were identified as originating primarily from one of the two subbasins. The data set was then trimmed of upper Salinas data points from the lowest and highest discharges in order to match the discharge range of the Arroyo Seco dominated subset to remove the potential bias of rating curves calculated over different ranges of discharge. These ‘dominant tributary’ subsets were then tested using

the ANCOVA methodology (see section 2.6.1 and Appendix 2.a).

### 2.8.2 Routing results

No significant differences in  $C_{SSf}$ - $Q$  behavior were identified between the Arroyo Seco and upper Salinas dominated flows (Table 2.4; Fig. 2.10a). Significant differences were found in terms of slope and offset for sand-sized suspended sediment rating curves partitioned by subbasin, with Arroyo Seco dominated samples resulting in a lower slope and higher offset (Table 2.4; Fig. 2.10b). Thus, subbasin water contribution control on fine suspended sediment behavior in the lower Salinas River was eliminated as a significant contributing mechanism to the overall positive hysteresis observed in fine suspended sediment in the lower Salinas, implicating significant lower Salinas control on fine sediment dynamics, and more distributed control of sand-sized sediment.

## 2.9 The channel bed and suspended sediment

### 2.9.1 Channel bed analyses

In the absence of an intensive channel-oriented field campaign, here the possibility of significant lower Salinas channel mediation of suspended sediment behavior through storage and resuspension of suspended sediment material was addressed through comparative particle size distribution characteristics between the channel bed and suspended sediment pools at S1 and S2 and through estimation of fine sediment content of the channel bed. Hydraulic geometry relationships were also calculated to assess how the lower Salinas flow characteristics changed with discharge.

Average particle size distribution characteristics were compared for bed sediment at stations S1 and S2 and suspended sediment samples in relation to discharge. Log-linear rating curves were constructed for USGS suspended sediment samples by standard USGS particle size classes of whole  $\phi$  intervals as well as the sand fraction that accounted for most of the bed sediment at both S1 and S2 (125 to 2000  $\mu\text{m}$ ) over the range of discharges shown to approximate log-linear behavior for  $C_{SSf}$  and  $C_{SSs}$  ( $q \geq 1 \text{ m}^3\text{s}^{-1}$ ). Particle size range rating curves were then compared by station (S1, S2) using the ANCOVA methods introduced in section 6. Suspended sediment concentration of particle size ranges that behaved

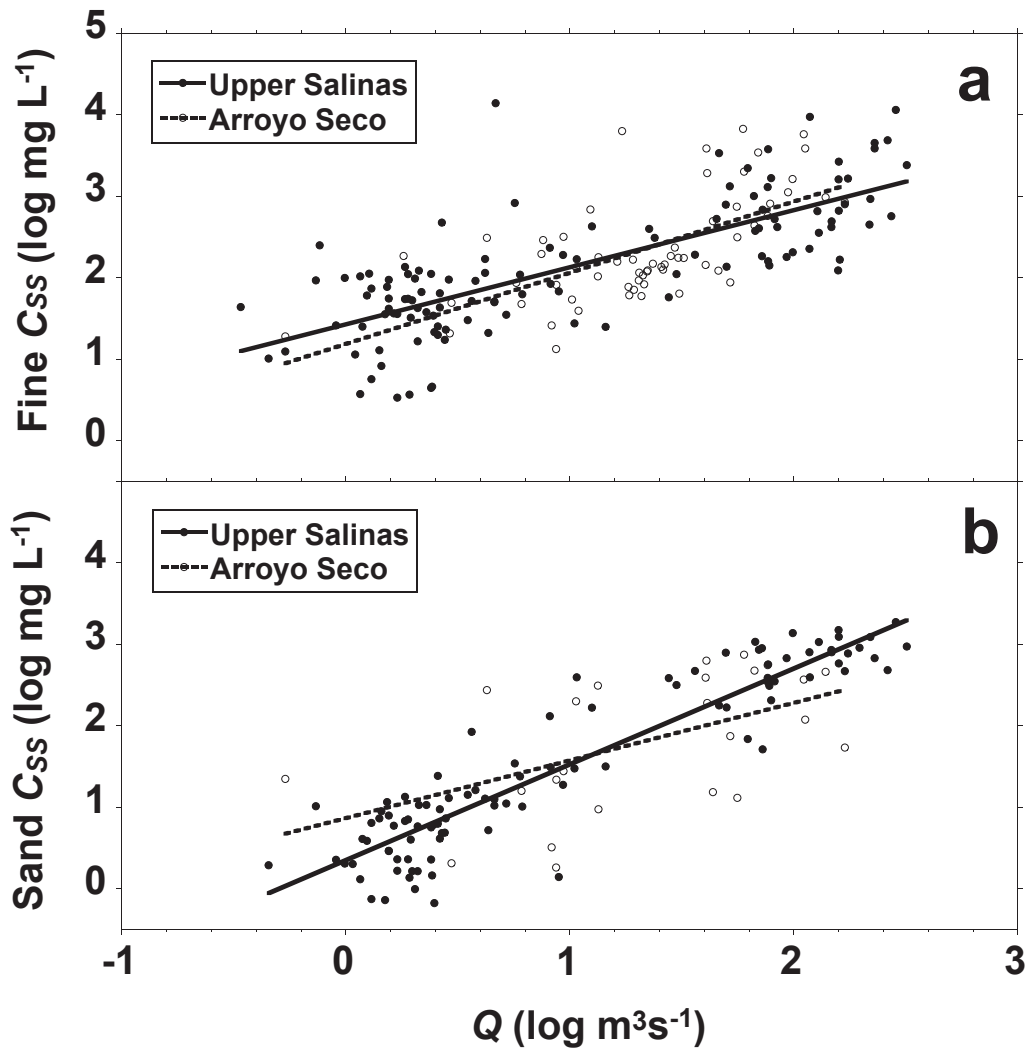


**Figure 2.10** (a) Fine and (b) sand-sized sediment in the lower Salinas linear regression rating curves sub-divided by subbasin water provenance (upper Salinas and Arroyo Seco). (a) Fine sediment behavior by water provenance was statistically coincident, while (b) sand behavior differed in terms of rating curve slope and offset.

in a statistically coincident manner between sites were then described by LOESS rating curves computed from joint S1 and S2 data, while size ranges with significantly different log-linear behavior were described with separate rating curves by station. Average particle size distributions by percent mass for each station for discharges spanning five orders of magnitude ( $0.1\text{--}1000\text{ m}^3\text{s}^{-1}$ ) were calculated from the particle size range LOESS curves. Particle size distribution characteristics and average lower Salinas channel width from S1 to S2 were used to estimate the mass of bed sediment by particle class for the top 10 cm of reach channel surface assuming a planimetric channel for simplicity of calculation. Width, average depth ( $d$ ), and mean velocity were related to  $Q$  through a power law function with exponential terms of  $b$ ,  $f$ , and  $m$ , respectively, for sites S1, S2, S3, and A1 (Leopold and Maddock, 1953).

### 2.9.2 Channel bed results

Rating curves constructed for each standard USGS particle size range by station exhibited very little difference in suspended sediment behavior between S1 and S2 for clay and silt particle sizes, although some sand classes appeared to increase in concentration between S1 and S2 (linear rating curve comparison not shown). This observation was confirmed by ANCOVA tests, which showed no statistically significant difference in rating curves between stations for all particle size ranges except 62.5–125, 125–250, and 125–2000  $\mu\text{m}$  sands. In each of these sand ranges, the condition of coincident rating curves was significantly violated, mostly because of differences in rating curve offsets, which were just below the  $p < 0.05$  threshold for significance (Table 2.4). Thus some sand concentrations slightly increase downstream from station S2 to S1, including the broad range encompassing most bed-sized sediment ( $d > 125\ \mu\text{m}$ ), but fine suspended sediment concentrations behave identically between stations.

Lower Salinas  $C_{SS} \sim Q$  LOESS rating curves by texture classes (clay, silt, and sand) showed that clay-sized particles rapidly become dominant between  $0.1$  and  $1\text{ m}^3\text{s}^{-1}$  and remain so for all higher flows (Fig. 2.11a). Sand  $C_{SS}$  values increase rapidly between  $1\text{--}10\text{ m}^3\text{s}^{-1}$  to join the silt curve, and the two follow nearly the same path for much of the discharge range between  $10$  and  $1000\text{ m}^3\text{s}^{-1}$ . Particle size range LOESS curves (Figs. 2.11b–e) were used to compute average particle size distributions at S1 and S2 for discharge classes  $0.1$ ,  $1$ ,  $10$ ,  $100$ , and  $1000\text{ m}^3\text{s}^{-1}$  (Fig. 2.12). Differences in suspended sand behavior between S1 and S2 were evident in the evolution of sharp, single-peaked sand distributions at

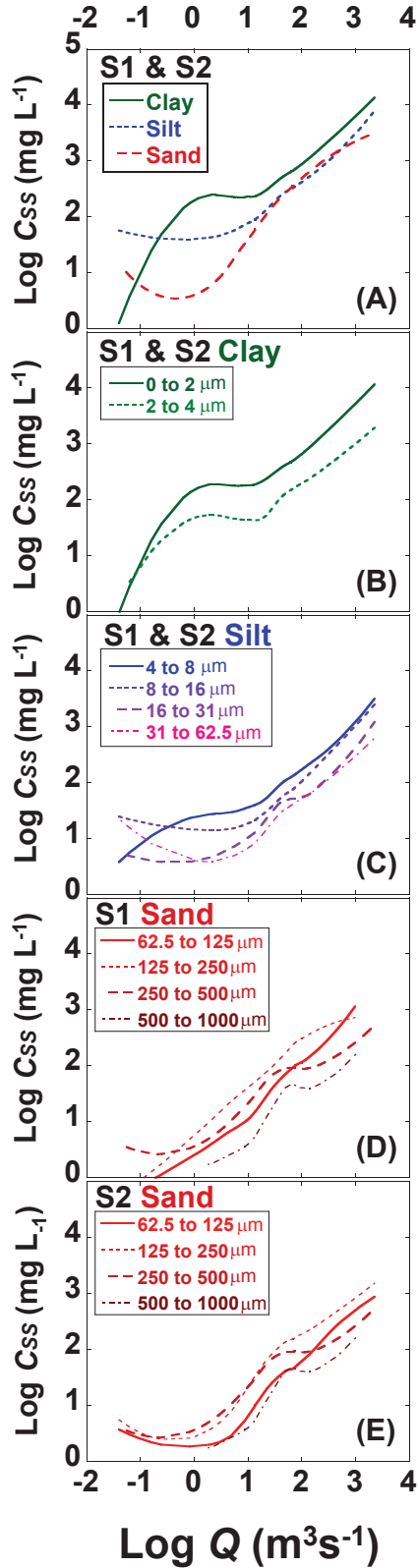


**Figure 2.11** LOESS rating curves fitted to lower Salinas suspended sediment by (a) texture class (clay, silt, and sand), (b) clay, (c) silt, and (d, e) sand particle size ranges. All LOESS curves were computed for combined stations S1 and S2 data sets, except for sand particle sizes 62.5–125 and 125–250  $\mu\text{m}$ , as log-linear rating curves for these ranges were significantly different between stations.

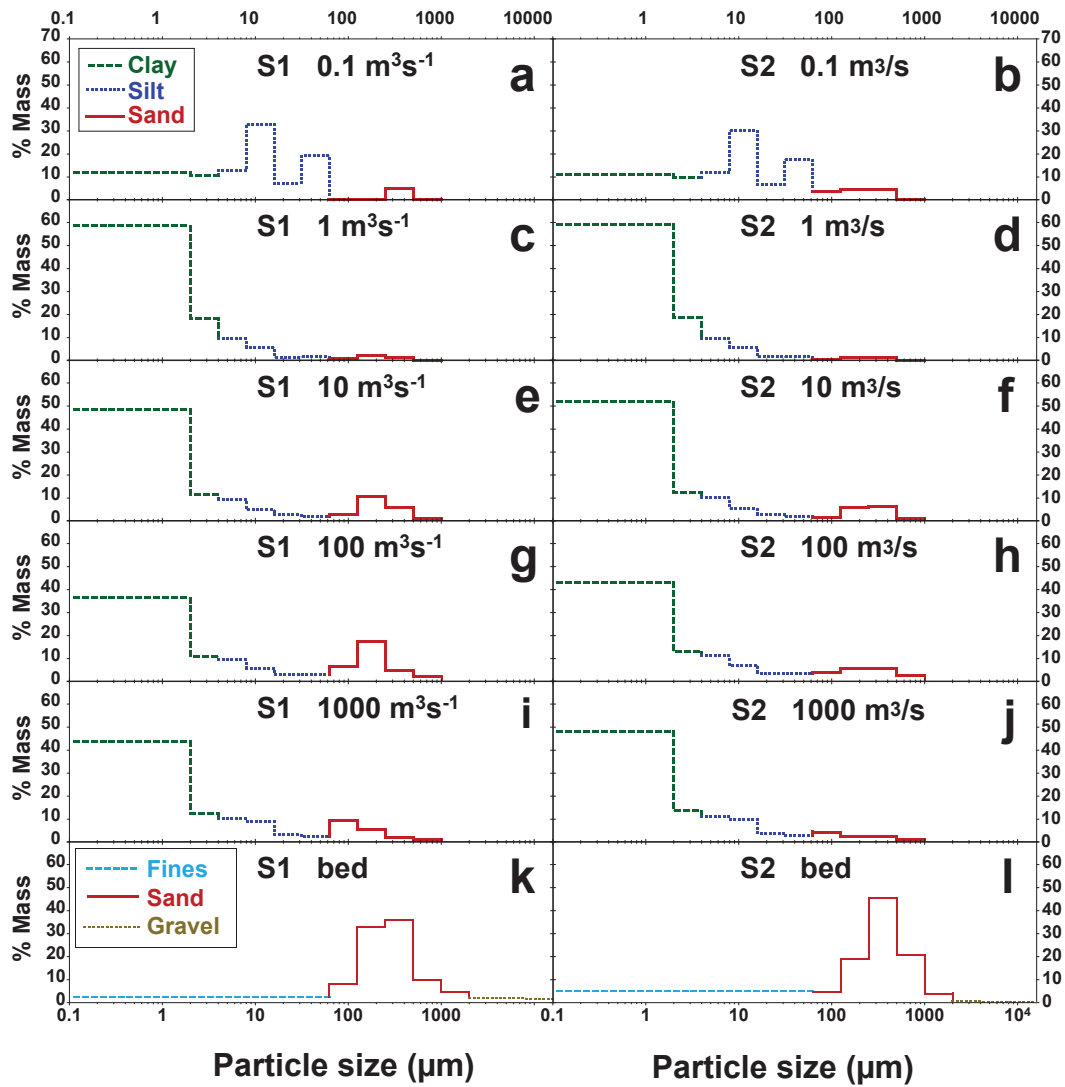


**Figure 2.12** Lower Salinas average suspended sediment particle size distributions for stations S1 (a, c, e, g, i) and S2 (b, d, f, h, j, l) by discharge magnitude, and channel beds (k, l). Distributions were calculated from LOESS curves plotted for each particle size range, and by station when log-linear regressions indicated significant differences in behavior between stations (62.5–125 and 125–250 μm) (see Fig. 2.11). All data derived from USGS sources.

**Table 2.5** Hydraulic geometry of Salinas stations<sup>a</sup>

	Width	Depth	Velocity		
Site	<i>b</i>	<i>f</i>	<i>m</i>	<i>b/f</i> ratio	<i>m/f</i> ratio
S1	0.49	0.34	0.17	1.44	0.48
S2	0.44	0.35	0.21	1.26	0.59
S3	0.50	0.34	0.16	1.50	0.48
A1	0.44	0.25	0.30	1.75	1.20

<sup>a</sup>Slope coefficients of power functions relating width, depth, and velocity to discharge are *b*, *f*, and *m*, respectively.

S1 with increasing discharge from 1 to 100 m<sup>3</sup>s<sup>-1</sup>, in comparison to the maintenance of a low percentage, flat-peaked sand distribution at S2 (Figs. 2.12c–h).

The average bed sediment composition between 1967 and 1992 at stations S1 and S2 was 2.7 and 5.2% fines ( $d < 62.5 \mu\text{m}$ ), respectively (Figs. 2.12k,l). Assuming a bulk density of 1.3 g cm<sup>-3</sup> for fine sediment, the channel bed at these sites could potentially yield 0.35–0.68 g cm<sup>-2</sup> of fines in the top 10 cm. Applying the average of these values and assuming the average flow width measured by the USGS at S1 and S2 of 161 m, a gross estimate of available fine in the reach between S1 and S2, and between S2 and S3 is  $\sim 2 \cdot 10^4$  and  $2.4 \cdot 10^4$  tons of fine sediment, respectively.

The results of hydraulic geometry analysis at S1, S2, S3, and A1 showed a dominance of width response to flow changes (Table 2.5). Depth was more responsive than velocity at Salinas sites, while the inverse was true for the steeper, rougher Arroyo Seco site; however, all four sites primarily responded through width adjustment. Because the capability to entrain sediment is dependent on stream power (in steady, uniform flow), which is dependent on depth, the ability to erode and transport sediment increases relatively slowly with discharge at these sites (Leopold and Maddock, 1953; Kale and Hire, 2004).

## 2.10 Discussion

### 2.10.1 Synthesis

The following antecedent hydrologic condition effects on suspended sediment behavior were found for the lower Salinas River:

- Fine sediment concentration decreased with:
  - Dry conditions over interannual time scales
  - Falling flows
- Fine sediment concentration increased with:
  - Rising flows
  - Longer elapsed time since the last moderate flow ( $10\text{--}20 \cdot Q_{mean}$ )
- Sand concentration decreased with:
  - Dry conditions over seasonal to interannual time scales

- Upper Salinas water provenance for 10–50· $Q_{mean}$  flows
- Sand concentration increased with:
  - Wetter conditions during the current and previous water year
  - Recent flow activity
  - Upper Salinas water provenance for low flows ( $< Q_{mean}$ )

Prolonged dry conditions were found to reduce both fine and sand-sized suspended sediment concentrations. No significant seasonal signal was observed for fine sediment in the lower Salinas, while sand supply to the suspended sediment transport appears to be strongly linked to preceding discharge magnitudes and to the amount of time that the channel experienced very low to no flow conditions over temporal scales that range from days to years. Fine sediment concentrations also increased in the lower Salinas with increasing elapsed time since moderate discharges of around  $100\text{--}200\text{ m}^3\text{s}^{-1}$ , long periods of which were also associated with prolonged droughts. Thus, there appear to be competing factors influencing fine sediment response to prolonged dry conditions, while sand supply is consistently suppressed.

The decrease in sand-sized sediment after the dry season and decreases in both fine and sand-sized sediment over seasonal to interannual periods of dry conditions is contrary to the pattern of sediment exhaustion commonly observed over the course of the wet season monsoonal systems (Paustian and Beschta, 1979; McCulloch et al., 2003; Kale and Hire, 2004; López-Tarazón et al., 2010; Warrick et al., 2013). The phenomenon of seasonal and interannual decreases in suspended sediment during dry periods in the lower Salinas may be caused in part by changes in surface erodibility. In coastal dry-summer subtropical climates such as that of the Salinas with warm, dry summers and cool, wet winters, the lack of flow and elevated temperatures of the summer dry season may dry out surficial channel sediments, particularly since the lower Salinas River bed is perched above groundwater. Fine, cohesive sediment is generally more difficult to entrain with increased deposition age, as interparticle bonding strength can increase drastically with dewatering; subaerial exposure can also lead to increases in the hydrophobicity of sediment (Mehta et al., 1989; Winterwerp et al., 1990). Prolonged intervals of low to no-flow conditions could also reduce channel and hillslope sediment contribution through the incursion

of vegetation in channels, gullies, and other intense precipitation/discharge-induced land surface disturbances such as slumps and mass wasting scars. Thus, summer dry seasons and multiyear droughts could lead to fine sediment that is less likely to be entrained, and once entrained more difficult to convey given increased roughness in vegetated channels, particularly in the case of early season flows that often must wet the channel and encounter vegetation not yet disturbed by flow. These possibilities remain to be tested in the field.

The flushing function of moderate discharges found for fine sediment in the lower Salinas is an understudied phenomenon, perhaps because of the focus on decadal to centennial scale sediment yield within the research community. Much of the work on hydrometeorological event preconditioning has focused on the effect of large, infrequent floods that generally transport large proportions of interdecadal sediment budgets and have been shown to have lasting geomorphic and sediment supply effects in steep, mountainous rivers on active margins (Brown and Ritter, 1971; Kelsey, 1980; Madej and Oseki, 1996; Warrick et al., 2013), although there has been some interest in terms of dam-release functionality (e.g., Batalla and Vericat, 2009). Sand concentrations on the other hand seem to be stimulated by ever larger and more recent hydrologic events, which is consistent with the northern California coast range systems that have exhibited increases in sediment supply immediately following large precipitation/discharge events, such as the widespread flooding of the December 1964 event (Warrick et al., 2013). Thus, fine and sand-sized sediments in the lower Salinas respond differently to previous hydrologic events, with sand supplies enriched by more recent and larger flows and fine sediment decreased after moderate threshold events.

### *2.10.2 Event characteristics and routing*

Why do fine sediment and sand respond differently to antecedent hydrologic events? Fine suspended sediment sources in most rivers – including moderately sized, steep coastal basins such as the Salinas – are generally known to be dominated by hillslope wash load, while sand supplies are often moderated to some degree by lower mainstem channel storage and transport competency (Walling and Moorehead, 1987). However, the Salinas River channel must moderate fine sediment transport to some extent, as suspended load must deposit when flows terminate in the channel with complete loss to

recharge. Investigation into event characteristics, hysteresis, water provenance, and evolution of particle size distribution with discharge magnitude and downstream position provided evidence that the Salinas channel does indeed influence both sand and fine suspended sediment behavior.

The positive correlation between  $\Delta Q_d$  and fine suspended sediment concentration suggests that the conditions leading to rapid increases in discharge, namely increased wash load resulting from the erosivity of intense precipitation events, and/or the energy imparted to the channel by rapid increases in discharge are significant contributing factors to positive fine suspended sediment hysteresis in the lower Salinas. The  $\Delta Q_d$  variable employed in this study is similar to the *Flashiness Index (FI)* developed by Batalla and Varicat (2009), where  $FI = \Delta Q/t$ , which has been successfully used as an index for energy expenditure on the channel (e.g., Tena et al., 2011). Fine suspended sediment in the lower Salinas displayed positive and negative hysteretic behavior with discharge, but the positive correlation with  $\Delta Q_d$  indicated that positive hysteresis effects slightly dominated the record. The major mechanisms generally associated with positive hysteresis include hydrodynamic phenomena such as increased boundary shear stress/shear velocity on the rising limb of the hydrograph because of a greater water surface slope than on the falling limb (Garcia and Parker, 1991), a larger proportional contribution of base flow/interflow on the falling limb (Gao and Pasternack, 2007), and routing considerations such as higher fine particle sediment supply from areas proximal to the channel and/or lower in the basin (Williams, 1989). Negative hysteresis has primarily been associated with routing characteristics, including higher sediment supply from distal portions of the basin and sediment transport lag in larger ( $> 10^3 \text{ km}^2$ ) basins, because suspended sediment downstream particle velocities are often lower than peak discharge wave celerity (Heidel, 1956; Williams, 1989). The provenance of storm waters above the lower Salinas was not a significant factor in determining  $C_{SSf}$  for low to moderate flows, which indicates that upper basin wash load signals attenuate before reaching the lower Salinas stations. This is counterintuitive, as the Arroyo Seco and the upper Salinas are on average very different subbasins in terms of relief, area, vegetation and soil characteristics, and fire regimes (Farnsworth and Milliman, 2003; Warrick et al., 2012); and one would expect wash load signatures to differ, as more moderate differences in subbasin characteristics have been shown to cause significant differences in suspended sediment behavior (e.g., Ankers et al., 2003).

### 2.10.3 Channel mediation

Thus upper basin provenance effects on fine sediment are overprinted by some combination of the following lower Salinas sediment sources: runoff, channel bed, and/or bank sediment. Routing analysis samples were identified by subbasin peak flow events and therefore, by definition, composed of very little lower Salinas storm water. This issue coupled with the fact that suspended sediment is deposited in the Salinas mainstem channel by early and late season flows, the evidence that  $C_{SSf}$  values increase with increasing energy imparted to the channel, and the lack of effect of hydrologic mode (summer base, storm, or winter recessional flow) on low flow  $C_{SS}$  supports the notion that lower Salinas fine suspended sediment dynamics for flows up to  $\sim 50 \cdot Q_{mean}$  are significantly affected by in-channel processes such as bank erosion as well as deposition and resuspension of fine sediment. Furthermore, much of the flow range sampled for the paired subbasin dominance analysis was below bankfull for the lower Salinas, which generally has a wide, complex channel composed of bar forms in various states of vegetation and multiple low water channels, as evidenced by the fact that lower Salinas hydraulic geometry changes most rapidly in width with increasing discharge. Therefore channel bank sediment control is probably not the major mechanism at play, as the banks of the lower Salinas are not interacting with flow over much of this discharge range. Thus, the lower Salinas appears to significantly alter upper basin fine suspended sediment signals toward a uniform behavior based primarily on in-channel dynamics at low to moderate water discharges. However, differences in sand-sized sediment behavior did persist to the lower Salinas, which suggests that subbasin sand signals are stronger than the overprinting of lower Salinas in-channel processes.

Bed and suspended sediment particle sized distribution analyses showed that bed sands likely play an increasing role in lower Salinas suspended sediment with increasing discharge, which is unsurprising as coarser sands are often transport limited in sand-bedded rivers. Moderate flows ( $\sim 100 \text{ m}^3 \text{ s}^{-1}$ ) found to cause a decrease in subsequent fine sediment concentration were accompanied by the highest proportion of bed-sized sediment at station S2 and especially S1 (Fig. 2.12). Increases in channel bed mobility exposing intermixed fines and the resuspension of surficial channel-deposited fines that otherwise slowly re-enter the water column over time may play a role in flushing associated with events of these magnitudes. The flushing effect may also operate on the hillslope by exhausting surficial,

easily mobilized sediment, as the hillslope sediment pool is far larger than that of the channel (Inman and Jenkins, 1999). Determination of the proportional role of channel and hillslope sediment sources is beyond the scope of this study, but further evidence does support the significance of in-channel processes.

The lower Salinas appears to be insensitive to flow regime differences over low to moderate discharge magnitudes (Table 2.4). Previous studies have shown that precipitation-driven storm flows often display dramatically different suspended sediment behavior in comparison to flows attributed to interflow, ground water discharge, or recharge-oriented dam releases (winter recessional or summer base flow), due primarily to the increased contribution of hillslope and channel margin sediment from precipitation events (Lana-Renault et al., 2007; López-Tarazón et al., 2010; Oeurng et al., 2010; Tena et al., 2011; Gao and Josefson, 2012). Lack of sensitivity in the lower Salinas further supports the idea that the channel plays a significant role in moderating suspended sediment concentration as water routed overland, through interflow or groundwater; and summer dam releases, which are almost devoid of sediment, are statistically coincident in suspended sediment rating curve behavior at low to moderate flow magnitudes. Previous studies have found that fine sediment may penetrate deeply into the coarser channel matrix and that these fines re-enter suspension only by flows large enough to mobilize bed sediment, even in reaches where bed sediment was sandy (López-Tarazón et al., 2011). Therefore, if the channel bed is generally of low mobility, surficial and intermixed channel deposits of incipient and recessional flows may contribute significantly to the fine sediment load of low flows.

In-channel storage has been found to play a significant role in fine sediment dynamics in other rivers, with fine sediment content of 0.04–8.0 g cm<sup>-2</sup> reported for a wide range of rivers using a method that involved the agitation of the top 5–10 cm of bed material (Lambert and Walling, 1988; Walling and Quine, 1993; Droppo and Stone, 1994; Walling et al., 1998, López-Tarazón et al., 2011). Most of these studies used a more expansive definition of fine sediment that included fine sand (< 150 μm) and were conducted on reaches with coarser bed material than the mainstem of the lower Salinas River, although the limited amount of work on sandy reaches suggests that they could store a higher proportion of fines than gravel beds (Walling and Quine, 1993). Average annual sediment load estimates based on Inman and Jenkins (1999) and Farnsworth and Milliman (2003) are ~ 30–60 times the amount estimated to have

been stored in the reach between S1 and S3, although both studies recognized that many years produced sediment fluxes of this magnitude or less. Thus, the fine sediment potentially stored in the lower Salinas main stem may only exert controls of a small scale relative to decadal- to centennial-scale suspended sediment yield, which is of a similar proportion to the channel storage effects found in another semi-arid catchment (López-Tarazón et al., 2011), but much less than has been found for more maritime climates (Walling et al., 1998).

#### *2.10.4 The power of antecedent conditions*

Unlike bed sediment alone, the hydrologic factors found in this study, though seemingly weak in terms of monotonic correlation coefficients, could have large effects on decadal- to centennial- scale sediment discharge, particularly if influencing the infrequent years responsible for most of the suspended sediment flux through the lower Salinas River. For example, monotonic trends in rating curve residuals against some hydrologic variables show up to 0.5 log unit or greater differences over the domain of variable values, which translates to approximately three times the difference in  $C_{SS}$  magnitude (see Fig. 2.6). As most sediment is transported through the lower Salinas River during a few high discharge days per year, and a few exceptional discharge years over the period of record (Farnsworth and Milliman, 2003), coincidence of discharge events with highly positive or negative hydrologic preconditions could result in large errors in sediment flux estimations that do not take these factors into account. This is particularly true for estimates applying suspended sediment data collected over only one decade to much longer discharge records, such as those of Farnsworth and Milliman (2003) and Inman and Jenkins (1999) for the Salinas River. Moreover, both channel and hydrologic factors could have significant proportional effects on sediment yields during years of lower suspended sediment production and over the range of low to moderate discharge magnitudes commonly found in the lower Salinas, which are of importance in terms of water quality.

## **2.11 Conclusions**

Suspended sediment rating curves often leave large residual variability in suspended sediment

concentration unexplained. Such was the case for the well-studied Salinas River located in a dry summer subtropical climate. Historical and event based hydrological characteristics were found to play a significant role in determining suspended sediment behavior in the lower Salinas. Prolonged drought was found to decrease both sand and fine sediment concentrations. Increased elapsed time since moderate hydrologic events with magnitudes of  $\sim 10\text{--}20 Q_{mean}$  resulted in increased fine sediment concentration. These moderate flows in the lower Salinas seem to flush the system, depressing subsequent concentrations of fines by exhausting some level of channel and hillslope storage. The importance of channel storage of sediment in the lower Salinas is highlighted by the positive effects of  $\Delta Q_d$  on fine concentrations, the prevalence of positive hysteresis, the preponderance of incipient flows in the early season and during droughts, and the insensitivity of the system to the dominance of upper Salinas or Arroyo Seco subbasin contributions and hydrologic regime (storm, winter recessional or summer base, and dam release flows) for moderate to low discharge magnitudes. Sand concentrations were found to increase as a result of wet conditions and more recent and larger hydrologic events and to decrease after seasonal scale dry conditions. Recent hydrologic activity also increased sand concentrations, with concentrations increasing when events over a broad range of discharges, from small ( $0.1 Q_{mean}$ ) to massive ( $100 Q_{mean}$ ), are more recent. Upper basin and Arroyo Seco sand signatures were also found to persist in the lower Salinas sand suspensions, which also display some evidence of distal basin lag effects relative to the more positive hysteresis domination of fine sediment. Thus, in-channel contributions to fine suspended sediment behavior is probably not a major control on decadal- to centennial- scale suspended sediment yield from the lower Salinas but may be significant in terms of water quality and annual scale sediment flux. Hydrologic preconditions identified in this study may also significantly influence long-term sediment flux dynamics in the lower Salinas, as they can effect changes in sediment concentration on the order of three times or greater.

The next step in this work is to identify the time dependent pattern of suspended sediment behavior in the lower Salinas and determine if these patterns are influenced by the time dependent behavior of hydrologic conditions and/or land surface change. Further field-based studies of hillslope, channel bed, and bank activity in the lower Salinas and upper basin are also required to directly address the mechanisms behind the antecedent hydrologic effects on suspended sediment behavior found here.

Extension of the approach employed here to other systems would benefit greatly from higher resolution water discharge and suspended sediment concentration time series available over longer temporal domains, which are expected to have limited this study from identification of further complexities in the interaction between antecedent conditions and sediment behavior.

## 2. 12 References

- Andrews ED, Antweiler RC, Neiman PJ, Ralph FM. 2004. Influence of ENSO on flood frequency along the California coast. *Journal of Climate* **17**: 337-348. DOI: 10.1175/1520-0442(2004)017<0337:ioeoff>2.0.co;2
- Ankers C, Walling DE, Smith RP. 2003. The influence of catchment characteristics on suspended sediment properties. *Hydrobiologia* **494**: 159-167
- Asselman NEM. 1999. Suspended sediment dynamics in a large drainage basin: the River Rhine. *Hydrological Processes* **13**: 1437-1450
- Batalla RJ, Vericat D. 2009. Hydrological and sediment transport dynamics of flushing flows: implications for management in large Mediterranean rivers. *River Research and Applications* **25**: 297-314. DOI: 10.1002/rra.1160
- Benda L, Dunne T. 1997. Stochastic forcing of sediment routing and storage in channel networks. *Water Resources Research* **33**: 2865-2880
- Brasington J, Richards K. 2000. Turbidity and suspended sediment dynamics in small catchments in the Nepal Middle Hills. *Hydrological Processes* **14**: 2559-2574
- Brown, CB. 1943. The Control of Reservoir Silting. U.S. Department of Agriculture, Miscellaneous Publication 21, Washington, D.C.
- Brown WM, Ritter JR. 1971. Sediment Transport and Turbidity in the Eel River Basin, California U.S. Geological Survey Water-Supply Paper 1986, Washington, D.C., 67pp.
- Brune, GM. 1953. Trap efficiency of reservoirs. *Trans. Am. Geophys. Union* **34**: 407-418
- Carson MA, Taylor CH, Grey BJ. 1973. Sediment production in a small Appalachian watershed during spring runoff - Eaton-Basin, 1970-1972. *Canadian Journal of Earth Sciences* **10**: 1707-1734

- Chakrapani GJ. 2005. Factors controlling variations in river sediment loads. *Current Science* **88**: 569-575
- Cleveland WS. 1979. Robust locally weighted regression and smoothing scatterplots. *J. Am. Stat. Assoc.* **74**, 829-836
- Cleveland WS, Devlin SJ. 1988. Locally weighted regression: an approach to regression analysis by local fitting. *J. Am. Stat. Assoc.* **83**(403): 596-610
- Constantine JA, Dunne T, PiÉGay H, Mathias Kondolf G. 2010. Controls on the alluviation of oxbow lakes by bed-material load along the Sacramento River, California. *Sedimentology* **57**: 389-407. DOI: 10.1111/j.1365-3091.2009.01084.x
- de Vente J, Poesen J, Arabkhedri M, Verstraeten G. 2007. The sediment delivery problem revisited. *Progress in Physical Geography* **31**: 155-178. DOI: 10.1177/0309133307076485
- Droppo IG, Stone M. 1994. In-channel surficial fine-grained sediment laminae .1. Physical characteristics and formational processes. *Hydrological Processes* **8**: 101-111. DOI: 10.1002/hyp.3360080202
- Estrany J, Garcia C, Batalla RJ. 2009. Groundwater control on the suspended sediment load in the Na Borges River, Mallorca, Spain. *Geomorphology* **106**: 292-303. DOI: 10.1016/j.geomorph.2008.11.008
- Farnsworth KL, Milliman JD. 2003. Effects of climatic and anthropogenic change on small mountainous rivers: the Salinas River example. *Global and Planetary Change* **39**: 53-64. DOI: 10.1016/s0921-8181(03)00017-1
- Farnsworth KL, Warrick JA. 2007. Sources, dispersal, and fate of fine sediment supplied to coastal California. U.S. Geological Survey Scientific Investigations Report 2007–5254, Washington, D.C., 77 pp.
- Ferguson, RI. 1986. River loads underestimated by rating curves. *Water Resour. Res.* **22**(1): 74-76
- Gao P, Pasternack GB. 2007. Dynamics of suspended sediment transport at field-scale drain channels of irrigation-dominated watersheds in the Sonoran Desert, southeastern California. *Hydrological Processes* **21**: 2081-2092. DOI: 10.1002/hyp.6398
- Gao P, Josefson M. 2012. Event-based suspended sediment dynamics in a central New York watershed. *Geomorphology* **139**: 425-437. DOI: 10.1016/j.geomorph.2011.11.007
- Garcia M, Parker G. 1991. ENTRAINMENT OF BED SEDIMENT INTO SUSPENSION. *Journal of Hydraulic Engineering-Asce* **117**: 414-435

- Gonzalez-Hidalgo JC, Batalla RJ, Cerda A, de Luis M. 2010. Contribution of the largest events to suspended sediment transport across the USA. *Land Degradation & Development* **21**(2): 83-91
- Gray AB, Pasternack GB, Watson EB. 2010. Hydrogen peroxide treatment effects on the particle size distribution of alluvial and marsh sediments. *Holocene* **20**: 293-301. DOI: 10.1177/0959683609350390
- Heidel SG. 1956. The progressive lag of sediment concentration with flood waves. *Trans. Am. Geophys. Union* **37**: 56-66
- Heinemann HG. 1981. A new sediment trap efficiency curve for small reservoirs. *Water Resources Bulletin* **17**: 825-830
- Heinemann HG. 1984. Reservoir trap efficiency. In: Hadley, R.F., Walling, D.E., (Eds.), *Erosion and Sediment Yield: Some Methods of Measurement and Modelling*. GeoBooks, Norwich, CT, 201-218.
- Helsel DR, Hirsch RM. 2002. Statistical methods in water resources—hydrologic analysis and interpretation. U.S. Geological Survey Techniques of Water-Resources Investigations book 4, chap. A3, Washington, DC, 510 pp.
- Hill PS, Nowell ARM, Jumars PA. 1988. Flume evaluation of the relationship between suspended sediment concentration and excess boundary shear-stress. *Journal of Geophysical Research-Oceans* **93**: 12499-12509. DOI: 10.1029/JC093iC10p12499
- Horowitz AJ. 2003. An evaluation of sediment rating curves for estimating suspended sediment concentrations for subsequent flux calculations. *Hydrological Processes* **17**: 3387-3409. DOI: 10.1002/hyp.1299
- Hudson PF. 2003. Event sequence and sediment exhaustion in the lower Panuco Basin, Mexico. *Catena* **52**: 57-76
- Inman DL, Jenkins SA. 1999. Climate change and the episodicity of sediment flux of small California rivers. *Journal of Geology* **107**: 251-270
- Kale VS, Hire PS. 2004. Effectiveness of monsoon floods on the Tapi River, India: role of channel geometry and hydrologic regime. *Geomorphology* **57**: 275-291. DOI: 10.1016/s0169-555x(03)00107-7
- Kelsey HM. 1980. A sediment budget and an analysis of geomorphic process in the Van-Duzen River

- Basin, north coastal California, 1941-1975 - summary. *Geological Society of America Bulletin* **91**: 190-195. DOI: 10.1130/0016-7606(1980)91<190:asbaaa>2.0.co;2
- Korup O. 2012. Earth's portfolio of extreme sediment transport events. *Earth-Science Reviews* **112**: 115-125. DOI: 10.1016/j.earscirev.2012.02.006
- Lambert CP, Walling DE, 1988. Measurement of channel storage of suspended sediment in a gravel-bed river. *Catena* **15**(1): 65-80.
- Lana-Renault N, Regues D, Marti-Bono C, Begueria S, Latron J, Nadal E, Serrano P, Garcia-Ruiz JM. 2007. Temporal variability in the relationships between precipitation, discharge and suspended sediment concentration in a small Mediterranean mountain catchment. *Nordic Hydrology* **38**: 139-150. DOI: 10.2166/nh.2007.003
- Langbein WB, Schumm SA. 1958. Yield of sediment in relation to mean annual precipitation. *Trans. Am. Geophys. Union* **39**: 1076-1084
- Larsen PV. 2003. ST111: Regression analysis and analysis of variance. <http://statmaster.sdu.dk/courses/st111/> (last accessed: 12/2012).
- Lenzi MA, Marchi L. 2000. Suspended sediment load during floods in a small stream of the Dolomites (northeastern Italy). *Catena* **39**(4): 267-282
- Leopold LB, Maddock TJ. 1953. Hydraulic geometry of stream channels and some physiographic implications. U.S. Geological Survey Professional Paper 252, Washington, D.C., 55 pp.
- Lopez-Tarazon JA, Batalla RJ, Vericat D, Balasch JC. 2010. Rainfall, runoff and sediment transport relations in a mesoscale mountainous catchment: The River Isabena (Ebro basin). *Catena* **82**: 23-34. DOI: 10.1016/j.catena.2010.04.005
- Lopez-Tarazon JA, Batalla RJ, Vericat D. 2011. In-channel sediment storage in a highly erodible catchment: the River Isabena (Ebro Basin, Southern Pyrenees). *Zeitschrift Fur Geomorphologie* **55**: 365-382. DOI: 10.1127/0372-8854/2011/0045
- Madej MA, Ozaki V. 1996. Channel response to sediment wave propagation and movement, Redwood Creek, California, USA. *Earth Surface Processes and Landforms* **21**: 911-927
- Mano V, Nemery J, Belleudy P, Poirel A. 2009. Assessment of suspended sediment transport in four alpine watersheds (France): influence of the climatic regime. *Hydrological Processes* **23**: 777-792.

DOI: 10.1002/hyp.7178

- McCulloch M, Fallon S, Wyndham T, Hendy E, Lough J, Barnes D. 2003. Coral record of increased sediment flux to the Great Barrier Reef since European settlement. *Nature* **421**(6924): 727-730
- McLeod AI. 2011. Package 'Kendall.' Kendall rank correlation and Mann-Kendall trend test. CRAN. Classification/MS C 62M10, 91B84. <http://www.stats.uwo.ca/faculty/aim>. (last accessed: 12/2012).
- Meade RH, Yuzyk TR, Day TJ. (Eds.), 1990. Movement and storage of sediment in rivers of the United States and Canada. In: *Surface Water Hydrology, The Geology of North America 0-1*. Geol. Soc. of Am., Boulder, CO. 255-280.
- Mehta AJ, Hayter EJ, Parker WR, Krone RB, Teeter AM. 1989. Cohesive sediment transport .1. process description. *Journal of Hydraulic Engineering-Asce* **115**: 1076-1093
- Milliman JD, Syvitski JPM. 1992. Geomorphic/Tectonic Control of Sediment Discharge to the Ocean: The Importance of Small Mountainous Rivers. *The Journal of Geology* **100**: 525-544
- Neagley JP, Robert T. O'Brien J. 1990. Market Allocation of Agricultural Water Resources in the Salinas River Valley. In *Management*. Naval Postgraduate School: Monterey, CA; 96 pp.
- Nutter EH. 1901. Sketch of the geology of the Salinas Valley, California. *Journal of Geology* **9**: 330-336
- Oeurng C, Sauvage S, Sanchez-Perez JM. 2010. Dynamics of suspended sediment transport and yield in a large agricultural catchment, southwest France. *Earth Surface Processes and Landforms* **35**: 1289-1301. DOI: 10.1002/esp.1971
- Pasternack GB, Brush GS, Hilgartner WB. 2001. Impact of historic land-use change on sediment delivery to a Chesapeake Bay subestuarine delta. *Earth Surface Processes and Landforms* **26**: 409-427. DOI: 10.1002/esp.189
- Paustian SJ, Beschta RL. 1979. Suspended sediment regime of an Oregon Coast range stream. *Water Resources Bulletin* **15**: 144-154
- Poesen JWA, Hooke JM. 1997. Erosion, flooding and channel management in Mediterranean environments of southern Europe. *Progress in Physical Geography* **21**: 157-199. DOI: 10.1177/030913339702100201
- R Development Core Team. 2012. R: A Language and Environment for Statistical Computing. R Foundation for Statistical Computing, Vienna, Austria. ISBN 3-900051-07-0, <http://www.R-project.org/>

(last accessed: 12/2012).

- Rosenberg LI, Joseph JC. 2009. Map of the Rinconada and Reliz Fault Zones, Salinas River Valley, California: U.S. Geological Survey Scientific Investigations Map 3059, scale 1:250,000 with pamphlet, <http://pubs.usgs.gov/sim/3059/> (last accessed: 12/2012).
- Rouse H. 1937. Modern conceptions of the mechanics of fluid turbulence. *Transactions of the American Society of Civil Engineers* **102**: 463-541
- Rouse H. 1938. Fluid mechanics for hydraulic engineers. Dover, New York, 422 pp.
- Sadeghi SHR, Mizuyama T, Miyata S, Gomi T, Kosugi K, Fukushima T, Mizugaki S, Onda Y. 2008. Development, evaluation and interpretation of sediment rating curves for a Japanese small mountainous reforested watershed. *Geoderma* **144**: 198-211. DOI: 10.1016/j.geoderma.2007.11.008
- Shi YL, Yang W, Ren ME. 1985. Hydrological characteristics of the Changjiang and its relation to sediment transport to the sea. *Continental Shelf Research* **4**: 5-15
- Syvitski JP, Morehead MD, Bahr DB, Mulder T. 2000. Estimating fluvial sediment transport: The rating parameters. *Water Resources Research* **36**: 2747-2760. DOI: 10.1029/2000wr900133
- Tena A, Batalla RJ, Vericat D, Lopez-Tarazon JA. 2011. Suspended sediment dynamics in a large regulated river over a 10-year period (the lower Ebro, NE Iberian Peninsula). *Geomorphology* **125**: 73-84. DOI: 10.1016/j.geomorph.2010.07.029
- Thompson JG, Reynolds R. 2002. Cultural evolution and water management in the Salinas River Valley. *Journal of the American Water Resources Association* **38**: 1661-1677. DOI: 10.1111/j.1752-1688.2002.tb04372.x
- U.S. Geological Survey National Water Information System (USGS NWIS). 2013. <http://waterdata.usgs.gov/nwis/sw> (last accessed: 03/2013).
- Walling DE. 1977. Assessing accuracy of suspended sediment rating curves for a small basin. *Water Resources Research* **13**: 530-538
- Walling DE, Moorehead PW. 1987. Spatial and Temporal Variation of the Particle-Size Characteristics of Fluvial Suspended Sediment. *Geografiska Annaler. Series A, Physical Geography* **69**: 47-59
- Walling DE, Quine TA. 1993. Using Chernobyl-derived fallout radionuclides to investigate the role of downstream conveyance losses in the suspended sediment budget of the river Severn, United-

- Kingdom. *Physical Geography* **14**: 239-253
- Walling DE, Owens PN, Leeks GJL. 1998. The role of channel and floodplain storage in the suspended sediment budget of the River Ouse, Yorkshire, UK. *Geomorphology* **22**: 225-242. DOI: 10.1016/s0169-555x(97)00086-x
- Warrick JA, Rubin DM. 2007. Suspended-sediment rating curve response to urbanization and wildfire, Santa Ana River, California. *Journal of Geophysical Research-Earth Surface* **112**. DOI: F0201810.1029/2006jf000662
- Warrick JA, Mertes LAK. 2009. Sediment yield from the tectonically active semiarid Western Transverse Ranges of California. *Geological Society of America Bulletin* **121**: 1054-1070. DOI: 10.1130/b26452.1
- Warrick JA, Hatten JA, Pasternack GB, Gray AB, Goni MA, Wheatcroft RA. 2012. The effects of wildfire on the sediment yield of a coastal California watershed. *Geological Society of America Bulletin* **124**: 1130-1146. DOI: 10.1130/b30451.1
- Warrick JA, Madej MA, Goni MA, Wheatcroft RA. 2013. Trends in the suspended-sediment yields of coastal rivers of northern California, 1955-2010. *Journal of Hydrology* **489**: 108-123. DOI: 10.1016/j.jhydrol.2013.02.041
- Watson EB, Pasternack GB, Gray AB, Goni M, Woolfolk AM. 2013. Particle size characterization of historic sediment deposition from a closed estuarine lagoon, Central California. *Estuarine Coastal and Shelf Science* **126**: 23-33. DOI: 10.1016/j.ecss.2013.04.006
- Wheatcroft RA, Goni MA, Hatten JA, Pasternack GB, Warrick JA. 2010. The role of effective discharge in the ocean delivery of particulate organic carbon by small, mountainous river systems. *Limnology and Oceanography* **55**: 161-171. DOI: 10.4319/lo.2010.55.1.0161
- Williams GP. 1989. Sediment concentration versus water discharge during single hydrologic events in rivers. *Journal of Hydrology* **111**: 89-106. DOI: 10.1016/0022-1694(89)90254-0
- Willis CM, Griggs GB. 2003. Reductions in fluvial sediment discharge by coastal dams in California and implications for beach sustainability. *Journal of Geology* **111**: 167-182. DOI: 10.1086/345922
- Winterwerp JC, Cornelisse JM, Kuijper C. 1990. Parameters to characterize natural muds. In: Abstract Volume, Int. Workshop on Cohesive Sediments, Brussels. KBIN, Brussels, 103-105.
- Wischmeier WH, Smith DD. 1978. Predicting rainfall erosion losses: A guide to conservation planning.

## **Appendix 2.A Supplemental Material**

### *Supplemental Material 2.i Bias Testing*

Merging suspended sediment samples from two studies extended the temporal range of analysis, but both sample sets (USGS and those collected for this study) included samples from two locations (S1 and S2), and the proportional contribution of these two sites to the total data set was not stable over time (Fig. 2.2). Selecting only USGS samples with particle size data could also bias analyses because of potential differences between samples with and without particle size data (Table 2.S.i).

Bias concerns were first addressed by constructing  $C_{SS}$ -Q rating curves (see section 4) for subgroups defined by sampling site (S1 or S2), or whether USGS particle size distribution analysis was performed. These subgroup rating curves were then tested for significant differences in the  $C_{SS}$ -Q relationship using ANCOVA methods (see section 6.1 and Supplemental Material II). The rating curves subgroups for the particle size distribution categories utilized total  $C_{SS}$  data ( $C_{SSf} + C_{SSs}$ ); all others were based on  $C_{SSf}$ . Assessment of differences between S1 and S2 suspended sediment behavior was based on data from water years when samples were collected from both sites, and was further broken down into two time periods: {1969,78,79,86} and 2008-2011 to avoid confounding with potential temporal trends. The particle size distribution subgroup comparisons were also performed on data from subsets defined by decade. In order to investigate the effect of omitting USGS samples without particle size data from this study, the rating curve for the entire USGS dataset was compared to the subgroup of samples with associated particle size data.

All bias investigations through rating curve comparisons produced no statistically significant differences for the entire period of record, except for one incidence of non-coincidence between samples with and without particle size data. The rating curves in this case were found to have offsets and slopes that were not significantly different, and the comparison of rating curves with particle size data to the entire USGS sample set showed that the rating curve was not significantly changed by the inclusion of samples without particle size data. Furthermore, only 30 of 317 suspended sediment samples collected

**Table 2.S.i** Samples by hydrologic regime and particle size distribution data

With particle size distribution data

Decade	Summer Base	Storm	Winter Recessional	Total
1960s	2	24	0	26
1970s	16	91	19	126
1980s	22	29	17	68
1990s	15	20	2	37
2000s	12	17	1	30

Without particle size distribution data

Decade	Summer Base	Storm	Winter Recessional	Total
1960s	0	0	0	0
1970s	2	0	0	2
1980s	5	4	4	13
1990s	0	0	0	0
2000s	12	1	2	15

Hydrologic regime: Summer base flow are those flows that occur between the last precipitation associated hydrologic event in the spring and the first of the fall. Storm flows are associated with precipitation events, excluding the change in concavity on the falling limb of the hydrograph. Winter recessional flows take place after a change in concavity on the falling limb of a storm flow hydrograph.

by the USGS were not processed for particle size distribution analysis (see Table 2.S.i). Thus, selection of the suspended sediment sample set for those that have associated particle size data, and inclusion of samples from stations S1 and S2 were found to have no significant biasing effect on the analyses of suspended sediment behavior in the lower Salinas River.

*Supplemental Material 2.ii The ANCOVA Method of Rating Curve Comparison*

For ANCOVA comparison between suspended sediment subgroups, multiple regression models were constructed from data subsets using the following general model for two group comparison as per Larsen (2003):

$$\text{Log}(C_{SS}) = \beta_0 + \beta_1 \text{Log}(Q_i) + \beta_2 Z + \beta_3 (\text{Log} Q_i) Z + \varepsilon \quad (\text{S2.ii.1})$$

where Z is a synthetic variable categorizing the data into any two subsets using a value of 1 or 0,  $\beta$  values are regression fitted coefficients and  $\varepsilon$  represents random variation not accounted for by the rest of the model. The model for the relationships between  $\text{Log}(Q)$  and  $\text{Log}(C_{SS})$  for the two groups can then be defined as:

$$\text{G1 (Z = 1):} \quad \text{Log}(C_{SS}) = (\beta_0 + \beta_2) + (\beta_1 + \beta_3) \text{Log}(Q_i) + \varepsilon \quad (\text{S2.ii.2})$$

$$\text{G2 (Z = 0):} \quad \text{Log}(C_{SS}) = \beta_0 + \beta_1 \text{Log}(Q_i) + \varepsilon \quad (\text{S2.ii.3})$$

These models form the basis for testing the subgroup rating curves for coincidence, where both subgroups should be described by the same rating curve, parallelism, the condition where rating curve slopes are statistically the same, and offset equivalence, where rating curve intercepts are equal. Coincident subgroups display the exact same relationship between the dependent and independent variables, in this case  $\text{log}(C_{SS})$  and  $\text{log}(Q)$ . In testing for coincidence the null hypothesis is:

$$H_0: \quad \beta_2 = \beta_3 = 0. \quad (\text{S2.ii.4})$$

If the null hypothesis cannot be discarded, then both groups are considered coincident, and the relationship between  $\log(C_{SS})$  and  $\log(Q)$  is described as Eq. 3 for the entire data set. If the null hypothesis is discarded, then further tests for parallelism and equivalence of offset (also known as equality of intercepts or elevation equivalence) are required to determine how the relationship between  $\log(C_{SS})$  and  $\log(Q)$  significantly differ. The null hypothesis of parallelism, the condition in which the slopes of the two subgroup regression lines are equal, is:

$$H_0: \beta_3 = 0. \quad (S2.ii.5)$$

Similarly, difference in offset requires only that the intercepts of the two subsets are significantly different, with a null hypothesis of:

$$H_0: \beta_2 = 0. \quad (S2.ii.6)$$

## Chapter 3

### **Decadal patterns in the suspended sediment behavior of a coastal dry-summer subtropical catchment: The role of hydrologic preconditions**

#### **Abstract**

Rivers display temporal dependence in suspended sediment – water discharge relationships. Although most work has focused on multi-decadal trends, river sediment behavior often displays sub-decadal scale fluctuations that have received little attention. The objectives of this study were to identify interannual to decadal scale fluctuations in the suspended sediment – discharge relationship of a dry-summer subtropical river, infer the mechanisms behind these fluctuations, and examine the role of El Niño Southern Oscillation climate cycles. The Salinas River (California) is a moderate sized (11,000 km<sup>2</sup>), coastal dry-summer subtropical catchment with a mean discharge ( $Q_{mean}$ ) of 11.6 m<sup>3</sup>s<sup>-1</sup>. It is located at the northern most extent of increased storm frequency during El Niño years for Pacific coastal North America. Even to interannual scale suspended sediment behavior in this system was known to be influenced by antecedent hydrologic conditions, whereby previous hydrologic activity regulates the suspended sediment concentration – water discharge relationship (Gray et al., 2014). The study presented here found that both fine and sand suspended sediment in the lower Salinas River exhibited persistent, decadal scale periods of positive and negative discharge corrected concentrations. The decadal scale variability in suspended sediment behavior was influenced by interannual to decadal scale fluctuations in hydrologic characteristics, including: elapsed time since small ( $\sim 0.1 \times Q_{mean}$ ), and moderate ( $\sim 10 \times Q_{mean}$ ) threshold discharge values, the number of preceding days that low/no flow occurred, and annual water yield. El Niño climatic activity was found to have little effect on decadal-scale fluctuations in the fine suspended sediment – discharge relationship due to low or no effect on the frequency of moderate to low discharge magnitudes, annual precipitation, and water yield. However, sand concentrations generally increased in El Niño years due to the increased frequency of moderate to high magnitude discharge events, which generally increase sand supply.

### 3.1 Introduction

Small to moderate sized basins ( $10\text{--}10^4$  km<sup>2</sup>) of high relief ( $> 2000$  m) are known to export the majority of the terrestrial sediment flux to the oceans (Milliman and Syvitski, 1992). Most river sediment is transported in suspension (Walling, 1977), and the relationship between suspended sediment concentration ( $C_{SS}$ ) and water discharge ( $Q$ ) is often highly variable in small systems (i.e. Bogen and Bonsnes, 2003; Farnsworth and Warrick, 2007). Furthermore, semi-arid rivers experiencing pronounced wet and dry seasons, such as the Salinas River of central California, often display particularly high variability in the  $C_{SS} - Q$  relationship (Warrick and Mertes, 2009; Farnsworth and Milliman, 2003; Gray et al., 2014).

Variability in the  $C_{SS} - Q$  relationship is determined by internal and external mechanisms that are highly dependent on temporal scale (Carson et al., 1973; Paustian and Beschta, 1979; Gao et al., 2007; Florsheim et al., 2011; Tote et al., 2011; Kuai and Tsai, 2012). Internal mechanisms are those that arise primarily from the characteristics of the basin, while external mechanisms stem primarily from environmental conditions exterior to the basin, such as climatic and solar forcings. Most estimations of decadal to multi-decadal suspended sediment flux assume stationarity in the  $C_{SS} - Q$  relationship and the mechanisms involved in its control (Helsel and Hirsch, 2002). Studies that have recognized temporal dependence in  $C_{SS} - Q$  relationships generally focused on multi-decadal trends forced by long term anthropogenic activity or large disturbances such as wildfire or rare floods (i.e. Pasternack et al., 2001; Willis and Griggs, 2003; Walling, 2006; Warrick and Rubin, 2007; Warrick et al., 2012; Warrick et al., 2013). Conversely, studies focused on event scale forcings in small mountainous basins generally have not examined their effects on interannual or decadal scale patterns in suspended sediment behavior (i.e. Hudson, 2003; Lenzi and Marchi, 2000; Estrany et al., 2009; Mano et al., 2009).

Some mechanisms operate exclusively over a narrow temporal domain, and cease to influence systematic differences in suspended sediment concentrations as the time period of comparison changes. For example, the event scale internal mechanism of differential peak  $C_{SS}$  and  $Q$  celerity downstream can lead to suspended sediment hysteresis – differing  $C_{SS} - Q$  relationships on the rising and falling limb of the hydrograph (Heidel, 1956; Marcus, 1989; Bull, 1997; Brasington and Richards, 2000). Differences in

the average  $C_{SS} - Q$  relationship from one decade to the next would be unaffected by differences in peak  $C_{SS}$  and  $Q$  transit speeds. This would be the case even if systematic changes in sediment and discharge celerity occurred at the decadal scale, as long as the event integrated  $C_{SS} - Q$  relationship did not change.

However, event scale mechanisms can also affect longer term variation in suspended sediment behavior. One set of mechanisms for this temporal 'up-scaling' are the effects of antecedent basin conditions. The external factors of storm track location and precipitation intensity interact with the internal factors of basin ground cover and substrate characteristics to largely determine the delivery of water and sediment to the channel (Hicks et al., 2000; Ankers et al. 2003). The most commonly available record of these interactions over time is the discharge time series, which can in turn be used to describe the hydrologic preconditioning of the system (Hudson, 2003; Gray et al, 2014). Antecedent conditions can affect subsequent suspended sediment behavior by increasing or decreasing sediment supply, particularly in systems that experience seasonal and highly variable conditions at interannual and greater scales (i.e. Abraham, 1969; Hudson, 2003; Lana-Renault et al., 2007; Lana-Renault and Regues, 2009; Gray et al., 2014). Furthermore, event to seasonal scale land surface and channel disturbances can also play a large role in changing suspended sediment behavior over short temporal scales by altering sediment availability (i.e. Colby, 1956; de Vente et al., 2007). Increased sediment availability in small to moderate sized basins has been observed after large floods in small mountainous basins (Abraham, 1969; Brown and Ritter 1971; Warrick et al., 2013). Flood events can also serve to flush semi-arid systems of sediment, exhausting sediment availability on an event basis or over the course of a storm season, which can have longer term effects on sediment supply (Hudson, 2003; Constantine et al., 2005; Batalla and Vericat, 2009; Gray et al., 2014).

In addition to the legacy effects of individual events,  $C_{SS} - Q$  relationships may also be steered by the seasonal, annual, or decadal scale patterns of persistent elevated or depressed hydrologic conditions. This is persistent dependency, or 'long-term-memory', wherein the previous states of a given parameter influences subsequent states over long time periods (Hurst, 1951; 1957). Discharge and transported constituent time series data from even relatively small basins ( $\sim 400 \text{ km}^2$ ) have displayed persistent dependency (Lawrence and Kottegoda, 1977; Montanari et al., 1997; Pelletier and Turcotte, 1997).

Perhaps the most studied examples of decadal scale patterns in a fine scale are the external controls on suspended sediment exerted by the regional effects of climate cycles on sediment flux. El Niño Southern Oscillation (ENSO) and Pacific Decadal Oscillation (PDO) patterns have been shown to affect annual and event scale precipitation magnitudes/intensities, and influence water and suspended sediment discharge variability at annual and decadal scales along the northeastern Pacific coast (Inman and Jenkins, 1999; Farnsworth and Milliman, 2003; Andrews et al., 2004; Andrews and Atweiler, 2012). However, these studies focused on the effects of climate cycles on discharge magnitude – frequency relationships applied to stationary  $C_{SS} - Q$  relationships.

This study directly addresses the assumption of a stationary suspended sediment – discharge relationship over multi-decadal time scales in the lower Salinas River, California. The central assertion is that decadal scale variability in the  $C_{SS} - Q$  relationship can be achieved through longer (interannual to decadal) temporal fluctuations or trends in the factors controlling event to annual scale suspended sediment behavior. The goals of this study were twofold. The first goal was to identify and describe the interannual to decadal scale patterns of suspended sediment – discharge behavior in the lower Salinas River, California. The second goal was to determine if interannual to decadal scale patterns in hydrologic conditions could explain the patterns observed in the  $C_{SS} - Q$  relationships. Event to annual scale hydrologic factors identified in previous work (Gray et al., 2014) were investigated for this purpose. The patterns in hydrologic factors were then examined in the context of regional climatic variability (ENSO cycling). Multi-decadal scale trends in suspended sediment behavior were then considered alongside trends in the discharge – precipitation relationship and in terms of decadal scale variability.

### **3.2 Study region**

The Salinas River drains a ~11,000 km<sup>2</sup> portion of the Central Coast Ranges of California from a maximum relief of ~ 1,900 m. Mean discharge ( $Q_{mean}$ ) is 11.6 m<sup>3</sup>s<sup>-1</sup> through the lowest gauging station in the basin (USGS gauge #11152500: *Salinas River near Spreckels*). This gauge and the next mainstem gauge 23.5 km upstream (USGS gauge # 11152300: *Salinas River near Chualar*,) are referred to in this study as S1 and S2, with drainage areas of 10,764 and 10,469 km<sup>2</sup>, respectively (Fig. 3.1). The period of

suspended sediment sampling between these two gauges spans 1967 to 2011, while discharge records extend from 1931 to present (USGS NWIS, 2013). The regional climate is dry-summer subtropical. Most annual precipitation originates from winter storms that occur from October through May, the largest of which are generally produced during strong El Niño years (Farnsworth and Milliman, 2003; Andrews et al., 2004). Geologic substrate is primarily Mesozoic sedimentary rock (Nutter, 1901; Rosenberg and Joseph, 2009). Land cover grades downslope from steep, forested headlands to chaparral and grassland assemblages in the lower hills, followed by lowlands that have been mostly converted to irrigation agriculture.

Agriculture is the largest anthropogenic disturbance in the Salinas River watershed in terms of area, followed by urbanization and dam emplacement (Thompson and Reynolds, 2002). Three major dams were constructed on the mainstem and two major eastern tributaries between 1941–1965 primarily for groundwater recharge purposes, motivated by irrigation demands that have led to overdrafting of Salinas aquifers since the early 20<sup>th</sup> century (Fig. 3.1) (Thompson and Reynolds, 2002). Urbanization has increased significantly in the basin from 172 to 230 km<sup>2</sup> between 1984 and 2010, although this remains a relatively low proportion of basin area (~ 2%) (California Department of Conservation, 2013). Groundwater extraction, primarily for irrigated agriculture, and the return of a portion of these waters to the channel are a significant component of the hydrology of the Salinas River (Thompson and Reynolds, 2002). Irrigation agriculture intensity has increased since the 1960s, but irrigation water demands stabilized beginning in the 1990s due to the rapid rise of drip irrigation, which has largely supplanted less hydrologically efficient sprinkler and furrow methods (Thompson and Reynolds, 2002).

### **3.3 Methods**

This study focused on suspended sediment samples collected by Gray et al. (2014) and historical USGS samples from the lower Salinas River. Gray et al. (2014) collected 43 samples between water years 2008 and 2011 from bridges crossing the Salinas River at Davis Street (4 river km below S1) and the USGS gauging stations S1 and S2 (Fig. 3.1). Water years begin on 1 October of the previous

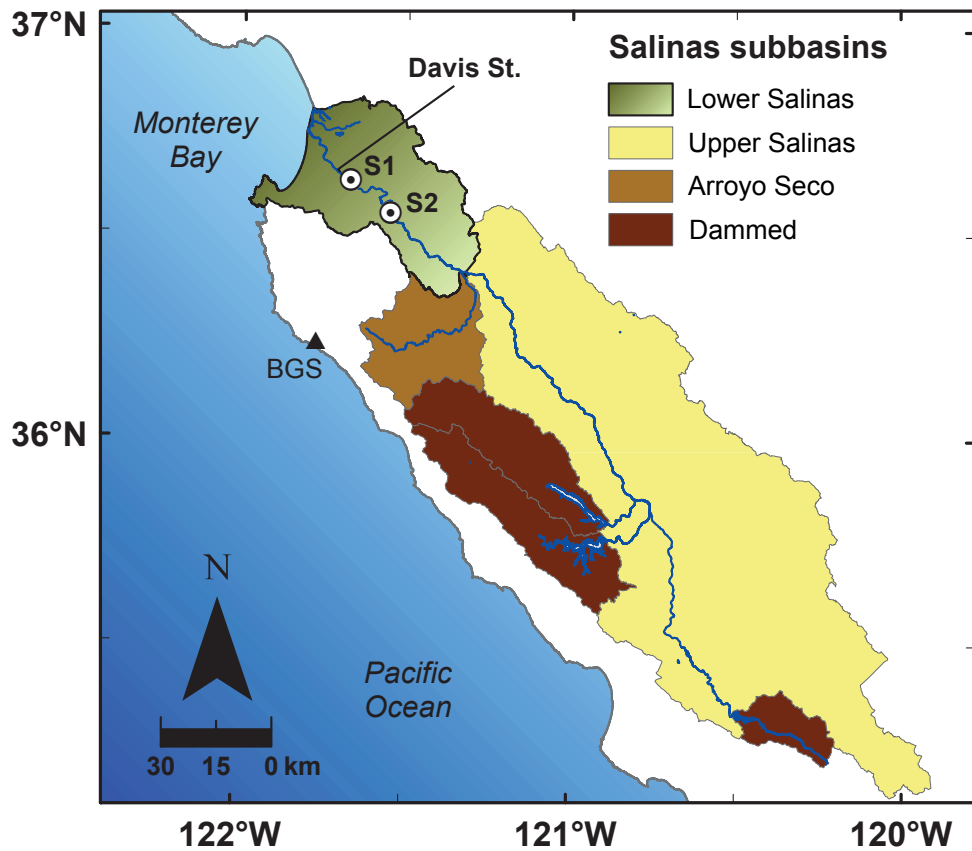


**Figure 3.1** The Salinas River watershed. The locations of U.S. Geological Survey (USGS) hydrologic gauging stations are marked with dotted circles and identification codes. Identification codes S1 and S2 correspond to gauge names: Salinas R. near Spreckels and Salinas River near Chualar (USGS gauge numbers 11152500 and 11152300), respectively. The Davis Street Bridge suspended sediment sampling location is indicated by a line. The National Oceanographic and Atmospheric Administration precipitation gauge 'Big Sur State Park' is indicated with a black triangle and the label BGS.

calendar year and end on 30 September of the calendar year. Samples were collected as per Warrick et al. (2012), with the following modifications. Samples were retrieved from the water surface at cross-channel stations of one-quarter, one-half, and three-quarters wetted channel width. Two 1-L samples from were collected from each cross-channel station for (i) total suspended sediment concentration ( $C_{SS}$ ) and (ii) particle size distribution analysis. One event was sampled at high resolution with 250-ml samples every 2 – 3 hours. Samples were measured volumetrically and then filtered through preweighed, combusted, Whatman GF/A, 0.7  $\mu\text{m}$  glass fiber filters. Filters were dried at 60°C for 24 h, cooled to room temperature under vacuum in a desiccator, and subsequently weighted to  $\pm 0.0001$  g. Sediment mass was obtained by subtracting filter mass from total mass. The  $C_{SS}$  was then calculated by dividing sediment mass by the initial sample volume.

Particle size distribution analysis was performed on sediment recovered from water samples through centrifugation at 3250 g in 500-mL bottles for 10 min. Sediment was transferred to 150-mL beakers and treated with unheated and heated 30%  $\text{H}_2\text{O}_2$  aliquots to oxidize organic constituents. Organic free sediment was then dispersed with 0.5% sodium metaphosphate solution, and run through a Beckman-Coulter LS 230 (Beckman Coulter Inc., Fullerton, CA, USA) laser diffraction granulometer using polarization intensity differential scattering (PIDS) as per Gray et al. (2010).

Suspended sediment samples were collected from the surface of river flow. For this reason coarse suspended sediment particles were expected to be underrepresented. Sediment suspension calculations by particle size based on the characteristics of the highest and lowest flows showed that fine particles in the clay to silt range (diameter ( $D$ ) < 62.5  $\mu\text{m}$ ) should be uniformly distributed throughout the vertical profile (Rouse, 1937, 1938; Hill et al., 1988). Based on these estimations, analysis of the suspended sediment samples collected by the authors was restricted to fine particles of  $D < 62.5$   $\mu\text{m}$ . Values for fine suspended sediment concentration ( $C_{SSf}$ ) were calculated by multiplying  $C_{SS}$  by the proportion of sediment occurring in the fine fraction:

$$C_{SSf} = \frac{C_{SS} \times (\% \text{ particles} < 62.5 \mu\text{m})}{100} \quad (3.1)$$

The USGS collected flow-integrated  $C_{SS}$  samples from the Salinas River at locations

corresponding to S1 and S2 from water years 1969 to 1986 and 1967 to 2010, respectively (USGS NWIS, 2013). The 277 USGS samples used in this study represented a given discharge event and were associated with both instantaneous discharge and particle size data. The USGS samples were processed by sieving to establish the relative contribution of fine, and sand ( $2000 \mu\text{m} > D > 63.5 \mu\text{m}$ ) fractions. The  $C_{SSf}$  for these samples was calculated using Eq. (1), and the concentration of sand suspended sediment ( $C_{SSs}$ ) was obtained by subtracting  $C_{SSf}$  from  $C_{SS}$ . Hereafter, the term  $C_{SS}$  is used generally when referring to tests that were conducted separately on  $C_{SSf}$  and on  $C_{SSs}$ .

All suspended sediment data from the USGS were associated with instantaneous discharge values. Samples collected by the authors were assigned discharge values through linear interpolation between adjacent 15-min discharge data from the appropriate USGS gauge. Davis Street sample discharge was estimated from the S1 record of 15-min discharge data by applying a time lag to account for the transit of flow stage downstream. The time lag was computed from the estimated transit time ( $t_t$ ), where  $t_t$  was equal to the distance between Davis Street and S1 divided by the transit speed ( $\text{m s}^{-1}$ ) of peak flow between S2 and S1 for each discharge event in question. Transit speeds were found to be highly variable, ranging from  $0.01$  to  $2.38 \text{ m s}^{-1}$ , yet most values fell between  $0.2$  and  $0.8 \text{ m s}^{-1}$ . When the lagged time fell between 15-min discharge records, the associated discharge was calculated through linear interpolation.

Monthly precipitation ( $P$ ) data was obtained from the National Weather Service for the Big Sur State Park (BGS) gauge; the gauge that correlates most closely with lower Salinas River streamflow (Warrick et al., 2012; Gray et al., 2014). Historic El Niño activity was characterized in this study by (i) the Oceanic Niño Index (ONI), an aggregate measurement of sea surface temperature defects from a 30 year base period average in the  $5^\circ\text{N}$  to  $5^\circ\text{S}$  by  $120^\circ$  to  $170^\circ\text{W}$  region and (ii) the extended Multivariate El Niño Index (MEI.ext), which incorporates the signals of several ENSO indices (Pedatella and Forbes, 2009; Wolter and Timlin, 2011). The National Oceanographic and Atmospheric Administration's (NOAA) three-month running average data for ONI were obtained for the interval of 1950 to 2011, while MEI.ext was retrieved from Wolter and Timlin (2011).

### 3.4 Computation and data analysis

Rating curves were used in this study to represent bivariate relationships between environmental parameters for given periods of time. The residuals of these relationships were then used to describe changes in these relationships over time. Residuals were obtained by subtracting the expected value on each rating curve from observed sample values, in effect correcting sample  $C_{SS}$  or  $Wy$  for the influence of  $Q$  or  $P$ , respectively. The rating curves employed to individually model  $C_{SSf} \sim Q$ ,  $C_{SSs} \sim Q$ , and annual water yield ( $Wy$ )  $\sim P$  relationships were constructed with simple linear regression and localized regression (LOESS) techniques applied to log-transformed data (Cleveland, 1979; Helsel and Hirsch, 2002; Gray et al., 2014). Suspended sediment rating curves were computed for the entire sediment sampling period (1967–2011), while  $Wy \sim P$  rating curves were calculated for the entire precipitation record (1930–2011) and just the 1967–2011 period. Rating curves were not corrected for log-transform bias as back-transformation for flux estimation in original units was not conducted here.

Persistent patterns in suspended sediment behavior were identified by sequentially summing  $C_{SSf} \sim Q$  and  $C_{SSs} \sim Q$  LOESS residuals over time. This method, referred to hereafter as cumulative residual analysis, was first developed by Hurst in the 1950s for estimating reservoir storage requirements (Hurst 1951; 1957). Periods of persistent positive or negative behavior were identified based on the local slope of the cumulative residual curve, with persistent positive or negative values recognized by positive or negative slopes maintained over ranges of residual values  $\geq 3\sigma$ , where  $\sigma$  is the standard deviation of the residuals.

Examination of persistent patterns in the hydrologic controls on suspended sediment behavior required variables representing these conditions. Gray et al. (2014) previously examined the effects of antecedent hydrologic conditions on suspended sediment behavior in the lower Salinas River. The significant hydrologic controls identified in that study were further examined here in terms of their decadal scale patterns of variability. The basic methodology of Gray et al. (2014) was to test for correlations between (i)  $C_{SSf} \sim Q$  or  $C_{SSs} \sim Q$  LOESS residuals and (ii) variables representing antecedent basin conditions using non-parametric Mann-Kendall analyses (Helsel and Hirsch, 2002). The following suites of variables were used to describe antecedent hydrologic conditions for each suspended sediment

sample: (i)  $\Sigma Q_{0.1}$ : the sum of days when  $Q_d \leq 0.1 \text{ m}^3\text{s}^{-1}$  for back cast summation windows of 1 to 2000 days; (ii)  $Q_j \text{ Time}$ : a measurement of the amount of time that has elapsed since the last hydrologic event greater than or equal to a given magnitude ( $Q_j$ ). Additionally, *annual water yield* for the current year was tested, as was  $\Delta Q_d$ , the change in daily discharge ( $Q_d$ ) from the day before sampling to the day of sampling.

The results of Gray et al. (2014) showed that  $C_{SSf} \sim Q$  LOESS residuals decreased with: (i) prolonged dry periods (increasing  $\Sigma Q_{0.1}$  with 1200 to 2000 day back cast summation windows), (ii) increased elapsed time since low discharge magnitudes ( $Q_j = \sim 1\text{--}4 \text{ m}^3\text{s}^{-1}$ ), and (iii) decreased elapsed time since moderate discharge magnitudes ( $Q_j = 100\text{--}200 \text{ m}^3\text{s}^{-1}$ ). Fine suspended sediment also displayed overall positive hysteresis (higher  $C_{SSf}$  concentrations on the rising limb of the hydrograph), which was reflected by a significant positive correlation with  $\Delta Q_d$ . In contrast,  $C_{SSs} \sim Q$  LOESS residuals decreased with: (i) seasonal to prolonged dry periods (increasing  $\Sigma Q_{0.1}$  with 10–2000 day back cast summation windows), and (ii) increasing elapsed time since a wide range of discharge magnitudes ( $Q_j = 1\text{--}1000 \text{ m}^3\text{s}^{-1}$ ), and increased with *annual water yield*.

Temporal patterns of the hydrologic conditions found by Gray et al. (2014) and the discharge time series were examined here to compare their decadal scale variability with that of fine, and sand suspended sediment. Individual variables were selected from the suites of  $\Sigma Q_{0.1}$  and  $Q_j \text{ Time}$  variables that had been found to display significant correlations with suspended sediment behavior by Gray et al. (2014). The variables selected were those that produced the highest correlations. For fines the variable that produced the most negative correlation was  $Q_1 \text{ Time}$ , and the variables with the highest positive correlations were  $Q_{114} \text{ Time}$ , and  $\Delta Q_d$ . The variables with the most negative correlations with sand were  $\Sigma Q_{0.1}$  with a 110 day sampling window, and  $Q_{400} \text{ Time}$ . The variable with the highest positive correlations with sand were current *annual water yield*.

Persistence in descriptors of antecedent hydrologic conditions and the discharge time series was visualized by subtracting their mean values, and then sequentially summing these mean corrected values over time. These sequential sums of mean corrected hydrologic variable behaviors were compared to suspended sediment cumulative residual analysis results to assess the role hydrologic conditions in determining decadal scale patterns in suspended sediment behavior. The hydrograph of mean daily

discharge values were also plotted to visualize the largest discharge events and longest droughts over the suspended sediment sampling record.

The role of ENSO was then investigated as a potential control on the hydrologic conditions found to influence suspended sediment behavior from 1950 to 2011. El Niño, or positive ENSO activity, has been associated with increased storm intensity in central to southern California region (Andrews and Antweiler, 2012). Previous studies have identified the Salinas basin as the northernmost of the central California rivers that respond to positive El Niño like conditions with an increased frequency of large P and Q events (Farnsworth and Milliman, 2003). To examine the coincidence of El Niño events and hydrologic event history of the lower Salinas River, plots of the annual sum of days with flows above threshold levels of 1, 100, 200 and 400 m<sup>3</sup>s<sup>-1</sup>, and below 0.1 m<sup>3</sup>s<sup>-1</sup> were compared to the three-month running mean ONI. To further examine the relationship between ENSO cycling and the discharge thresholds of interest, the annual sum of days satisfying the hydrologic criteria detailed above and annual P were plotted against annual peak ONI.

Finally, temporal trend analyses of ( $C_{SS} \sim Q$ ) or ( $Wy \sim P$ ) residuals were conducted using linear regression or Mann-Kendall methods to assess the multi-decadal trajectory of  $C_{SS}$  and  $Wy$  changes in the basin. These approaches can be characterized as parametric (linear regression trends of linear regression residuals), mixed parametric/nonparametric (linear regression trends of LOESS residuals, or Mann-Kendall trends of linear regression residuals) or nonparametric (Mann-Kendall trends of LOESS residuals) (Helsel and Hirsch, 2002). All analyses were performed using R 3.0.1 with package “Kendall” (McLeod, 2011; R Development Core Team, 2013).

### 3.5 Results

Linear and LOESS rating curves showed strong, generally linear relationships between Q and  $C_{SS}$  for  $Q > \sim 1 \text{ m}^3\text{s}^{-1}$ , with curved or flat tails for  $Q < \sim 1 \text{ m}^3\text{s}^{-1}$  (Fig. 3.2a,b, Table 3.1). The  $R^2$  values for  $C_{SSf}$  and  $C_{SSs}$  log linear rating curves were similar at 0.55 and 0.58, respectively, while the  $C_{SSf}$  slope was lower than that of  $C_{SSs}$  (0.71 vs. 0.92), but with a  $\sim 2x$  higher offset (1.57 vs. 0.73). LOESS models accommodated this low Q curvature, which resulted in slightly lower RMSE values in comparison to log-

linear regressions. Linear regression based  $Wy$  models also missed slight curvature in the response to  $P$ , which was slightly better described (e.g. resulted in lower RMSE values) by LOESS models for both temporal domains (Fig. 3.2c,d). The LOESS curves were used for subsequent suspended sediment and water yield rating curve residual analysis, as this better fit resulted in less systematic bias with discharge.

Cumulative residual analysis revealed that that Salinas River experienced periods of persistent higher-than-expected  $C_{ss}$  as well as the converse (Fig. 3.3). Fine sediment displayed persistent periods of higher  $C_{SSf}$  from 1967–1979 and 1990–1993, and persistent periods of lower  $C_{SSf}$  from 1980–1989 and 1994–2011 (Fig. 3.3a). The latter period of lower  $C_{SSf}$  was characterized by a period of relatively constant values from about 2002 – 2009, followed by a rapid decline in values. Sand displayed persistent periods of higher  $C_{SSs}$  from 1967–1986, followed by a period of persistent lower  $C_{SSs}$  during 1987–2010 (Fig. 3.3f). The period of persistent low sand concentrations was also characterized by a period of near constant values from about 1993 to 2005.

Plots of cumulative mean corrected values of the antecedent hydrologic condition descriptors revealed patterns in hydrologic history that may have played a role in decadal scale suspended sediment behavior (Fig. 3b–d ,g–i), with the hydrograph at S1 included for reference (Fig. 3.3e,j). The most striking feature of these plots is a persistent dry period spanning the mid-1980s to early 1990s. Two hydrologic variables used to estimate fine sediment concentration,  $Q_1$  *Time* and  $Q_{114}$  *Time*, displayed very similar persistent behaviors over much of the sample period, with notable exceptions (Fig. 3.3b,c). The cumulative residual results for  $Q_1$  *Time* showed displayed steady decreases in the mean corrected residual sums over periods from roughly 1966–1987 and 1993–2011, separated by a dramatic positive period that spanned the late 1980s to mid-1990s (Fig. 3.3b). On the other hand,  $Q_{114}$  *Time* displayed constant values (with some variability) from 1965 – 1980 and 2000 – 2011, and persistent decreases from 1980 – 1990 and 1995 – 2000 (Fig. 3.3c). The period of rapidly increasing mean corrected residual sums was also present for  $Q_{114}$  *Time*, but extended from the late 1980s to the early 1990s. The cumulative mean corrected plot for  $\Delta Q$  did not display persistent behavior, but rare large flood events did appear with their rapid, consecutive increases in discharge magnitude, including the three largest peak events of the period of suspended sediment record, which occurred on 2/26/1969, 3/3/1983 and 3/12/1995 (Fig. 3.3d,e).

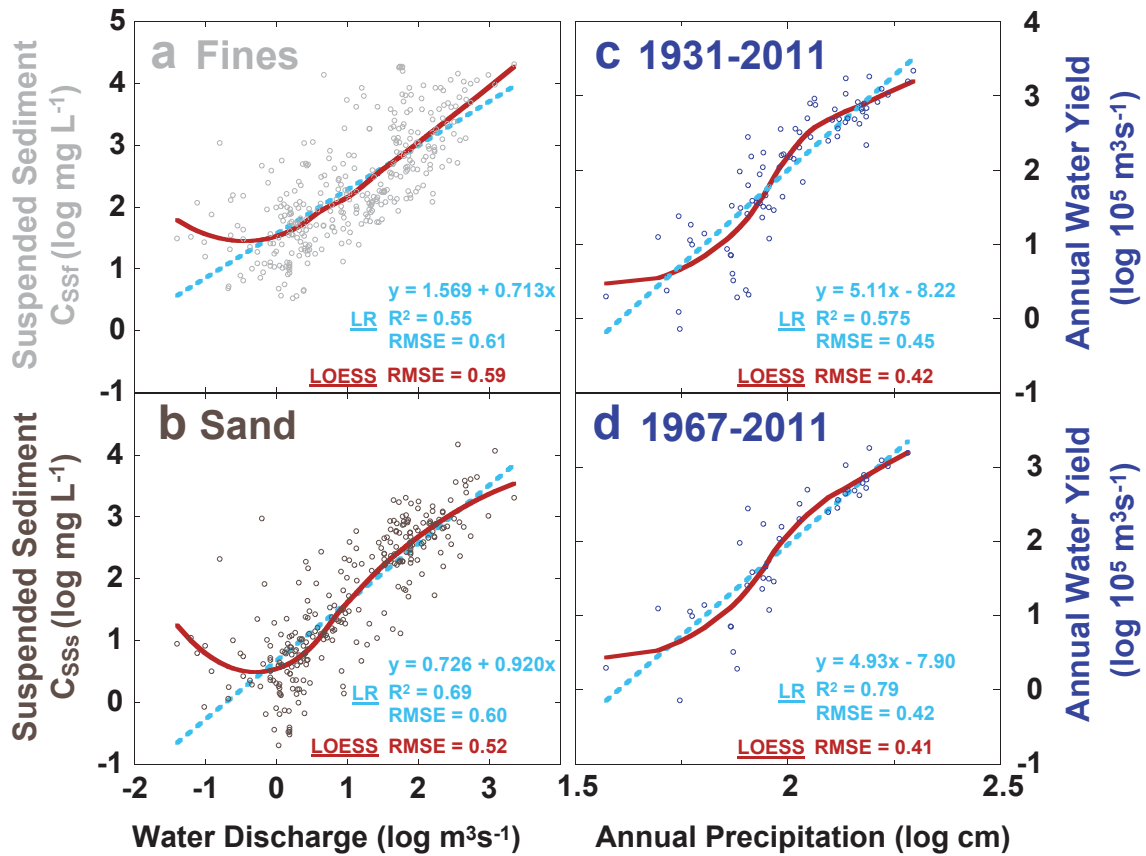


**Figure 3.2** Linear regression (LR) and LOESS rating curve models for suspended sediment concentration – water discharge behavior in log-log space for (a) fine and (b) sand sized sediment over the sampling period (1967–2011). Water yield – precipitation relationships are similarly modeled with linear regression and LOESS techniques for the entire period of S1 discharge measurement (c) 1931–2011, and the suspended sediment sampling period (d) 1967–2011.

**Table 3.1 Suspended Sediment Rating Curves  
Suspended Sediment Concentration ~ Water Discharge Linear Regression and LOESS Rating Curves**

Sediment Size	Temporal Zone <sup>a</sup>	Model	Model Equation	R <sup>2</sup>	RMSE <sup>b</sup>
Fine	Total Range (1967 - 2011)	Linear Regression	$\log C_{ss} = 1.569 + 0.713 * \log Q$	0.55	0.61
		LOESS	-	-	0.59
	1967 - 1979	Linear Regression	$\log C_{ss} = 1.896 + 0.634 * \log Q$	0.56	0.57
		LOESS	-	-	0.56
	1980 - 89, 1994 - 2011	Linear Regression	$\log C_{ss} = 1.326 + 0.651 * \log Q$	0.6	0.43
		LOESS	-	-	0.42
1990 - 1993	Linear Regression	$\log C_{ss} = 2.233 + 0.850 * \log Q$	0.45	0.78	
Sand	Total Range (1967 - 2010)	Linear Regression	$\log C_{ss} = 0.726 + 0.920 * \log Q$	0.69	0.60
		LOESS	-	-	0.55
	1967 - 1986	Linear Regression	$\log C_{ss} = 0.670 + 0.947 * \log Q$	0.70	0.60
		LOESS	-	-	0.52
	1987 - 2010	Linear Regression	$\log C_{ss} = 0.228 + 1.125 * \log Q$	0.71	0.53
		LOESS	-	-	0.48

**Annual Water Yield<sup>c</sup> ~ Precipitation<sup>d</sup> Linear Regression and LOESS Rating Curves**

Dependent Var.	Temporal Zone <sup>a</sup>	Model	Model Equation	R <sup>2</sup>	RMSE <sup>b</sup>
Water Yield	Total Range (1931 - 2011)	Linear Regression	$\log W_y = 5.11 * \log P - 8.22$	0.75	0.45
		LOESS	-	-	0.42
Water Yield	1967 - 2011	Linear Regression	$\log W_y = 4.93 * \log P - 7.90$	0.79	0.42
		LOESS	-	-	0.41

<sup>a</sup>All years reported as water years, beginning on October 1 of the previous year and running through September 30 of indicated year.

<sup>b</sup>Indicates root mean squared error (RMSE) values for the entire model. All RMSE values reported in log units.

<sup>c</sup>Annual water yield in units of  $10^5 \text{ m}^3$  at USGS station 'Salinas River near Spreckles' ID# 11152500, referred to here as 'S1'.

<sup>d</sup>Annual precipitation in units of cm from NOAA gauge 'Big Sur State Park' (BGS).

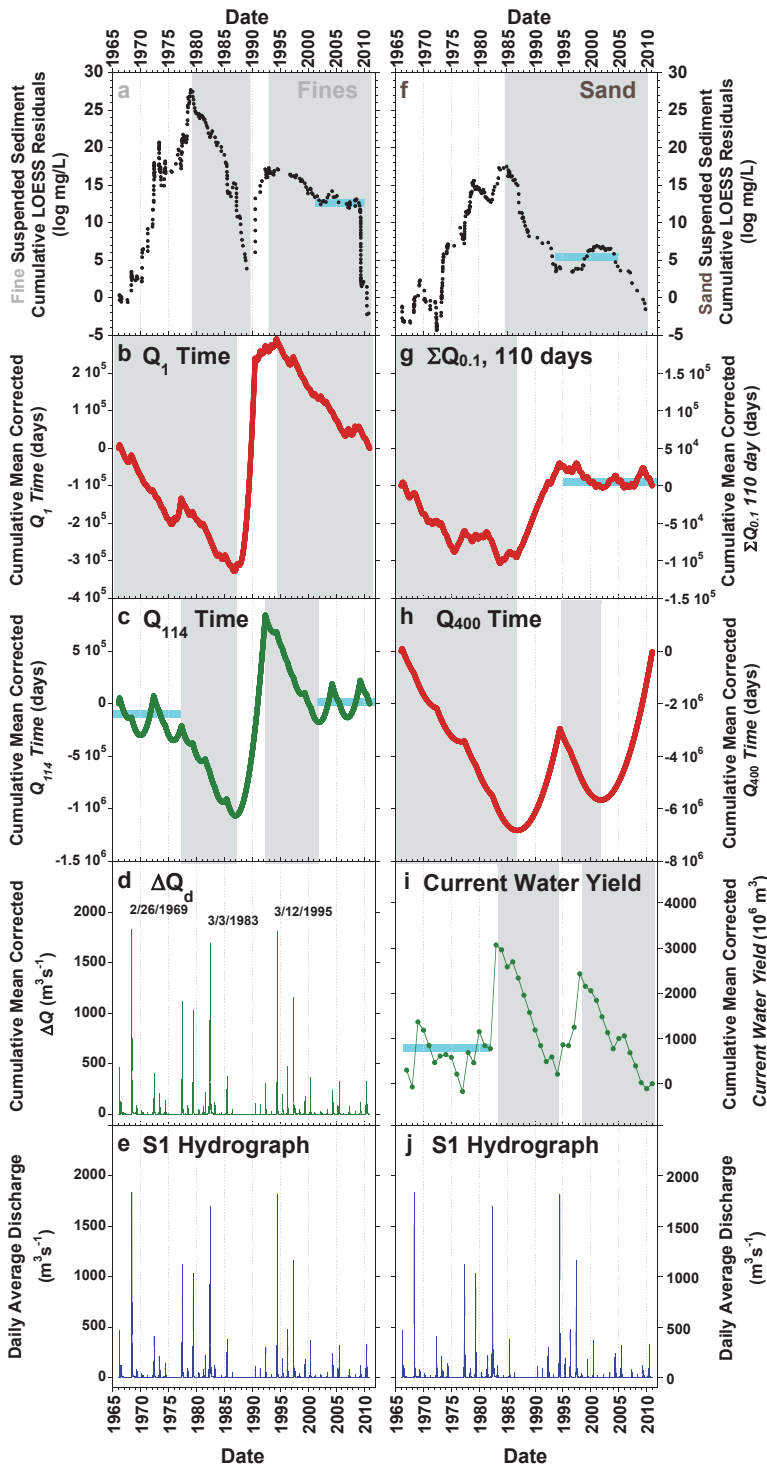


**Figure 3.3** Plots of (a) fine and (f) sand LOESS residuals sequentially summed over time. (b–d, g–i) Arrayed beneath each sediment class are the sequential sums of the mean corrected hydrologic variables found to exert significant control at the event to inter-annual scale, and (e,j) the daily discharge hydrograph at gauge S1. Gray shading indicates zones of persistent low residual values, un-shaded zones are positive, and relatively stable periods are highlighted with light blue bars. The dates of the three highest discharge events during the suspended sediment record are indicated on the (e) hydrograph.

The two hydrologic factors that negatively affected sand concentration calculations,  $\sum Q_{0.1}$  with a 110 day counting window, and  $Q_{400}$  Time, also displayed a transition from persistent low to high values around the mid-1980s, with transition placement  $\sim 1987$  (Fig. 3.3f,g). The behavior of  $\sum Q_{0.1, 110 \text{ day}}$  was generally stable after the end of the positive excursion ( $\sim 1995$ ), while  $Q_{400}$  Time went through another cycle of persistent low (1995–2002) and high (2002–2011) values. *Current water yield*, the hydrologic factor that exerted a positive effect in the sand, exhibited a relatively stable period between 1967 and 1979, followed by a wetter period from 1979–1983, a prolonged dry period from 1983–1994, and brief wet interval from 1994–1998, and another prolonged dry period from 1998–2011 (Fig. 3.3i).

In summary, the early portion of the suspended sediment record, from 1967 to mid-1980s, was characterized as hydraulically active with most days experiencing lower than average elapsed time since the last  $Q \geq 1, 114, \text{ and } 400 \text{ m}^3\text{s}^{-1}$ , and lower sums of previous very low to no flow days ( $Q \leq 0.1 \text{ m}^3\text{s}^{-1}$ ). Four of the six hydrologic events with peak  $Q > 1000 \text{ m}^3\text{s}^{-1}$  also occurred during this period (Fig. 3.3e,j). This was followed by a very dry period that extended from the mid-1980s to the mid-1990s, with very little water flux through the lower Salinas River from 1988–1990 and no  $Q > 114 \text{ m}^3\text{s}^{-1}$  events until 1993. The period of the mid-1990s to present began with two large events, including the flood of 1995, which ushered in a short wet period that ended in the late 1990s, after which water yields and peak hydrologic events were generally low.

The period of persistent high fine sediment concentrations from 1967 to 1980 coincided with a period of persistently low  $Q_1$  Time values, and relatively constant  $Q_{400}$  Time values. Both periods of persistent low fine sediment concentration generally coincided with periods of persistent low  $Q_{114}$  Time values. The second period of low fine sediment concentration (1993–2011) also experienced a period of stable concentrations that coincided with a return to relatively constant  $Q_{114}$  Time values. However this period of stable concentration was followed by a return to persistent low concentrations, despite persistently low  $Q_1$  Time and stable  $Q_{114}$  Time values. The long dry interval spanning the late 1980s through the early 1990s lined up with the positive excursion of fine suspended sediment concentration in the early 1990s. This dry period also resulted in persistent increases in both  $Q_1$  Time and  $Q_{114}$  Time sums.

The mid-1980s transition to drought also marked the transition in persistent excess sand concentration from positive to negative. However, subsequent transitions to wetter periods did not result in a break in persistent negative sand concentrations, although a small, contemporaneous positive excursion was observed (Fig. 3.3f).

The effects of ENSO activity on lower Salinas River discharge history were most evident for higher discharge events. Of 78 events with  $Q \geq 400 \text{ m}^3\text{s}^{-1}$  since 1950, 74 occurred during El Niño years, with most ( $n = 55$ ) occurring during stronger ( $\text{ONI} > 1$ ) El Niño years, including in 1969, 1983 and 1995 (Figs. 3.4, 3.5a). Moderate flows ( $Q \geq 100$  and  $> 200 \text{ m}^3\text{s}^{-1}$ ) mostly occurred during El Niño years (Figs. 3.4, 3.5b,c), while the number of days with  $Q_d \geq 1 \text{ m}^3\text{s}^{-1}$  and the sum of low flow ( $Q_d \leq 0.1 \text{ m}^3\text{s}^{-1}$ ) days as well as annual precipitation were insensitive to El Niño cycles (Figs. 3.4, 3.5d,e,f). Of note is the fact that during many El Niño years the lower Salinas River did not experience any high or moderate flows. Thus the El Niño cycle can be considered a condition of increased high flow frequency or risk, which is in agreement with the findings of Farnsworth and Milliman (2003).

Monotonic temporal trends in ( $C_{SSf} \sim Q$ ) and ( $C_{SSs} \sim Q$ ) residuals from 1967 – 2011 were found to be negative for all four tests, with two-sided  $p$ -values well below 0.05 (Table 3.2, Fig. 3.6). The  $Wy - P$  relationships for 1931–2011 and 1967–2011 showed decreasing trends, though most were not statistically significant (Table 3.2, Fig. 3.7). The longer  $Wy - P$  dataset showed some indication of a decreasing trend in water yield, as the fully parametric test (linear regression of linear regression residuals) and the fully nonparametric test (Mann-Kendall analysis of LOESS residuals) yielded decreasing trends with  $p$  values slightly below 0.05 (Fig. 3.7a). This was expected due to the emplacement of dams in the mid-20<sup>th</sup> century. None of the tests for temporal trends in the 1967–2011 subgroup of ( $Wy \sim P$ ) residuals showed temporal trends that were statistically significant (Fig. 3.7b). Thus there was no significant multi-decadal scale change in the ( $Wy \sim P$ ) relationship over the period of suspended sediment record (1967 – 2011).

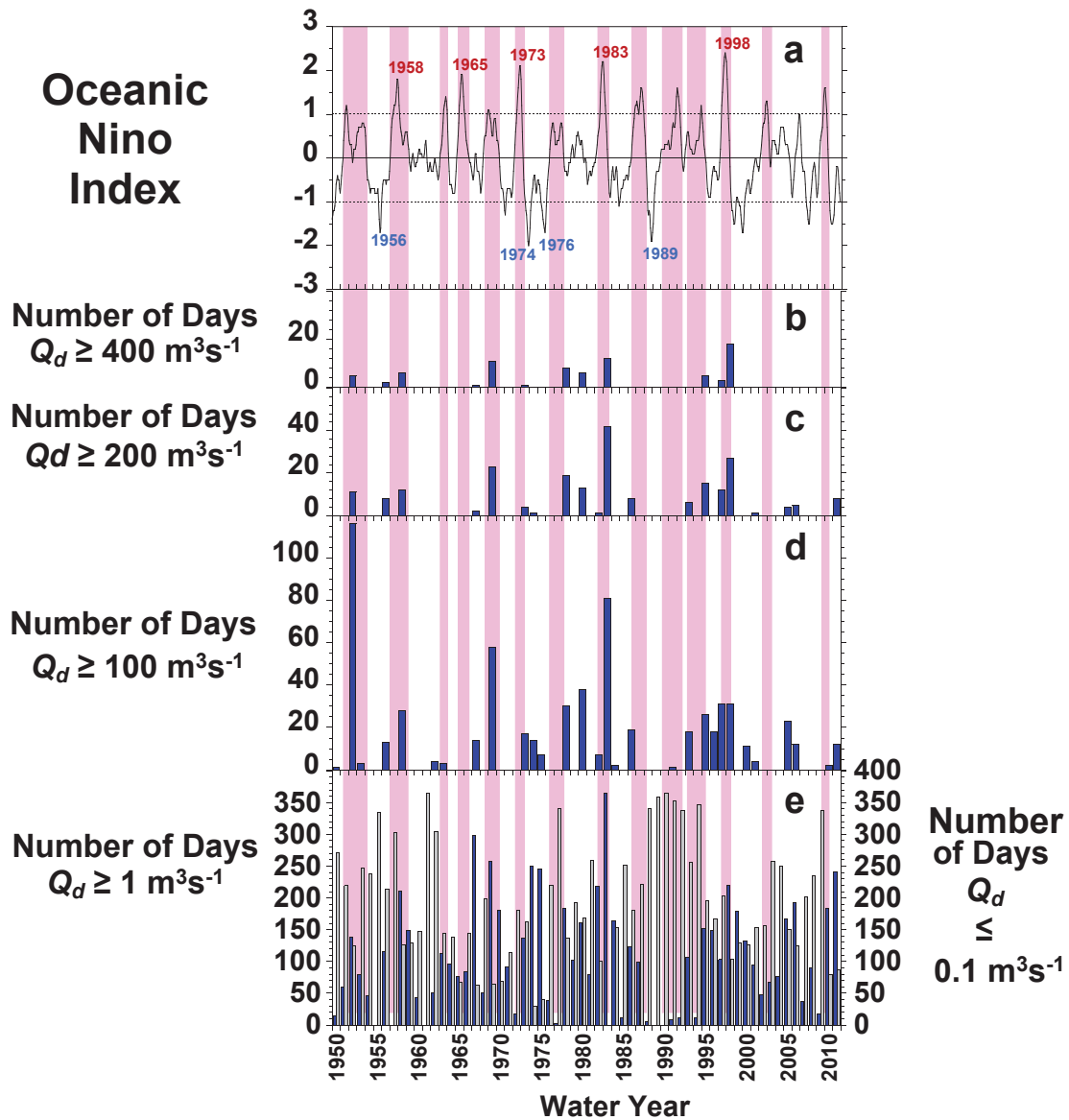


**Figure 3.4** El Niño and lower Salinas discharge events: (a) Oceanic Niño Index (ONI) plotted as a 3 month running mean of sea surface temperature anomaly in the Niño 3.4 region; (b,c,d,e) The number of days when daily discharge ( $Q_d$ ) was  $\geq 400$ , 200, 100, 1  $\text{m}^3\text{s}^{-1}$ , or  $\leq 0.1 \text{ m}^3\text{s}^{-1}$  respectively, by water year. Plot (a) is offset to accommodate the water year abscissa for plots (b) through (e). Shaded zones mark strong to moderate El Niño years, with upper years in plot (a) identifying strong El Niño years and lower years indicating strong La Niña years.

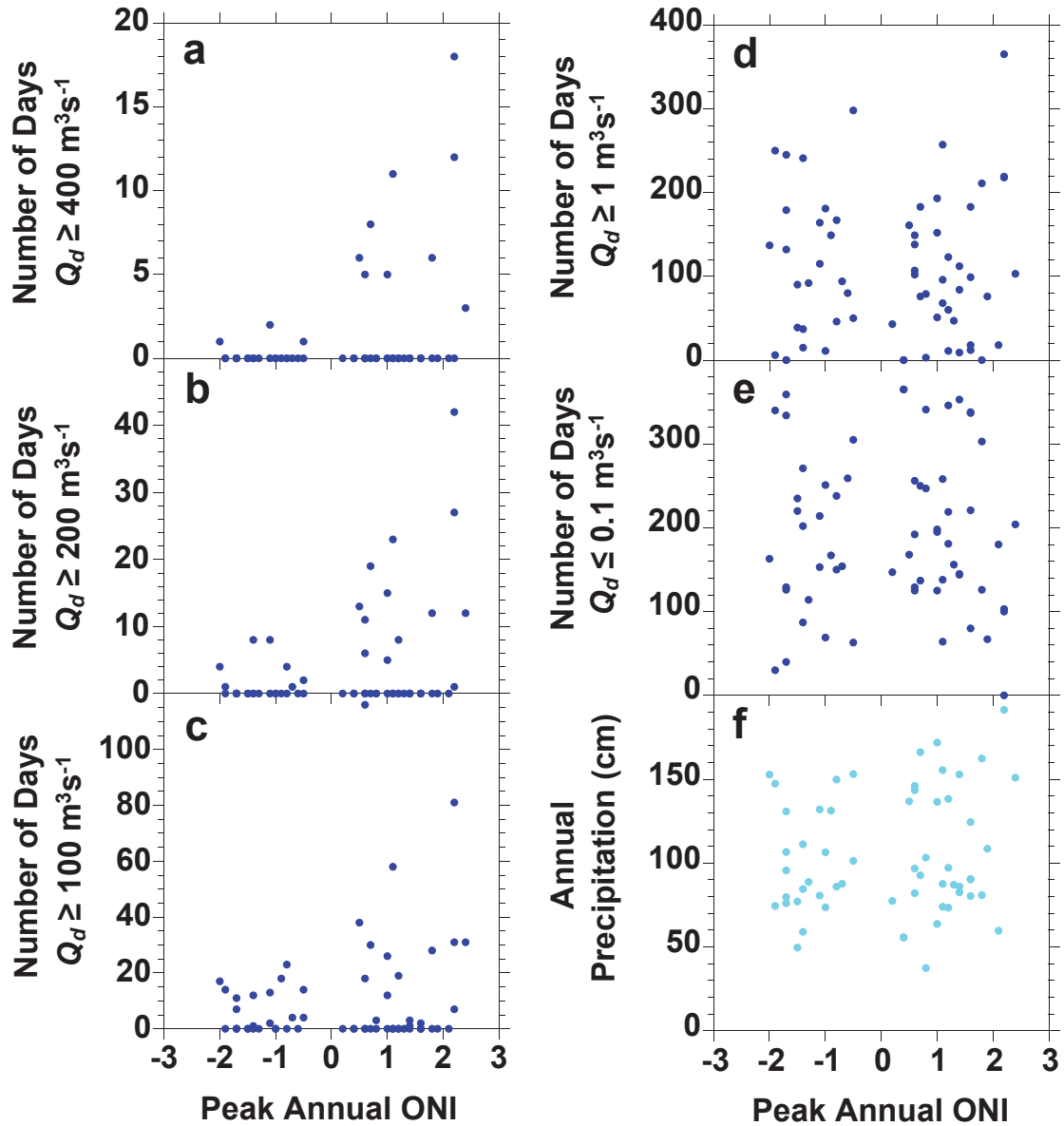


**Figure 3.5** The lower Salinas River gauge S1 annual sum of days with daily discharge greater than or equal to (a) 400, (b) 200, (c) 100, (d) 1  $\text{m}^3\text{s}^{-1}$ , (e) less than or equal to 0.1  $\text{m}^3\text{s}^{-1}$  vs, and (f). annual precipitation at the NOAA Big Sur State Park (BGS) gauge vs. peak annual Ocean Niño Index (ONI).

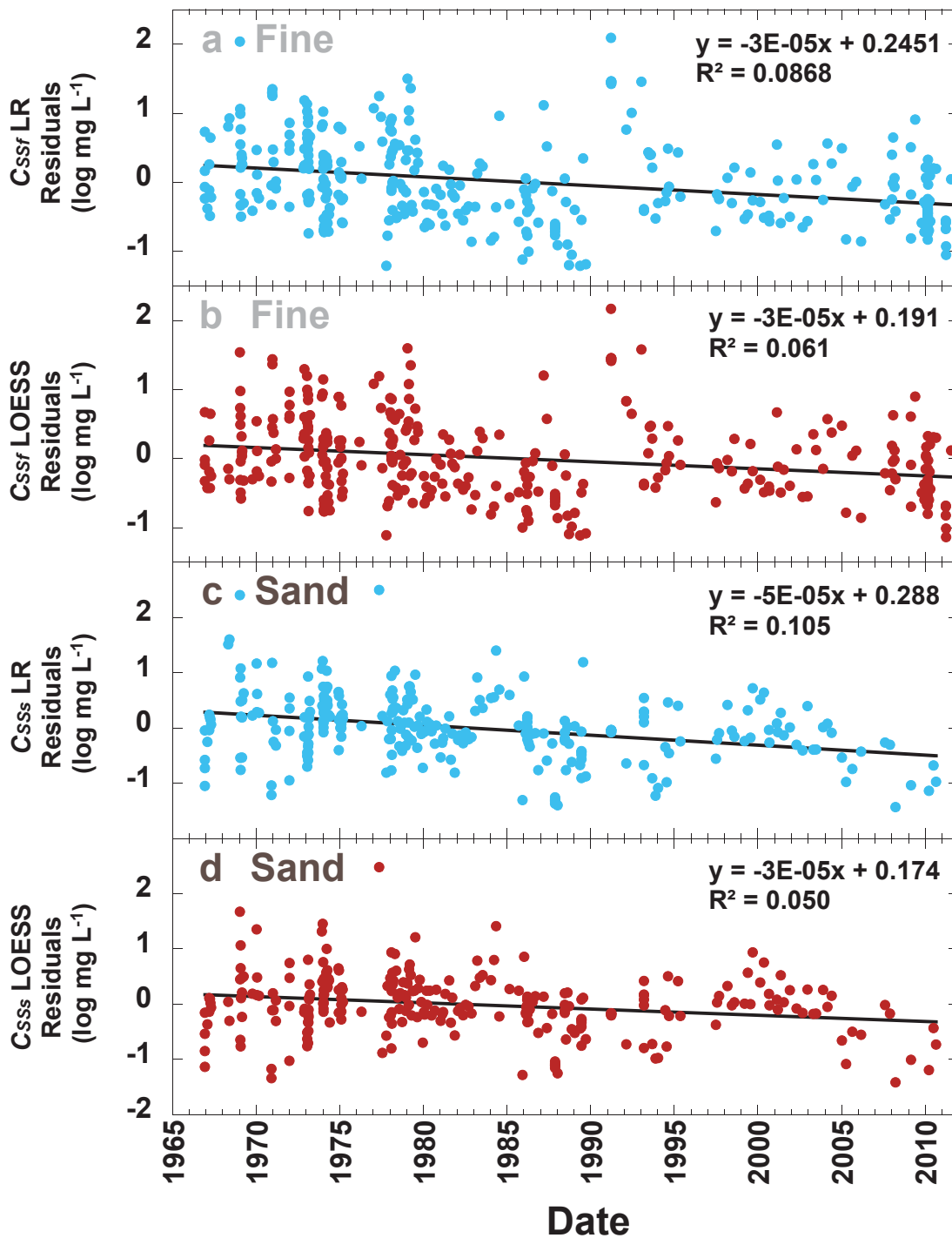


**Figure 3.6** (a, b) Fine and (c, d) sand sized suspended sediment (a, c) log linear regression residuals and (b, d) LOESS  $C_{SS} \sim Q$  residuals plotted over time with fitted linear temporal trend estimations.

**Table 3.2** Temporal Trends

Temporal Range	Relationship	Test	Kendall tau	Kendall P-value	LR Coeff.	LR R <sup>2</sup>	LR P-value
1967-2011	Fine Sediment ( $C_{ssf} \sim Q$ )	LR residuals	-0.23	2.3E-10	-3.0E-05	0.09	5.0E-08
1967-2011		LOESS residuals	-0.20	1.7E-07	-3.0E-05	0.06	5.9E-06
1967-2010	Sand ( $C_{sss} \sim Q$ )	LR residuals	-0.22	5.7E-08	-5.0E-05	0.11	3.2E-08
1967-2010		LOESS residuals	-0.14	6.3E-04	3.1E-05	0.050	1.8E-04
1931-2011	$Wy \sim P$	LR residuals	-0.03	0.72	-4.2E-03	0.05	0.05
1931-2011		LOESS residuals	-0.18	0.02	-3.4E-03	0.04	0.09
1967-2011		LR residuals	-0.10	0.34	-4.9E-03	0.03	0.32
1967-2011		LOESS residuals	-0.12	0.29	-4.2E-03	0.02	0.35

Temporal trend statistics for suspended sediment concentration - discharge and water yield - precipitation relationships in the lower Salinas River. Fine sediment is defined as particles with a diameter (D) < 62.5  $\mu\text{m}$ . Sand is defined as 62.5  $\leq$  D  $\leq$  2000  $\mu\text{m}$ . LR = linear regression,  $C_{ssf}$  = fine suspended sediment concentration,  $C_{sss}$  = sand suspended sediment concentration, Q = discharge, Wy = water yield, P = precipitation.

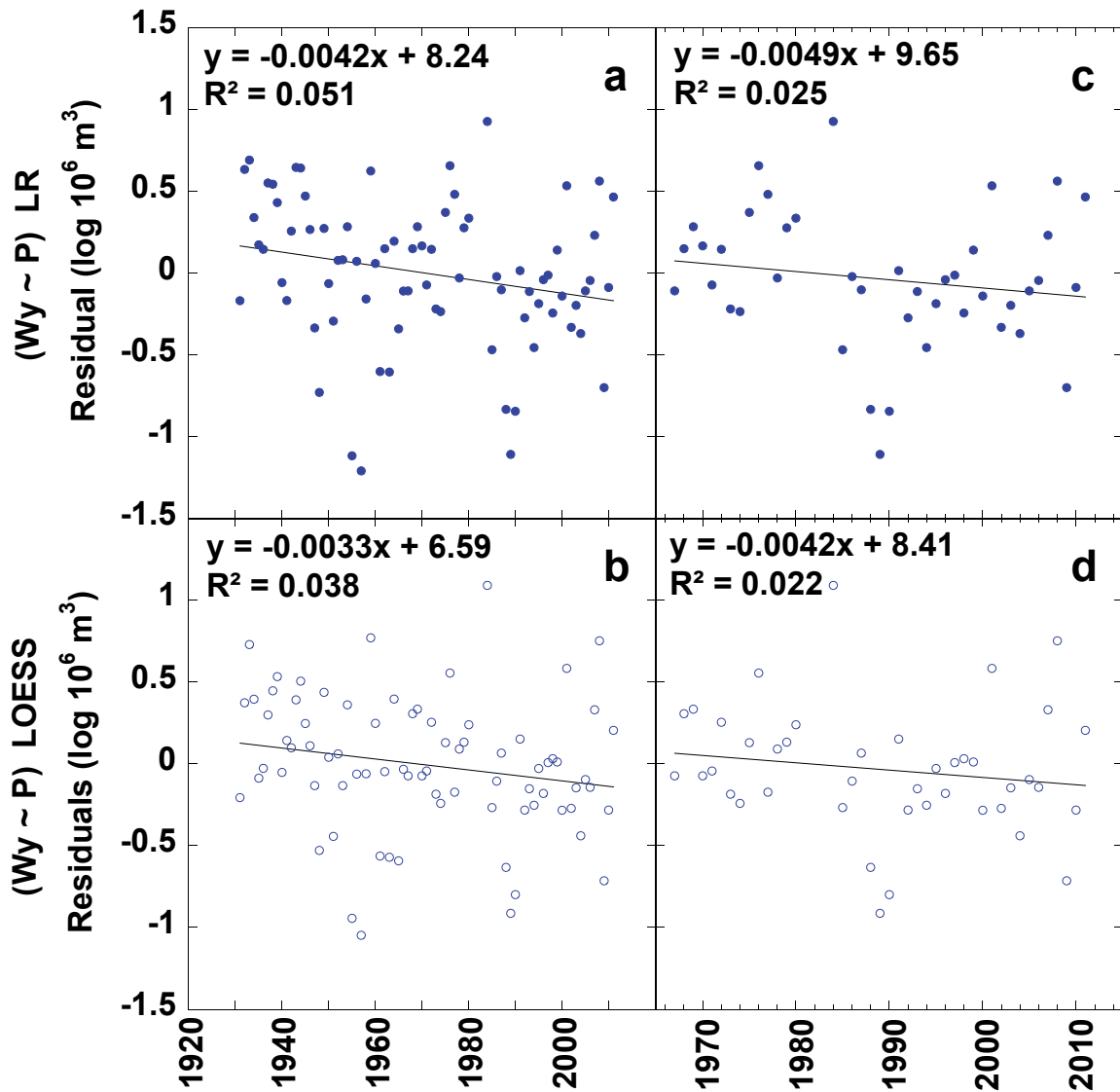


**Figure 3.7** Water yield ~ precipitation residuals (a, b) plotted over the period of discharge measurement at S1 on the lower Salinas River (1930–2011), and (c, d) the period of record for suspended sediment (1967–2011). Residuals were derived from (a, c) linear regression, and (b, d) LOESS curves.

### 3.6 Discussion

Persistent decadal scale fluctuations in positive and negative suspended sediment excursions from expected, discharge-controlled values occurred for fine and sand fractions between water years 1967 and 2011. Decadal scale patterns in antecedent hydrologic conditions appeared to match the observed persistence in suspended sediment behavior in some cases, particularly for fines before the early-2000s and sand over the entire sample period. ENSO activity does not appear to be responsible for most of the antecedent hydrologic precondition characteristics that influence suspended sediment behavior, with the exception of increases in sand supply after larger events ( $Q > \sim 10x Q_{mean}$ ) and the flushing of fine sediment by moderate discharge events ( $10\text{--}20x Q_{mean}$ ). Slight decreasing multi-decadal trends in both fine and sand sediment behavior between 1967 and 2011 do not appear to have been affected by changes in the water yield – precipitation relationship.

Furthermore, no high discharge event triggers were found for interannual to decadal scale alterations in suspended sediment behavior. This was not surprising for fine sediment, as Gray et al. (2014) found no relationship between the timing of large discharge events and fine sediment behavior in the lower Salinas River. Recent large discharge events had been found to increase sand concentrations, but apparently these events did not lead to decadal scale shifts in sand behavior. Extreme flooding events have been shown to exert interannual to inter-decadal effects on suspended sediment behavior in other river systems (Syvitski et al, 2000; Smith et al., 2003; Warrick et al., 2013). For example, Warrick et al. (2013) found that the large 1965 floods resulted in very high  $C_{SS}$  states in northern California rivers and that these states decayed for years thereafter, leading to inter-decadal, negative trends in  $C_{SS}$  residuals. Other systems have also shown this decaying sediment augmentation associated with extreme events (e.g. Morehead et al., 2003). These effects are often found in systems with large tracts of steep, unstable hillslopes prone to mass wasting (Korup, 2012), such as the Eel River of Northern California (Brown and Ritter et al., 1971). In these cases, large, high-intensity precipitation events can speed up existing slides, trigger new slides, and initiate or expand gully style drainage of the resulting land surface scars, while high river discharge can truncate landslide snouts that reach the valley floor and cause further increases in downslope transport of sediment (Kelsey, 1980). In contrast, the Salinas basin

is underlain by more stable bedrock and is not subject to the level of mass wasting found in the Eel River watershed (Nutter, 1901).

The lack of evidence for persistent effects of large floods on sediment behavior in the lower Salinas River may also be due to the fact that no 'extreme' events were captured during the period of suspended sediment sampling. The two largest hydrologic events during 1967–2011 occurred in 1969 and 1995 and produced peak discharges on the order of  $1800 \text{ m}^3\text{s}^{-1}$ , which translates to a return period of only  $\sim 20$  years. In contrast, the 1964 event on the Eel River was estimated to be a 200–400 year flood (Brown and Ritter, 1971; Sloan et al. 2001). Although sediment concentrations were generally high in the lower Salinas River after the 1969 event, they were also high for the few years sampled before it, while the 1995 event was in a period of low  $C_{SS}$ , which did not appear to be altered by the passing of this moderately large flood (see Fig. 3.4).

More moderate discharge magnitudes appear to have a larger bearing on decadal scale suspended sediment behavior than floods in the lower Salinas River. Time series of more moderate in-channel flows experienced by the Salinas River expressed persistent behavior over time scales similar to that of suspended sediment (i.e. interannual to decadal, see Fig. 3.4). These flow magnitudes have been shown to exert statistically significant effects on suspended sediment behavior (Gray et al., 2014). Indeed, decadal scale patterns in hydrologic variable states seemed to reveal a simple and consistent underpinning for the patterns in sand behavior (see Fig. 3.3). Wetter conditions prevailed in the early part of the record (late 1960s to mid-1980s), which led to persistent low values in hydrologic variables shown to have negative effects on  $C_{SSs}$ , and relatively stable to positive values for variables shown to have positive effects. This temporal zone coincides with that of high sand concentrations, which supports the notion that hydrologic preconditions could be the major factor controlling the behavior of  $C_{SSs}$ . A shift to dry conditions around the mid-1980s led to generally high values in variables with 'negative' forcing, and low values of variables with 'positive' forcing. This coincides with the onset of the negative period of sand sediment behavior, which ran from the mid-1980s to the end of sampling in 2010. A short wet period in the late 1990s also coincides with a minor period of positive sand activity in this otherwise negative period. Thus, interannual to decadal scale patterns in sand behavior seems to be controlled in part by decadal scale basin wetness and the frequency of moderate to large hydrologic events.

The relationship between fine suspended sediment and hydrologic preconditions was more complicated, but also generally consistent (see Fig. 3.3). The two hydrologic variables that expressed decadal scale persistence,  $Q_1$  Time, which decreases  $C_{SSf}$  through time, and  $Q_{114}$  Time, which increases  $C_{SSf}$  through time (Gray et al., 2014), follow similar patterns of persistent deviation from their respective mean states. The third variable used in this study,  $\Delta Q_d$ , operated at the event scale and did not exhibit interannual or decadal scale persistent behavior. In this case the decadal scale variability in fine sediment behavior seems to display a distinct sensitivity to  $Q_{114}$  Time rather than  $Q_1$  Time. Persistent periods of low  $Q_{114}$  Time generally coincided with periods of low fine sediment concentration, while stable or high values of  $Q_{114}$  Time generally coincided with periods of stable or high fine sediment concentration. In contrast, shifts in fine sediment behavior do not appear to be sensitive to the persistent patterns of the negative controls exerted by  $Q_1$  Time. Thus, depletion of subsequent fine sediment concentrations by moderate ( $100\text{--}200\text{ m}^3\text{s}^{-1}$ ) ‘flushing’ flows, appears to exert a larger control on the decadal scale behavior of fine sediment than the timing of very low ( $1\text{ to }4\text{ m}^3\text{s}^{-1}$ ) flows. However, a notable discrepancy is apparent at the end of the record, as persistent low fine sediment concentrations continue despite stable  $Q_{114}$  Time values.

But how do flows of these low to moderate magnitudes respond to regional climate controls? The large infrequent flood events ( $Q \geq 40x Q_{mean}$ ) that transport the majority of the sediment through the Salinas River (Farnsworth and Milliman, 2003) occur almost exclusively during El Niño years (see Fig. 3.6). Short elapsed time, from days to years, since the last moderate to high discharge event has been shown to increase sand concentrations in the lower Salinas River (Gray et al, 2014). In contrast, this study found that moderate Q peaks ( $100\text{--}200\text{ m}^3\text{s}^{-1}$ , or  $\sim 10\text{--}20 Q_{mean}$ ), which act as a flushing function on fine suspended sediment supplies, were only slightly influenced by El Niño activity. Furthermore, neither total precipitation nor low flow days were influenced by El Niño. Therefore, ENSO cycles appear to increase total  $C_{SS}$  by augmenting sand sediment supply due to closer timing of high peak Q’s, while fine suspended sediment behavior remains relatively insensitive to ENSO cycles. This finding suggests that ENSO cycles lead to increases in suspended sediment flux through increased frequency of high discharge events that move much of the sediment through the Salinas Basin (Farnsworth and Milliman,

2003; Wheatcroft et al., 2010). Furthermore, ENSO cycles enhance this effect by augmenting sand rating curves.

Slightly negative, multi-decadal trends in both fines and sand were found over the period of record (see Fig. 3.7). Decadal scale patterns in behavior are implicated in these longer scale trends, as the sampling period began with positive, and ended with negative zones of persistent behavior for both texture classes. Multi-decadal trends in suspended sediment behavior are often attributed to anthropogenic changes to the land surface (Kallache et al., 2005, Walling, 2006), including urbanization (Espey, 1969; Hollis, 1975; Trimble, 1997; Warrick and Rubin, 2007), agricultural practices (Walling and Fang, 2003; McHugh et al., 2008, Deasy et al., 2009), and channel modification (Vorosmarty et al., 2003; Willis and Griggs, 2003). Very little change in proportional urban area has occurred in the Salinas basin (California Department of Conservation, 2013), and the major damming projects of the upper Salinas River mainstem and tributaries were already in place years before the initiation of sediment monitoring (SRCMP, 2009). Furthermore, no significant change was observed in the relationship between precipitation and discharge from 1967 – 2011 (see Fig. 3.7), which is one of the major mechanisms related to changing sediment – discharge behavior with urbanization and channel modification (Willis and Griggs, 2003; Warrick and Rubin, 2007).

However, agricultural intensity increased over this period and irrigation practices shifted from sprinkler and furrow to drip irrigation (Monterey County, 2013). This change in agricultural technology may have contributed to the negative trends in suspended sediment concentration, and the prolonged negative zone of fine sediment behavior from the mid-1990s to 2011. Wildfire may also be at play, as Warrick et al. (2012) found that sediment flux from the Arroyo Seco, a major subbasin of the Salinas River, was highly controlled by wildfire and large precipitation event sequences. Further investigation would be required to explicitly link agricultural practices and wildfire activity to the suspended sediment behavior patterns observed here.

### 3.7 Conclusions

The lower Salinas River displayed decadal scale persistence in the suspended sediment – discharge behavior of fine and sand sized suspended sediment. Fine sediment displayed two couplets of alternating positive/negative periods of behavior, while sand exhibited only one positive and one negative period.

These patterns of suspended sediment behavior appear to have been caused in part by decadal scale persistence in hydrologic conditions. The initial positive periods of both fine and sand behavior occurred during a hydrologically active period when low to moderate discharge events were frequent (1967 – 1980). Sand transitioned to its negative period with the transition to less hydrologically active conditions, and has remained in this state through the rest of the record. Transitions between positive and negative periods of persistent fine sediment behavior were consistently correlated with persistent patterns in the positive effect of longer elapsed time since moderate ( $\sim 10x Q_{mean}$ ) flows. This generally swamped out the negative effects on fine sediment concentration exerted by longer elapsed times since very low ( $\sim 1/10x Q_{mean}$ ) flows. This suggests that a flushing function associated with moderate discharges ( $10\text{--}20x Q_{mean}$ ) is a dominant control on interannual to decadal scale fine sediment behavior in the lower Salinas River.

A minimal effect was found for ENSO cycles on these hydrologic conditions, and by extension suspended sediment behavior at decadal scales. Positive ENSO periods led to increases in the frequency of moderate to large events, with an increase in effect found between moderate ( $Q = 10 - 20x Q_{mean}$ ) and large ( $Q \geq 40x Q_{mean}$ ) events. The lack of effect on drought/small discharge magnitude frequency and weak control on moderate discharge frequency suggests that ENSO plays a small role in modulating decadal scale fine sediment behavior. However, increased sand concentration due to large discharge events suggested that positive ENSO phases do augment sand concentration.

Finally, inconsistencies in decadal scale behavior of fine sediment vis-à-vis hydrologic conditions implied that additional, unstudied factors are at play. This notion is supported in part by overall negative trend in both fine and sand suspended sediment concentrations. Future mechanistic studies of land

scape forcing factors are required to address this issue, with particular regard to agricultural practices – the largest anthropogenic influence in the basin.

### 3.8 References

- Abraham CE. 1969. Suspended sediment discharges in streams. U.S. Army Corps of Engineers. Hydrologic Engineering Center. Davis, CA. Technical Paper 19, 10 pp.
- Andrews ED, Antweiler RC. 2012. Sediment Fluxes from California Coastal Rivers: The Influences of Climate, Geology, and Topography. *Journal of Geology* **120**: 349-366
- Andrews ED, Antweiler RC, Neiman PJ, Ralph FM. 2004. Influence of ENSO on flood frequency along the California coast. *Journal of Climate* **17**: 337-348
- Ankers C, Walling DE, Smith RP. 2003. The influence of catchment characteristics on suspended sediment properties. *Hydrobiologia* **494**: 159-167
- Batalla RJ, Vericat D. 2009. Hydrological and sediment transport dynamics of flushing flows: implications for management in large Mediterranean rivers. *River Research and Applications* **25**: 297-314
- Bogen J, Bonsnes TE. 2003. Erosion and sediment transport in High Arctic rivers, Svalbard. *Polar Research* **22**: 175-189. DOI: 10.1111/j.1751-8369.2003.tb00106.x.
- Brasington J, Richards K. 2000. Turbidity and suspended sediment dynamics in small catchments in the Nepal Middle Hills. *Hydrological Processes* **14**: 2559-2574
- Brown WM, Ritter JR. 1971. Sediment transport and turbidity in the Eel River Basin, California: U.S. Geological Survey Water-Supply Paper 1986, 67pp.
- Bull LJ. 1997. Relative velocities of discharge and sediment waves for the River Severn, UK. *Hydrological Sciences Journal-Journal Des Sciences Hydrologiques* **42**: 649-660
- California Department of Conservation. 2013. Monterey County land use data. (last accessed 12/2013) <http://www.conservation.ca.gov/Index/Pages/Index.aspx>.
- Carson MA, Taylor CH, Grey BJ. 1973. Sediment production in a small Appalachian watershed during spring runoff - Eaton-Basin, 1970-1972. *Canadian Journal of Earth Sciences* **10**: 1707-1734

- Cleveland WS. 1979. Robust locally weighted regression and smoothing scatterplots. *J. Am. Stat. Assoc.* **74**: 829-836
- Colby BR. 1956. Relationship of sediment discharge to streamflow. U.S. Geological Survey. Reston, VA. Open file report. 170 pp.
- Constantine JA, Pasternack GB, Johnson ML. 2005. Logging effects on sediment flux observed in a pollen-based record of overbank deposition in a northern California catchment. *Earth Surface Processes and Landforms* **30**: 813-821
- de Vente J, Poesen J, Arabkhedri M, Verstraeten G. 2007. The sediment delivery problem revisited. *Progress in Physical Geography* **31**: 155-178
- Deasy C, Brazier RE, Heathwaite AL, Hodgkinson R. 2009. Pathways of runoff and sediment transfer in small agricultural catchments. *Hydrological Processes* **23**: 1349-1358
- Estrany J, Garcia C, Batalla RJ. 2009. Suspended sediment transport in a small Mediterranean agricultural catchment. *Earth Surface Processes and Landforms* **34**: 929-940. DOI: 10.1002/esp.1777.
- Espey WH. 1969. Urban effects on the unit hydrograph. Effects of watershed changes on streamflow (Moore, W. L. and Morgan, C. W., eds.), University of Texas Press, Austin. 215-228.
- Farnsworth KL, Milliman JD. 2003. Effects of climatic and anthropogenic change on small mountainous rivers: the Salinas River example. *Global and Planetary Change* **39**: 53-64
- Farnsworth, KL, Warrick, JA. 2007. Sources, Dispersal, and Fate of Fine Sediment Supplied to Coastal California. U.S. Geological Survey Scientific Investigations Report 2007-5254, Washington, D.C., 77pp.
- Florsheim JL, Pellerin BA, Oh NH, Ohara N, Bachand PAM, Bachand SM, Bergamaschi BA, Hernes PJ, Kavvas ML. 2011. From deposition to erosion: Spatial and temporal variability of sediment sources, storage, and transport in a small agricultural watershed. *Geomorphology* **132**: 272-286. DOI: 10.1016/j.geomorph.2011.04.037.
- Gao P, Pasternack GB, Bali KM, Wallender WW. 2007. Suspended-sediment transport in an intensively cultivated watershed in southeastern California. *Catena* **69**: 239-252. DOI: 10.1016/j.catena.2006.06.002.

- Gray AB, Pasternack GB, Watson EB. 2010. Hydrogen peroxide treatment effects on the particle size distribution of alluvial and marsh sediments. *Holocene* **20**: 293-301
- Gray AB, Warrick JA, Pasternack GB, Watson EB, Gofñi MA. 2014. Suspended sediment behavior in a coastal dry-summer subtropical catchment: effects of hydrologic preconditions. *Geomorphology* **214**: 485-501
- Heidel SG. 1956. The progressive lag of sediment concentration with flood waves. *Trans. Am. Geoph. Union*. **31**: 56-66
- Helsel DR, Hirsch RM. 2002. Statistical methods in water resources—hydrologic analysis and interpretation: U.S. Geological Survey Techniques of Water-Resources Investigations. 510 pp.
- Hicks DM, Gomez B, Trustrum NA. 2000. Erosion thresholds and suspended sediment yields, Waipaoa River Basin, New Zealand. *Water Resour. Res.* **36**: 1129-1142
- Hill PS, Nowell ARM, Jumars PA. 1988. Flume evaluation of the relationship between suspended sediment concentration and excess boundary shear-stress. *Journal of Geophysical Research-Oceans* **93**: 12499-12509. DOI: 10.1029/JC093iC10p12499.
- Hollis GE. 1975. The effect of urbanization on floods of different recurrence interval. *Water Resour. Res.* **11**: 431-434
- Hudson PF. 2003. Event sequence and sediment exhaustion in the lower Panuco Basin, Mexico. *Catena* **52**: 57-76
- Hurst HE. 1951. Long-term storage capacity of reservoirs. *Transactions of the American Society of Civil Engineers* **116**: 770-799
- Hurst HE. 1957. Suggested statistical model of some time series which occur in nature. *Nature* **180**: 494-494
- Inman DL, Jenkins SA. 1999. Climate change and the episodicity of sediment flux of small California rivers. *Journal of Geology* **107**: 251-270
- Kallache M, Rust HW, Kropp J. 2005. Trend assessment: applications for hydrology and climate research. *Nonlin. Proc. in Geophys.* **12**: 201-210

- Kelsey HM. 1980. A sediment budget and an analysis of geomorphic process in the Van-Duzen river basin, north coastal California, 1941-1975 - summary. *Geological Society of America Bulletin* **91**: 190-195
- Korup O. 2012. Earth's portfolio of extreme sediment transport events. *Earth-Science Reviews* **112**: 115-125
- Kuai KZ, Tsai CW. 2012. Identification of varying time scales in sediment transport using the Hilbert-Huang Transform method. *Journal of Hydrology* **420**: 245-254. DOI: 10.1016/j.jhydrol.2011.12.007.
- Lana-Renault N, Regues D. 2009. Seasonal patterns of suspended sediment transport in an abandoned farmland catchment in the Central Spanish Pyrenees. *Earth Surface Processes and Landforms* **34**: 1291-1301
- Lana-Renault N, Regues D, Marti-Bono C, Begueria S, Latron J, Nadal E, Serrano P, Garcia-Ruiz JM. 2007. Temporal variability in the relationships between precipitation, discharge and suspended sediment concentration in a small Mediterranean mountain catchment. *Nordic Hydrology* **38**: 139-150
- Lawrence A, Kottegoda N. 1977. Stochastic modelling of river-flow time series, *J. R. Stat. Soc.* **140**: 1-47
- Lenzi MA, Marchi L. 2000. Suspended sediment load during floods in a small stream of the Dolomites (northeastern Italy). *Catena* **39**: 267-282
- Mano V, Nemery J, Belleudy P, Poirel A. 2009. Assessment of suspended sediment transport in four alpine watersheds (France): influence of the climatic regime. *Hydrological Processes* **23**: 777-792
- Marcus WA. 1989. Lag-time routing of suspended sediment concentrations during unsteady-flow. *Geological Society of America Bulletin* **101**: 644-651. DOI: 10.1130/0016-7606(1989)101<0644:ltross>2.3.co;2.
- McHugh AD, Bhattarai S, Lotz G, Midmore DJ. 2008. Effects of subsurface drip irrigation rates and furrow irrigation for cotton grown on a vertisol on off-site movement of sediments, nutrients and pesticides. *Agronomy for Sustainable Development* **28**: 507-519
- McLeod AI. 2011. Package 'Kendall.' Kendall rank correlation and Mann-Kendall trend test. CRAN. Classification/MSB 62M10, 91B84. <http://www.stats.uwo.ca/faculty/aim>. (last accessed: 10/2013).
- Milliman JD, Syvitski JPM. 1992. Geomorphic/tectonic control of sediment discharge to the ocean: the importance of small mountainous rivers. *Journal of Geology* **100**: 525-544

- Montanari A, Rosso R, Taqqu M. 1997. Fractionally differenced ARIMA models applied to hydrologic time series: Identification, estimation and simulation. *Water Resour. Res.* **33**: 1035-1044
- Monterey County Agricultural Commissioner's Office Crop Reports. 2013.  
<http://ag.co.monterey.ca.us/resources/category/crop-reports> (last accessed 12/2013)
- Morehead MD, Syvitski JP, Hutton EWH, Peckham SD. 2003. Modeling the temporal variability in the flux of sediment from ungauged river basins. *Global and Planetary Change* **39**: 95-110
- Nutter EH. 1901. Sketch of the geology of the Salinas Valley, California. *Journal of Geology*. **9**: 330-336
- Pasternack GB, Brush GS, Hilgartner WB. 2001. Impact of historic land-use change on sediment delivery to a Chesapeake Bay subestuarine delta. *Earth Surface Processes and Landforms* **26**: 409-427
- Paustian SJ, Beschta RL. 1979. Suspended sediment regime of an Oregon Coast Range stream. *Water Resources Bulletin* **15**: 144-154
- Pedatella NM, Forbes JM. 2009. Interannual variability in the longitudinal structure of the low-latitude ionosphere due to the El Nino-Southern Oscillation. *Journal of Geophysical Research-Space Physics* **114**: A12316.
- Pelletier JD, Turcotte DL. 1997. Long-range persistence in climatological and hydrological time series: analysis, modeling and application to drought hazard assessment. *Journal of Hydrology* **203**: 198-208
- R Development Core Team. 2013. R: A language and environment for statistical computing. R Foundation for Statistical Computing, Vienna, Austria. <http://www.R-project.org/> (last accessed: 10/2013).
- Rosenberg LI. and Joseph JC. 2009. Map of the Rinconada and Reliz Fault Zones, Salinas River Valley, California: U.S. Geological Survey Scientific Investigations Map 3059, scale 1:250,000 with pamphlet URL <http://pubs.usgs.gov/sim/3059/>.
- Rouse H. 1937. Modern conceptions of the mechanics of fluid turbulence. *Transactions of the American Society of Civil Engineers* **102**: 463-541
- Rouse H. 1938. Fluid mechanics for hydraulic engineers, Dover, New York, 422 pp.
- Sloan J, Miller JR, Lancaster N. 2001. Response and recovery of the Eel River, California, and its tributaries to floods in 1955, 1964, and 1997. *Geomorphology* **36**: 129-154

- Smith BPG, Naden PS, Leeks GJL, Wass PD. 2003. The influence of storm events on fine sediment transport, erosion and deposition within a reach of the River Swale, Yorkshire, UK. *Science of the Total Environment* **314**: 451-474
- SRCMP (Salinas River Channel Maintenance Program). 2009. Monterey County Water Resources Agency. 81 pp.
- Syvitski JP, Morehead MD, Bahr DB, Mulder T. 2000. Estimating fluvial sediment transport: The rating parameters. *Water Resour. Res.* **36**: 2747-2760
- Thompson JG, Reynolds R. 2002. Cultural evolution and water management in the Salinas River Valley. *Journal of the American Water Resources Association* **38**: 1661-1677
- Tote C, Govers G, Van Kerckhoven S, Filiberto I, Verstraeten G, Eerens H. 2011. Effect of ENSO events on sediment production in a large coastal basin in northern Peru. *Earth Surface Processes and Landforms* **36**: 1776-1788. DOI: 10.1002/esp.2200.
- Trimble SW. 1997. Contribution of stream channel erosion to sediment yield from an urbanizing watershed. *Science* **278**: 1442-1444
- U.S. Geological Survey National Water Information System (USGS NWIS). 2013  
<http://waterdata.usgs.gov/nwis/sw> (last accessed: 03/2013).
- Vorosmarty CJ, Meybeck M, Fekete B, Sharma K, Green P, Syvitski JPM. 2003. Anthropogenic sediment retention: major global impact from registered river impoundments. *Global and Planetary Change* **39**: 169-190
- Walling DE. 1977. Assessing accuracy of suspended sediment rating curves for a small basin. *Water Resour. Res.* **13**: 530-538
- Walling DE. 2006. Human impact on land-ocean sediment transfer by the world's rivers. *Geomorphology* **79**: 192-216
- Walling DE, Fang D. 2003. Recent trends in the suspended sediment loads of the world's rivers. *Global and Planetary Change* **39**: 111-126
- Warrick JA, Mertes LAK. 2009. Sediment yield from the tectonically active semiarid Western Transverse Ranges of California. *Geol. Soc. Am. Bull.* **121**: 1054-1070

- Warrick JA, Rubin DM. 2007. Suspended-sediment rating curve response to urbanization and wildfire, Santa Ana River, California. *Journal of Geophysical Research-Earth Surface* **112**. DOI: F0201810.1029/2006jf000662.
- Warrick JA, Hatten JA, Pasternack GB, Gray AB, Goni MA, Wheatcroft RA. 2012. The effects of wildfire on the sediment yield of a coastal California watershed. *Geological Society of America Bulletin* **124**: 1130-1146. DOI: 10.1130/b30451.1.
- Warrick JA, Madej MA, Goni MA, Wheatcroft RA. 2013. Trends in the suspended-sediment yields of coastal rivers of northern California, 1955-2010. *Journal of Hydrology* **489**: 108-123. DOI: 10.1016/j.jhydrol.2013.02.041.
- Wheatcroft RA, Goni MA, Hatten JA, Pasternack GB, Warrick JA. 2010. The role of effective discharge in the ocean delivery of particulate organic carbon by small, mountainous river systems. *Limnology and Oceanography* **55**: 161-171. DOI: 10.4319/lo.2010.55.1.0161.
- Willis CM, Griggs GB. 2003. Reductions in fluvial sediment discharge by coastal dams in California and implications for beach sustainability. *Journal of Geology* **111**: 167-182
- Wolter K, Timlin MS. 2011. El Nino/Southern Oscillation behaviour since 1871 as diagnosed in an extended multivariate ENSO index (MEI.ext). *International Journal of Climatology* **31**: 1074-1087. DOI: 10.1002/joc.2336.

## Chapter 4

### **Effects of antecedent hydrologic conditions, time dependence, and climate cycles on the suspended sediment load characteristics of the Salinas River, California**

#### **Abstract**

Previous estimations of sediment flux for the Salinas River of central California were based on data collected in the 1970s and used assumptions of time invariant suspended sediment – discharge behavior. The goals of this study were to estimate sediment flux from the Salinas River using data from 1967–2011 by incorporating time dependent behavior and reassess the role of El Niño Southern Oscillation patterns in inter-decadal sediment load. This study builds on previous work that found that time-dependent suspended sediment behavior in this system is controlled in part by antecedent hydrologic conditions. The condition of temporal dependence was further tested herein through comparison of flux estimates obtained through time-dependent formulations and a multivariate approach incorporating hydrologic factors. Longer sampling records and incorporation of decadal scale behavior or antecedent hydrologic conditions resulted in average annual load estimates of 2.1 or 2.4 Mt, in comparison to earlier estimates of ~ 3.3 Mt. Previous overestimation of sediment load is due to the extrapolation of suspended sediment behavior from a decade of high sediment concentrations to the entire record. The majority of suspended sediment was transported by flows of ~ 25–90 times mean discharge depending on transport constituent (fines or sand) and estimation method. Periods of differential suspended sediment behavior changed the relative importance of rare, peak floods due to changes in the relationship of suspended sediment concentration versus discharge. El Niño years dominated the sediment budget by producing on average ten times more sediment than non-El Niño years. Antecedent hydrologic conditions appear to have caused much of the temporal dependence of suspended sediment behavior, until the last 20 years of the record when fine sediment seems to have been further reduced, perhaps due to changes in agricultural practices.

## 4.1 Introduction

Most of the mass flux from terrestrial to oceanic spheres occurs as suspended river sediment, and most suspended sediment is transported by small ( $10$  to  $10^4$  km<sup>2</sup>), high relief rivers (Milliman and Syvitski, 1992). Such rivers are often prone to highly episodic sediment load behavior due to highly variable hydrologic regimes and nonlinear relationships between the supply of sediment and water to the channel. These suspended sediment concentration ( $C_{SS}$ ) – discharge ( $Q$ ) ‘rating’ relationships can also change over time due to changes in the conditions moderating sediment and/or water supply. Thus, accurate, multi-decadal estimates of suspended sediment flux from small rivers is complicated by highly variable behavior over time, the dynamics of which are often poorly described due to a lack of field data.

It has long been recognized that suspended sediment behavior can be dependent on antecedent conditions across a broad domain of temporal scales. Hysteresis, or path dependence, is the most common event scale phenomenon in suspended sediment behavior, whereby different  $C_{SS} - Q$  relationships are observed for the rising and subsequent falling limbs of a given event hydrograph (Williams, 1989). Seasonal effects are also commonly considered, particularly in areas that experience cold winters with prolonged frozen conditions or areas with monsoonal precipitation regimes that may experience sediment exhaustion as the rainy season progresses (e.g. Walling, 1977). More recent studies have also incorporated temporal dependence in suspended sediment rating curves. Interannual to inter-decadal patterns of sediment behavior due to the effects of large flooding events (Kelsey, 1980; Klein and Anderson, 2012; Warrick et al. 2013), wildfire (Shakesby and Doerr, 2006; Warrick et al., 2012) and urbanization (Warick and Rubin, 2007) and combined land use changes (Pasternack et al., 2001) have all been shown to significantly affect decadal to inter-decadal scale suspended sediment flux.

Suspended sediment load is the product of  $C_{SS}$  and  $Q$  over time. Thus the concentration of any given transported constituent (e.g., any grain size fraction) together with the frequency distribution of discharge can be used to understand which flows are most significant for transport for that constituent. Effective discharge  $Q(e)$ , a concept coined by Wolman and Miller (1960), is the magnitude of discharge that produces the most of a given transported constituent over a given period. Effective discharge has been a measure of great interest in a wide range of environmental research including those concerned

with fluvial geomorphic control (Andrews, 1980; Webb and Walling, 1982), terrestrial organic carbon flux to the oceans (Wheatcroft et al., 2010) and suspended sediment load behavior (Nash, 1994; Gao et al., 2007). Another useful method for examining discharge frequency control on water and water-transported constituents is the 'half-load discharge' ( $Q_{1/2}$ ) (Vogel et al., 2003). Whereas  $Q(e)$  is the estimation of the discharge class that transports the most of a given constituent,  $Q_{1/2}$  is the discharge magnitude below which 50% of the constituent is transported over time.

Flood frequency characterizations required for these analyses generally employ techniques that also assume stationarity in annual peak flow time series. However, it is now widely recognized that discharge magnitude/frequency behavior is also prone to non-stationarity, which can be the result of climatic cycles (Potter, 1958; Pelletier and Turcotte, 1997). On the west coast of the United States, El Niño Southern Oscillation (ENSO) cycles have been shown to cause interannual to decadal scale patterns in river discharge behavior due largely to steering of moisture convection from the tropical western Pacific. To account for the effect of climate cycles, peak annual discharge series subdivided by climatic states can be used to assess differences in peak discharge frequency between alternating climatic conditions, such as ENSO phases (Kahana et al., 2002).

The objectives of this study were to investigate the effects of decadal scale suspended sediment behavior, antecedent hydrologic conditions, and ENSO climate cycles on suspended sediment load from the Salinas River in central California as an indicator of small mountainous river behavior in a dry-summer subtropical climate. This work adds to a growing body of international research underscoring the importance of temporal dependence in suspended sediment behavior on multi-decadal sediment flux estimates, and the diversity of mechanisms behind these dependencies.

## 4.2 Study region

The Salinas River drains a ~11,000 km<sup>2</sup> portion of the Central Coast Ranges of California from a maximum relief of ~ 1,900 m with a mean discharge ( $Q_{mean}$ ) calculated from the period of record as 11.6 m<sup>3</sup>s<sup>-1</sup>. The regional climate is dry-summer subtropical, and most annual precipitation originates from winter storms, the largest of which are generally produced during strong El Niño years (Farnsworth and

Milliman, 2003; Andrews et al., 2004). Three dams were emplaced on the mainstem and two major eastern tributaries previous to the initiation of suspended sediment sampling (Fig. 4.1). This study was based on data obtained from the two lowest USGS hydrologic gauging stations in this basin: Salinas River near Spreckels (gauge # 11152500) and Salinas River near Chualar (gauge # 11152300), hereafter referred to as S1 and S2, respectively (Fig. 4.1).

Two previous studies have addressed temporal patterns in lower Salinas suspended sediment load. Inman and Jenkins (1999) conducted a regional scale study on suspended sediment flux from central and southern California coastal rivers with a focus on episodic events and their relationship to regional climate cycles. They found that large events with recurrence intervals of 5 to 10 years dominated sediment transfer from the rivers in this region, including the Salinas, and that multi-decadal scale wet and dry cycles lead to concomitant increases and decreases in suspended sediment flux to the ocean, respectively. Their approach to calculating suspended sediment load utilized a rating curve constructed from data at S1 collected by the USGS from water years 1969–1979, which they applied to monthly averages of daily water discharge from 1944–1995, which resulted in an estimated average annual suspended sediment load of 1.7 Mt/yr. Farnsworth and Milliman (2003) also examined the role of large discharge events in the estimation of total suspended sediment load at S1, and used the same set of S1 USGS data to compute a power law rating curve that was then applied to daily discharge data from 1930–2000 for an average annual suspended sediment discharge of 3.3 Mt/yr.

### **4.3 Experimental overview**

The experimental approach was to estimate independent loads for suspended fine- and sand-sized sediment, each through either (i) a single rating curve based on the entire temporal domain, (b) separate rating curves for each respective period of persistent suspended sediment behavior, or (iii) a multiple linear regression rating curve incorporating the variables describing antecedent hydrologic conditions outlined above. The estimates involving antecedent hydrologic conditions were compared to decadal behavior-based estimates to further assess the role of antecedent conditions in decadal scale

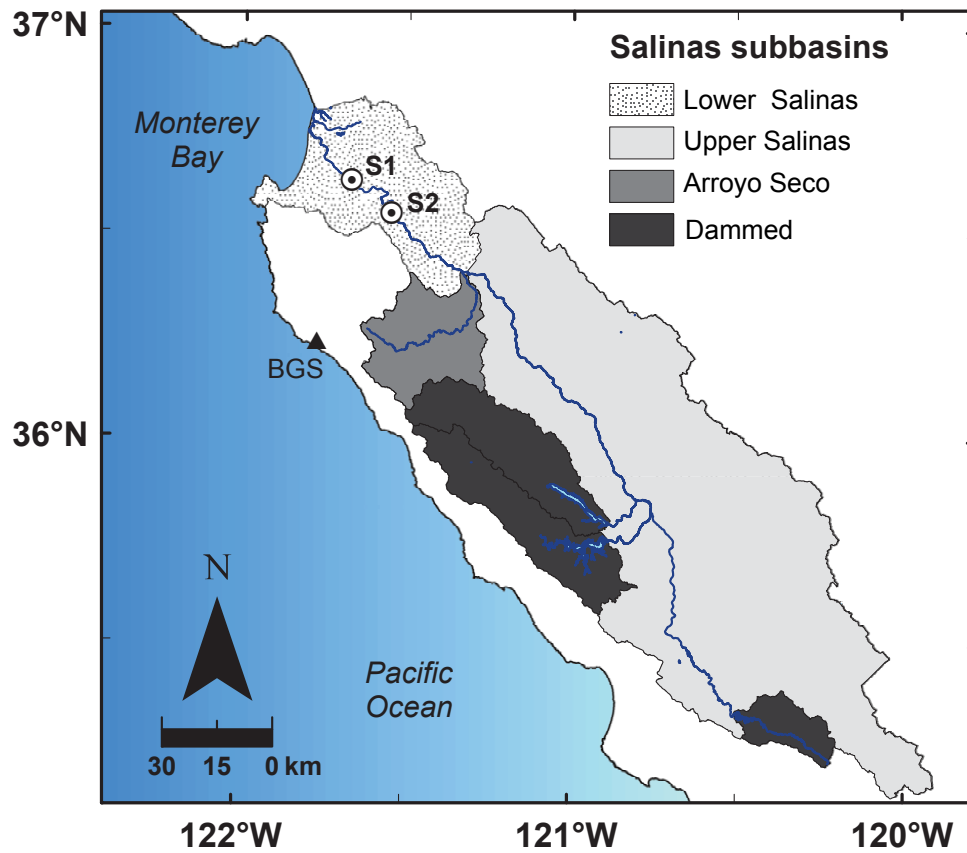


**Figure 4.1** The Salinas River watershed. The locations of USGS hydrologic gauging stations are marked with dotted circles and identification codes. Identification codes S1 and S2 correspond to gauge names: Salinas R. near Spreckels and Salinas River near Chualar (USGS gauge numbers 11152500, 11152300) respectively. The NOAA precipitation gauge is indicated with a black triangle and the label BGS, which stands for gauge names Big Sur State Park.

patterns. All estimates were then placed in the context of ENSO cycles and assessed using magnitude frequency analyses to examine the discharges responsible for moving most of the sediment through the lower Salinas.

#### **4.4 Data**

A brief summary of the data used for this study follows. For in depth reporting on available suspended sediment, water discharge and precipitation data see Chapter 2.

The USGS collected flow-integrated suspended sediment samples from the Salinas at locations corresponding to the S1 and S2 gauges during 1967–2010, while the authors collected near-surface samples during 2008–2011 respectively (USGS NWIS; Chapter 2). Sample associated discharges were instantaneous or computed from linear interpolation of associated 15-minute discharge data. Daily discharge data from S1 were available for 1930–2011 and were used for suspended sediment load calculations. Historic El Niño activity was characterized in this study by (i) the Oceanic Niño Index (ONI), an aggregate measurement of sea surface temperature defects and (ii) the extended Multivariate El Niño Index (MEI.ext), which incorporates the signals of several ENSO indices (Pedatella and Forbes, 2009; Wolter and Timlin, 2011). The National Oceanographic and Atmospheric Administration's three-month running average data for ONI were used for the interval 1950–2011, and MEI.ext for 1931–1950.

#### **4.5 Suspended sediment rating curve development**

Available  $C_{SS}$  and associated  $Q$  data were used to model the dependence of  $C_{SS}$  on  $Q$  for the system (hereafter referred to in the form of  $C_{SS} \sim Q$ ) after log-transformation using (a) linear, (b) LOESS and (c) multiple regression techniques.

##### *4.5.1 Linear regression and LOESS rating curves*

A log-linear sediment rating curve describes the  $C_{SS} \sim Q$  relationship as:

$$\log(C_{SS}) = \log(a) + b \log(Q) + \varepsilon \quad (4.1)$$

where  $a$  is the offset of the linear curve,  $b$  is the slope and  $\varepsilon$  is the error function. To avoid potential bias from the systematically poor fit of log-linear curves previously found for the Salinas River, LOESS rating curves for suspended fines ( $C_{SSf}$ ) and sand ( $C_{SSs}$ ) were also computed, using  $\alpha = 0.75$  and 2<sup>nd</sup> degree polynomials (Cleveland, 1979; Cleveland and Devlin, 1988; Helsel and Hirsch, 2002, Gray et al, in press).

Log-linear and LOESS rating curves constructed for the lower Salinas  $C_{SSf}$  and  $C_{SSs}$  datasets over the entire temporal domain showed that linear curves fail to account for the curvature in the  $C_{SS} \sim Q$  relationship at high and low  $Q$  (Table 4.1, Fig. 4.2). For this reason, LOESS curve residuals (the difference between observed and fitted values) were used to identify periods of high or low  $C_{SS}$  (see below).

#### 4.5.2 Temporally zoned rating curves

Identification of persistent periods of high or low  $C_{SS}$  behavior was established in previous work (Gray, 2014). Determination of which periods exhibited significantly distinct rating curves is accomplished here through ANCOVA analysis. Periods were previously identified on the basis of the local slope of sequentially summed  $C_{SS} \sim Q$  residuals obtained from total temporal domain LOESS curves. Positive or negative behavior was recognized by positive or negative slopes on the sequentially summed residual curves maintained over ranges of residual values  $\geq 3$  times the standard deviation of the residuals (Fig. 4.3). Zones of high  $C_{SSf}$  were identified from 1967–1979, and 1990–1993, with lower concentrations from 1980–1989, and 1994–2011. The  $C_{SSs}$  was persistently high from 1967–1986, and low from 1987–2011.

Here positive and negative temporal zones were used to define subgroups of the  $C_{SSf}$  and  $C_{SSs}$  datasets, which were each fitted with linear regression rating curves after log transformation of  $C_{SSf}$  and  $Q$  values. An ANCOVA method was used to compare the  $C_{SSf}$  and  $C_{SSs}$  subgroups for statistically significant differences in rating curve slope and offset. For a detailed treatment of the ANCOVA approach to comparing rating curves, see Gray et al. (in press).

All linear regression rating curves for fine sediment periods appeared to be parallel, with the exception of 1990–1993, with higher offset for positive cumulative residual zones, and lower offset for

**Table 4.1** Suspended Sediment Rating Curves

Linear Regression and LOESS Rating Curves										Shapiro-Wilk Normality Test		Log Bias Correction Factors ( $BCF_i$ )	
Size	Time Period	Model	Model Equation	$R^2$	RMSE <sup>a</sup>	$W$	$P$ -value <sup>c</sup>	Ferguson	Duan	(F + D)/2 <sup>e</sup>			
Fine	Total Range (1967 - 2011)	LR	$\log C_{SS} = 1.569 + 0.713 \cdot \log Q$	0.55	0.61	0.97	***	1.530	3.365	2.447 <sup>b</sup>			
		LOESS	-	-	0.59	0.96	***	1.489	3.167	2.328 <sup>b</sup>			
	1967 - 1979	LR	$\log C_{SS} = 1.896 + 0.634 \cdot \log Q$	0.56	0.57	0.99	Normal	1.448	2.316	1.882 <sup>b</sup>			
		LOESS	-	-	0.56	0.99	Normal	1.435	1.565	1.500 <sup>b</sup>			
	1980 - 89, 1994 - 2011	LR	$\log C_{SS} = 1.326 + 0.651 \cdot \log Q$	0.6	0.43	0.98	*	1.240	1.768	1.504 <sup>b</sup>			
		LOESS	-	-	0.42	0.98	*	1.226	1.346 <sup>b</sup>	1.286			
	1990 - 1993	LR	$\log C_{SS} = 2.233 + 0.850 \cdot \log Q$	0.45	0.78	0.95	*	2.021	2.494	2.496 <sup>b</sup>			
		LOESS	-	-	0.81	0.92	Normal	2.133	2.553	2.343 <sup>b</sup>			
	Sand	Total Range (1967 - 2010)	LR	$\log C_{SS} = 0.726 + 0.920 \cdot \log Q$	0.69	0.60	0.98	*	1.511 <sup>b</sup>	4.073	2.792		
			LOESS	-	-	0.55	0.97	**	1.411 <sup>b</sup>	3.097	2.254		
1967 - 1986		LR	$\log C_{SS} = .670 + 0.947 \cdot \log Q$	0.70	0.60	0.97	**	1.511 <sup>b</sup>	4.224	2.867			
		LOESS	-	-	0.52	0.97	**	1.364 <sup>b</sup>	2.755	2.059			
1987 - 2010		LR	$\log C_{SS} = 0.228 + 1.125 \cdot \log Q$	0.71	0.53	0.97	*	1.388 <sup>b</sup>	2.391	1.890			
		LOESS	-	-	0.48	0.99	Normal	1.305 <sup>b</sup>	1.716	1.511			

Multiple Linear Regression Rating Curves										Shapiro-Wilk Normality Test		Log Bias Correction Factors ( $BCF_i$ )	
Size	Time Period	Model	Variables	Coefficients	VIF <sup>d</sup>	$R^2$	RMSE	$W$	$P$ -value	Ferguson	Duan	(F+D)/2	
Fine	Total Range (1967 - 2011)	MLR	-	-	-	0.53 <sup>a</sup>							
			Intercept	1.459	-	6.3E-02							
			$\log Q$	0.677	1.42	0.65	3.7E-02	0.97	***	1.384	2.782	2.083 <sup>b</sup>	
			$Q_{114}$ Time	-2.12E-03	1.34		3.4E-04						
			$Q_{114}$ Time	5.71E-04	1.15		6.4E-05						
			$\Delta Q$	7.75E-04	1.09		3.3E-04						
Sand	Total Range (1967 - 2010)	MLR	-	-	-	0.52 <sup>a</sup>							
			Intercept	0.9819	-	0.10							
			$lq$	0.8255	1.31	0.76	3.9E-02	0.96	***	1.368 <sup>b</sup>	4.350	2.859	
			$\Sigma Q_{0.1, 110}$ day	-2.66E-03	1.42		1.0E-03						
			$Q_{400}$ Time	-1.77E-04	1.54		3.9E-05						
			current Wy	1.46E-04	1.40		6.8E-05						
previous Wy	1.54E-04	1.34		7.2E-05									

<sup>a</sup> indicates root mean squared error (RMSE) values for the entire model. All RMSE values reported in log units.

<sup>b</sup> indicates log bias correction factors ( $BCF_i$ ) found to most closely estimate observed mean  $CSS$ . These values were used in subsequent  $Q_{SS}$  estimations. All  $BCF_i$  values reported in multiplicative form.

<sup>c</sup> Shapiro-Wilk test result  $P$ -value ranges: Normal  $\geq 0.5$ ;  $0.5 > * > 0.001$ ;  $0.001 > ** > 1E-5$ ;  $1E-5 > ***$

<sup>d</sup> Variance inflation factor (VIF) values close to 1 indicate little collinearity issues between variables in multiple regressions, while VIF values near 5 or greater would indicate considerable collinearity.

<sup>e</sup> (F+D)/2 = the log bias Ccorrection factors (Ferguson + Duan)/2.

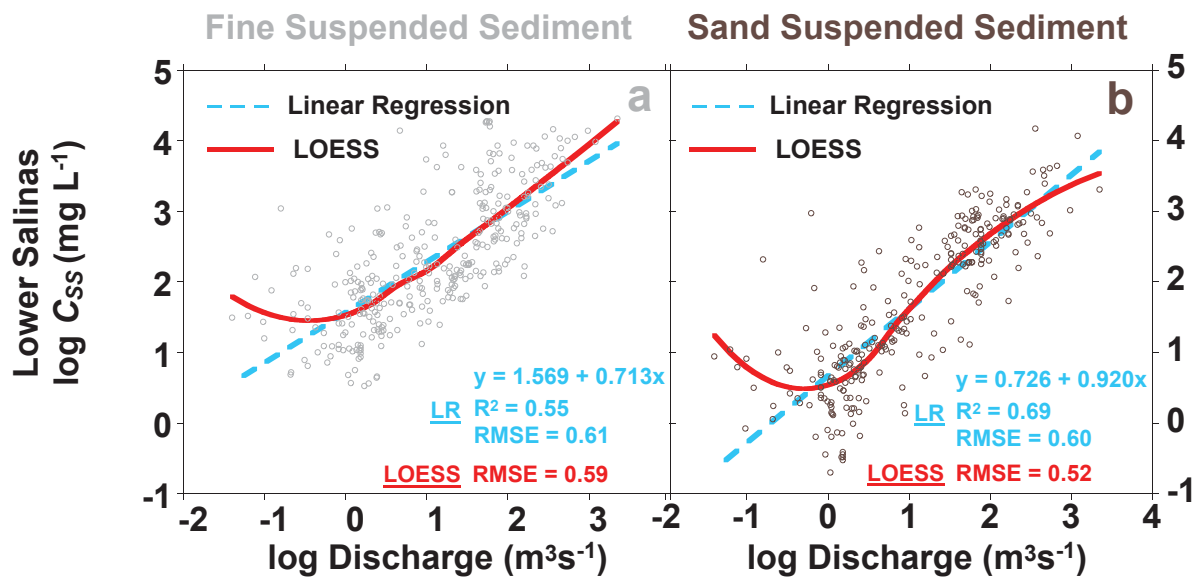


**Figure 4.2** Linear regression and LOESS rating curve models of  $C_{SS}$  –  $Q$  behavior in log-log space for (a) fine and (b) sand sized sediment with sample values.

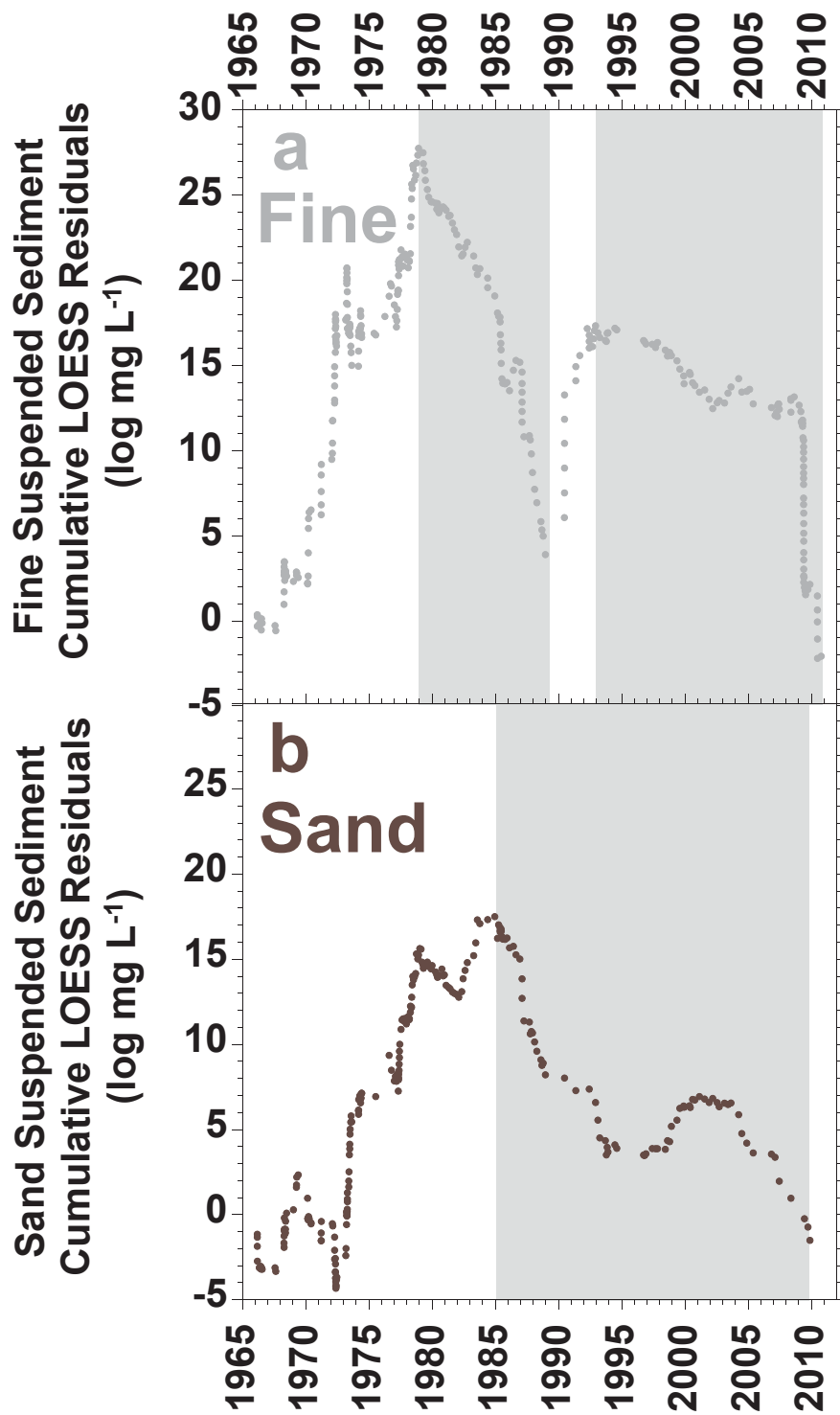


**Figure 4.3** Plots of (a) fine and (b) sand LOESS residuals sequentially summed over time. Gray shading indicates zones of persistent negative residual behavior, un-shaded zones are positive.

negative zones (Fig. 4.4a). Conversely, the two periods for sand appeared to have differing slope and offset, with the negative cumulative residual zone displaying a lower offset, but higher slope, resulting in a convergence of rating curves at the highest values of  $Q$  (Fig. 4.4b). ANCOVA comparisons of fine sediment rating curves at a  $p < 0.05$  significance threshold showed that the two negative cumulative residual zones (1980–89, 1994–2011) were offset equivalent, as were the two positive zones (1967–79, 1990–93), with no significant difference in rating curve slopes (e.g, all fine sediment rating curves were parallel) (Table 4.2).

LOESS based temporally zoned rating curves generally displayed a transition from curved to log-linear relationships found for the entire temporal domain located around  $1 \text{ m}^3\text{s}^{-1}$  (0 log units) (Fig. 4.5). This resulted in decreased RMSE values for LOESS curves in comparison to linear regression curves, except for the 1990–1993 fine sediment period, which displayed a small increase (Table 4.1). Temporally zoned linear regression models generally accounted for slightly more variance in  $C_{SS}$  than found for the linear models based on the entire temporal domain, again with the exception of the 1990–1993 period.

#### 4.5.3 Multiple regression rating curves

Stepwise multiple linear regression models were constructed with the inclusion of hydrologic variables to account for more variation in  $C_{SSf}$  and  $C_{SSs}$  than resolved by  $Q$  alone. The authors previously examined the effects of antecedent hydrologic conditions on suspended sediment behavior in the lower Salinas River at event to interannual (Gray et al., in press), and decadal timescales (Gray, 2014). Results of those studies showed that fine suspended sediment (particle size ( $D$ )  $< 62.5 \mu\text{m}$ ) behavior displayed overall positive (clockwise) hysteresis at the event scale (rising versus falling limb of the event hydrograph), with fine sediment supply suppressed by both prolonged drought periods and flushing flows of a moderate flow ( $\sim 100\text{--}200 \text{ m}^3\text{s}^{-1}$ ). The  $C_{SSs}$  decreased with increasing elapsed time since a wide range of discharge thresholds (from  $1 \text{ m}^3\text{s}^{-1}$  to  $500 \text{ m}^3\text{s}^{-1}$ ), and seasonal as well as long term (multi-annual) arid conditions also resulted in decreased  $C_{SSs}$ . Elapsed time since a given  $Q_j$  is defined as  $Q_j$  Time. Drought is represented by  $\Sigma Q_{0.1}$ , the sum of days when  $Q_d \leq 0.1 \text{ m}^3\text{s}^{-1}$  for back cast summation windows of 1–2000 days. The one-day change in  $Q$  from the day before the day of sampling was described as  $\Delta Q_d$ .

**Table 4.2** Cumulative residual analysis time period rating curve ANCOVA results

Regression Pair		Coincidence	Parallelism	Offset
Sediment size	Time periods			
Fines	1967 - 79 vs. 1980 - 89	***	P	***
Fines	1967 - 79 vs. 1990 - 93	**	P	E
Fines	1967 - 79 vs. 1994 - 2011	***	P	**
Fines	1980 - 89 vs. 1990 - 93	***	P	***
Fines	1980 - 89 vs. 1994 - 2011	C	P	E
Fines	1990 - 93 vs. 1994 - 2011	***	P	*
Sand	1967 - 86 vs. 1987 - 2010	***	***	*

C = coincident, P = parallel, and E= offset equivalent at a  $P > 0.05$  threshold. Significant differences are indicated over ranges of P-values as: \* P-value < 0.001, \*\* P-value < 1E-4, \*\*\* P-value < 1E-5.

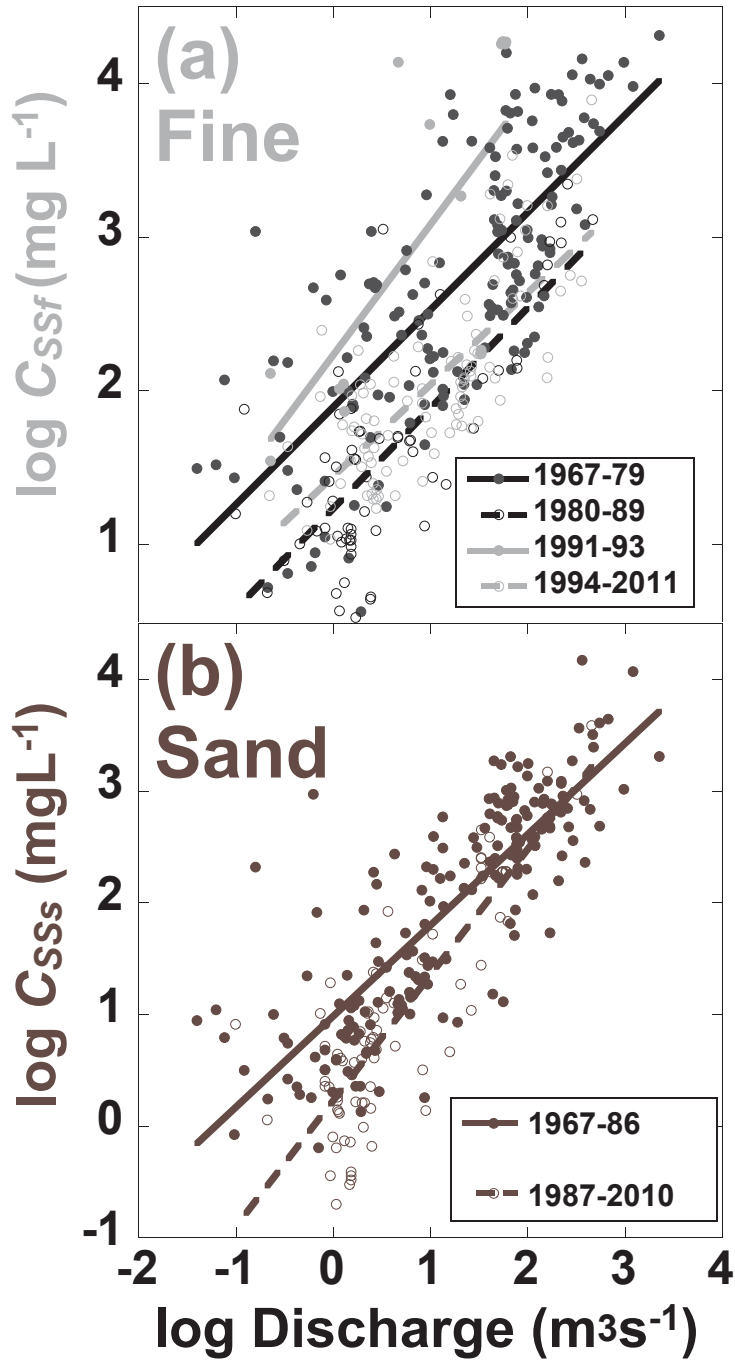


**Figure 4.4** Log-linear regression rating curves for (a) fine and (b) sand sized suspended sediment over temporal zones of persistent positive (solid lines) and negative (dash lines) behavior.

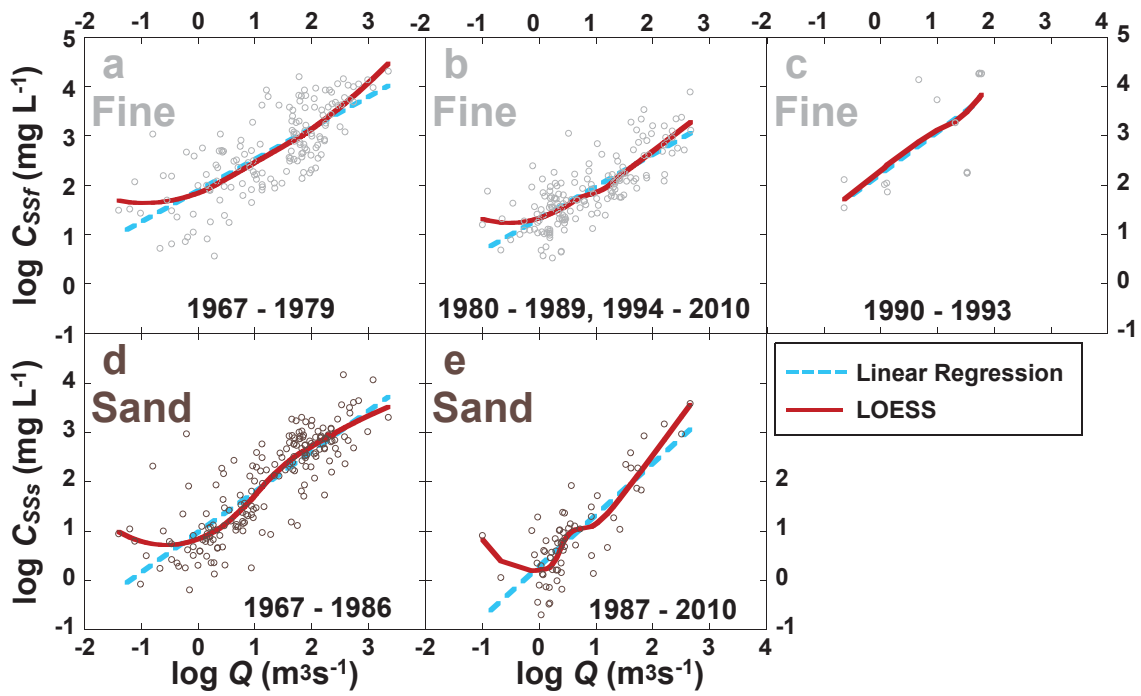


**Figure 4.5** Linear and LOESS rating curve models for (a–c) fine and (d, e) sand sized  $C_{SS} - Q$  behavior by temporal zones of persistent suspended sediment behavior.

The only variables included in multiple regression calculations were those that (i) were not collinear with other variables (defined by pairwise linear correlation analysis resulting in an  $R^2 < 0.8$ ; as per Montgomery and Peck (1992)) and (ii) resulted in statistically significant correlations with discharge-corrected  $C_{SS}$  (Chatterjee et al., 2000; Warrick and Mertes, 2009). Thus, the multiple regression rating curve for  $C_{SSf}$  employed  $Q_1$  Time,  $Q_{114}$  Time and  $\Delta Q_d$ , while that for  $C_{SSs}$  included  $\Sigma Q_{0.1, 110 \text{ days}}$ ,  $Q_{400}$  Time, Current Water Yield and Previous Water Yield. Overall  $R^2$  values were adjusted for the increasing predictor variable pool (Chatterjee et al., 2000).

## 4.6 Suspended sediment load

### 4.6.1 $Q_{SS}$ estimation methods

Daily suspended sediment load ( $Q_{SS}$ ) was estimated for fine and sand fractions by modifying rating curve estimations of  $C_{SSf}$  and  $C_{SSs}$  to account for systematic biases and then multiplying by daily water yield values as per Warrick and Mertes (2009):

$$C_{SS} = BCF_d \cdot BCF_l \cdot C_{SS \text{ rating curve}(Q)} \quad (4.2)$$

$$Q_{SS} = Q_d \cdot C_{SS} \quad (4.3)$$

where  $BCF_d$  corrects for bias introduced by using daily rather than instantaneous discharge and  $BCF_l$  corrects for the logarithmic transformation consequence of calculating regression parameters using geometric rather than arithmetic mean.

Estimates of  $C_{SSf \text{ rating curve}(Q)}$  and  $C_{SSs \text{ rating curve}(Q)}$  values were first obtained for all unique  $Q$  values in the S1 gauge record using linear regression, multiple linear regression and LOESS rating curves developed above. LOESS techniques alone do not allow for extrapolation beyond the domain of sampled discharge values. For LOESS rating curves supported by discharge data that fell short of the highest  $Q$  values present in the 1967–2011 S1 dataset, estimations of  $C_{SS}$  for higher  $Q$  were extrapolated by fitting a linear regression to LOESS estimations for the five highest sampled  $Q$  values. Like many coastal

California rivers, low Q regime  $C_{SS} \sim Q$  relationships were found to be relatively flat or convex up (e.g. Farnsworth and Warrick, 2007). Thus  $C_{SS}$  estimates for low Q were obtained by extending LOESS curves for all sample sets except fine sediment during 1991–1993 by applying a fixed mean log  $C_{SS}$  value estimated from the sampled values with Q's below the transition to positive log-linear behavior. This transition was identified by visual examination of the LOESS curve and was consistently positioned at about  $\log Q = 0$  (or  $1 \text{ m}^3\text{s}^{-1}$ ) for all data sets. Fine sediment samples from the 1991–1993 did not display a departure from log-linear behavior, perhaps in part due to the fact that the minimum sampled Q at  $0.23 \text{ m}^3\text{s}^{-1}$  was not as low as in all other data sets. In this case the low Q regime was estimated in the same manner explained for the high Q regime.

The parameter  $BCF_d$  was estimated to be 1.01 by comparing fine sediment loads estimated from  $Q_d$  values to fine sediment loads estimated with  $Q_{15min}$  data for water years with complete  $Q_{15min}$  time series (1992, 1994, 2001, 2003-2006, 2008, 2009) (Warrick and Mertes, 2009).  $BCF_l$  was calculated using a combination of the parametric method of Ferguson (1986), and the nonparametric 'smearing' method of Duan (1983). The Ferguson correction for log-transform bias ( $BCF_{lf}$ ) is calculated as:

$$BCF_{lf} = 10^{\frac{s^2}{2}} \quad (4.4)$$

where  $s^2$  is the mean squared error of the residuals. Use of  $BCF_{lf}$  is contingent upon the assumption of normality in the distribution of rating curve residuals. However, the distribution of residuals for most rating curves used in this study were found to differ significantly from normal using the Shapiro-Wilk test, where the null hypothesis is that a distribution is normal, and  $p$ -values below 0.05 were considered to indicate significant departures from normal (see Table 4.1) (Cohn et al., 1989; Hicks et al., 2000; Helsel and Hirsch, 2002). Thus the Duan smearing correction factor ( $BCF_{ld}$ ) was also investigated, as it does not require residual distribution normality:

$$BCF_{ld} = \frac{\sum_{i=1}^n 10^{e_i}}{n} \quad (4.5)$$

where  $e_i$  is each residual value generated by subtracting observed  $C_{SS}$  values from the  $C_{SS}$  rating curve ( $Q$ ) estimates and  $n$  is the number of samples (Rasmussen et al., 2009). The suitability of these factors in correcting log transformation bias was examined by computing the arithmetic mean  $C_{SS}$  for each sample set using uncorrected rating curve estimations of  $C_{SS}$ , and those corrected by either  $BCF_{f_i}$ ,  $BCF_{d_i}$  or the arithmetic mean of the two ( $BCF_{(f+d)/2}$ ), and then comparing these values to the observed sample arithmetic mean  $C_{SS}$ . The BCF (or lack thereof) that resulted in a mean  $C_{SS}$  closest to the observed was chosen for inclusion in the estimation of  $Q_{SS}$ . As residuals for all rating curves were found to be homoscedastic using the nonparametric Filgner-Killeen test of homogeneity of variances,  $BCF_i$  corrections were applied uniformly to calculations across the entire discharge domain.

#### 4.6.2 Comparison of suspended sediment load estimations

Estimated mean annual  $Q_{SS}$  ranged from 2.89 Mt/year (based on two LOESS rating curves: one for fines and one for sand, over the entire temporal domain) to 2.01 Mt/year (estimated from several temporally zoned, linear regression rating curves computed separately for fines and sands) (Table 4.3). Moving from entire temporal domain rating curves to temporally zoned rating curves resulted in decreased total mean annual  $Q_{SS}$  values for LOESS and linear regression methods, with reductions of 0.76 and 0.24 Mt/year, respectively. In both cases the reduction in  $Q_{SS}$  was affected by a decrease in fine sediment load ( $Q_{SSf}$ ), countered to some extent by an increase in sand load ( $Q_{SSs}$ ), resulting in an increase in the mean percent sand in the suspended sediment budget. Including hydrologic variables in multiple linear regressions resulted in a 0.11 Mt/year increase in total mean annual  $Q_{SS}$  relative to linear regression with  $Q$  as the lone independent variable. The increase in  $Q_{SS}$  was driven by a 0.16 Mt/year increase in sand, which was only slightly counterbalanced by a 0.05 Mt/year decrease in fine load.

Large interannual variability in both  $Q_{SSf}$  and  $Q_{SSs}$  was observed for estimates produced from all methods employed in this study, with differences between maximum and minimum sediment flux amounting to ~ 5–7 orders of magnitude (Fig. 4.6). Linear regression and LOESS methods with total time domain rating curves produced the same rank for 33 out of 45 water years in terms of total annual  $Q_{SS}$ , including the top 18 years, whereas comparison of linear and LOESS estimates based on temporal zones resulted in only 10 years with the same rank. Moving from total temporal domain to temporally zoned

**Table 4.3** Lower Salinas suspended sediment load

Method <sup>a</sup>	Time period <sup>b</sup>	Megatons per year				% Sand
		Fine Q <sub>SS</sub>	Sand Q <sub>SS</sub>	Total Q <sub>SS</sub>	s of total Q <sub>SS</sub> <sup>c</sup>	
LOESS All	1967 - 2011	2.42	0.47	2.89	6.24	16.2
LOESS Tzone	1967 - 2011	1.39	0.75	2.13	4.59	35.1
LOESS Tzone	1967 - 2011, El Niño only	2.42	1.37	3.79	6.01	27.5
LOESS Tzone	1967- 2011, La Niña & La Nada	0.20	0.12	0.33	0.45	30.7
LR All	1967 - 2011	1.72	0.54	2.26	4.71	23.8
LR All	1944 - 1995	1.40	0.44	1.83	4.70	15.9
LR All	1930 - 2000	1.87	0.59	2.46	4.73	16.9
LR Tzone	1967 - 2011	1.45	0.56	2.01	4.34	27.7
MR All	1967 - 2011	1.67	0.70	2.37	5.62	29.6
MR All	1967 - 2011, El Niño only	2.87	1.25	4.12	7.31	15.6
MR All	1967- 2011, La Niña & La Nada	0.29	0.08	0.37	0.43	16.3

<sup>a</sup>LOESS is local, low order polynomial regression, LR is linear regression with discharge as the single independent variable, MR is multiple linear regression multiple linear regression with hydrologic variables in addition to discharge as independent variables. 'All' indicates a single rating curve for the total temporal domain of suspended sediment samples, 'Tzone' indicates separate rating curves employed for each time period of persistent suspended sediment behavior.

<sup>b</sup>'El Niño only' are years determined to be in positive ENSO condition. 'La Niña & La Nada' are all other years. 1944 - 1995 is the time period used by Inman and Jenkins (1998) for an average annual Q<sub>SS</sub> estimation, and 1930 - 2000 is the temporal domain utilized by Farnsworth and Milliman (2003).

<sup>c</sup>'s' is standard deviation

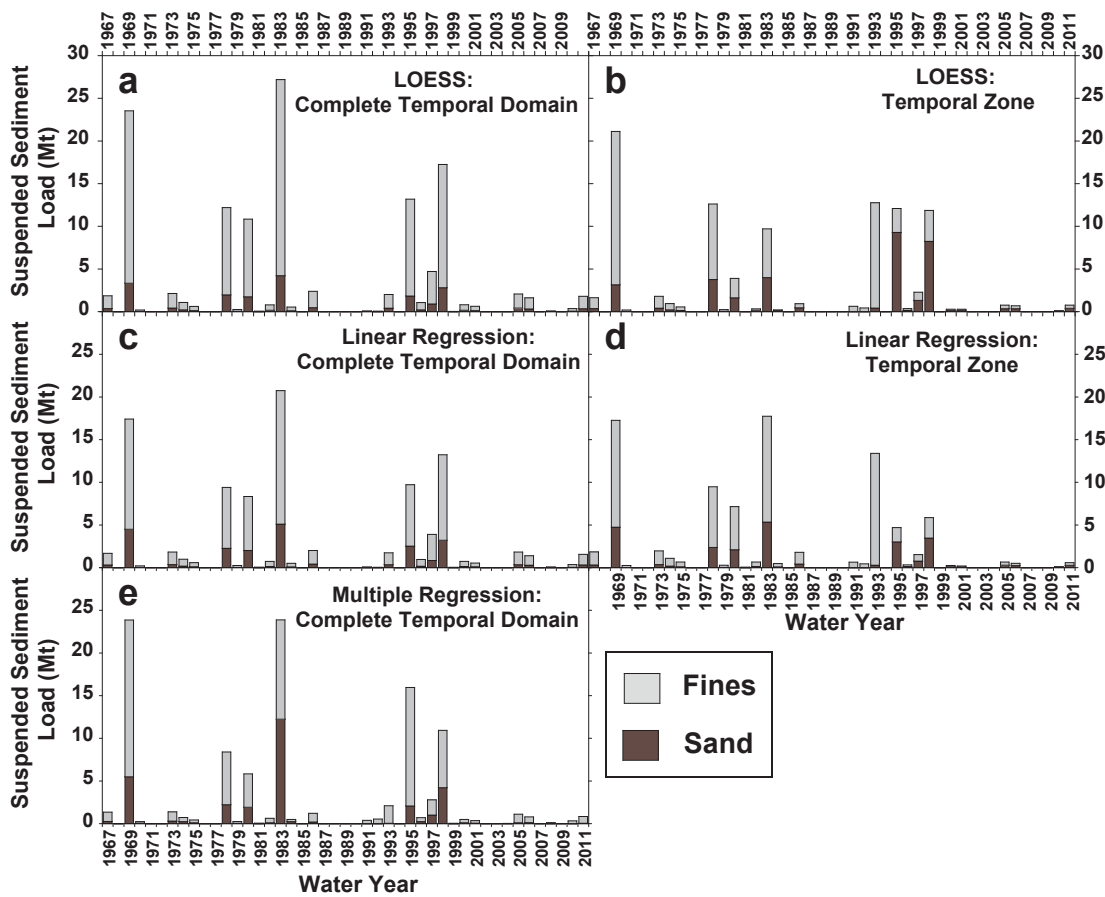


**Figure 4.6** Lower Salinas River annual suspended sediment discharge ( $Q_{SS}$ ) by estimation method. All methods employed separate estimations for fine and sand sized sediment. (a,b) LOESS and (c,d) linear regression methods were applied as (a, c) single regression curves computed from suspended sediment data collected over the complete temporal domain of suspended sediment sampling (1967–2011), or (b, d) with different rating curves for each temporal zone of persistent residual behavior. (e) Multiple regression models were constructed using the entire temporal domain of suspended sediment data.

rating curves using LOESS or linear regression techniques resulted in changing the rank of all but 7 or 8 water years respectively. Ranking of annual  $Q_{SS}$  magnitude was the same for simple linear and multiple linear methods in 20 out of 45 years. Despite differences in ranking, all methods of  $Q_{SS}$  estimation recognized water years 1969, 1978, 1980, 1983, 1995 and 1998 as among the years of highest  $Q_{SS}$ .

Some similarities were present in the differences found for  $Q_{SS}$  by water year for total temporal domain vs. temporally zoned rating curves, and total temporal domain, simple linear versus multiple linear rating curves (Fig. 4.7). Patterns in total temporal domain versus temporally zoned differences for fines and sand were similar for LOESS and linear regression techniques (Fig. 4.7 a–f). Generally smaller magnitude differences were observed for the linear regression models (excepting a large increase in fine sediment discharge in 1993), and particularly large increases in sand sized sediment were found for 1995 and 1998 LOESS temporal zone estimates (Fig. 4.7b). As the LOESS and linear regression sand curves for the 1987–2010 temporally zoned differed primarily over low ( $< 1 \text{ m}^3 \text{ s}^{-1}$ ) and high ( $> 100 \text{ m}^3 \text{ s}^{-1}$ ) discharge domains (Fig. 4.7e), sensitivity tests were used to remove one or the other of these differences, which showed that higher sand concentrations for the LOESS model at high  $Q$  were responsible for the resultant differences in  $Q_{SS}$  estimations (results not shown). Of the years that displayed a reduction of fine sediment discharge for linear regression temporal zone  $Q_{SS}$  estimates in comparison rating curve methods (1969, 1980, 1983, 1985, 1995–1998, 2001, 2002, 2004, 2005, 2010, 2011) (Fig. 4.7d), all but 1969 and 1995 were also reduced by moving from simple linear regression over the total temporal domain to including hydrologic variables for multiple regressions (Fig. 4.7g). Increases in fine  $Q_{SS}$  estimated for 1969 and 1995 estimated through the multiple regression approach were the two largest departures from the simple linear model, and were directly opposed to the differences obtained from employing simple linear regression by temporal zone. The multiple regression approach also resulted in small negative differences in fine sediment  $Q_{SS}$  for years 1973, 1974 and 1978, which were not observed between the single rating curve and temporally zoned models, and also produced much lower increases than found between the linear regression methods for 1992 and especially 1993. Similarities were also observed between sand linear regression (temporally zoned – single rating curve) and (multiple regression – single linear regression curve) differences (Fig. 4.7e, h). The years 1969, 1983 and 1998 delivered increases in sand load in both cases, while 1993, 2005, 2006 and 2011 showed decreases for

both cases as well. However, the magnitude of difference was generally greater for the multiple regression – total temporal domain curve comparison, and opposite responses were observed for the years 1978, 1980, and 1995, when temporally zoned difference was positive and multiple regression difference was negative, and 1984, 1996, 1997, when multiple regression difference was positive and temporally zoned difference was negative or null.

Thus, the inclusion of hydrologic variables in the estimation of  $Q_{SS}$  had an effect similar to that of subdividing the total temporal domain linear regression curves into roughly decadal scale zones of behavior for the later part of the record (1996–2011) (Fig. 4.7f,i), but did not capture the largest differences obtained through temporal zonation in the earlier part of the record, namely for years 1969, 1983, 1993, and 1995, due to large difference between multiple regression and temporally zoned linear regression in fine (1969, 1993, 1995) (Fig. 4.7d,g) and sand (1983, 1995) (Fig. 4.7e,h) estimations for those years.

#### 4.6.3 Differences in $Q_{SS}$ estimation for critical years

Focusing on the years 1969, 1983, 1993, and 1995, identified as most critical to the differences in sediment flux changes obtained by shifting from linear regression over the total temporal domain (single rating curve), to temporally zoned or multiple regression curves, the following questions were posed: how did these temporal zone and multiple regression rating result in different estimations of  $Q_{SS}$  and which method is in better agreement with observations?

Examination of cumulative  $Q_{SS}$  over the domain of  $Q$  values for each of the water years in question showed that the larger magnitude fine  $Q_{SS}$  values found for 1969 and 1995 from multiple regression were primarily the result of 1 to 4 days when discharge was  $\geq 1000 \text{ m}^3 \text{ s}^{-1}$ , with gains of  $\sim 12 \text{ Mt}$  in both cases (Fig. 4.8a,c). For fine sediment in 1969 and 1995, cumulative multiple regression estimates from  $0\text{--}1000 \text{ m}^3 \text{ s}^{-1}$  were lower than linear regression estimates based on the single, total temporal domain rating curve, and below temporally zoned linear regression estimates as well for 1969. In contrast, temporally zoned linear regression resulted in much higher  $Q_{SSf}$  for most of 1993, while multiple regression only diverged from the total temporal domain linear estimates due to a few discharge days between  $\sim 80\text{--}175 \text{ m}^3 \text{ s}^{-1}$  (Fig. 4.8b). For  $Q_{SSs}$  in 1983, cumulative multiple regression estimates

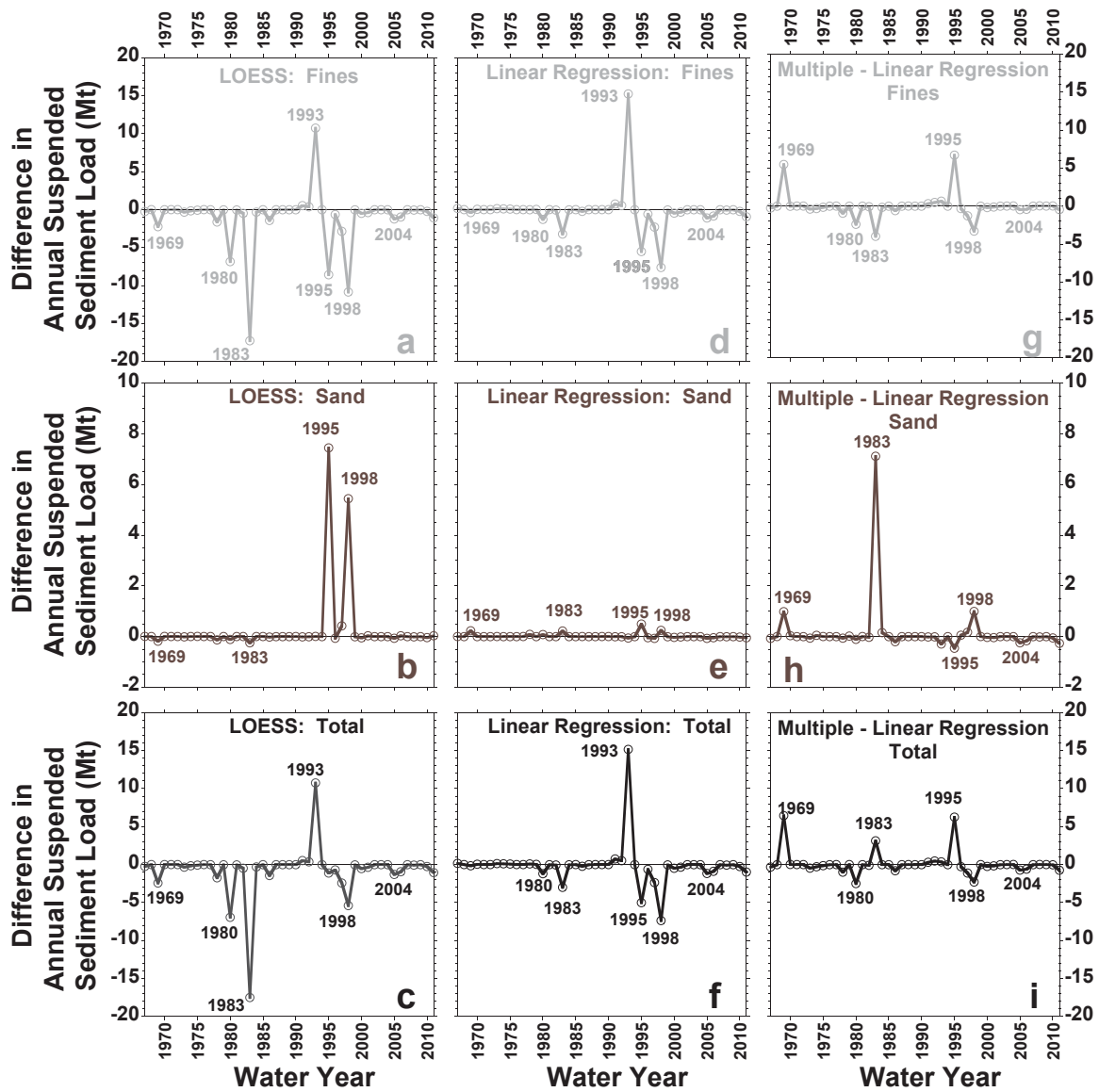


**Figure 4.7** Differences in annual suspended sediment discharge ( $Q_{SS}$ ) estimations for fine, sand and total sediment. (a–c) LOESS temporal zone based estimations – LOESS complete temporal domain estimations. (d–f) Linear regression temporal zone based estimations – linear regression complete temporal domain estimations. (g–i) Multiple regression estimations – linear regression complete temporal domain estimations.

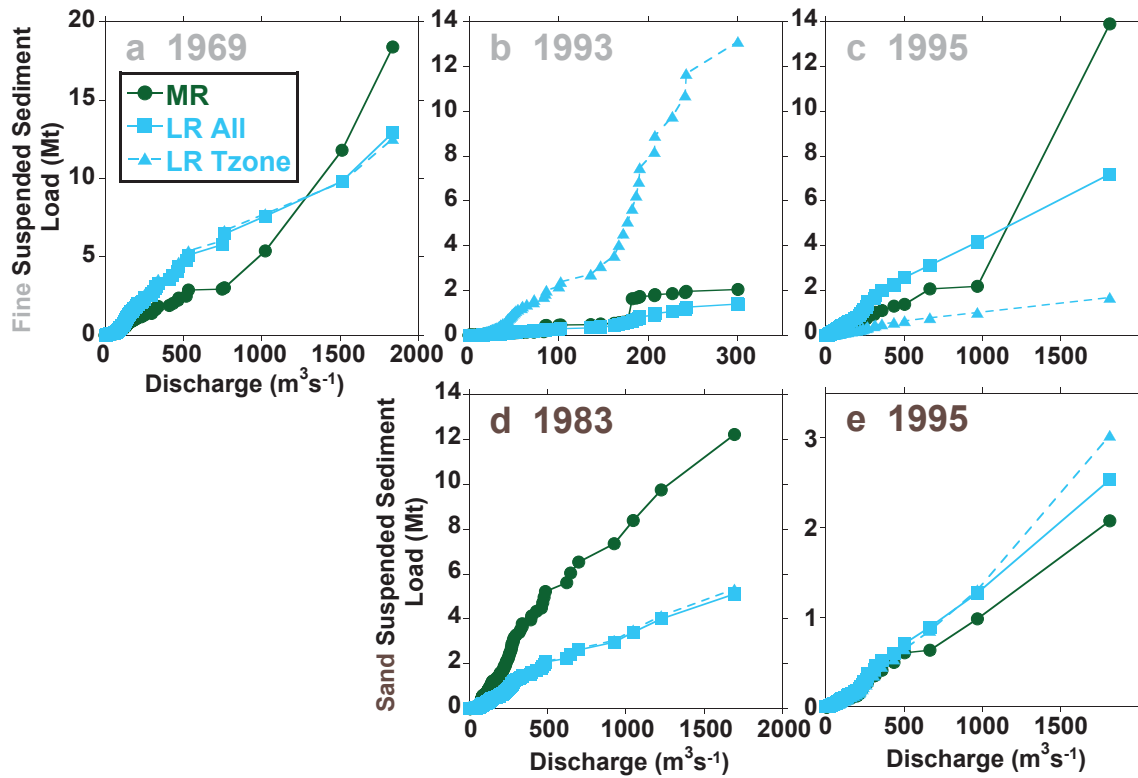


**Figure 4.8** Cumulative suspended sediment discharge estimates by daily water discharge magnitude for water years 1969, 1983, 1993 and 1995. Fine suspended sediment is featured in (a), (b) and (c); sand sized suspended sediment in (d) and (e). “MR” stands for multiple linear regression including water discharge and hydrologic variables. “LR” stands for linear regressions with water discharge as the independent variable. “All” indicates a single rating curve used for the total temporal domain of sampling (1967–2011), while “Tzone” indicates separate rating curves for temporal zones of persistent suspended sediment behavioral characteristics.

dominated over the entire flow domain, while simple linear methods were almost indistinguishable (Fig. 8d). All methods produced similar  $Q_{SSs}$  for 1995 up to the three days with  $Q > 500 \text{ m}^3\text{s}^{-1}$ , after which multiple regression estimates were lower than linear regression methods by  $\sim 0.25\text{--}0.75 \text{ Mt}$ , and temporally zoned linear regression diverged from total temporal domain estimates only for the peak day with  $1812 \text{ m}^3\text{s}^{-1}$ , resulting in a  $\sim 0.25 \text{ Mt}$  higher  $Q_{SS}$  (Fig. 4.8e).

Comparisons of observed  $C_{SS}$  to daily estimates based on multiple regression and simple linear regression were then used to examine the relative efficacy of these methods (Fig. 4.9). For 1969, 1983 and 1995 (Fig. 4.9a,c,d,e) multiple regression values were plotted for all days between the first and last sample collection dates of the water year and the day before and after those dates, while the plot for the 1991–1993 water years included multiple regression  $C_{SS}$  estimations for all days with non-zero  $Q$  (Fig. 4.9b). For water year 1969, all methods of estimating  $C_{SSf}$  plotted lower than observed values for low  $Q$  ( $0.16\text{--}0.24 \text{ m}^3\text{s}^{-1}$ ) and were in close agreement with observed values for  $\sim 60 < Q < 470 \text{ m}^3\text{s}^{-1}$  (Fig. 4.9a). While both linear regression methods plotted close to observed for high  $Q$  estimates ( $> 1000 \text{ m}^3\text{s}^{-1}$ ), as the regression curves converged in this domain, multiple regression estimates were well above observed values and the linear regression curve estimates. These three  $Q$ 's  $> 1000 \text{ m}^3\text{s}^{-1}$  were largely responsible for the high estimations of annual  $Q_{SSf}$  found with multiple regression for 1969 (see Fig. 4.8a).

It should be noted that the highest observed  $C_{SSf}$  value on record of 20,566 mg/L was collected on 2/26/1969, and thus the three high  $Q$  multiple regression estimates of  $C_{SSf}$  at 26,350 – 48,647 mg/L are higher than any found in 45 years of sampling. Of course very few samples have been collected from such high flows in the lower Salinas. High  $C_{SSf}$  estimations for these three days were driven by high  $\Delta Q$  values, as shown by the proportional contribution of this variable to the multiple regression  $C_{SSf}$  estimates for these days (Table 4.4).

A more complex pattern of  $C_{SSf}$  behavior and estimations emerges for water years 1991 – 93 (Fig. 4.9b). Observed values from water years 1991–1992 plot along a generally linear corridor described by all multiple regression estimates for these two years and the linear regression line for the 3-year period. The first observed value for the 1993 water year (collected on 1/12/1993) also fell within this zone in  $C_{SSf} - Q$  space, while observed values collected later in the year (between 3/9–9/8/1993) plotted with or below the total temporal domain linear regression curve. Multiple regression estimations of  $C_{SSf}$  were

found to be highly contingent on the behavior of the  $Q_{114}$  *Time* variable, which increased steadily throughout this period of prolonged low flow until the first daily  $Q$  in excess of  $114 \text{ m}^3\text{s}^{-1}$  in 2493 days (e.g. almost 7 years) was reached on 1/15/1993 (Table 4.4). Thus, when multiple regression estimates for daily  $Q$  in 1993 were plotted separately based on whether they occurred before or after the 1/15 – 16/1993 transition in  $Q_{114}$  *Time* values, the “early” 1993 estimates plot with the other multiple regression estimates and observations for 1991–1992 as well as the temporal zone linear regression, while the “late” 1993 multiple regression estimates plotted with the total temporal domain linear regression and the “late” 1993 observed  $C_{SSf}$  values. Therefore the multiple regression approach seems to capture the general pattern of both inter- and intra-annual suspended sediment dynamics in this case, whereas the temporal zonation approach missed the transition to lower  $C_{SSf}$  behavior, which resulted in a much higher estimation of  $Q_{SS}$  (see Fig. 4.8b).

Only two samples were collected in 1995, one at low ( $8.2 \text{ m}^3\text{s}^{-1}$ ) and moderately high ( $453 \text{ m}^3\text{s}^{-1}$ ) discharge, which limited the comparisons between estimated and sampled  $C_{SS}$  values. However, it was apparent that both fine (Fig. 4.9c) and sand (Fig. 4.9e) multiple regression estimates followed a similar pattern, with  $C_{SS}$  estimates above the low discharge observation, below the high discharge observation, and generally following a linear pattern. The  $Q_{SSf}$  multiple regression estimations plotted between the higher total temporal domain linear regression and the lower temporal zone curve, whereas  $Q_{SSs}$  multiple regression estimates were greater than linear regression estimates over the sampled discharge domain. The maximum daily discharge in 1995 was  $1812 \text{ m}^3\text{s}^{-1}$  (3.258 log units), and the fine  $C_{SS}$  multiple regression estimate of 74,088 mg/L (4.870 log units) (see Fig 9c) resulted in an estimate of 11.72 Mt of fine sediment flux in a single day (Fig. 4.8c). It should be noted that this multiple regression estimate is also well above the highest  $C_{SSf}$  values observed in the lower Salinas. In contrast, steep linear regression sand rating curves both lead to higher annual  $Q_{SS}$  estimates due to higher sediment loads than found with multiple regression, as the multiple regression estimate for the peak  $Q$  of this year fell approximately on the linear path shared by the lower discharge multiple regression estimates (Fig. 4.8e, 4.9e).

The large differences found for water year 1983  $Q_{SSs}$  between multiple regression and the linear regression techniques was the result of consistently higher  $C_{SSs}$  estimates across the  $Q$  domain, while total temporal domain and temporally zoned linear methods produced nearly the same rating curve, and

**Table 4.4** Average proportional contribution of hydrologic variables<sup>a</sup> to multiple regression  $C_{ss}$  estimates

Water years	Time period	Q ( $m^3 s^{-1}$ )	Fine (Mt)			Sand (Mt)		
			$Q_1$ Time	$Q_{114}$ Time	$\Delta Q$	Sum $Q_{0.1}$ , 110 day	$Q_{400}$ Time	Wy Current
1967 - 1979	10/1/1966 - 9/30/1979	0 - 1834	-0.15	0.21	0.00	-	-	-
1980 - 1989	10/1/1979 - 9/30/1989	0 - 1693	-0.31	0.28	0.00	-	-	-
1994 - 2011	10/1/1993 - 9/30/2011	0 - 1812	-0.05	0.11	0.00	-	-	-
1969	1/27/1969, 2/26 - 27/1969	1022 - 1834	0.00	0.00	0.15	-	-	-
1983	sample dates + 10 day buffers	9 - 487	0.00	0.02	0.00	-0.01	-0.02	0.14
1991-92, 1993 (early)	10/1/1991 - 1/15/1993	0 - 107	-0.07	0.34	0.00	-	-	-
1993 (late)	1/15/1993 - 9/30/1993	0 - 300	0.00	0.01	0.00	-	-	-
1995	3/20 - 28/1995	90 - 436	0.00	0.00	0.00	-0.03	0.00	0.05
1995	5/11 - 15/1995	5 - 9	0.00	0.01	0.00	0.00	0.00	0.08

<sup>a</sup> The following hydrologic variables were included:  $Q_1$  Time,  $Q_{114}$  Time and  $Q_{400}$  Time, are the elapsed times since the last daily discharge  $\geq 1, 114$  or  $400 m^3 s^{-1}$ , respectively.  $\Delta Q$  is change in daily discharge.  $\Sigma Q_{0.1}$ , 110 day is the number of days with daily discharge values  $\leq 0.1 m^3 s^{-1}$ . Wy Current is the water yield of the water year of sample collection. Wy Previous is the water year before the year of sample collection.

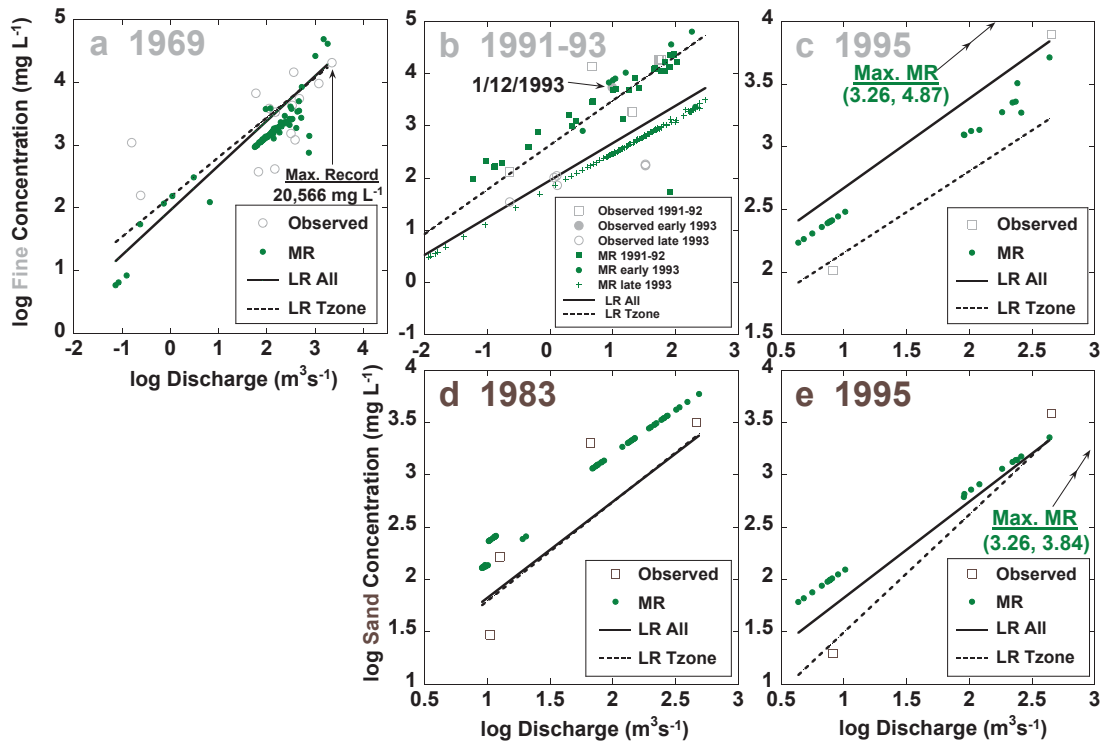


**Figure 4.9** Comparisons of observed and estimated suspended sediment concentrations for water years 1969, 1983, 1991–93 and 1995. Observed values are subdivided in the 1991–93 plot (b) into water years 1991–92, early 1993 (1/9–15/1993), and late 1993 (after 1/15/1993). Estimation methods plotted are multiple regression (MR), and linear regression (LR) utilizing total temporal domain rating curves (All) and temporal zone rating curves (Tzone), all of which have been corrected for log and daily discharge bias (see section 4.4.3). Multiple regression estimates are shown as points values for daily discharge values corresponding to the days within the temporal domain defined by the first and last days when samples were collected in a given water year, plus one day on either end for the 1969, 1983 and 1995 water year plots (a, c, d, e), and all non-zero discharge days for 1991–93 (b). Linear regressions values are shown as their corresponding regression curves. “Max. MR” in (c) and (e) indicates the maximum daily  $C_{SS}$  estimate produced from multiple regression with corresponding ( $C_{SS}$ , water discharge) values in log units, which and double arrows indicating that they would plot outside of frame in both cases.

hence similar  $Q_{SS}$  estimates (Figs. 4.8d, 4.9d). Multiple regression estimates thus appear to more closely fit the admittedly small set of observed values than the estimations from linear regressions for the case of sand sized suspended sediment in 1983. Multiple regression  $C_{SS}$  estimates for the dates around sample collection plot around three out of four of the observed values, while linear curves plotted below the same three out of four values. Sand  $Q_{SS}$  is augmented in 1983 multiple regression estimates due to the high current water yield value for that year, which contributed to low aridity values ( $Sum Q_{0.1}$ , 110 day) and relatively recent high discharge ( $Q > 400 \text{ m}^3\text{s}^{-1}$ ) events (Table 4.4).

#### 4.7 Magnitude and frequency analysis of Q and $Q_{SS}$

##### 4.7.1 Methods of magnitude and frequency analysis

Determination of effective discharge ( $Q(e)$ ) requires the computation of the transport efficacy ( $e(Q)$ ) of the range of discharges experienced:

$$e(Q) = Q_{SS}(Q) \cdot f_{(Q)}(Q) \quad (4.6)$$

where  $Q_{SS}(Q)$  is the constituent discharge (in this case suspended sediment) as a function of discharge, and  $f_{(Q)}(Q)$  is a representation of the probability density function (*pdf*) of discharge (Wolman and Miller, 1960; Wolman and Shick, 1967; Klonsky and Vogel, 2011). Effective discharge is the value of discharge that results in the maximum value of  $e(Q)$  for a given transport constituent. Assignment of  $Q(e)$  is highly dependent on the method employed for estimating the *pdf*, and recent studies have shown that switching from (i) arbitrary binning (histogram) and generalized, parametric frequency function methods to (ii) nonparametric kernel density estimations with optimized spacing yields more stable approximations of  $Q(e)$  (Klonsky and Vogel, 2011). This study employed the R package ‘KernSmooth’ with a Gaussian kernel and the sample variance based ‘oversmoothed bandwidth selector’ as per Wand and Jones (1995, p.61) to generated the kernel density estimation for the daily discharge record at S1 from 1930–2011 (Wand, 2012) (R Development Dore Team, 2013). Discharge-based estimates of fine, sand and total suspended sediment load were computed by discharge bin using each of the rating curve techniques

detailed above. Effective discharge was then estimated for the aforementioned suspended sediment fractions as well as water discharge from the basin.

Half load discharge ( $Q_{1/2}$ ) was calculated for fine, sand and total suspended sediment as well as  $Q$  by summing  $Q_{SS}$  and water yields for all unique daily discharges from 1930–2011 at S1, and then creating a running sum of the proportional contributions of these discharge values to the total loads of each suspended sediment constituent and water yield over the period of record. Both  $Q(e)$  and  $Q_{1/2}$  for suspended sediment loads and  $Q$  were compared to  $Q_{mean}$ .

#### 4.7.2 Magnitude/frequency results

Transport efficacy of suspended sediment was generally characterized as highly multimodal, with many peak  $e(Q)$  values of similar magnitude, producing a wide range of effective discharge estimations (Table 4.5, Figs. 4.10, 4.11, 4.12). Water yield  $e(Q)$ , on the other hand, was strongly unimodal with a  $Q(e)$  of  $9.9 \text{ m}^3\text{s}^{-1}$ , or  $\sim 0.85x Q_{mean}$  (Fig. 4.10j). As  $e(Q)$  is the product of frequency and  $Q_{SS}$  for a given  $Q$ , and discharge frequency in this study is expressed as a fixed set of kernel density estimations, the differences in  $e(Q)$  and resultant  $Q(e)$  values are the result of differences in the formulation of  $Q_{SS}$  estimations. Fine suspended sediment effective discharge ( $Q(e)_f$ ) ranged from 14.8–1979  $\text{m}^3\text{s}^{-1}$ , with most methods producing values of either 14.8 or 460–465  $\text{m}^3\text{s}^{-1}$  (Fig. 4.10a–c, Fig. 4.11). Sand suspended sediment effective discharge ( $Q(e)_s$ ) was generally higher, falling between 124 and 1979  $\text{m}^3\text{s}^{-1}$ , with multiple methods producing estimates of 124, 465 and 1979  $\text{m}^3\text{s}^{-1}$  (Fig. 4.10d–e, Fig. 4.12). As fine sediment represents the majority of suspended sediment flux, total suspended sediment  $Q(e)$  estimates were dominated by fine  $e(Q)$  values, which resulted in total sediment  $Q(e)$  estimates that agreed with  $Q(e)_f$  for each method (Fig. 4.10g–i).

Cumulative discharge patterns also exhibited a wide range of behavior depending on particle size range (total, fine or sand fraction of suspended sediment) and method of  $Q_{SS}$  estimation, which resulted in a wide range of  $Q_{1/2}$  estimations (Fig. 4.13, Table 4.5). However, most cumulative discharge curves displayed steeper sections from  $\sim 1\text{--}500 \text{ m}^3\text{s}^{-1}$ , followed by a lower angle curve from  $\sim 500$  to a high discharge value varying from  $\sim 1700\text{--}1800 \text{ m}^3\text{s}^{-1}$ , after which a second steep jump the cumulative discharge curve occurred. This pattern of paired ‘low’ range ( $\sim 1\text{--}500 \text{ m}^3\text{s}^{-1}$ ) and high range ( $> 1700 \text{ m}^3\text{s}^{-1}$ )

**Table 4.5** Effective and half-load discharge

Method <sup>a</sup>	Q(e): Effective Discharge <sup>b</sup> (m <sup>3</sup> s <sup>-1</sup> )			Q <sub>1/2</sub> : Half Load Discharge <sup>c</sup> (m <sup>3</sup> s <sup>-1</sup> )			
	Fine <sup>d</sup> Q <sub>SS</sub>	Sand <sup>e</sup> Q <sub>SS</sub>	Total Q <sub>SS</sub>	Fine Q <sub>SS</sub>	Sand Q <sub>SS</sub>	Total Q <sub>SS</sub>	Water
LOESS All	465	124	465	528	423	512	-
LOESS Tzone	1979, 460, 465	124, 1979	-	451	699	498	-
LR All	14.8	465	14.8	459	558	464	-
LR Tzone	14.8, 14.8, 465	465, 1979	-	298	657	385	-
MR All	1811	252	1811	919	617	814	-
Water yield	-	-	-	-	-	-	134

<sup>a</sup> All methods except 'Water yield' employed log transformed suspended sediment concentration and water discharge data. LOESS stand for low order polynomial local regression, LR = linear regression, MR = Multiple Regression. Water yield calculations were based on daily average discharge data. 'All' indicates use of single rating curves for data over the complete temporal domain of suspended sediment data collection, 'Tzone' indicates separate rating curves applied to temporal zones, or time periods, of persistent LOESS rating curve residual behavior.

<sup>b</sup> Effective discharge is the water discharge magnitude responsible for the greatest flux of a given constituent over time.

<sup>c</sup> Half load discharge is the magnitude of water discharge where the cumulative flux of a given constituent has reached half of the total flux over the period of record.

<sup>d</sup> LOESS and LR Tzone Q(e) estimations for fine sediment are listed in order for the following time periods: (1967 - 79);(1980 - 89, 1994 - 2011); (1990 - 93).

<sup>e</sup> LOESS and LR Tzone Q(e) estimations for sand are listed in order for the following teime periods: (1967 - 1986); (1987 - 2011).

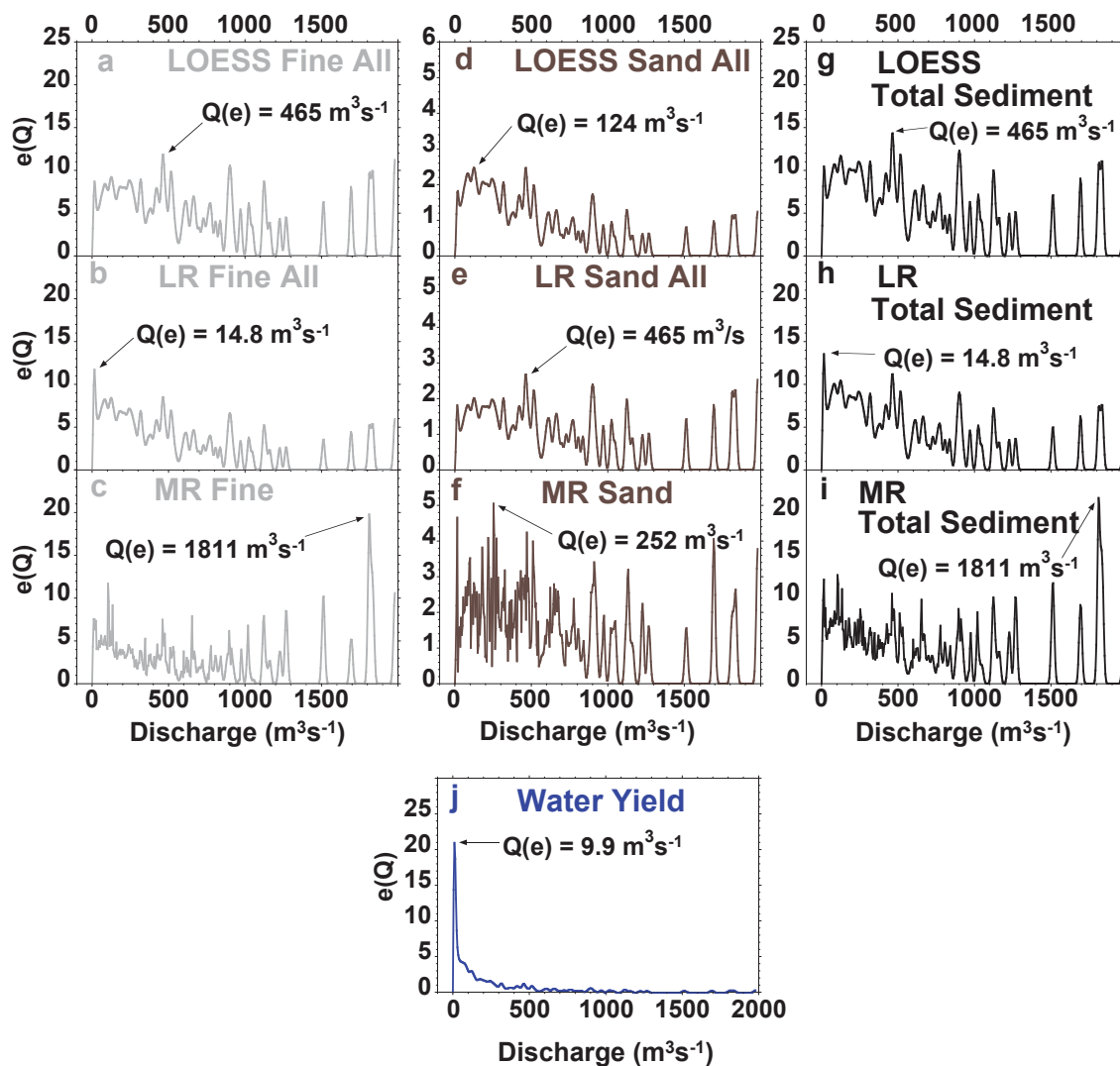


**Figure 4.10** Plots of discharge efficacy ( $e(Q)$ ) for (a-c) fines, (d-f) sand, (g-i) “total sediment” (fines + sand), and (j) water yield. Effective discharge ( $Q(e)$ ) is identified for each case. All methods for sediment flux estimation employed the complete temporal domain of suspended sediment data, as indicated by for the LOESS and LR (linear regression) plots. “MR” indicates estimation with multiple regression rating curves employing variables representing antecedent hydrologic conditions. Water yield was computed from daily discharge values.

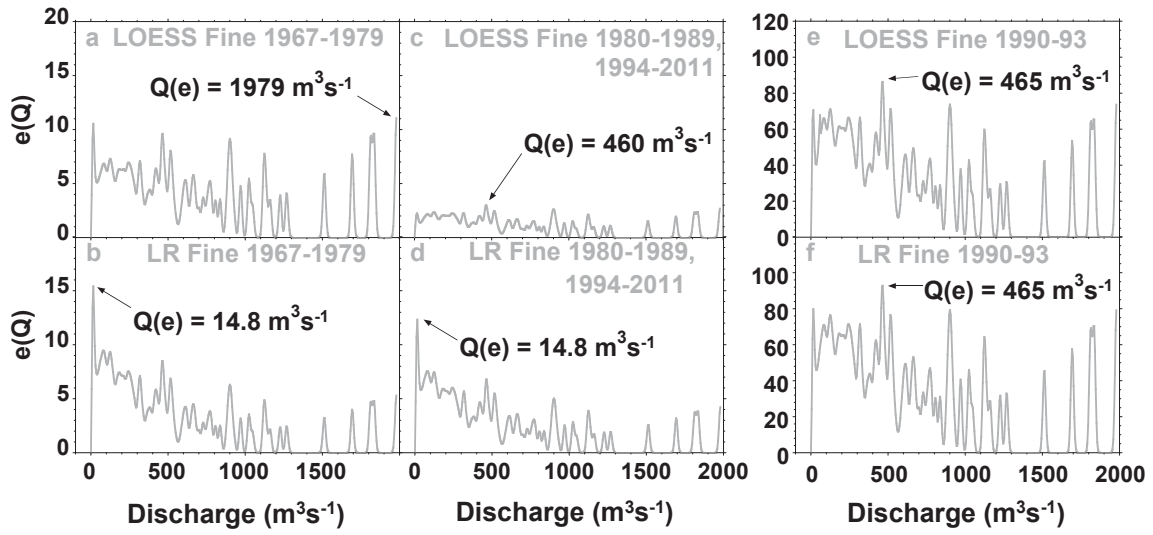


**Figure 4.11** Plots of fine suspended sediment discharge efficacy ( $e(Q)$ ) for (a, c, e) LOESS and (b, d, f) linear regression estimation methods by temporal zone. Effective discharge ( $Q(e)$ ) identified for each case.

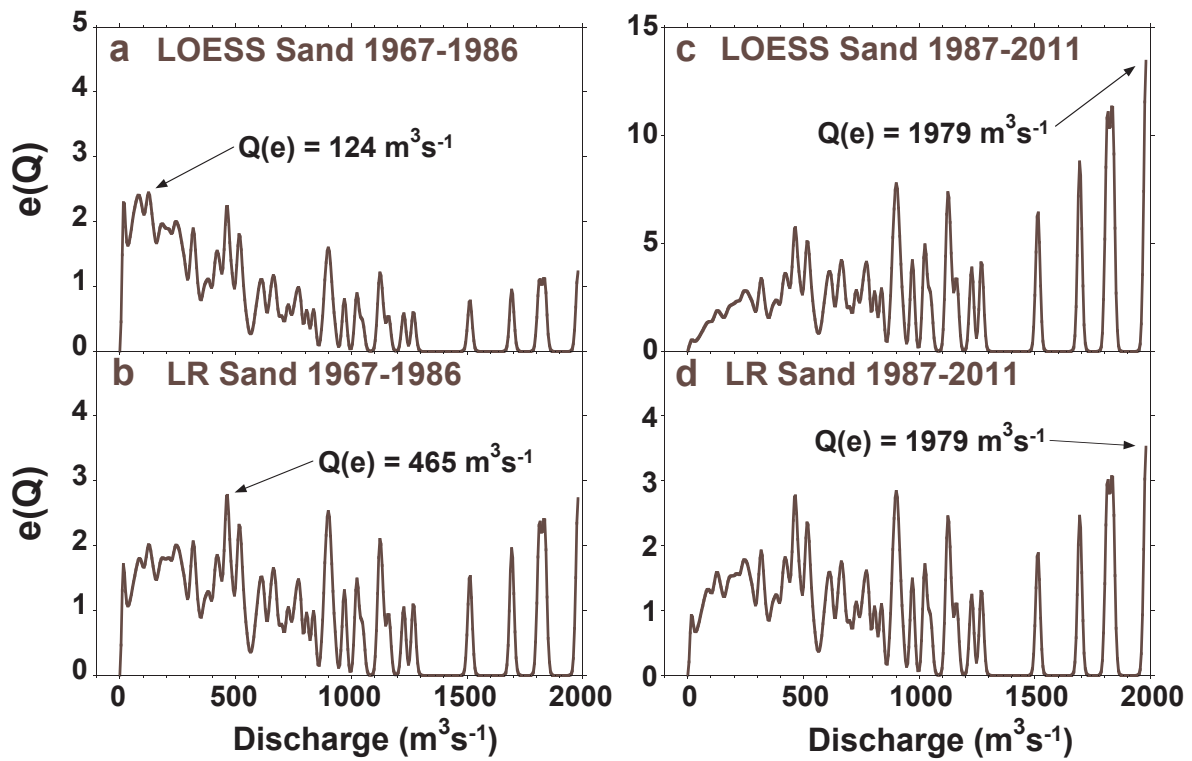


**Figure 4.12** Plots of sand sized suspended sediment discharge efficacy ( $e(Q)$ ) for (a, c) LOESS and (b, d) linear regression estimation methods by temporal zone, for discharge classes generated from kernel density estimations, with effective discharge ( $Q(e)$ ) identified for each case.

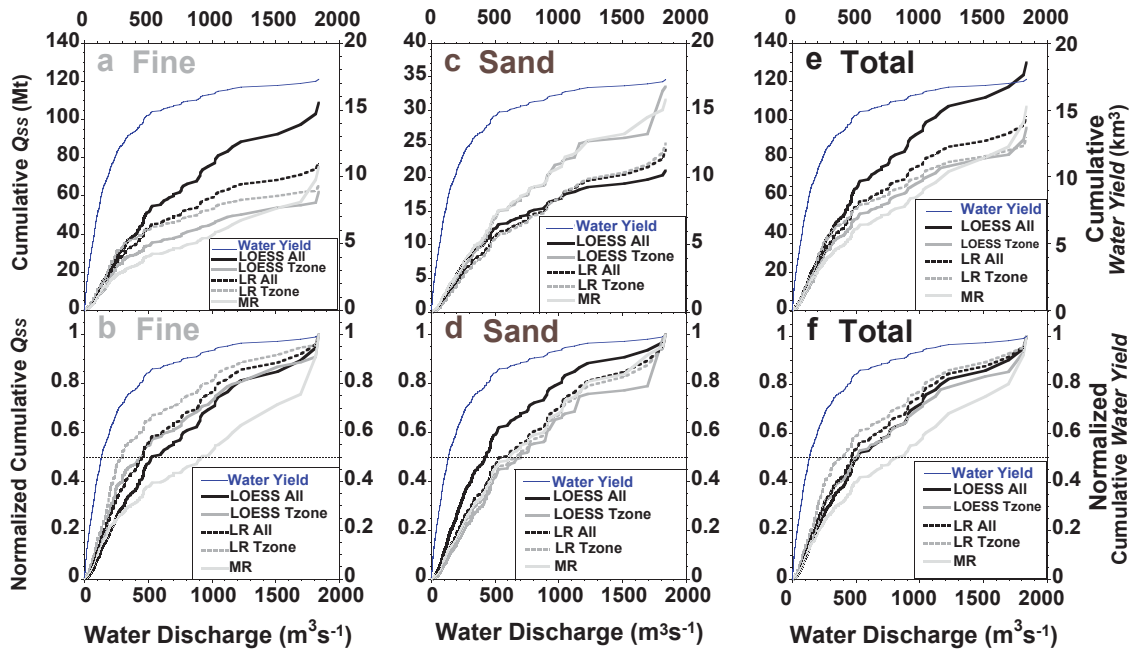


**Figure 4.13** Cumulative discharge curves for the lower Salinas River representing (a, b) fine, (c, d) sand, and (e, f) total suspended sediment discharge estimates for the period of (1967–2011) plotted by method and sequentially summed by increasing water discharge. Water yield over the same period summed by water discharge magnitude are included in each plot for reference. Plots (b, d, and f) show values normalized by corresponding cumulative suspended sediment discharge.

<sup>1</sup>) rapid flux accumulation is driven by the high frequency of discharge over the low discharge domain, and the massive rate of sediment flux at the much less frequent, higher discharge domain. Resulting  $Q_{1/2}$  for fines, sand and total suspended sediment were between 298–919  $\text{m}^3\text{s}^{-1}$ , 423–699  $\text{m}^3\text{s}^{-1}$ , and 385–814  $\text{m}^3\text{s}^{-1}$ , respectively, with variation on the basis of  $Q_{SS}$  estimation method (Table 4.5, Fig. 4.13b,d,f). The  $Q_{1/2}$  for water yield (134  $\text{m}^3\text{s}^{-1}$ ) was lower than that of any suspended sediment constituent.

#### **4.8 ENSO controls on flood frequency and sediment discharge**

To examine flood frequency for given discharge magnitudes and climatic states, the lower Salinas (S1) peak annual water discharge record in its entirety, as well as the El Niño and La Niña data subsets were subjected to a Log Pearson III type flood frequency analysis using HEC-SSP 2.0 software with standard settings as per Bulletin 17B of the Interagency Advisory Committee on Water Data (IACWD, 1982; USACE, 2010). Peak annual discharge records for S1 were subdivided on the basis of ENSO activity into years that contained an El Niño, La Niña or neutral (La Nada) signal (Fig. 4.14). The presence of dominant El Niño or La Niña like conditions was defined as  $(\text{MEI.ext, ONI}) > 0.5$  or  $< -0.5$  respectively during the general precipitation phase of the Salinas water year (October – April), and La Nada for the remaining years that didn't satisfy these conditions. Years classified on this basis were then examined in terms of annual  $Q_{SS}$ .

Flood frequency analysis stratified by ENSO phases yield almost identical in the 50 to 95 % exceedance range (corresponding to an annual peak flow of  $\sim 1\text{--}200 \text{ m}^3\text{s}^{-1}$ ) (Fig. 4.15). However, flood frequencies diverged for the rarest peak magnitudes, with 100-year floods estimated at  $\sim 6000 \text{ m}^3\text{s}^{-1}$  for El Niño years as compared to only  $\sim 2000 \text{ m}^3\text{s}^{-1}$  for La Niña years.

#### **4.9 Discussion**

##### **4.9.1 $Q_{SS}$ magnitude**

All methods of mean annual  $Q_{SS}$  estimation in this study fall between the low estimate of Inman and Jenkins (1999) and high estimate of Farnsworth and Milliman (2003), both of which were based on

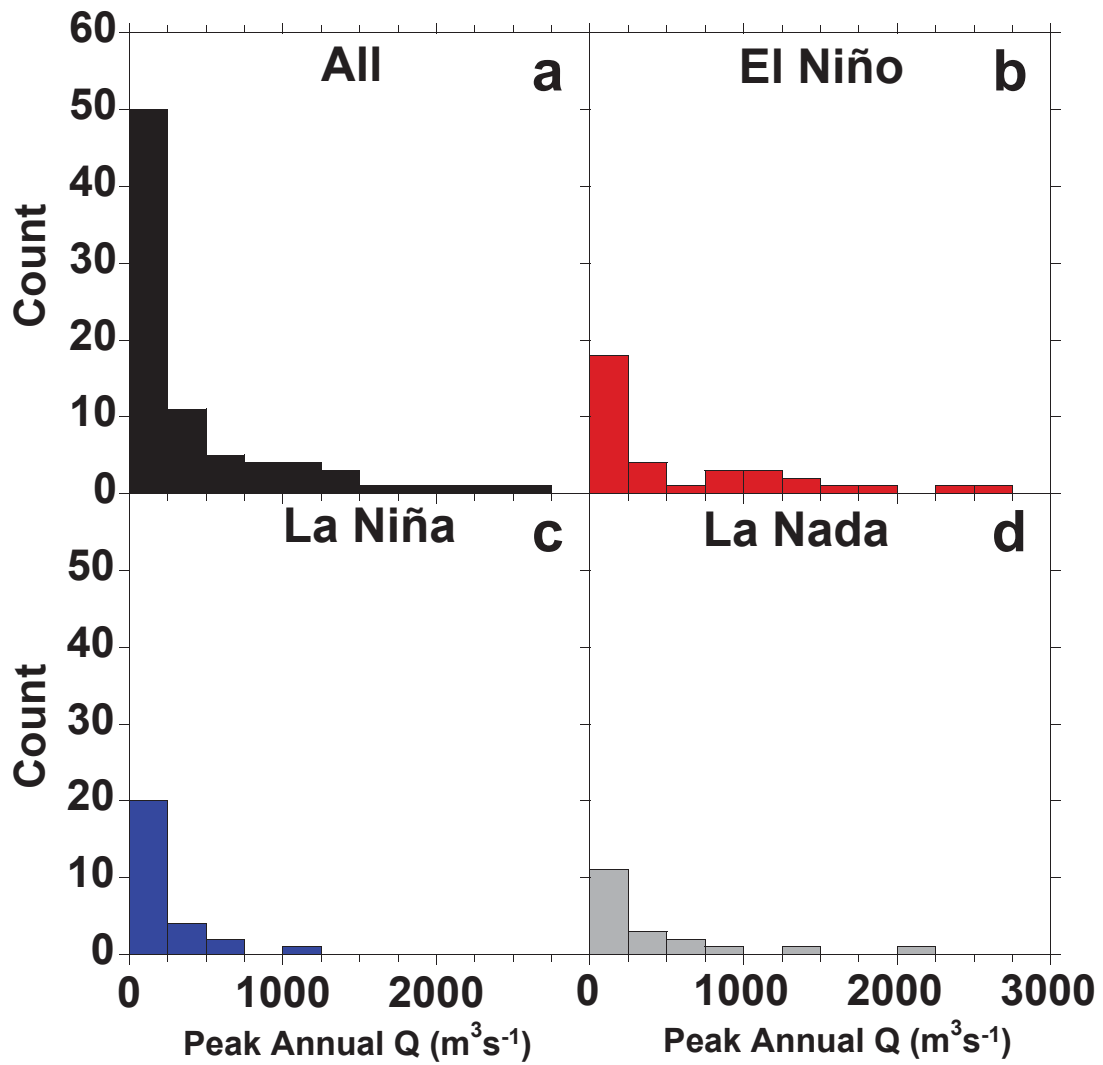


**Figure 4.14** Histograms of peak annual flow values at S1 for (a) the total record, (b) El Niño, (c) La Niña, and (d) La Nada years.

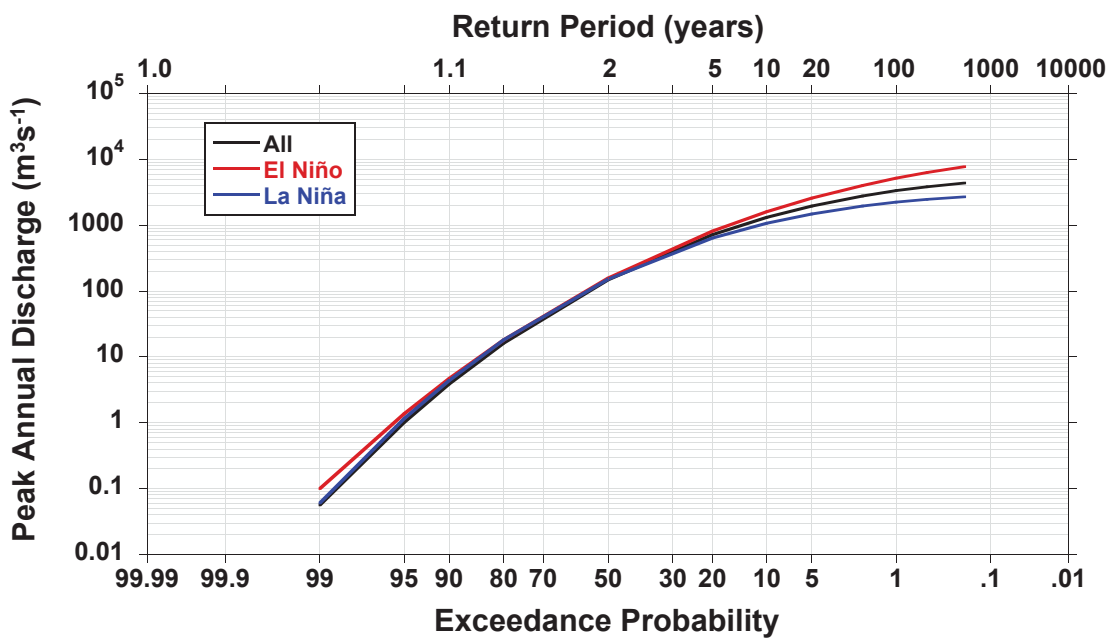


**Figure 4.15** Flood frequency analysis results for the lower Salinas at gauge S1 using Bulletin 17B calculations applied to peak instantaneous discharge values for the the hydrologic record 1930–2011. "All" indicates the probability curve calculated from the entire data set. "El Niño" and "La Niña" indicate curves based on sub-sets of peak discharge defined by water years dominated by either El Niño or La Niña like conditions.

log-linear regressions of USGS suspended sediment samples at S1 from the 1970s. Inman and Jenkins (1999) applied monthly average values, which probably caused their low estimate of 1.7 Mt/year, as monthly averaging of discharge values would decrease estimates due to the non-linear  $C_{SS} \sim Q$  relation. Additionally, Inman and Jenkins (1993) may have not employed a bias correction factor for logarithmic transformation, as none was mentioned in their methods, which would further lower their estimates. Farnsworth and Milliman (2003) used daily  $Q$  in their computations, and presumably a Ferguson-based correction factor for log bias, although this was unspecified in their report. Extrapolation of the 1970s, a decade of persistently high suspended sediment concentration, to the entire water discharge record resulted in their high  $Q_{SS}$  estimate of 3.3 Mt/year. Results of this study showed that estimations from a single linear regression rating curve for the longer (45 year) suspended sediment record used in this study reduced average annual  $Q_{SS}$  to 2.26 Mt/year (see Table 4.4). Although this and the preceding two studies obtain their averages over different temporal domains (this study: 1967–2011, Inman and Jenkins: 1944–1995, Farnsworth and Milliman: 1930–2000), comparisons between this study's average  $Q_{SS}$  estimations using log-linear regression over these three temporal domains revealed a 19% decrease and 9% increase by averaging over the respective studies' domains. Thus, the high Farnsworth and Milliman estimate is primarily the result of assuming stationarity in inter-decadal scale suspended sediment behavior.

Because even small to moderate sized river systems such as the Salinas often express decadal scale persistence in suspended sediment behavior, a sampling interval of a single decade can lead to under or over estimation of multi-decadal sediment flux averages if samples are collected from one period of persistent behavior. When the decadal scale variability of the lower Salinas River is explicitly acknowledged through separate rating curves, log-linear estimates are further reduced to 2.01 Mt/year, highlighting the effects of reducing a multi-decadal sample record with persistent cycles to a single relationship.

As found for other west coast river in the United States, this study found that the  $C_{SS} \sim Q$  relation is described better by a log LOESS curve than a log-linear curve (Williams, 1989; Farnsworth and Warrick, 2007; Warrick et al., 2013). Transitioning to a LOESS curve led to increases in average  $Q_{SS}$  estimates due to higher fine  $C_{SS}$  values over the low ( $< 1 \text{ m}^3\text{s}^{-1}$ ) and high ( $> 100 \text{ m}^3\text{s}^{-1}$ ) discharge domains

relative to linear regression predictions. Including hydrologic variables into multiple regression also increased the overall estimation of  $Q_{SS}$ . As these are the best estimates for  $Q_{SS}$  found in this study due to accounting for additional suspended sediment concentration variability, average annual  $Q_{SS}$  estimates for the lower Salinas are reported here as between the LOESS temporally zoned estimate of 2.13 Mt/year and the multiple regression estimate of 2.37 Mt/year. There was evidence of better fit from the multiple regression method for some years when LOESS temporal zone curves were lower than observed values (e.g., 1991–1993) including years critical to overall sediment flux, such as 1983. However, there were also indications that multiple regression estimates were over predicting  $C_{SS}$ , particularly in 1969.

Despite these limitations, this study represents a step forward toward enhancing the precision of sediment flux estimation by accounting for the effects of non-stationarity. Better estimates of  $Q_{SS}$  in the lower Salinas were achieved by using a longer sample records, and explicitly acknowledging persistent patterns in suspended sediment behavior and the effects of hydrologic preconditions.

#### 4.9.2 *Effective discharge of suspended sediment*

The overall picture of suspended sediment discharge for the lower Salinas River is one dominated by rare, large events at the multi-decadal scale. Greater than half the  $Q_{SS}$  is transported by discharges only exceeded once every  $\sim 3$  to 7 years. In contrast, the most effective transport of water takes place at magnitudes near  $Q_{mean}$ , and the majority of water is transported by discharges with return intervals of  $< \sim 2$  years. However, lower magnitude discharges, on the order of  $1-2 Q_{mean}$  move a significant amount of sediment in this system, on par with some of the rare, high discharge events ( $> 1500 \text{ m}^3\text{s}^{-1}$ , or  $\sim 130 Q_{mean}$ ).

The two estimates forwarded by this study as the most accurate, based on LOESS temporally zoned and multiple regression rating curves, each bore widely different effective discharge estimations (465 versus  $1811 \text{ m}^3\text{s}^{-1}$ , corresponding to 40 and 156 times  $Q_{mean}$ , respectively) and  $Q_{1/2}$  (498 versus  $814 \text{ m}^3\text{s}^{-1}$ , corresponding to 42 and 72 times  $Q_{mean}$ , respectively) for  $Q_{SS}$ . Indeed, the many methods of  $Q_{SS}$  estimation employed in this study produced a wide range of magnitude/frequency estimates, although  $Q_{1/2}$  for sand were generally higher than for fines and temporally zoned estimates of  $Q(e)$  were generally the same or higher than for total temporal domain estimates. All of these values are much higher than

the corresponding effective and half-load discharges of water, which are  $9.9$  and  $134 \text{ m}^3\text{s}^{-1}$  ( $0.9$  and  $11.6$  times  $Q_{mean}$ ) respectively. Thus, a relatively small fraction of water is transported by the moderate to very high magnitude events which transport most of the suspended sediment through the lower Salinas River.

This characteristic of the Salinas is similar to the transport effectiveness of suspended sediment in other highly episodic, small rivers draining the Coast Ranges of California. For example, the lower Eel River has been found to have a wide range of similar magnitude  $e(Q)$  values from  $\sim 5$ – $25 Q_{mean}$ , with a distinct  $Q(e)$  peak at  $\sim 31 Q_{mean}$  (Klonsky and Vogel, 2011). The lower  $Q(e)/Q_{mean}$  value of the Eel relative to the Salinas is most likely due to its position in the wetter north coast ranges. In contrast, larger rivers with more continuous flow characteristics generally have lower  $Q(e)$  and  $Q_{1/2}$  values, which are generally closer to  $Q_{mean}$  and more in line with the magnitude/frequency characteristics of water in those systems (Nash 1994).

Temporal zones of persistent sediment behavior varied in  $Q(e)$  placement due to changes in sediment rating curve shape. Sand behavior displayed a consistent shift in effective discharge from the moderate discharge  $e(Q)$  cluster ( $10$ – $40 Q_{mean}$ ) to extremely high discharge ( $170 Q_{mean}$ ) when moving from the high  $C_{SS}$  period (1967–1986) to the low  $C_{SS}$  period (1987–2010), due to the steeper rating curve for the latter zone (see Fig. 4.6d,e, Fig. 4.12). In contrast, fine sediment periods based on LOESS curves resulted in very similar  $Q(e)$  values for the 1991–1993 positive period and the joint negative periods (1980–1989, 1994–2011), while the positive period (1967–1979) resulted in a much higher  $Q(e)$  due to steep curvature of the rating curve in the upper discharge domain (see Fig. 4.5a–c, Fig. 4.11). Thus, even for a given distribution of flood probabilities, it is clear that non-stationarity in suspended sediment behavior leads to non-stationarity in effective discharge, which can cause the lower Salinas to behave more like a larger or wetter river, or like a smaller, more arid system depending on the period of activity.

#### 4.9.3 *The role of ENSO in suspended sediment discharge*

As reported by Farnsworth and Milliman (2003), large infrequent events almost always occur during positive El Niño years. Magnitude/frequency analysis clearly shows that moderate to high discharges accounts for most of the sediment transported through the lower Salinas at the inter-decadal scale. Furthermore, short elapsed time since the last moderate to high discharge activity has been

shown to increase sand concentrations (Chapter 2). Thus, El Niño cycles appear to increase total  $Q_{SS}$  and augment sand supply due to closer timing of these high discharge events. Indeed, the two best estimates of  $Q_{SS}$  advanced here (temporally zoned LOESS, and multiple regression with hydrologic variables) both showed that El Niño years transported an order of magnitude more sediment on average than non-El Niño years, with slightly higher proportional increases in sand (though absolute % sand decreased) (see Table 4.5). These conclusions are in broad agreement with the findings of previous studies that have highlighted the importance of El Niño on sediment transport in southern California (Inman and Jenkins, 1999; Farnsworth and Milliman, 2003; Andrews and Antweiler, 2012).

Investigation into the proportional contribution of these variables to fine  $C_{SS}$  estimations from the multiple regression showed that  $Q_{114}$  *Time* was on average greater than the negative adjustment of  $Q_1$  *Time* during 1967–1979, while the negative adjustments from  $Q_1$  *Time* were on average larger than the positive contributions of  $Q_{114}$  *Time* from 1980–1989 (see Table 4.4). However,  $Q_{114}$  *Time* also beat out  $Q_1$  *Time* during the negative fine sediment zone 1994–2011. Multi-decadal replacement of sprinkler and furrow with drip irrigation coincident with the latter half of the suspended sediment record found in Chapter 3 may be responsible in part for this departure in hydrologic variable control.

#### 4.10 Conclusions

This study produced the following results regarding lower Salinas suspended sediment behavior and flux:

- Sediment discharge estimates are best approximated by LOESS estimates utilizing separate temporally zoned rating curves or multiple regression curves that utilize hydrologic variables.
- Use of suspended sediment data sets collected over longer time spans, acknowledging decadal scale patterns and hydrologic variable affects resulted in a ~ 1 Mt/year (~ 30%) reduction of average annual  $Q_{SS}$  estimates in comparison to the most recent previous estimate.

- Most  $Q_{SS}$  through the lower Salinas occur during large ( $Q > 40 Q_{mean}$ ) rare events with return intervals  $> 3$  years, which is consistent with highly episodic, steep coastal systems on active margins, but not as extreme as observed on truly arid rivers.
- However, periods of persistent sediment behavior can 'down-regulate' the system toward moving a higher proportion of sediment during lower discharges, as well as 'up-regulate' toward emphasis on even rarer events (return interval  $\sim 20$  year) due to changes in the  $C_{SS} \sim Q$  relationship.
- El Niño years were responsible for  $\sim 10$  times more  $Q_{SS}$  on average than non-El Niño years from 1967–2011.

Despite these limitations,  $Q_{SS}$  in most systems continues to be estimated through the product of  $Q$  and  $C_{SS}$  estimated from simple sediment rating curves based on samples representing relatively narrow ranges of basin conditions and short temporal domains. The simple fact remains that suspended sediment data is time consuming and costly to collect. With a reduction in funding toward these sampling efforts across the United States, the possibility of achieving or maintaining the long-term records required to decipher long term sediment flux dynamics is reduced.

#### 4.11 References

- Andrews, ED. 1980. Effective and bankfull discharge of streams in the Yampa River Basin, Colorado and Wyoming: *Journal of Hydrology* **46**: 311-330
- Andrews ED, Antweiler RC. 2012. Sediment Fluxes from California Coastal Rivers: The Influences of Climate, Geology, and Topography. *Journal of Geology* **120**: 349-366. DOI: 10.1086/665733
- Andrews ED, Antweiler RC, Neiman PJ, Ralph FM. 2004. Influence of ENSO on flood frequency along the California coast. *Journal of Climate* **17**: 337-348. DOI: 10.1175/1520-0442(2004)017<0337:ioeoff>2.0.co;2
- Chatterjee S, Hadi AS, Price B. 2000. Regression Analysis by Example: New York, John Wiley & Sons, Inc., 359 pp.

- Cleveland WS. 1979. Robust locally weighted regression and smoothing scatterplots. *Journal of the American Statistical Association* **74**: 829-836
- Cohn TA, Delong LL, Gilroy EJ, Hirsch RM, Wells DK. 1989. Estimating constituent loads. *Water Resources Research* **25**: 937-942. DOI: 10.1029/WR025i005p00937
- Duan N. 1983. Smearing estimate - a nonparametric retransformation method. *Journal of the American Statistical Association* **78**: 605-610
- Farnsworth KL, Milliman JD. 2003. Effects of climatic and anthropogenic change on small mountainous rivers: the Salinas River example. *Global and Planetary Change* **39**: 53-64. DOI: 10.1016/s0921-8181(03)00017-1
- Farnsworth KL, Warrick JA. 2007. Sources, dispersal, and fate of fine sediment supplied to coastal California: U.S. Geological Survey Scientific Investigations Report 2007-5254, 77 pp.
- Ferguson RI. 1986. River loads underestimated by rating curves. *Water Resources Research* **22**: 74-76
- Gao P, Josefson M. 2012. Event-based suspended sediment dynamics in a central New York watershed. *Geomorphology* **139**: 425-437. DOI: 10.1016/j.geomorph.2011.11.007
- Gao P, Pasternack GB, Bali KM, Wallender WW. 2007. Suspended-sediment transport in an intensively cultivated watershed in southeastern California. *Catena* **69**: 239-252. DOI: 10.1016/j.catena.2006.06.002
- Helsel DR, Hirsch RM. 2002. Statistical methods in water resources—hydrologic analysis and interpretation: U.S. Geological Survey Techniques of Water-Resources Investigations. 510 pp.
- Hicks DM, Gomez B, Trustrum NA. 2000. Erosion thresholds and suspended sediment yields, Waipaoa River Basin, New Zealand. *Water Resources Research* **36**: 1129-1142
- Inman DL, Jenkins SA. 1999. Climate change and the episodicity of sediment flux of small California rivers. *Journal of Geology* **107**: 251-270
- Interagency Committee on Water Data (IACWD). 1982. Guidelines for determining flood flow frequency, Bulletin No. 17B (revised and corrected), Hydrology Subcommittee, Washington, D. C.
- Kahana R, Ziv B, Enzel Y, Dayan U. 2002. Synoptic climatology of major floods in the Negev Desert, Israel. *International Journal of Climatology* **22**: 867-882. DOI: 10.1002/joc.766

- Kelsey HM. 1980. A sediment budget and an analysis of geomorphic process in the Van-Duzen River Basin, north coastal California, 1941-1975 - summary. *Geological Society of America Bulletin* **91**: 190-195. DOI: 10.1130/0016-7606(1980)91<190:asbaaa>2.0.co;2
- Klein RD, Anderson JK. 2012. Declining sediment loads from Redwood Creek and the Klamath River, north coastal California. In: Proceedings of the Coastal Redwood Forests in a Changing California: A Symposium for Scientists and Managers, U.S. Department of Agriculture, Forest Service General Technical Report PSW-GTR-238, 79–88.
- Klonsky L, Vogel RM. 2011. Effective measures of "effective" discharge. *Journal of Geology* **119**: 1-14
- Milliman JD, Syvitski JPM. 1992. Geomorphic/tectonic control of sediment discharge to the ocean: the importance of small mountainous rivers. *Journal of Geology* **100**: 525-544
- Montgomery DC, Peck EA. 1992. Introduction to linear regression analysis: New York, John Wiley & Sons, Inc., 527 pp.
- Nash DB. 1994. Effective sediment-transporting discharge from magnitude-frequency analysis. *Journal of Geology* **102**: 79-95
- Pasternack GB, Brush GS, Hilgartner WB. 2001. Impact of historic land-use change on sediment delivery to a Chesapeake Bay subestuarine delta. *Earth Surface Processes and Landforms* **26**: 409-427
- Pedatella NM, Forbes JM. 2009. Interannual variability in the longitudinal structure of the low-latitude ionosphere due to the El Nino-Southern Oscillation. *Journal of Geophysical Research-Space Physics* **114**: A12316.
- Pelletier JD, Turcotte DL. 1997. Long-range persistence in climatological and hydrological time series: analysis, modeling and application to drought hazard assessment. *Journal of Hydrology* **203**: 198-208
- Potter, WD., 1958. Upper and lower frequency curves for peak rates of runoff, *Transactions Amer. geophys. Union* **39**: 100-105
- R Development Core Team. 2013. R: A language and environment for statistical computing. R Foundation for Statistical Computing, Vienna, Austria. <http://www.R-project.org/> (last accessed: 10/2013).
- Rasmussen PP, Gray JR, Glysson GD, Ziegler AC. 2009. Guidelines and procedures for computing time-series suspended-sediment concentrations and loads from in-stream turbidity-sensor and streamflow

- data: U.S. Geological Survey Techniques and Methods book 3, chap. C4, 53 pp.  
<http://pubs.usgs.gov/tm/tm3c4/> (last accessed 3/13/2013).
- Shakesby RS, and Doerr SH. 2006. Wildfire as a hydrological and geomorphological agent. *Earth-Science Reviews* 74: 269–307
- U.S Army Corps of Engineers (USACE), 2010. HEC-SSP, Statistical Software Package, User's Manual, Version 2.0, CPD-86, Institute for Water Resources, Davis, CA, USA.
- U.S. Geological Survey National Water Information System (USGS NWIS),  
<http://waterdata.usgs.gov/nwis/sw> (last accessed: 03/2013).
- Vogel RM, Stedinger JR, Hooper RP. 2003. Discharge indices for water quality loads. *Water Resources Research* 39. DOI: 10.1029/2002wr001872
- Walling DE. 1977. Assessing accuracy of suspended sediment rating curves for a small basin. *Water Resources Research* 13: 530-538
- Wand MP. 2012. KernSmooth: Functions for kernel smoothing for Wand & Jones (1995). R package version 2.23-8. <http://CRAN.R-project.org/package=KernSmooth> (last accessed 3/13/2013).
- Wand MP, Jones MC. 1995. Kernel Smoothing. Chapman and Hall, London. 212 pp.
- Warrick JA, Mertes LAK. 2009. Sediment yield from the tectonically active semiarid Western Transverse Ranges of California. *Geol. Soc. Am. Bull.* 121: 1054-1070
- Warrick JA, Rubin DM. 2007. Suspended-sediment rating curve response to urbanization and wildfire, Santa Ana River, California. *Journal of Geophysical Research-Earth Surface* 112. DOI: F0201810.1029/2006jf000662.
- Warrick JA, Hatten JA, Pasternack GB, Gray AB, Goni MA, Wheatcroft RA. 2012. The effects of wildfire on the sediment yield of a coastal California watershed. *Geological Society of America Bulletin* 124: 1130-1146. DOI: 10.1130/b30451.1.
- Warrick JA, Madej MA, Goni MA, Wheatcroft RA. 2013. Trends in the suspended-sediment yields of coastal rivers of northern California, 1955-2010. *Journal of Hydrology* 489: 108-123. DOI: 10.1016/j.jhydrol.2013.02.041.
- Webb BW, Walling DE. 1982. The magnitude and frequency characteristics of fluvial transport in a Devon drainage basin and some geomorphic implications. *Catena* 9: 9-23

- Williams GP. 1989. Sediment concentration versus water discharge during single hydrologic events in rivers. *Journal of Hydrology* **111**: 89-106
- Wheatcroft RA, Goni MA, Hatten JA, Pasternack GB, Warrick JA. 2010. The role of effective discharge in the ocean delivery of particulate organic carbon by small, mountainous river systems. *Limnology and Oceanography* **55**: 161-171. DOI: 10.4319/lb.2010.55.1.0161
- Wolman MG, Miller JP. 1960. MAGNITUDE AND FREQUENCY OF FORCES IN GEOMORPHIC PROCESSES. *Journal of Geology* **68**: 54-74
- Wolman MG, Shick AP. 1967. Effects of construction on fluvial sediment; Urban and suburban areas of Maryland. *Water Resources Research* **3**: 451-464
- Wolter K, and Timlin MS. 2011. El Nino/Southern Oscillation behaviour since 1871 as diagnosed in an extended multivariate ENSO index (MEI.ext). *International Journal of Climatology* **31**: 1074-1087

## Chapter 5

### **Abandoned channel fill sequences in the tidal estuary of a small mountainous, dry-summer river**

#### **Abstract**

Abandoned river channel fills are important sedimentological structures that remain understudied, particularly in tidal settings that experience bi-directional flow and highly seasonal fluvial activity. This study proposes a modification of the current generic model for abandoned channel fill stratigraphy produced in unidirectional flow river reaches to incorporate seasonal tidal deposition. Evidence supporting the new concept came from a thorough study of two consecutive channel abandonment sequences in Ropers Slough of the lower Eel River Estuary in northern California. Aerial photographs showed that Ropers Slough had been abandoned around 1943, then reoccupied after a ~ 200-year recurrence interval flood in 1964, only to be abandoned again in 1974 to fill in up to the present day 40 years later. Planform geomorphic characteristics derived from these images were used in conjunction with sub-cm resolution stratigraphic analyses to describe the depositional environment processes and their resultant sedimentary deposits. Study results found that both abandonment sequences recorded quasi-annual scale fluvial/tidal deposition couplets. In both cases tidal deposits were higher in organic and inorganic carbon content, containing very little or no sand. However, the two abandonment fills differed significantly in terms of the temporal progression of channel narrowing and fluvial sediment deposition characteristics. The first abandonment sequence led to a much more rapid narrowing of Ropers Slough, and produced deposits with a general positive relationship between grain size/deposit thickness and discharge magnitude. The second abandonment resulted in a much slower narrowing of Ropers Slough and generally thinner fluvial deposits with no clear relationship to discharge magnitude. Differences in fill sequences appear to have been caused in part by the position of the Ropers Slough channel entrance relative to channel meander morphology. Thus, the abandoned channel fill sequences appeared to differ due to the topographic steering of bed sediment transport and deposition previously

identified in rivers experiencing only unidirectional flow, while also expressing the seasonal dichotomy of fluvial and tidal deposits.

## **5.1 Introduction**

### *5.1.1 Background*

Tidally influenced abandoned channel deposits are important as valuable records of autogenic processes and allogenic signatures related to tectonism, climate, hydrology, and upper basin environmental history. Abandoned channel fills of lowland meandering and anabranching rivers comprise a significant proportion of the terrestrial sedimentary record, yet very few studies have focused on their generation and structure (Toonen et al., 2012). Although Fisk (1947) developed an initial conceptual model for abandoned channel fill development, only a handful of case studies have examined the stratigraphy of abandoned channels produced under conditions recorded over historic time (e.g. Hooke, 1995; Werritty et al., 2006; Constantine et al., 2010). These studies, and that of Shields and Abt (1989) on human constructed fluvial lakes, have shown that the progression of sedimentation in abandoned fluvial channels is highly dependent on autogenic factors such as the morphology of the bifurcation zone and the bed level/downstream channel slope of each bifurcate. The main autogenic control on abandoned channel alluviation is divergence angle – the angle between the mean directions main and abandoned channel flows; initially identified by Fisk (1947) and supported by these observational studies. Allogenic controls have also been observed, including discharge magnitude/frequency characteristics (Citterio and Piégay, 2009; Hoek et al., 2011). Numerical modeling exercises have confirmed the mechanisms behind the effects of local and upstream channel morphology on abandoned channel sedimentation (Constantine et al., 2010; Kleinhans et al., 2011), in addition to bank strength (Sun et al., 1996), and upstream meander position (Kleinhans et al., 2008).

Generic models of abandoned channel fill architecture have been developed from the above studies – the most recent of which was produced by Toonen et al. (2012). The Toonen model describes two end members driven by fluvial sediment connectivity between the major channel and abandoned channel, which is largely controlled by the development of plug bars at the entrances of the abandoned

channel (Fig. 5.1). On one end of the spectrum abandoned channels continue to receive regular throughflow and entrained bedload. In these cases the abandoned channel geometry (width, depth) is reduced relatively rapidly over time, and the resultant channel fill will include thick deposits of material similar to the underlying channel bed. On the other end of the spectrum are abandoned channels with no regular throughflow connectivity and no entrainment of bedload from the main channel. These channels, commonly referred to as 'oxbow lakes', only receive fluvial sediment during overbank events (Allen, 1965). As such, they tend to fill much more slowly, and with much finer sediment that can contain seasonal and event based laminations. Abandoned channel fills commonly progress from the former to latter end members over time, as plug bars form at the entrance/exit of abandoned channels due to flow separation/backwater effects, and eventually block bedload connectivity (Fisk, 1947). Increased divergence angle, and by extension local sinuosity, increases the rate of plug bar formation, which decreases the time period of effective bed load advection into the abandoned channel, and more rapidly disconnects it from main channel flows and all classes of fluvial sediments.

### *5.1.2 New conceptual model*

Despite these advances in the understanding of abandoned channel development and alluviation, the current generic model does not incorporate tidal effects. Most of the studies that established the principles of channel fill dynamics listed above focused on meandering gravel to coarse sand bedded rivers that accomplished meander abandonment through neck or chute cut-offs, and without reoccupying abandoned channels. These rivers were also driven by strictly fluvial regimes, far upstream from the influence of tides. In contrast, tidally influenced river reaches can exhibit strong bi-directional flow, and they also experience channel abandonment and fill. When such a system experiences periodic low fluvial output, the geomorphology and stratigraphy could be governed by an interplay between two distinct and

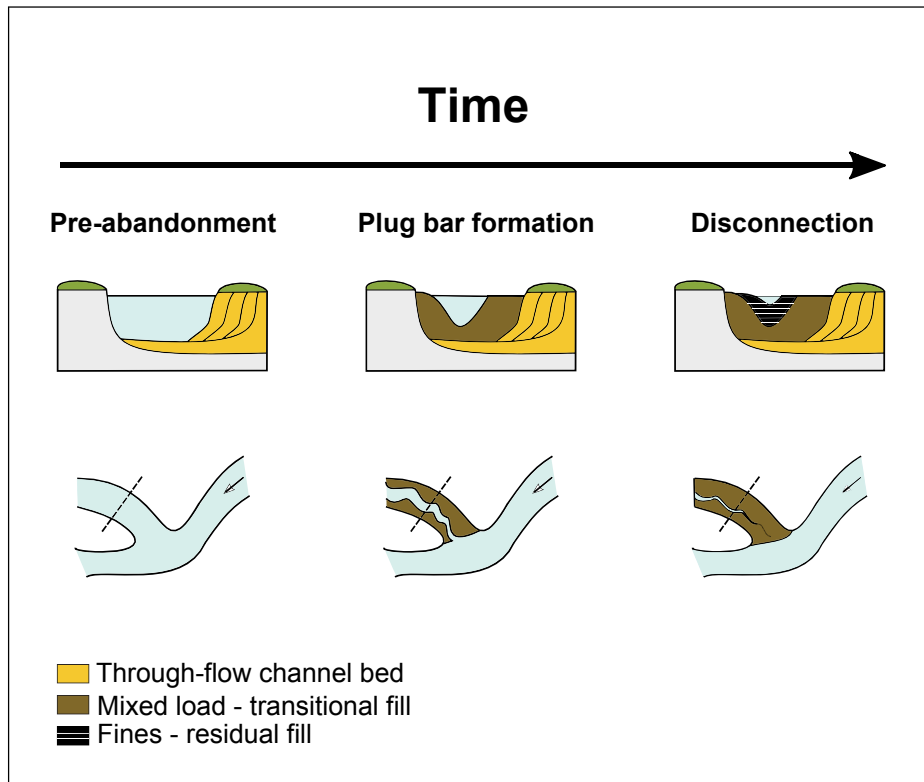


**Figure 5.1** Toonen et al. (2012) conceptual model of abandoned channel fill sequence progression.

oscillating regimes: (i) fluvial deposits produced during high discharge periods (wet seasons), and (ii) tidally dominated deposits during low discharge periods (dry seasons). Periodic low flow conditions are typical of river systems that are small (drainage area  $< 10^4$  km<sup>2</sup>), and/or experience a highly variable precipitation regime with inundation cycles at seasonal to inter-annual time scales typical of semi-arid, dry-summer or monsoonal climates (e.g. Puckridge et al., 2000; Andrews et al., 2004). At low diversion angle/early plug bar formation, abandoned channels are expected to act as a high water sub-channel subject to throughflow (with or without bed load transport) during peak winter flows, and then as a tidal slough fed through the downstream entrance during low discharge periods. Tidal action may also influence the evolution of these systems over periods greater than the time scale of abandonment, as tidal flows can maintain the downstream entrance opening (Kleinhans, 2009), and prolong a gradient benefit that may increase the likelihood of reoccupation during high flow events (Smith et al., 1998; Stouthamer, 2005).

The objectives of this study were to: (i) link the sediment fill of a tidally influenced, abandoned fluvial channel in a dry summer coastal system to precise periods of geomorphic activity, (ii) determine if the resultant sedimentary characteristics could also serve as indices for historical river discharge magnitude, (iii) identify the mechanisms behind differences in the geomorphic and stratigraphic fill sequences, and (iv) use the insights of this case study to modify the generic through flow and overbank channel fill model of Toonen et al. (2012). It was expected that the same autogenic and allogenic factors operating in strictly fluvial systems would greatly affect the overall progress of channel filling, namely diversion angle and upstream bend placement effects on bedload entrainment. The general approach to these issues employed a combination of sedimentary, aerial image and hydrologic analyses.

## **5.2 Study region**

The Eel River drains 9500 km<sup>2</sup> of mostly steep, forested terrain of the north California Coast Ranges to the NNW through a highly episodic hydrologic and sediment transport regime. Regional climate is dry summer temperate with cold, wet winters, and dry warm summers. A high gradient of precipitation (250 – 50 cm yr<sup>-1</sup>) extends from the coast region to the interior of the watershed. Mean

discharge ( $Q_{mean}$ ) at the lowest gage in the basin (USGS #11477000, *Eel River at Scotia, CA*) is  $206 \text{ m}^3 \text{ s}^{-1}$ , with 10- and 100-year recurrence interval mean daily flows estimated as  $9200 \text{ m}^3 \text{ s}^{-1}$  and  $14,300 \text{ m}^3 \text{ s}^{-1}$ , respectively, through log Pearson Type III flood frequency analysis (USGS NWIS, 2014).

This study focused on the vicinity of Ropers Slough, an abandoned channel in the Eel River Estuary, which lies  $\sim 7 \text{ km}$  south of Humboldt Bay ( $40^\circ 38' 21.46'' \text{N}$ ,  $124^\circ 16' 11.79'' \text{W}$ ). The Eel River Estuary is the fourth largest in California, with  $\sim 11 \text{ km}^2$  of intertidal/subtidal area (Schlosser & Eicher, 2012). Reaches in the study area were defined on the basis of bifurcation and convergence nodes in the lower Eel Estuary (Fig. 5.2). A major bifurcation (Node 1) splits the lower Eel River Estuary channel into two bifurcates defined as (i) the South Channel and (ii) the Ropers Slough/Central Channel Complex (RSC). The RSC was further subdivided due to a secondary bifurcation (Node 2) into Ropers Slough and the Central Channel. Downstream convergence nodes are defined as the confluence of Ropers Slough and the Central Channel (Node 3) and the confluence of the RSC and the South Channel (Node 4). Ropers Slough has existed at times as the major channel in the RSC complex, and at others as an abandoned high water channel/tidal slough, the details of which will be explored more fully in the following sections.

Early reports from settlers in the 19<sup>th</sup> Century indicated that the Eel River Estuary was largely forested with pine, spruce, alder and redwoods, almost all of which was cleared by the late 1800s (Schlosser and Eicher, 2012). Today tidal mudflats and marshland mostly exist along main and recently abandoned fluvial channels in the central portion of the estuary, and along the northern tidal slough complexes. Vegetation assemblages in tidal marshes include *Sarcocornia pacifica*, *Distichlis spicata*, *Jaumea carnosa*, and *Jaumea carnosa* (Schlosser and Eicher, 2012; personal observations of the author).

Tides are mixed semi-diurnal, and tidal influence currently extends about 11 river km upstream during the low water summer months. Tidal prism was most likely decreasing by the early 20<sup>th</sup> century, and is estimated to have experienced a  $\sim 40\%$  decrease since 1900 (SCS, 1989). Much of this

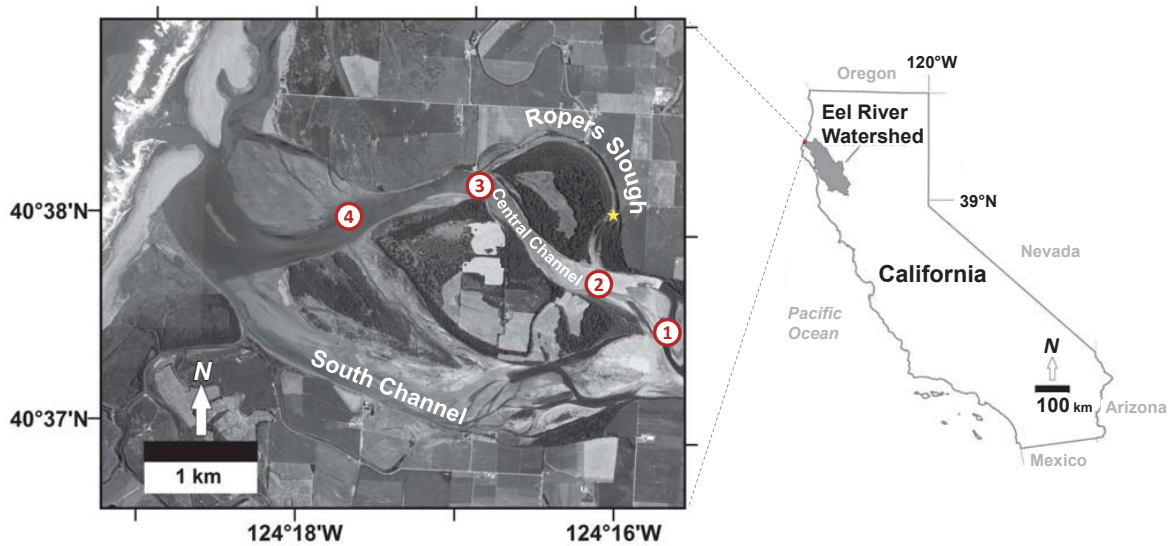


**Figure 5.2** The lower Eel River Estuary study region (image date 6/27/2009). Fluvial flow direction is generally right to left, with the Eel River mouth to the Pacifica Ocean visible in the upper left corner. The main northern Eel River channel system (the RSC complex) proceeds from Node 1 to Node 4. The Central Channel currently is the primary conveyance, while Ropers Slough is a tidal slough that receives high flows during the wet season. The star located toward the south east end of Ropers Slough indicates the location of the EDRS cores.

reduction is attributed to a ~ 200 year flood event (peak discharge  $> 20,000 \text{ m}^3\text{s}^{-1}$ ) that occurred in December of 1964 (described more fully below), and drastically filled the deeper pools of the south channel (Li et al., 1992; Van Kirk, 1996).

Rare high discharge events on the Eel have produced larger sediment yields than perhaps any other river in the U.S. (Brown and Ritter, 1971; Kelsey, 1980; Warrick et al., 2013; USGS NWIS, 2014). The high sediment load of the Eel River is driven by large storm events acting upon extremely erodible geology, especially the mass wasting prone Franciscan mélangé, a highly deformed class of Cenozoic metasedimentary marine rock that underlies the central portion of the basin (Kelsey, 1980, McLaughlin et al., 1989). High sediment loads appear to have been exacerbated by large scale industrial timber harvesting, which began in the late 19<sup>th</sup> Century and continues to be the largest human impact in the watershed (Kelsey, 1980; Warrick et al., 2013). Small pockets of urbanization and agriculture take advantage of the few lowlands present in this region, including the Eel River Estuary (Schlosser and Eicher, 2012).

The extraordinary amount of sediment moved by the 1964 flood and the widespread geomorphic effects that followed inspired a great deal of scientific interest, mostly from the coastal marine sediment, fluvial sediment transport, and hillslope geomorphology communities. Subsequent studies focused on sediment load estimation (Brown & Ritter, 1971; Kelsey, 1980; Sommerfield et al., 2002; Warrick et al., 2013), hillslope processes governing the delivery of sediment to the channel (i.e. Mackey et al., 2011), or the fate of these sediments on the continental shelf (Wheatcroft et al., 1997; Nittrouer, 1999; Blair et al., 2004, Sommerfield and Wheatcroft, 2007). The latest studies on suspended sediment dynamics of the Eel River and neighboring systems have shown that the 1964 flood engendered a period of increased suspended sediment load that has relaxed over the latter half of the 20<sup>th</sup> and beginning of the 21<sup>st</sup> Centuries (Madej et al., 2012; Warrick et al., 2013; Warrick, 2014). Gravel bedded reaches upstream have continued to express the effects of the 12/1964 event 35 years later (Sloan et al., 2001).

Previous geomorphic and sedimentological work in the Eel Estuary documented the channel aggradation/avulsion history in the vicinity of Ropers Slough, and estuarine scale sedimentation. Haley (1970) described the major morphological changes in the Eel River Estuary between 1950 and 1969, including the aggradation of deep pools in the south channel after the 1964 flood. Puckett (1977)

documented subsequent changes to the Eel Estuary channels through the initiation of the second abandonment of Ropers Slough in 1974. Boles et al. (1977) characterized channel bed sediment in terms of texture classes on the basis of samples collected from 1975 – 1976. Li et al. (1991) collected three sediment cores from the Eel Estuary and posited that late Holocene deposition at the estuarine scale was controlled by infrequent episodes of rapid subsidence. A recent report by Schlosser and Eicher (2012) characterized changes in Eel River Estuary benthic habitat types from 1948 to 2009 on the basis of high resolution aerial imagery and ground based surveys.

### 5.3 Materials and methods

#### 5.3.1 Sedimentology

A single stratigraphic record was sought from a middle-zone, brackish, tidal marsh surface (hereafter referred to as the single coring location 'EDRS'), vegetated with *Spartina* and located on the interior portion of Ropers Slough, in the lower Eel River Estuary on 7/23/2008 (Fig. 5.2). To avoid problems caused by coring through a vegetated mat, the record was obtained using a pair of sediment cores of overlapping depth- one including the vegetation (0–38 cm depth) and one obtained 50 cm laterally from the first starting below the vegetation (21.5 to 303 cm depth). The short section was hammer driven, while the long section was recovered with the vibracoring method with a piston to generate suction up the tube. Cores were transported to the laboratory, split, photographed, and described. Archival acrylic D-channels were digital x-radiographed at the University of California at Davis Veterinary Medical Teaching Hospital. Sediment horizons were sub sampled on the basis of stratigraphic intervals for particle size distribution, inorganic and organic carbon content, stable carbon isotopes and  $^{14}\text{C}$  radiometric dating.

Particle size distribution analyses were run on 195 horizons. Sediments with diameters less than gravel (diameter (D) < 2000  $\mu\text{m}$ ), were subsampled in volumes of  $\frac{1}{4}$  to  $\frac{1}{2}$  cc, processed to remove organic material, dispersed, and run with three replicate pulses through a Beckman Coulter LS-230 with polarized differential intensity of scattered light (PIDS) for measurement to a minimum size of 0.04  $\mu\text{m}$  as per Gray et al. (2010). Additionally, gravel bearing horizon masses of 40 to 400 g were subsampled,

dispersed with 0.5 % sodium hexametaphosphate solution, agitated for 16 hours and then wet sieved to remove the fine fraction (clay ( $D < 4 \mu\text{m}$ ) + silt ( $D = 4$  to  $63 \mu\text{m}$ )). The retained mix of sand and gravel was dried at  $60 \text{ }^\circ\text{C}$  for 24 hours, weighed to  $\pm 0.001 \text{ g}$ , then sieved for 10 minutes on a Thomas sieve shaker, and reweighed as pan fractions. Particle size distributions for the gravel range were constructed by obtaining the % mass for each gravel fraction relative to the total sample mass. Total sample mass was calculated by summing the weighted gravel and sand mass with a calculated fine fraction mass, which was obtained by applying the laser granulometry based volumetric relationship between fines and sand to the sieving sand mass.

Additional particle size distribution data for channel bed, bed load and suspended sediment samples collected by the USGS from the *Eel River at Scotia, CA* gaging station (#11477000) were processed by the USGS using mass based sieving and settling techniques (USGS NWIS, 2014). Log-linear rating curves of suspended sediment concentration ( $C_{SS}$  (mg/L)) vs. water discharge ( $Q$ , ( $\text{m}^3\text{s}^{-1}$ )) were also plotted for each  $\phi$  interval and texture class.

All particle size distribution data were analyzed with GRADISTAT v.8 to compute descriptive statistics in units of  $\mu\text{m}$  and  $\phi$  based on the logarithmic method of moments (Folk, 1974; Tanner, 1995; Blott and Pye, 2001,). Sediment texture classes (e.g. clay, silt, sand, etc.) were reported as per the Blott and Pye (2001) modified Udden/Wentworth scale (Wentworth 1922), with the exception that the original clay/silt transition of  $4 \mu\text{m}$  was maintained.

Carbon content measurements were performed on bulk sediment samples. Sediment samples of 1 cc were dried at  $60 \text{ }^\circ\text{C}$  for 24 hours, equilibrated to ambient temperature over desiccant in vacuum, weighed, combusted at  $550 \text{ }^\circ\text{C}$ , and then reweighed. Total carbon content (%TC) was approximated by calculating the loss on ignition mass and normalizing to the mass of the initial dried sample percent inorganic carbon was (Goñi et al., 2000; Goñi et al., 2005). Total inorganic carbon (%TIC) was measured using an automated carbonate system (Ostermann et al., 1990), and the organic carbon content (%OC) was calculated as the difference between %TC and %TIC. The stable isotopic compositions of OC ( $\delta^{13}\text{C}_{\text{OC}}$ ) were measured on pre-acidified sediments using a CHN analyzer coupled to a Finnigan Delta-S mass spectrometer (Fry et al., 1992). Organic carbon  $^{13}\text{C}/^{12}\text{C}$  ( $\delta^{13}\text{C}_{\text{OC}}$ ) was measured for with a Finnigan Delta-S mass spectrometer and is reported relative to the PDB standard (VPDB) (Fry et al., 1992).

The chronostratigraphic model for EDRS was based on post-bomb radiocarbon techniques due to the recent deposition of EDRS sediment. Above ground nuclear explosions in the 1950s and 1960s caused a rapid increase in atmospheric  $^{14}\text{C}$  levels, which have been declining since the mid-1960s due primarily to mixing of global  $\text{CO}_2$  reservoirs (Rafter and Fergusson, 1957; Buchholtz, 2009). Collection of radiocarbon samples from EDRS horizons was constrained to autochthonous seeds and leaves to minimize the time lag between the biological material generation and horizon sequestration. Samples were cleaned and processed for accelerator mass spectrometry (AMS) measurements of fraction modern  $^{14}\text{C}$  ( $F^{14}\text{C}$ ) and  $\delta^{13}\text{C}$  using the standard acid/alkali/acid procedure followed by graphitization at the National Ocean Sciences Accelerator Mass Spectrometry Facility (NOSAMS) and the Lawrence Livermore National Laboratory Center for Accelerator Mass Spectrometry (CAMS). Estimations of  $F^{14}\text{C}$  were calculated as per Reimer et al. (2004) with corrections for  $\delta^{13}\text{C}$  and background interference. In cases where  $\delta^{13}\text{C}$  was not measured at the AMS facility due to small sample size, the average  $\delta^{13}\text{C}$  obtained through mass spectrometry of 56 EDRS horizons was used to revise  $F^{14}\text{C}$ . The  $F^{14}\text{C}$  error in these cases was also revised based on  $\delta^{13}\text{C}$  measurement error and the standard deviation of EDRS horizon  $\delta^{13}\text{C}$  values combined in quadrature. Date ranges for  $F^{14}\text{C}$  values were calibrated using the CaliBomb program set to NH Zone 2 (Reimer et al., 2013). Although EDRS is located near the border of NH Zones 1 and 2, the differences in calibrated dates were on the order of  $< 1$  year, and insignificant for the purposes of this study.

### 5.3.2 *Planform geomorphology*

The planform evolution of Eel River channel structure in the vicinity of Ropers Slough was reconstructed from 20 aerial photographs collected between 1940 and 2009, and obtained from the USGS (USGS Earth Explorer, 2014) (Table 5.1). This photo sequence includes two cycles of Ropers slough channel abandonment (Fig. 5.3). Channel abandonment times were assigned to the date of highest daily discharge at the Scotia gage between the date of the most recent photographs before and after abandonment. Photographs without spatial references were georectified in ArcGIS 10.1 with a 3<sup>rd</sup> degree polynomial transformation using 11 to 30 georeferenced control points tied to 0.5-m resolution orthorectified photographs collected in 2009 for the Humboldt Bay and Eel River Estuary Benthic Habitat

Project (Hughes et al., 2006; Schlosser and Eicher, 2012). Median spatial resolution (raster cell size,  $R$ ) for the entire time series of photographs was 2.24 m with a range of 0.50 to 8.16 m. The median RMSE of referencing errors (spatial distortion,  $o$ ) was 0.85 m with a range of 0.08 to 4.7 m.

Serial photographs were used to compile the following time series: (i) the depositional/erosional environment at the EDRS collection site, (ii) the location of the upstream entrance to Ropers Slough relative to the meander morphology of the RSC complex, and (iii) measurements of channel characteristics. The geomorphic setting of the EDRS location was determined for each photo as (i) major fluvial through-flow channel bed, (ii) minor fluvial channel/tidal slough channel bed, or (iii) emergent marsh. Assigned geomorphic setting was highly certain, as EDRS was sufficiently far from geomorphic boundaries for each time period to be unaffected by the combination of spatial error ranges. The entrance of Ropers Slough was identified as located either on the outer bank or inner bank of meander bends in the RSC complex.

Three channel characteristics as defined below were measured for each reach using ArcGIS 10.1: cutoff ratio, diversion angle, and average active channel width. For channel cutoff events, the cutoff ratio is the length of the abandoned channel divided by the length of the cutoff channel. To calculate cutoff ratio, channel lengths were measured in ArcGIS 10.1 along the estimated thalweg between characteristic nodes. Diversion angle is the angle between average flow direction in the cutoff channel and flow into the entrance of the abandoned channel (Fisk, 1947). Diversion angle was calculated from the vertices of main channel and sub-channel centerlines measured from the earliest photograph after the cut-off. Active channel width was defined as the distance between vegetated banks normal to the channel centerline. It was measured in 20 equally spaced increments for each reach. Planimetric measurement errors ( $\epsilon_m$ ) were assumed to be isotropic and thus calculated as the sum of ground feature identification error and residual distortion error:

$$\epsilon_m = \sqrt{2}pR + 2o \quad (5.1)$$

where  $p$  is the imprecision of identifying ground features, as an integer of pixels size (resolution,  $R$ ) and  $o$  is the spatial distortion (Mount et al., 2003). A value of  $p = 2$  was estimated by replicate measurements of the highest and lowest resolution images used in this study.

#### 5.4 Data analysis

A general stratigraphic zonation of the EDRS core was developed on the basis of sediment texture and layering. Basic horizon types were then defined by particle size distribution characteristics, and stratigraphic units of adjacent similar horizons were composed. This lithostratigraphy was then set within a chronostratigraphic model and accompanied by carbon composition results. The chronostratigraphic model was based on a combination of bomb calibrated  $^{14}\text{C}$  dates in the context of the geomorphic conditions interpreted from aerial photographs, the Eel River hydrograph and stratigraphic changes. These factors contributed to the assignment of depositional environments to core levels with further aid from aerial photograph based geomorphic mapping over the time of core accretion. Comparisons of particle size distribution descriptors between populations of samples were achieved through mean state comparisons using T-tests (threshold of significance  $p \leq 0.05$ ) with the conservative assumption of unequal variance (Helsel and Hirsch, 2002).

Sedimentary characteristics were then examined in light of the chronostratigraphic model, and geomorphic and hydrologic time series. Sums of fine/coarser stratigraphic unit couplets for the abandoned channel sequences were compared to (i) the duration of deposition, and (ii) the number of events satisfying threshold discharge magnitudes to explore the possibility of seasonal hydrologic regime (fluvial/tidal) and event magnitude controls. Maximum daily discharge for each water year was then compared graphically with the following stratigraphic characteristics: (i) unit thickness, (ii) maximum  $D_{90}$  and (ii) maximum % coarse (sand + gravel) of the measured horizons in each unit. The water discharge time series and fluvial sediment particle size characteristics were considered in terms of the stratigraphic model and EDRS particle size metrics.

Particle size distribution characteristics were then plotted in statistical domains developed by Tanner to further evaluate shifts in transport agency and depositional regimes (Tanner, 1991; Larrío et al.,

**Table 5.1** Aerial photograph source data

Date	Agency <sup>b</sup>	Resolution (m)	Spatial distortion (m) <sup>c</sup>	GCP <sup>d</sup>
7/27/2009	NOAA	0.50	-	-
6/29/2005	USDA, NAIP	1.00	-	-
9/3/1998	USGS	3.49	0.47	14
6/15/1993	USGS	3.23	0.49	>10
4/28/1989	USGS	4.06	0.08	>10
8/28/1985	USGS	2.24	0.10	11
7/8/1982	USGS	6.90	0.67	>10
6/27/1980	USGS	7.11	4.33	14
5/29/1979	USGS	8.16	1.73	13
5/8/1978	USGS	5.69	0.91	13
1/4/1977	USGS	6.51	0.71	11
4/29/1974	USGS	6.64	0.89	14
4/3/1974	USGS	7.47	1.39	12
1/21/1974	USGS	6.19	0.88	12
4/4/1973	USGS	5.31	0.83	13
7/15/1972	USGS	1.00	0.55	13
summer, 1965 <sup>a</sup>	HBHRCD	0.70	4.70	30
9/13/1956	USGS	1.10	1.46	16
summer, 1948 <sup>a</sup>	HBHRCD	0.70	2.58	26
12/13/1940	USGS	1.09	0.82	14

<sup>a</sup>The 1965 and 1948 high resolution mosaics were collected over an undetermined time period during the respective summer seasons.

<sup>b</sup>The Agencies are: NOAA= National Oceanographic and Atmospheric Administration, USDA; NAIP = U.S. Department of Agriculture, National Agriculture Imagery Program; USGS = U.S. Geological Survey.

<sup>c</sup>Spatial distortion reported as the maximum if multiple digital photographs used for a given date

<sup>d</sup>GCP = Georeferenced control points. The values listed indicate the minimum number of control points if multiple digital photographs were used for a given date.

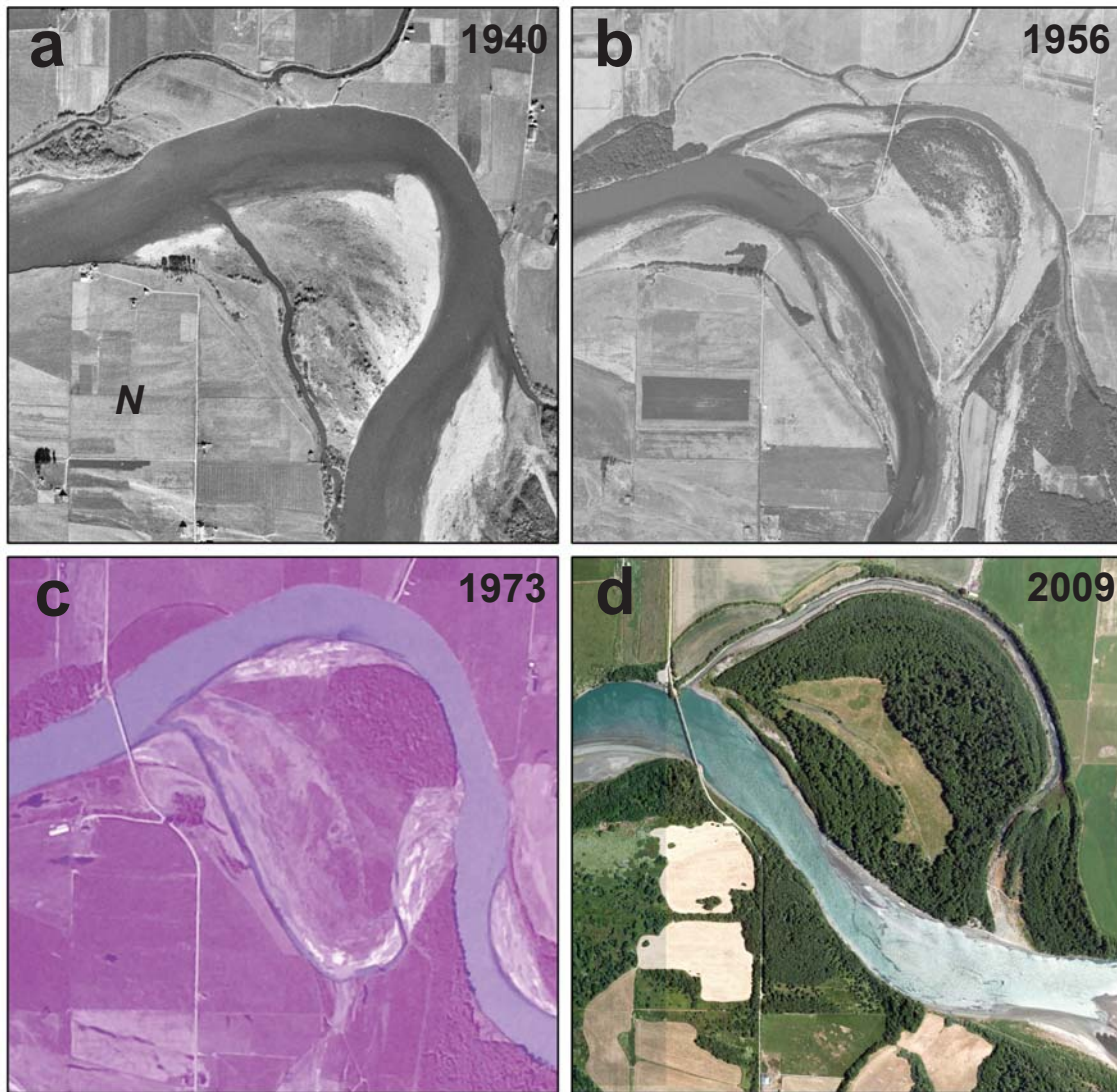


**Figure 5.3** Aerial photo sequence of the Ropers Slough and Central Channel region in 1940, 1956, 1973, 2009. Ropers Slough is in the upper right portion of the frame and the Central Channel occupies center frame. All images are in the same scale and represent the same spatial extent.

2002; Watson et al., 2013). Suite mean values of the following sample statistics (all in  $\phi$  units): mean, sorting, skewness, and kurtosis, as well as suite standard deviations of means ( $\sigma\mu$ ) and sorting ( $\sigma\sigma$ ) were calculated for each sample type (suspended sediment, bedload, channel bed, and stratigraphic units). These were then plotted into (i) mean vs. sorting, (ii)  $\sigma\mu$  vs.  $\sigma\sigma$ , (iii) skewness vs. kurtosis, and (iv) sorting vs. skewness spaces.

## 5.5 Results

### 5.5.1 Stratigraphic zones

The major textural dichotomy found in EDRS was the presence of horizons composed entirely of fines, and horizons containing sand. Four general stratigraphic zones were defined on the basis of sediment texture and the presence of plant macrofossils (Fig. 5.4).

Zone 1, which extends from the surface to a depth of 164 cm is composed of a series of two alternating characteristic units (i) distinct sandy silt horizons lacking internal structure and ranging from 0.5 to 5 cm thick, and (ii) finely laminated (mm scale) clayey silts of ~ 1 to 40 cm thick, which occasionally contain sandy laminations (Fig. 5.4). No trends in particle size in the particle size distribution metrics  $D_{10}$ ,  $D_{50}$  and  $D_{90}$  were found for Zone 1 with depth. Both unit types contained abundant plant macrofossils to a depth of about 1 m, and were penetrated by roots to a depth of 140 cm, becoming less abundant down core.

Zone 2 extends from 164 to 195 cm and is composed entirely of sandy silts, and sands (Fig. 5.4). Unlike the unstructured coarse layers of Zone 1, Zone 2 sandy silts also appeared to have mm scale laminations. Sand dominated layers display wavy bedding structures, apart from the lowest unit, which contain sand supported clay clasts. Examination of horizon  $D_{50}$  values showed that the overall Zone 2 particle size depth trend is that of a fining up sequence. Coarse fraction trends as indicated by  $D_{90}$  were stable with the exception of the lowest, coarsest, clay-clast bearing zone. Plant macrofossils and roots are notably sparse in Zone 2.

Zone 3, extending from depths of 195 to 221.5 cm is characterized by a 20 cm thick gravely sand unit (depth 201 to 221 cm) bound above and below by thin layers of silty sand, the upper of which fines

up into an unstructured layer of clayey silt (Fig. 5.4). The upper silt layer was the only found to contain plant macrofossils. Gravel sizes display a double peak with depth, the coarser of which (depth range 205 to 209 cm,  $D_{90} = 9045.6 \mu\text{m}$ ) coincides with the highest proportion of gravel. Very little organic material was present in Zone 3.

Zone 4 (depth 221.5 to 303 cm, end of core) is composed of three unstructured sandy horizons (two dominated by sand, one dominated by silt) alternating with laminated silty clay units (Fig. 5.4). The two sand dominated horizons (depth ranges 227 to 235 cm, and 245 to 301 cm) are coarser than those found in Zones 1 and 2 above, with  $D_{90}$  ranging from 149.5 to 270.5  $\mu\text{m}$ . The relative coarseness of the sandy silt horizon (depth 238 to 243 cm) is similar to those up-core ( $D_{90}$  of  $\sim 100 \mu\text{m}$ ), and was horizontally laminated. This silty sand unit is overlain by a fining-up sequence of clayey silts (depth 235 to 238) capped by a silty clay with the highest clay content found in the core (62.2 % clay). The lowest and coarsest unit was a massive sand body extending from 245 to 301 cm, bound below by a rooted horizon of organic rich silt. The silt layer capping this large sand body is another fining-up sequence topped by the second highest clay content found in the core (33.7 % clay). Plant macrofossils found in Zone 4 were limited to the units of laminar fines.

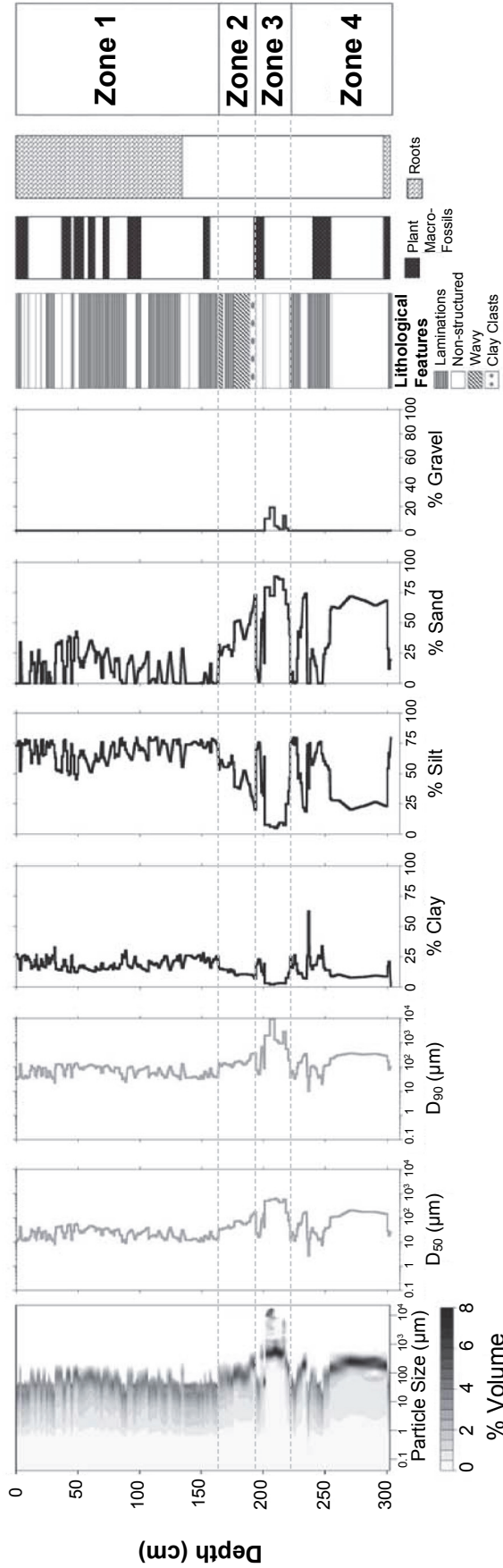


**Figure 5.4** Stratigraphic and sedimentological results for the EDRS cores. See text for in depth descriptions.

### 5.5.2 Particle size distribution characteristics of stratigraphic zones

Of the 46 measured fine horizons, 37 were present in Zone 1, and 9 in Zone 4 (Table 5.2). Fine horizons were poorly sorted, mesokurtic, and fine skewed, displaying single or bimodal peaks in the medium to very coarse silt range (11 to 38  $\mu\text{m}$ ) and a characteristic clay shoulder around 2 – 4  $\mu\text{m}$  (Table 5.2, Fig. 5.5). Clay/Silt ratios were generally 1:3. Comparison between fine horizon descriptors revealed that only skewness and kurtosis differed significantly between Zones 1 and 4 (slightly higher in Zone 1) (Table 5.3).

Sandy horizons displayed a higher range of particle size distribution characteristics than fine horizons (Table 5.3, Fig. 5.5). In general, sandy horizons were very poorly sorted, mesokurtic to very leptokurtic, fine skewed, and unimodal, with a small proportion of bimodal and poly-modal horizons found mostly in Zones 3 and 4. Primary modes in Zones 1, 2 and 4 were generally in the coarse silt to very fine sand range (31 to 125  $\mu\text{m}$ ). The few secondary modalities in these zones were generally finer, plotting in the coarse to very coarse silt range. In contrast, the majority of Zone 3 horizons were fine skewed, meso to leptokurtic, and bimodal or poly-modal mixes of sand and gravel. Zone 3 primary modes ranged from fine to medium sand (125 to 500  $\mu\text{m}$ ), while secondary modes were generally coarser, plotting in the very coarse sand to medium gravel range ( $1 \cdot 10^3$  to  $1.6 \cdot 10^5$   $\mu\text{m}$ ). High variability in texture class composition also belied the range of sediments represented by this group, as horizons varied between clayey silts, with trace amounts of sand, to sand and gravel mixes with very low (<10%) fines (Fig. 5.5).

Differences in the population means of sandy horizon particle size distribution characteristics between zones ranged from equivalence in nearly every characteristic to significant differences for all characteristics (Table 5.3). By this array of tests, Zone 2 and Zone 4 sandy horizons were most similar, with equivalence of every characteristic except for % clay. The Zone pairs 1 vs. 4 and 2 vs. 3 each showed equivalence in three metrics, while pairs 1 vs. 3 and 3 vs. 4 were only equivalent in terms of skewness.

**Table 5.2** EDRS particle size distribution metrics by horizon type and zone

Metric <sup>c</sup>	Unit	Fine Horizons <sup>a</sup>					Sandy Horizons <sup>b</sup>					All Zones
		Zone1	Zone2	Zone3	Zone4	Zones	Zone1	Zone2	Zone3	Zone4	Zones	
Horizons	n	37	0	0	9	46	89	16	14	30	149	
Unimodal	n	13	0	0	4	17	87	14	5	22	128	
Bimodal	n	24	0	0	5	29	1	1	5	5	12	
Modality > 2	n	0	0	0	0	0	1	1	4	3	9	
1° Mode mean	µm	28.68	-	-	25.05	27.97	45.80	76.59	318.43	80.16	90.03	
1° Mode (s)	µm	8.97	-	-	10.20	9.22	20.70	45.19	203.74	74.80	102.74	
2° Mode mean	µm	23.65	-	-	20.86	23.17	36.63	16.42	1198.65	45.80	1105.60	
2° Mode (s)	µm	7.71	-	-	12.95	8.60	7.20	0	5651.15	42.69	3787.89	
Sorting mean	φ	1.77	-	-	1.75	1.76	2.00	2.15	2.40	2.14	2.08	
Sorting (s)	φ	0.04	-	-	0.08	0.05	0.12	0.12	0.31	0.19	0.20	
Skewness mean	φ	0.86	-	-	0.80	0.85	0.95	1.13	1.19	1.05	1.01	
Skewness (s)	φ	0.05	-	-	0.08	0.06	0.11	0.24	0.53	0.28	0.25	
Kurtosis (mean)	φ	3.18	-	-	3.03	3.15	3.37	3.84	4.78	3.60	3.60	
Kurtosis (s)	φ	0.11	-	-	0.17	0.14	0.24	0.64	2.34	0.59	0.89	
% Clay mean	%	25.42	-	-	31.42	26.60	17.20	12.41	9.72	14.12	15.36	
% Clay (s)	%	2.06	-	-	12.09	5.93	2.96	1.93	0.53	4.87	4.55	
% Silt mean	%	74.58	-	-	68.58	73.40	67.02	51.02	31.53	51.55	58.85	
% Silt (s)	%	2.06	-	-	12.09	5.93	9.26	10.04	24.52	20.40	17.99	
% Coarse mean	%	0	-	-	0	0	15.78	36.57	58.74	34.34	25.79	
% Coarse (s)	%	0	-	-	0	0	11.88	11.62	28.09	24.92	22.27	

<sup>a</sup>Fine horizons are defined as those that were composed only of clay and silt size classes. <sup>b</sup>Sandy horizons are those that contain any amount of sand sized or coarser inorganic material. <sup>c</sup>All mean values are arithmetic. (s) indicates sample standard deviation. Sorting, skewness and kurtosis computed through the logarithmic method of moments.

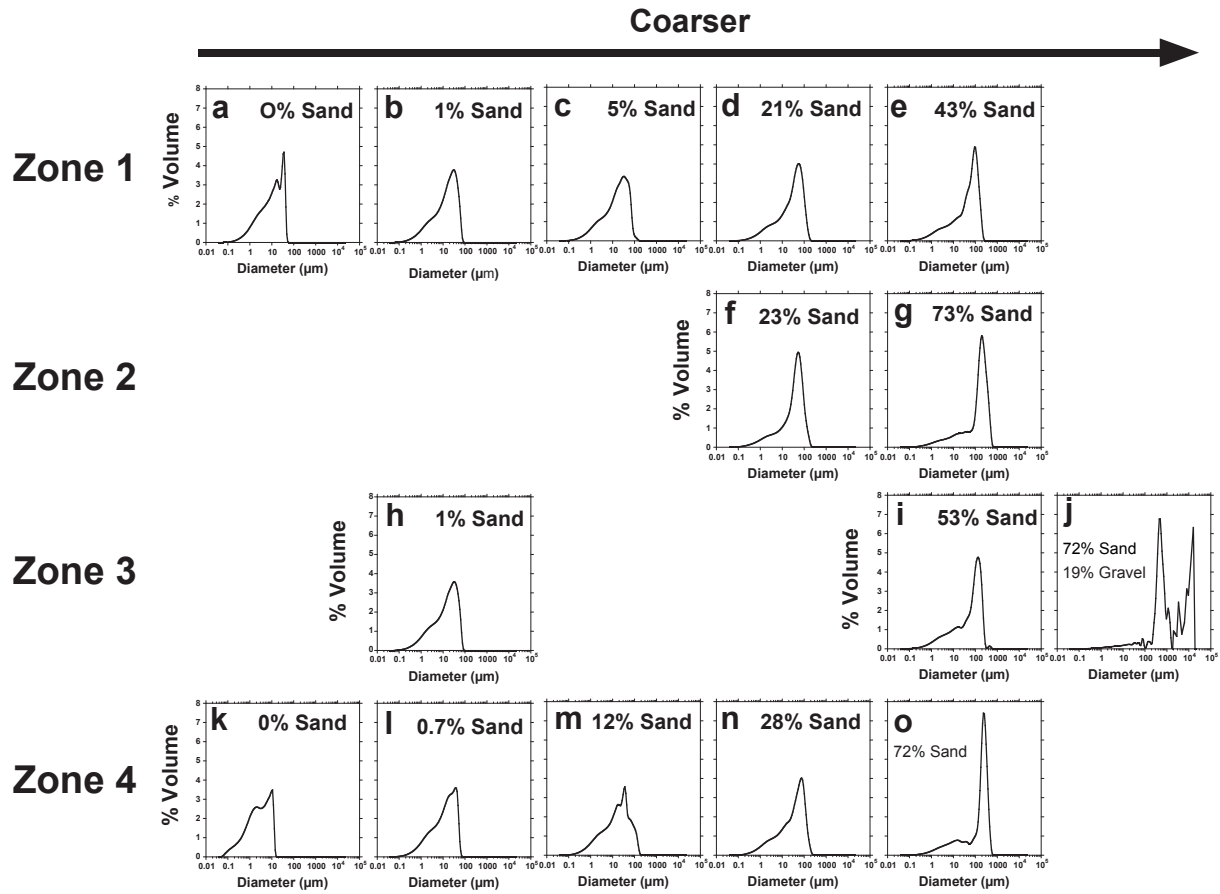


**Figure 5.5** Characteristic particle size distributions for horizon types by zone and general coarse (sand + gravel) content. Figures correspond to the following EDRS depths (cm): (a) 24–24.5, (b) 127–127.5, (c) 27–28, (d) 82–83, (e) 48–49 43, (f) 174–175, (g) 193–194, (h) 196–197, (i) 220–221, (j) 205–209, (k) 236–237, (l) 237.25–238, (m) 301–302, (n) 239–240, (o) 270–271.

**Table 5.3** Comparisons of EDRS mean particle size distribution and carbon content characteristics<sup>a</sup>.

Particle size distribution characteristics by horizon type an zone. <sup>b</sup>											
Horizon type	Zones	1° Mode	Sorting	Skewness	Kurtosis	D <sub>10</sub>	D <sub>50</sub>	D <sub>90</sub>	% Clay	% Silt	% Coarse <sup>b</sup>
	Z1 vs. Z4	Eq.	Eq.	*	*	Eq.	Eq.	Eq.	Eq.	Eq.	-
Fine	Z1 vs. Z2	**	***	**	**	***	***	***	***	***	***
Sandy	Z1 vs. Z3	***	***	Eq.	*	**	**	*	***	***	***
Sandy	Z1 vs. Z4	***	Eq.	Eq.	*	***	***	***	Eq.	***	***
Sandy	Z2 vs. Z3	***	**	Eq.	Eq.	**	**	*	Eq.	**	*
Sandy	Z2 vs. Z4	Eq.	Eq.	Eq.	Eq.	Eq.	Eq.	Eq.	*	Eq.	Eq.
Sandy	Z3 vs. Z4	**	**	Eq.	*	**	**	*	*	**	**
Particle size distribution characteristics by stratigraphic unit.											
Stratigraphic Unit <sup>c</sup>											
	1° Mode	Sorting	Skewness	Kurtosis	D <sub>10</sub>	D <sub>50</sub>	D <sub>90</sub>	% Clay	% Silt	% Coarse <sup>b</sup>	
Fine	vs. Medium	***	***	*	*	***	***	***	***	***	***
Fine	vs. Coarse	***	***	***	**	***	***	***	***	***	***
Fine	vs. Very Coarse	**	**	Eq.	*	**	Eq.	***	***	***	***
Medium	vs. Coarse	***	***	***	**	***	***	***	***	***	***
Medium	vs. Very Coarse	**	*	Eq.	*	**	Eq.	***	***	***	***
Coarse	vs. Very Coarse	**	Eq.	Eq.	Eq.	**	Eq.	**	**	**	**
Carbon content by stratigraphic unit											
Stratigraphic Unit <sup>c</sup>											
	Organic Carbon	Inorganic Carbon									
Fine	vs. Medium	***	***	***							
Fine	vs. Coarse	***	***	***							
Fine	vs. Very Coarse	***	***	***							
Medium	vs. Coarse	***	*	***							
Medium	vs. Very Coarse	***	***	***							
Coarse	vs. Very Coarse	*	Eq.	Eq.							

<sup>a</sup>Results for one sided T-tests listed as follows: (Eq.) indicates the H<sub>0</sub> of equivalent means was not rejected (P-value > 0.05), (\*) for P-values < 0.05, (\*\*) for P-values < 0.01, (\*\*\*) for P-values < 0.001.

<sup>b</sup>The descriptor % coarse is the sum of % sand and % gravel.

<sup>c</sup>Stratigraphic units refer to all horizons with the indicated ranges of % coarse: Fine = (0-7%); Medium = (7-50%); Coarse = (>50% no gravel); Very Coarse = (>50% w/gravel).

### 5.5.3 Stratigraphic units

Horizons were aggregated into stratigraphic 'units', defined as contiguous horizons of a given type. First, horizon types were refined, as highly variable sandy horizon particle size characteristics within and between zones suggested that further delimitation was necessary. A histogram of sandy horizons by % coarse revealed that three disparate populations of sandy samples were likely: samples with trace (< 7%), moderate (7 to 50 %) and high (> 50%) coarse content with and without gravel (Fig. 5.6). All sandy populations were found to significantly differ from each other in terms of all mean particle sized distribution descriptors, with the exception of some comparisons to samples with gravel, which were obscured by the high variance of most particle size distribution metrics for these samples (Table 5.3). Thus, horizons were grouped into four characteristic stratigraphic unit types: (i) Fine (0 to 7 % sand), (ii) Medium (7 to 50 % sand), (iii) Coarse (> 50% sand, no gravel), and (iv) Very Coarse (gravelly sand) and were numbered down core by zone (Fig. 5.7).

### 5.5.4 Carbon composition by stratigraphic unit

Down core variations in organic and inorganic (carbonate) content were informative in terms of marsh development and also provided supporting evidence for tidal vs. fluvial sedimentation regimes. Organic carbon content was highest near the surface, where roots and large plant debris were most abundant, and sharply trailed off with depth, only to increase again in the last few centimeters of the core where another rooted horizon appeared (Fig. 5.7). Inorganic carbon content appeared to be more closely linked with differences at the horizon or unit level (Fig. 5.7). Indeed, both organic and inorganic carbon content generally decreased with increasing unit coarseness (Fig. 5.8), and the difference in mean values between each unit type were found to be statistically significant in all cases except for Coarse and Very Coarse CaCO<sub>3</sub> content (Table 5.3).

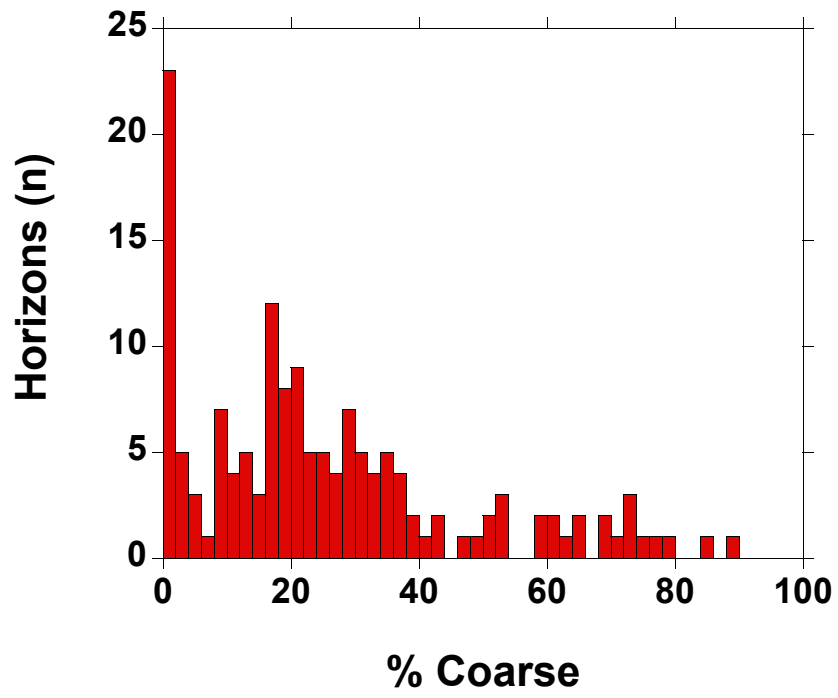
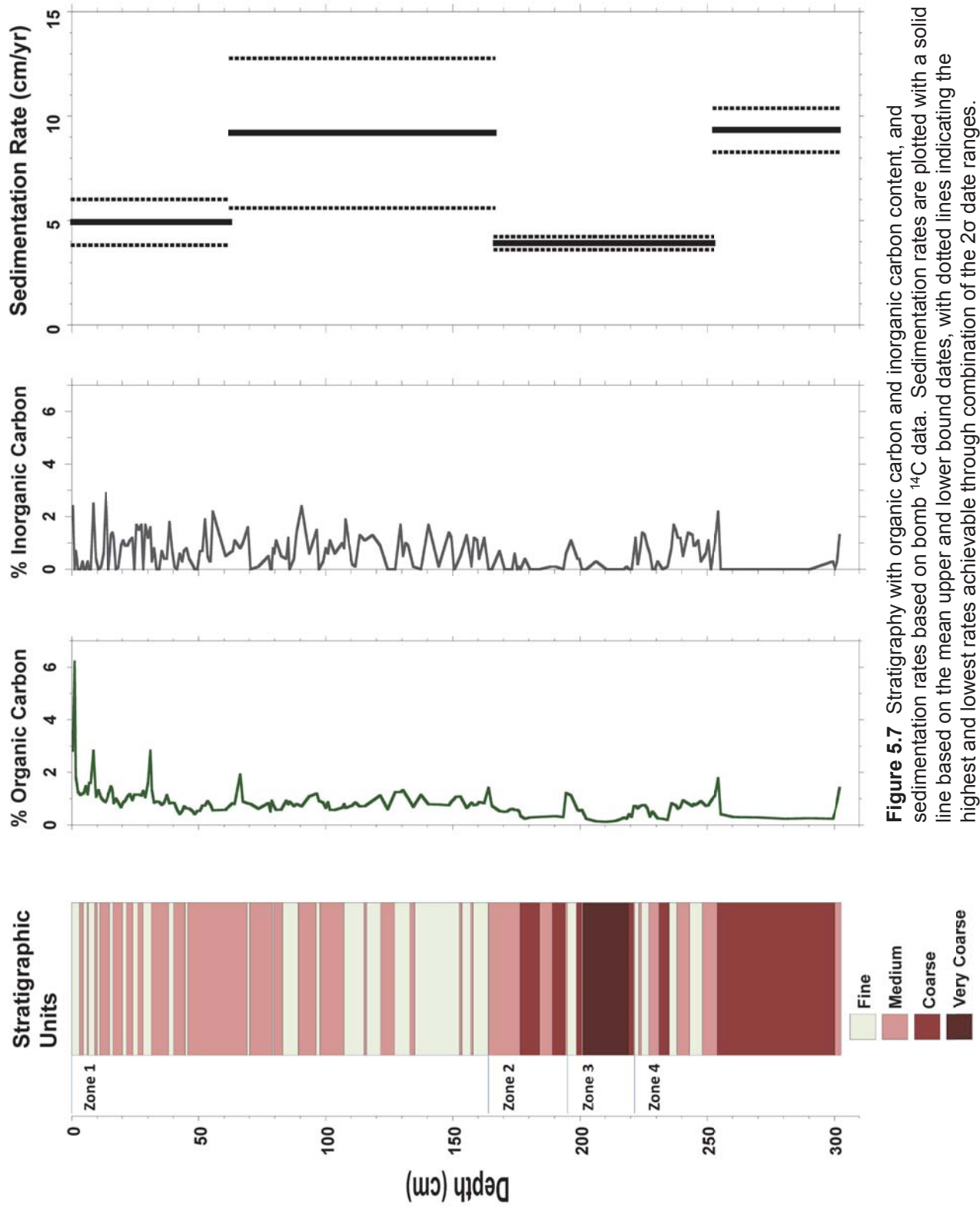
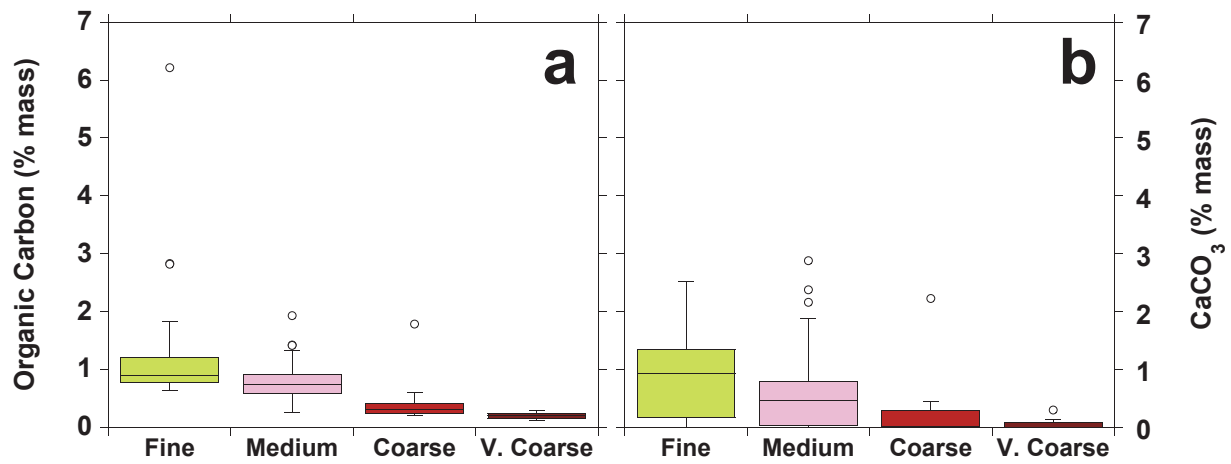


Figure 5.6 Coarse (sand + gravel) content histogram.



**Figure 5.7** Stratigraphy with organic carbon and inorganic carbon content, and sedimentation rates based on bomb  $^{14}\text{C}$  data. Sedimentation rates are plotted with a solid line based on the mean upper and lower bound dates, with dotted lines indicating the highest and lowest rates achievable through combination of the  $2\sigma$  date ranges.



**Figure 5.8** Box and whisker plots of (a) organic and (b) inorganic content by stratigraphic unit. Open circles indicate outlier values, whiskers the maximum and minimum values of the non-outlier range, upper and lower box extent the 75% and 25% quantile, respectively, and the central line the mean.

### 5.5.5 Chronostratigraphic model

Post-bomb radiocarbon dating revealed that EDRS was accreted over the last half of the 20<sup>th</sup> to early 21<sup>st</sup> Centuries (Table 5.4). As this time period traverses the rise and fall of the bomb derived <sup>14</sup>C spike in the atmosphere, and as such produces two age ranges for each F<sup>14</sup>C value, directional input of sedimentary sequence is used to guide age range selection. Sediment superposition and photographic evidence of the timing of geomorphic change at the site, particularly the fact that the site was located in the main RSC channel complex from at least 1965 through 1974, allowed for a confident choice of age ranges for the resultant stratigraphic model. Accretion rates varied from  $3.6 \pm 0.3$  to  $9.2 \pm 3.6$  cm yr<sup>-1</sup> between dated horizons (Fig. 5.7).

### 5.5.6 Depositional environments

The two channel abandonment cycles of Ropers Slough resulted in three depositional environments at EDRS over the period of accretion: (i) major fluvial channel, (ii) abandoned channel with seasonal throughflow, and (iii) tidal slough marginal emergent marsh (Table 5.5). It was assumed that the first abandonment, which occurred between the 1940 and 1948 photographs, took place during the highest magnitude event of that time range ( $8920 \text{ m}^3\text{s}^{-1}$ , 1/21/1943). The 1943 discharge event was  $2000 \text{ m}^3\text{s}^{-1}$  greater than any other event during this time period. Channel avulsion/reoccupations generally occur during high discharge events in low gradient rivers (Hook, 1995; Constantine et al., 2010), and were observed to do so in other abandonment scenarios on the Eel River by the authors, including the second Ropers Slough abandonment, which was photo documented during the  $8000 \text{ m}^3\text{s}^{-1}$  event of 1974.

**Table 5.4** Radiocarbon measurements

Mean Depth (cm)	Sample ID <sup>a</sup>	F <sup>14</sup> C	F <sup>14</sup> C Error	$\delta^{13}\text{C}$	Cal Year AD	2 $\sigma$ year ranges <sup>b</sup>		Probability
						Probability	Cal Year AD	
62.5	CAMS-163329	1.118801	0.0054	-25.93	1957.8 : 1958.6	0.067	<b>1993.1 : 1998.7</b>	0.933
166.5	CAMS-163330	1.214663	0.0035	-27.79	1959.0 : 1961.5	0.341	<b>1983.0 : 1986.2</b>	0.659
252.5	CAMS-163331	1.387876	0.0078	-25.93	<b>1962.5 : 1962.8</b>	0.143	1973.3 : 1976.5	0.857
302	CAMS-163332	1.072338	0.0041	-25.93	<b>1957.1 : 1957.8</b>	0.086	2002.1 : 2007.2	0.914
302	OS-71195	1.064300	0.0021	-27.24	<b>1956.9 : 1957.6</b>	0.104	2004.0 : 2009.5	0.896

<sup>a</sup>Identification code prefixes as follows: CAMS = Lawrence Livermore National Laboratory Center for Accelerator Mass Spectrometry, OS = National Ocean Sciences Accelerator Mass Spectrometry Facility.

<sup>b</sup>Year ranges and associated probabilities are the product of calibrating F<sup>14</sup>C with F<sup>14</sup>C error using the CaliBomb model of post bomb pulse <sup>14</sup>C levels in zone NH2. This produces a low probability, 'old' distribution of dates, and a high probability 'young' distribution, due to the rapid rate of <sup>14</sup>C increase in the atmosphere at the beginning of the bomb pulse, and the relatively slower decline in <sup>14</sup>C levels after the mid 1960s. Most likely year ranges indicated in bold were chosen with consideration for stratigraphic sequence and the time series of planform geomorphology.

**Table 5.5** EDRS depositional environments and planform geometry of the Ropers Slough region

Date	Width (m)			E.		W.		Cutoff <sup>a</sup> Ratio	Depositional Environment	Ropers <sup>b</sup> Entrance
	South mean	Central mean	Ropers mean	Ropers Mouth	Ropers Mouth	Ropers Mouth				
12/13/1940	381.37	20.03	316.17	364.67	325.83	n/a	Main channel	-		
summer, 1948	387.10	211.50	112.84	85.37	128.77	1.96	Abandoned	Outer bank		
9/13/1956	348.52	220.55	46.19	45.33	90.58	-	Abandoned	Outer bank		
summer, 1965	593.71	201.85	40.64	closed	33.79	-	Main channel	Outer bank		
7/15/1972	838.31	74.14	181.68	184.70	180.50	1.01	Main channel	-		
4/4/1973	833.40	60.34	189.47	182.95	367.73	-	Main channel	-		
1/21/1974	832.85	75.40	230.37	256.55	370.18	1.58	Main channel	-		
4/29/1974	882.26	136.09	240.90	275.92	394.81	1.70	Main channel	Inner Bank		
1/4/1977	881.13	129.35	221.94	270.10	390.58	1.74	Abandoned	Inner Bank		
5/8/1978	917.04	189.55	235.72	558.23	206.24	1.63	Abandoned	Inner Bank		
5/29/1979	n/a	197.31	194.39	363.00	169.19	1.89	Abandoned	Inner Bank		
6/27/1980	949.76	204.55	194.66	463.00	196.53	1.77	Abandoned	Inner Bank		
7/8/1982	853.82	197.47	169.06	384.80	137.99	1.60	Abandoned	Inner Bank		
8/28/1985	870.56	233.18	109.52	355.19	155.46	1.60	Abandoned	Inner Bank		
4/28/1989	880.89	258.15	107.51	188.88	385.61	1.59	Abandoned	Inner Bank		
6/15/1993	811.23	276.12	82.55	365.74	142.89	1.59	Abandoned	Inner Bank		
9/3/1998	578.68	264.89	74.23	90.92	96.73	1.47	Abandoned	Inner Bank		
6/29/2005	479.69	259.94	37.18	30.27	-	-	Emergent marsh	Inner Bank		
6/27/2009	421.09	279.18	30.56	33.95	-	-	Emergent marsh	Inner Bank		

<sup>a</sup>See methods section for description of cutoff ratio.

<sup>b</sup>The position of the upstream entrance to Ropers Slough (E: Ropers Mouth) relative to the meander morphology of the RSC complex.

### 5.5.7 Channel geometry

Diversion angle, the basic geometric relationship between the post abandonment main channel flow direction and channel inlet flow direction, was almost identical for the two abandonments at  $66.2$  and  $67.3 \pm 3^\circ$ , respectively (Table 5.5). Cut-off ratios were also equivalent. However, progression of subsequent channel narrowing was very different, with Ropers Slough narrowing much more rapidly after the 1943 abandonment than after 1974 (Figs. 5.9, 5.10). Geomorphic differences between the two eras of Ropers Slough abandonment included the morphology of the entrance of the RSC complex (Node 1), and the morphology of the Ropers Slough channel entrance (Node 2) (Table 5.5, see Figs. 5.3, 5.9).

Fluvial sediment supply to Ropers Slough after each cutoff event may have been controlled in part by location of the entrance to Ropers Slough relative to the meander morphology of the RSC complex. During the 1943 to ~ 1965 abandonment sequence the entrance of Ropers Slough was located on the outside of a north east facing meander bend in the RSC complex (Table 5.5, see Figs. 5.3, 5.9). During the second abandonment sequence from 1974 to the present (2014), the entrance to Ropers Slough is located on the inside of a very low sinuosity bend of the RSC complex. Furthermore, the entrance of Ropers slough itself in this case was a bend of the RSC complex that was actively accreting a point bar before abandonment. This point bar became the basis for the plug bar that continued to accrete across the entrance of Ropers Slough after abandonment.

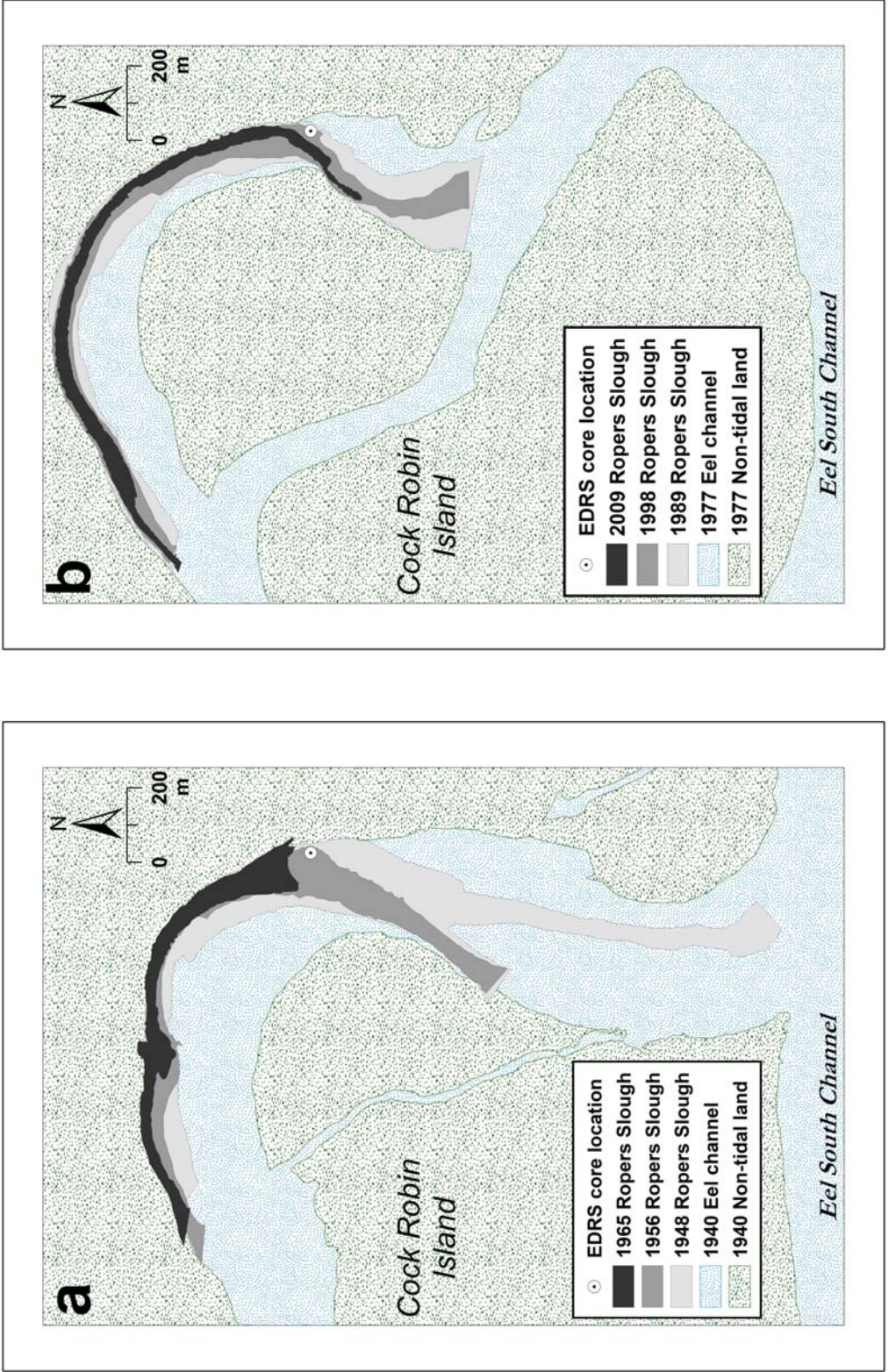


**Figure 5.9** Ropers Slough channel area diagrams for the (a) first (1948 – 1965) and (b) second (1974 to present) abandonment sequences. Both frames display the same scale and spatial extent.

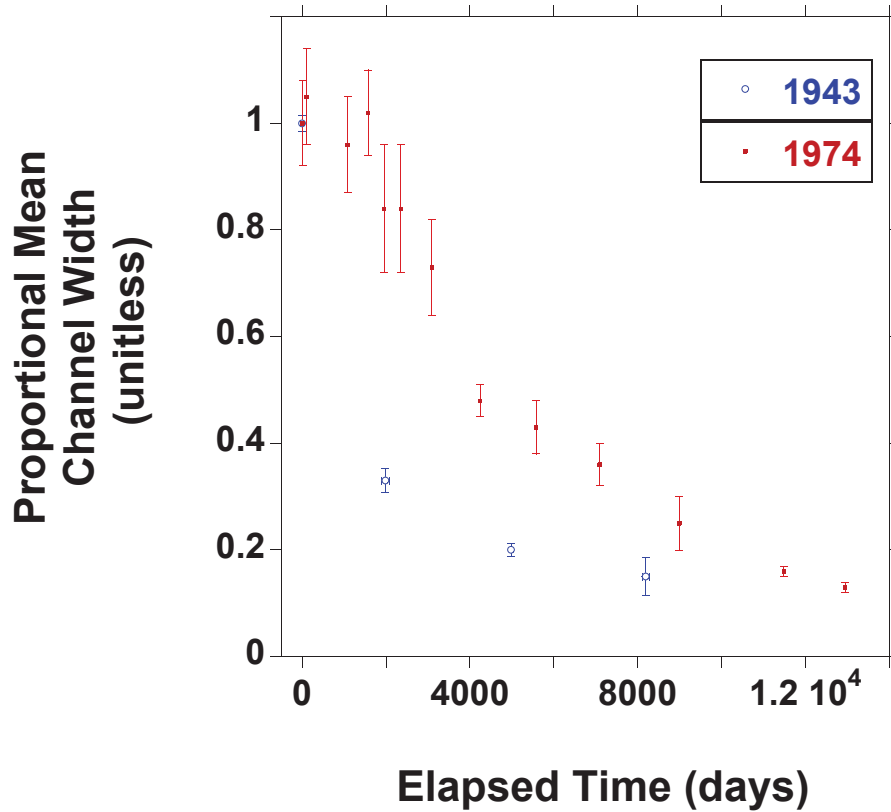


**Figure 5.10** Ropers Slough channel width adjustment after the first (1943) and second (1974) abandonment events. Channel width values normalized to average channel width in the most recent aerial photograph before abandonment. Channel widths in all cases refer to active channel width defined by vegetated channel banks. Error ranges in temporal domain were only applied to measurements from image mosaics, which were collected in the summer of the given year, but without exact associated dates.

### 5.5.8 Hydro-stratigraphy

The  $^{14}\text{C}$  based chronostratigraphic model was slightly modified with regard to the time series of discharge events and stratigraphic characteristics to assign time periods of deposition to the abandoned channel fill sequences of Zones 1 and 4. The Zone 1 depositional period was estimated as (1987–2008), based on the age of material deposited at depths of 62.5 and 166.5 cm. The  $2\sigma$  date range for material at 166.5 was 1983.0 to 1986.2. This upper most unit of Zone 2 was assigned a depositional date of 1986. Further supporting evidence for this date choice were: (i) the unit was coarser and thicker than surrounding units, and (ii) the 1986 water year produced a maximum  $Q_d$  of  $8600 \text{ m}^3\text{s}^{-1}$ , which was  $2000 \text{ m}^3\text{s}^{-1}$  higher than any water year within  $\pm 9$  years. The Zone 4 depositional period was estimated as (1960 to 1964). Two  $^{14}\text{C}$  samples collected near the bottom of the core (depths of 302 cm) dated to 1957. The lowest Coarse unit of Zone 4 was the thickest found in the entire core, and was assigned to 1960 as the maximum  $Q_d$  of  $7400 \text{ m}^3\text{s}^{-1}$  was  $\sim 1400 \text{ m}^3\text{s}^{-1}$  greater than the year with the second highest  $Q_d$  (1963) and at least  $2500 \text{ m}^3\text{s}^{-1}$  greater than those of 1957–1959.

The Stratigraphic unit and wet season periodicity were found to be very similar in Zones 1 and 4, with 19 couplets deposited over 22 years in Zone 1, and 4 couplets deposited over 5 years in Zone 2 (Fig. 5.11). Departure from a strictly annual resolution may have been related to threshold discharge considerations. A discharge event threshold near  $3000 \text{ m}^3\text{s}^{-1}$  would result in the same number of events as stratigraphic couplets for Zone 1, while a threshold of near  $2000 \text{ m}^3\text{s}^{-1}$  would produce the same number of events as stratigraphic couplets for Zone 4 (Fig. 5.11).

Comparison of the maximum daily discharge for each water year with Zone 1 unit characteristics revealed patterns related to the highest discharge events and the longest period of low discharge (Fig. 5.12). The occurrence of the year with the largest daily discharge value (1997) within the time period of deposition is generally consistent with the depth of the thickest medium textured unit. This unit possesses the highest horizon  $D_{90}$  and % coarse values of Zone 1, although only slightly elevated above several others (Fig. 5.12). The period of low flows between 1987 and 1992, with maximum annual  $Q_d$  values between  $2000$  and  $3000 \text{ m}^3\text{s}^{-1}$ , was consistent with the lowest Zone 1 units. The Medium units in this position were generally thin (mostly between 1 and 2 cm, with one 5.5 cm unit), while the Fine units were mostly thick (mostly between 6 and 17.5 cm, with one 3.5 cm unit) (Fig. 5.12). Fine unit particle size

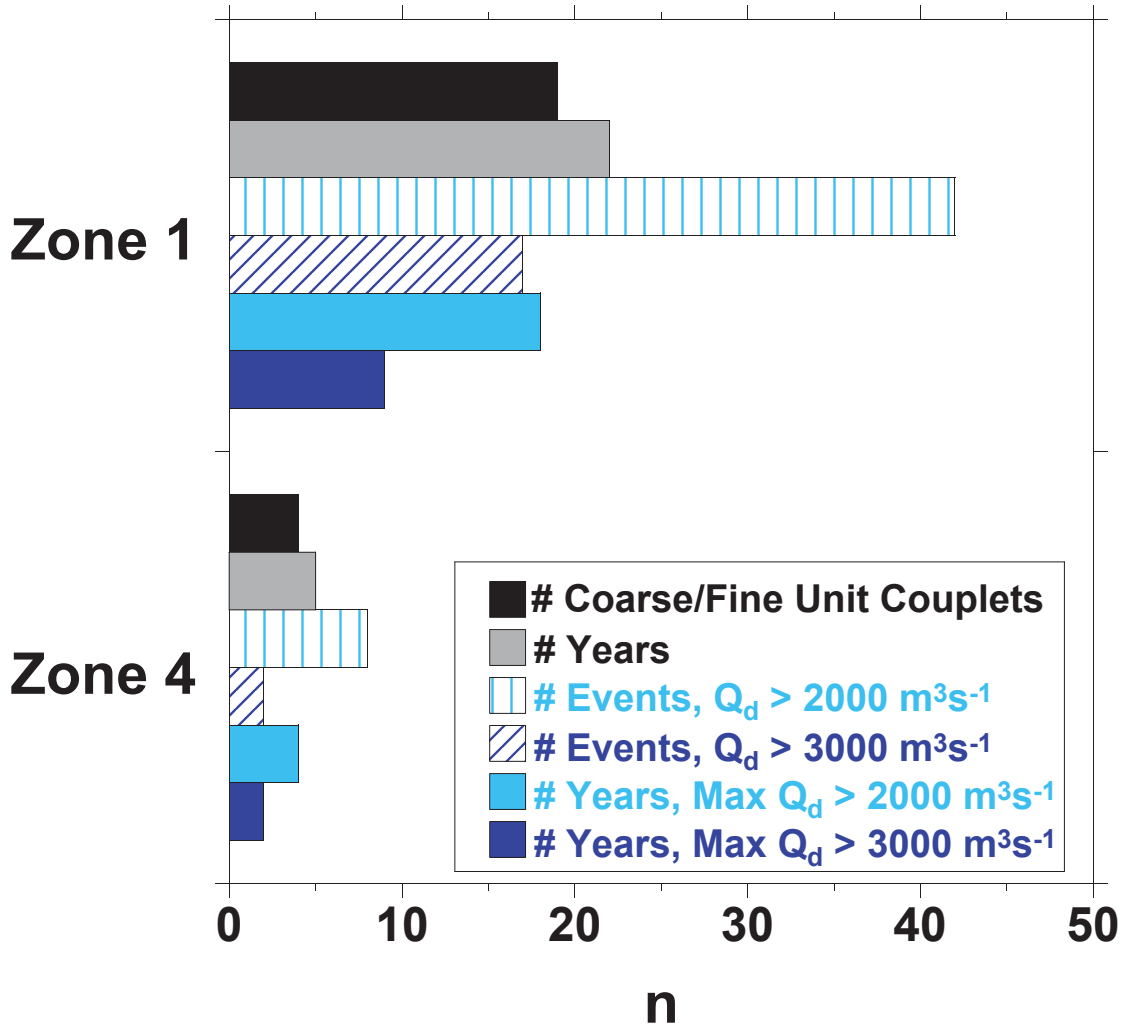


**Figure 5.11** Comparison of abandon channel fill stratigraphy with the number of years and hydrologic characteristics of the time period of deposition for Zones 1 and 4.

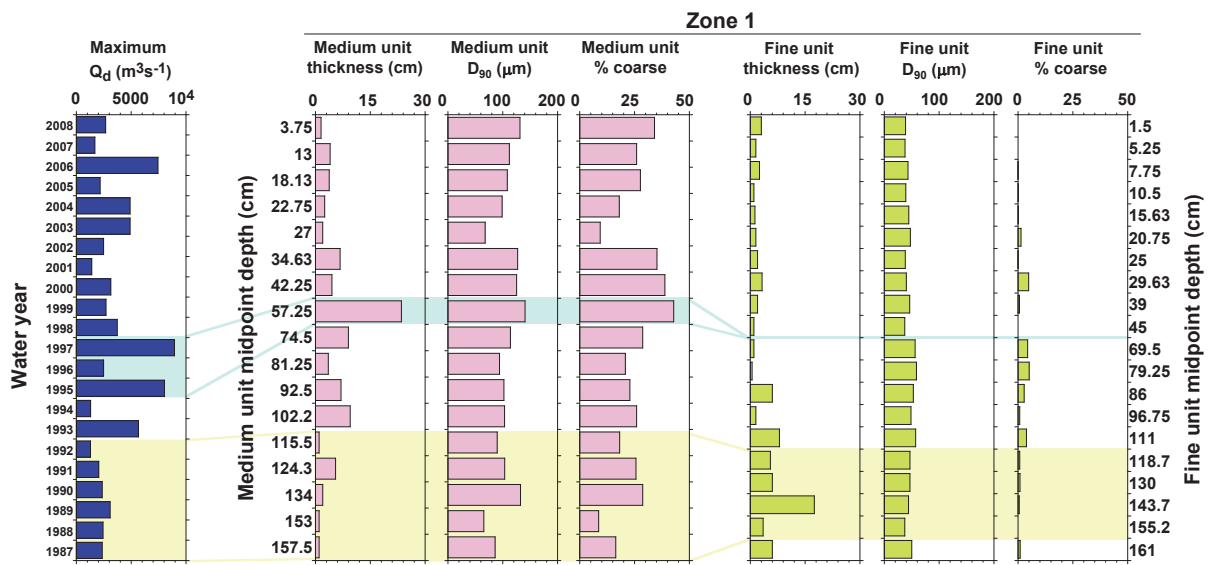


**Figure 5.12** Zone 1 stratigraphic unit characteristics and the annual maximum daily discharge ( $Q_d$ ) values at Scotia over the period of deposition.

characteristics ( $D_{90}$ , % coarse) appeared to be insensitive to these discharge patterns.

To examine Zone 4 annual hydrologic and stratigraphic fine/coarser unit couplets, Medium and adjacent Coarse units were combined to form 'Med/Coarse' unit assemblage. The two years with the highest annual  $Q_d$  (1960 and 1963) values may have resulted in the thickest and coarsest unit assemblages, with the lower and thicker of the two corresponding with 1960. Maximum  $D_{90}$  and % coarse values were almost identical between these two unit assemblages, although 1960 maximum  $Q_d$  was  $7400 \text{ m}^3\text{s}^{-1}$  in comparison to  $6000 \text{ m}^3\text{s}^{-1}$  in 1963. In contrast, 1961 and 1962 had maximum  $Q_d$  values of  $2700$  and  $2300 \text{ m}^3\text{s}^{-1}$  respectively and appear to have only resulted in the accretion of a single 5 cm thick Medium unit (Fig. 5.13).

#### 5.5.9 Eel River suspended, bed, and bedload sediment characteristics

Eel River suspended sediment particle size distributions were generally very poorly sorted, symmetrical, platykurtic, and bi- or poly-modal, with nearly equal proportions of clay, silt and sand (Table 5.6, Fig. 5.14). None of the 180 suspended sediment samples contained particles coarser than  $2000 \mu\text{m}$  (very coarse sand). Bed sediment samples displayed a range of modalities and were generally poorly sorted, fine skewed, leptokurtic and composed mostly of equal parts sand and gravel, with only a trace amount of fines (< 2%). Bedload sediment also displayed a range of modalities and was generally poorly sorted, fine skewed, very leptokurtic and composed of primarily sand and gravel. Although no data was presented on fines, the 0 to  $250 \mu\text{m}$  particle size bin averaged ~3% of total sample mass, thus the upper limit of fine contribution to bedload was similar to the fine content of the bed.

Concentration-discharge log-linear rating curves revealed that Eel River suspended sediment particle size distribution was relatively insensitive to discharge (Fig. 5.15). However, notable changes in distribution were found. At  $Q \approx 200 \text{ m}^3\text{s}^{-1}$  silt supplants clay as the primary textural constituent (Fig. 5.15a) and very fine sand ( $63$  to  $125 \mu\text{m}$ ) supersedes fine sand ( $125$  to  $250 \mu\text{m}$ ) (Fig. 5.15b). At  $Q > 2000 \text{ m}^3\text{s}^{-1}$  silt concentrations  $\approx 2x$  clay concentrations, as does the proportionality between fine and very fine sand. Results of tests for differences in mean particle size distribution characteristics on the following sample populations: (i)  $Q < 200 \text{ m}^3\text{s}^{-1}$ , (ii)  $200 < Q < 2000 \text{ m}^3\text{s}^{-1}$ , and (iii)  $Q > 2000 \text{ m}^3\text{s}^{-1}$ , indicated that these populations were indeed distinct in terms of particle size distribution (Table 5.7).

**Table 5.6** Eel River suspended, bed and bedload particle size distribution metrics<sup>a</sup>

Metric <sup>e</sup>	Unit	Suspended Sediment <sup>b</sup>				Bed <sup>c</sup>	Bedload <sup>d</sup>
		0 - 200 (m <sup>3</sup> s <sup>-1</sup> )	200 - 2000 (m <sup>3</sup> s <sup>-1</sup> )	2000 - 10000 (m <sup>3</sup> s <sup>-1</sup> )	All Samples	All Samples	All Samples
Samples	n	5	117	58	180	7	6
Unimodal	n	1	1	0	2	2	2
Bimodal	n	1	23	20	44	4	3
Modality > 2	n	3	93	38	134	1	1
1° Mode mean	µm	3	66.66	22.84	50.77	12133.93	2812.50
1° Mode (s)	µm	0	143.82	56.71	122.11	11844.06	4615.70
2° Mode mean	µm	14.88	119.29	86.43	106.24	10650.00	20562.50
2° Mode (s)	µm	5.75	167.69	76.62	143.49	20907.05	32719
D <sub>10</sub> mean	µm	2.40	2.80	2.74	2.77	286.65	432.28
D <sub>10</sub> (s)	µm	0.12	0.42	0.18	0.36	161.70	283.42
D <sub>50</sub> mean	µm	9.13	34.59	28.15	31.80	6352.05	2176.67
D <sub>50</sub> (s)	µm	5.81	28.37	15.27	24.91	5758.70	2820.34
D <sub>90</sub> mean	µm	113.44	308.67	197.31	267.36	18622.08	10113.96
D <sub>90</sub> (s)	µm	100.25	149.67	0.00	136.74	17379.99	7903.82
Sorting mean	φ	1.88	2.45	2.26	2.37	2.12	2.21
Sorting (s)	φ	0.54	0.29	0.10	0.28	0.41	0.25
Skewness mean	φ	-0.91	-0.08	-0.03	-0.09	0.98	1.29
Skewness (s)	φ	1.80	0.30	0.23	0.32	1.07	0.69
Kurtosis (mean)	φ	3.25	1.79	1.83	1.85	5.29	7.57
Kurtosis (s)	φ	7.33	0.25	0.16	0.41	3.57	1.90
% Fines <sup>f</sup> mean	%	86.20	63.79	68.24	65.85	1.57	-
% Fines <sup>f</sup> (s)	%	16.72	11.00	6.96	11.09	2.64	-
% Clay mean	%	53.80	31.70	30.31	31.87	-	-
% Clay (s)	%	16.30	8.28	5.40	8.59	-	-
% Silt mean	%	32.40	32.09	37.93	33.98	-	-
% Silt (s)	%	3.71	7.24	4.40	7.01	-	-
% Sand mean	%	13.80	36.21	31.76	34.15	49.00	58.50
% Sand (s)	%	10.38	11.33	8.30	11.13	35.15	27.16
% Gravel mean	%	0	0	0	0	49.43	41.50
% Gravel (s)	%	-	-	-	-	36.95	27.16

<sup>a</sup>All samples collected and measured by the U.S. Geological Survey.

<sup>b</sup>Suspended sediment is further subdivided into populations based on discharge range.

<sup>c</sup>Bed samples were not processed for clay and silt classes, only the aggregate class 'Fines.'

<sup>d</sup>No characterization of fines was performed on Bedload samples.

<sup>e</sup>All mean values are arithmetic. (s) indicates sample standard deviation. Sorting, skewness and kurtosis computed through the logarithmic method of moments.

<sup>f</sup>Fines includes the clay and silt classes.

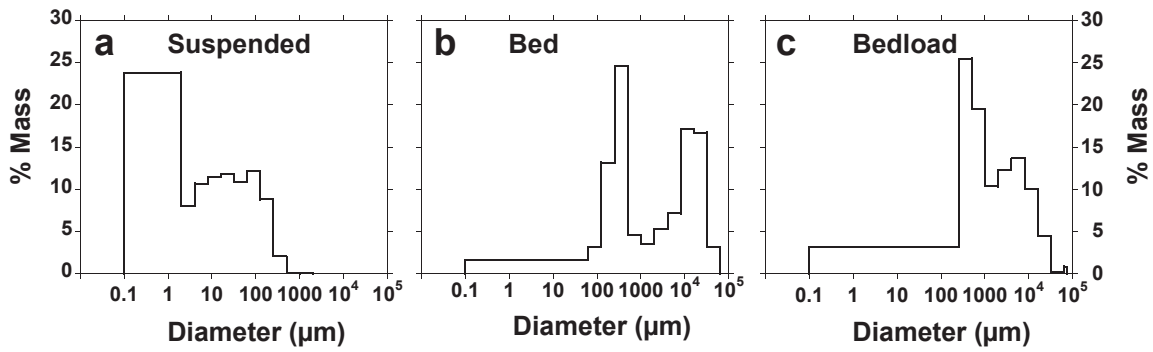


**Figure 5.14** Eel River (a) suspended, (b) bed, and (c) bedload particle size distribution diagrams. All samples collected by the USGS at the Scotia gauge (#11477000) (USGS NWIS, 2014).

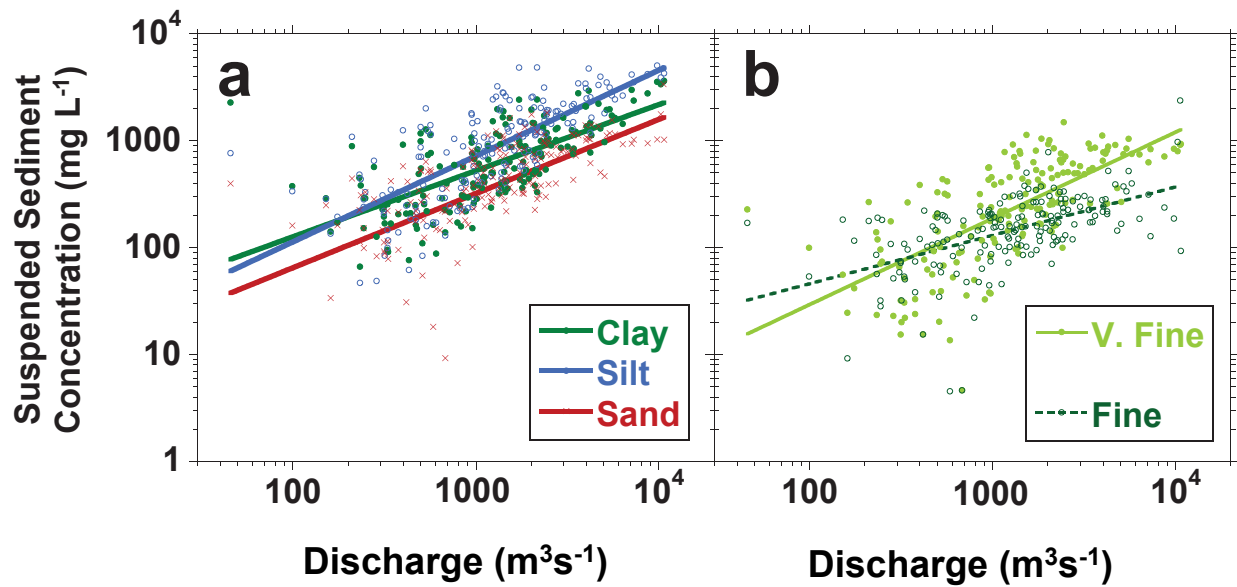


**Figure 5.15** Log-linear concentration – discharge rating curves of Eel River suspended sediment by (a) texture class, and (b) the sand size classes ‘very fine’ (62.5 to 125  $\mu\text{m}$ ) and fine (125 to 250  $\mu\text{m}$ ).

#### 5.5.10 Tanner domains: EDRS and Eel River sediment suite statistics

The EDRS horizons and Eel river sediments (suspended, bed and bedload) were compared by plotting suite particle size distribution values in bivariate statistical spaces (Fig. 5.16). EDRS and suspended sediment sub-populations were further defined by stratigraphic unit and discharge range, respectively. The suite mean vs. sorting space has been commonly used to discriminate between fluvial and settling environments (Tanner, 1991; 1995; Lario et al., 2002; Watson et al. 2013) (Fig. 5.16a). With increasing mean particle sizes (decreasing  $\phi$ ), sorting increased in a generally linear fashion for fine through coarse EDRS units and suspended sediment. Increasing mean particle size through the very coarse unit to bedload and bed sediment range resulted in decreasing sorting values. Fine units and low discharge suspended sediment plotted in the 'closed basin' domain, while medium/coarse units and medium/high discharge suspended sediment samples plotted in the 'fluvial' domain, as defined by Tanner (1991) and refined by Lario et al. (2002). Samples segregated into distinct regions of skewness vs. kurtosis space, one of which was occupied by suspended sediment, another by fine through coarse units, and a third region with very coarse units, bed and bedload samples (Fig. 5.16b). The depositional domains defined for this space did not correspond well with this lower Eel system, as none of these fluviially derived samples plotted near the pre-established fluvial zone. In contrast, all samples plotted into the pre-defined fluvial zone in sorting vs. skewness space, with EDRS units, bed and bedload samples occupying a narrow, fine skewed range, and suspended sediment samples plotting below in the symmetrical to coarse skewed range (Fig. 5.16c). Standard deviation of means vs. standard deviation of sorting space has been used to infer increasing stream gradients as both values increase (Fig. 5.16d). Indeed, this pattern holds up if very coarse EDRS units are compared to Eel River bed sediments, which were collected from a somewhat steeper reach upstream. Coarsening unit progression followed a linear like increase in both parameters from fine through coarse units, whereas the progress from low to high discharge samples led to a decrease in the standard deviation of means and sorting.

## 5.6 Discussion

### 5.6.1 Stratigraphic and geomorphic synthesis

The sediments sampled by the EDRS cores were deposited between 1957 and 2008. The major features of this deposit (from the bottom up) were: (i) the last years of an abandoned channel fill sequence (Zone 4), (ii) an interval as the main northern channel (RSC complex) (Zone 3), and (iii) a second sequence of abandonment and fill (Zones 2 and 1). The upper contact of the first abandoned fill sequence (Zone 3/4 transition) is most likely an unconformity, as the newly forged RSC complex must have scoured through the top layers of sediment. The differences in inundation between the reach of Ropers Slough that had been reoccupied as main channel and that which remained abandoned in 1965 clearly showed that scouring must have taken place. The reorganization of the RSC complex most likely occurred during the large December 1964 flood. Significant geomorphic changes occurred during that event and the new RSC complex was still very narrow in the summer of 1965. Over subsequent years the RSC complex widened and reorganized further by routing through the rest of Ropers Slough and abandoning the Central Channel by 1972.

Although the exact dating of the channel bed deposits in Zone 3 was unclear, a simple interpretation would identify these coarsest of deposits as the product of the largest discharge event, namely the December 1964 flood. However, geomorphic change in the Eel Estuary suggests that this was not the case. The dilation of the RSC complex between 1965 and 1972 was in part the result of the shoaling of the main South Channel by the December 1964 flood. Successive high discharge events did not change this trend, but rather established the northern channel (the RSC complex) as the main channel, scouring it to accommodate greater flow. It is highly unlikely that a channel would increase in width and discharge capacity to this degree without increasing in depth to some extent.

Furthermore, Boles *et al.* (1977) found that the Ropers Slough channel bed surface in 1975–1976 was composed of a mixture of fines, sand, and fine gravel. Thus, the coarse deposit in Zone 3 is more likely related to the 1974 flood, which had a peak discharge of  $10,959 \text{ m}^3\text{s}^{-1}$  at Scotia, and was the third largest discharge of the hydrologic record. Zone 2 then recorded the transition from major to abandoned channel that occurred between ~ 1977 and 1986.

**Table 5.7** Comparisons of Eel River sediment mean particle size distribution characteristics<sup>a</sup>.

Suspended sediment samples by discharge range.		1° Mode									
Discharge ranges <sup>b</sup>		Mode	Sorting	Skewness	Kurtosis	D <sub>10</sub>	D <sub>50</sub>	D <sub>90</sub>	% Clay	% Silt	% Sand
(Q < 200)	vs. (Q > 200)	***	Eq.	*	Eq.	***	***	*	*	Eq.	**
(200 > Q > 2000)	vs. (Q > 2000)	**	***	Eq.	Eq.	Eq.	*	***	Eq.	***	**

<sup>a</sup>Results for one sided T-tests listed as follows: (Eq.) indicates the H<sub>0</sub> of equivalent means was not rejected (P-value > 0.05), (\*) for P-values < 0.05, (\*\*) for P-values < 0.01, (\*\*\*) for P-values < 0.001.

<sup>b</sup>Discharge ranges are reported in units of m<sup>3</sup>s<sup>-1</sup>.

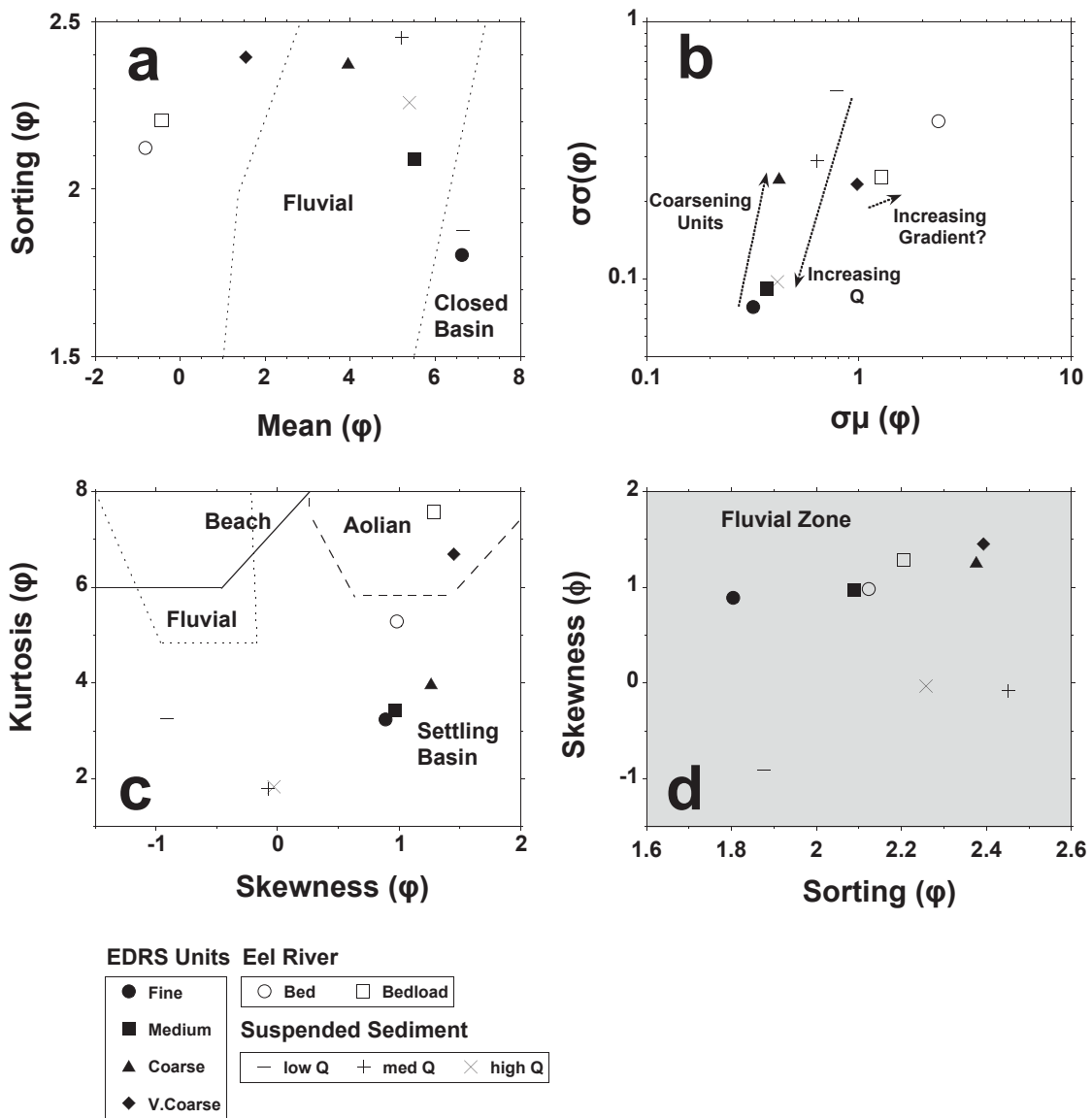


**Figure 5.16** Tanner (1991) domains of particle size distribution suite statistics for EDRS stratigraphic units and Eel River suspended, bed and bedload sediments. All figures are plotted in  $\phi$  units, which increase in value with finer particle size.

The abandoned channel fill sequences of Zones 1 and 4 were typified by (i) sandy, generally unstructured units of lower organic and inorganic carbon content alternating with (ii) finely laminated units of low to no sand with higher organic and inorganic carbon content. The frequency of these stratigraphic units closely matched the wet/dry seasonal cycle counts for the time periods of deposition within the error range of chronologic control. It is with great confidence that these units are identified as recording seasonal scale deposition.

After the 1943 cutoff event Ropers Slough maintained a higher degree of sediment connectivity with the main channel over a longer period of time, allowing for a more rapid rate of filling and narrowing due a higher degree of bed and coarse suspended sediment entrainment relative to the aftermath of the 1974 cutoff. This later cutoff event was followed by an early transition from main channel, high discharge bed sediments to a sub channel aggrading with sand. After rapid sill/plug bar formation, the EDRS sediment further accreted through deposition from high water sub-channel flows carrying fluvial suspended sediment, and bidirectional tidal flows redistributing fines during low water conditions.

### *5.6.2 Sedimentology and discharge magnitude*

There were three pieces of evidence for controls of discharge magnitude on stratigraphic characteristics within the second fill sequence (Zone 1, see Figs. 5.11, 5.12). (i) There were more years during this deposition period than Medium/Fine unit couplets, while a threshold discharge magnitude of slightly less than  $3000 \text{ m}^3\text{s}^{-1}$  would result in the same number of events and stratigraphic couplets. (ii) The year with the largest discharge event (1997) may have deposited the thickest and coarsest sedimentary unit in Zone 1 (depth 45.5–69 cm). (ii) The six year period at the beginning of the record (1987–1992) also corresponded with a sequence of relatively thick Fine units at the base of Zone 1.

Simple relationships with discharge magnitude were not apparent beyond these broad patterns. This finding runs contrary to the expectation that larger floods would result in thicker deposits, which has been found in numerous studies of overbank deposits in small systems (i.e. Constantine and Pasternack, 2005; Werrity, 2006; Watson et al., 2013) and large systems(i.e. Aalto et al., 2008). Suspended sediment rating curves showed a strong positive relationship between concentration and discharge, and larger floods should result in greater depths of inundation if other hydrodynamic factors remain constant for

events of a given magnitude. Thus, in an idealized settling scenario (e.g., single channel-floodplain couplet), larger discharge events should produce thicker sediment deposits. However, abandoned channel hydrodynamics can violate some of these assumptions if the inundating waters generally remain in motion (Constantine, 2010; Toonen et al., 2012). Furthermore, differences in tidal stage during the incidence of peak sediment discharge may impact the dynamics of water and sediment routing through the abandoned channel. Although no consistent event scale hysteresis in suspended sediment concentration has been found for the lower Eel River (Warrick et al., 2013), differences in the timing of peak sediment load relative to peak discharge could also play a role in obscuring a deposition thickness – flood discharge relationship. Intra-unit relationships between discharge and particle size distribution descriptors (e.g.,  $D_{50}$ ,  $D_{90}$ , etc.) were also absent in the latter abandoned channel fill sequence, as little variability in coarse particle sizes was observed. This result is expected for an abandoned channel receiving fluvial inundation from moderate flows ( $Q > 2000 \text{ m}^3\text{s}^{-1}$ ) and above, as Eel River suspended sediment particle size distributions generally did not coarsen with discharge in the moderate to high discharge range.

In contrast, the first abandoned channel fill sequence (Zone 4) displayed potentially more consistent relationships between discharge magnitude and both unit thickness and particle size descriptors. The thickest and coarsest layer may belong to the 1959/60 winter flood season, which had a peak discharge of  $9713 \text{ m}^3\text{s}^{-1}$  and was the largest flood event to deposit sediment in this zone. This coarse unit is more than 7x thicker than any other sandy Zone 4 unit, with a peak  $D_{90}$  of  $361 \mu\text{m}$  and 72% sand. A thinner, fining up sequence higher in Zone 4 may have been deposited in 1963, with a peak discharge of  $7136 \text{ m}^3\text{s}^{-1}$ . The peak sand content of this sequence is a coarse unit of only 4 cm thickness, but with a nearly identical sand content and  $D_{90}$  values as the 1959/60 unit. Other sandy units in this zone were only 1 to 5 cm thick and much finer with sand contents on the order of 40-55% and  $D_{90}$  values from 69 to  $190 \mu\text{m}$ .

### 5.6.3 Particle size distribution domains and sediment source

In agreement with the findings of Lario *et al.* (2002) and Watson *et al.* (2013), suspended sediment suite statistical analysis was found to be an informative component of a broader analysis

sedimentological analysis. Suite statistics provided another line of supporting evidence for changes in sediment source and depositional environments. The bed sediments deposited in Zone 3 consistently plotted with upstream bed and bedload samples collected at the Scotia station on the Eel River. Suspended sediment and abandoned channel fill also plotted in adjacent zones in involving means, sorting and the standard deviation of these values. Abandoned channel fill units were also correctly identified as fluvial/closed basin in the domains of mean vs. sorting space established by Tanner (1991). A break in the relationship between mean and sorting was observed between the abandoned channel fill/suspended sediment samples and the bed/bedload samples in this space. Only channel fill sediment plotted into their established depositional domain in skewness vs. kurtosis space. However, bed/bedload and suspended sediment also segregate into distinct zones. The overall pattern of sediment samples in these spaces further supported the similarity between Zone 3 samples and bed/bedload material, and the abandoned channel fill with fluvial material.

#### *5.6.4 Mechanisms*

What caused the differences in fill characteristics between the first and second abandoned channel sequences? Both sequences began as main channels that experienced abandonment through chute cut-offs of nearly identical diversion angles ( $\sim 67^\circ$ ) and cutoff ratios. In both cases the EDRS site was positioned about the same distance from the RSC/Ropers Slough bifurcation (Node 2). However, the first abandonment resulted in a much more rapid narrowing of Ropers Slough, and after 15 to 20 years of narrowing and shoaling the first abandoned channel fill produced wet season fluvial deposits that were generally sandier, coarser, and thicker than those found in the second fill sequence. In fact, the fluvial deposits of the first fill sequence more closely resemble the earliest units deposited just after the second abandonment.

Differences in stratigraphy between the first and second abandoned channel fill sequences were due to differences in some combination of (i) external forcing factors such as flood magnitudes and sediment load, and (ii) internal factors such as local bed/channel geometry, and their effects on local hydraulics and sediment transport (Toonen et al., 2012). Large flooding events during the winters of 1955/56 and 1964/65 with return intervals of 100 and 200 years respectively are known to have

augmented suspended sediment loads, an effect that has decreased over the subsequent decades (Warrick et al., 2013). Higher sediment loads during the 1950s and 1960s may be responsible in part for the rapid filling of the first sequence, however, much of the observed narrowing occurred by 1948, well before the 1956 event. Sediment loads in the 1940s may have also been very high, but we there are not suspended sediment data from this time period (Warrick *et al.*, 2013). Furthermore, the largest discharge event between the first abandonment and 1948 was only  $6768 \text{ m}^3\text{s}^{-1}$ , or about a 5 year return interval flow.

Alternatively, the first and second abandonment sequences were influenced by the position of the entrance to Ropers Slough relative to RSC complex meander bend morphology. While the factors of accommodation space and higher sediment load may have some bearing on the rapidity of first sequence fill, local channel curvature is perhaps the most compelling contributing factor. The massive floods of 1955 and 1964 could not have influenced the early narrowing of the first abandonment between 1943 and 1948. Furthermore, accommodation space must have been substantially reduced by the time that the lowest EDRS strata were deposited in the late 1950s. Channel curvature controls on water and sediment apportioning, however, would have been operational over the entirety of each fill period.

The meander bends associated with the bifurcation at the entrance Ropers Slough were accreting point bars. Bed sediment can be expected to behave differently in the entrance region of each bifurcate located on a meander bend, particularly if the inner bend is accreting a point bar (Kleinhans, 2008; Seminara, 2001). When this is the case, others have found that the bifurcate extending from the inner bank would be expected to have more bed accreted in the mouth region than the bifurcate extending from the outer bank (Hooke, 1995; Constantine et al., 2010; Toonen et al., 2012). Indeed, the entrances of bifurcates located on inner bends, namely the RSC complex from 1940 to ~1965, and Ropers Slough from 1974 to the present appeared to rapidly accrete point bars. Conversely, the Ropers Slough entrance from 1940 to ~1965 was located on the outer bend, and did not appear to seal off due to plug bar formation over time.

#### 5.6.5 Conceptual model evaluation

Modification of the Toonen et al. (2012) conceptual model for abandoned channel stratigraphic architecture to include seasonal scale tidal deposits appeared to be well supported by the case of Ropers Slough. Both of the abandoned channel fill sequences examined in this study recorded periods of fluvial and tidal deposition with almost seasonal resolution. Furthermore, previous generic mechanisms for abandoned channel fill evolution were supported by the differences in both geomorphic and stratigraphic evolution between the first and second fill sequences. Differences in the topographic steering of bedload and plug bar formation rates related to the position of the abandoned channel mouth relative to meander morphology led to the expected directions of difference in channel narrowing and sediment texture. Slower plug bar formation during the first fill sequence may have led to generally lower threshold discharge values required for inundation of Ropers Slough than those required after the rapid plug bar formation experienced over the second fill sequence.

## **5.7 Conclusions**

Abandoned channel fill sequences in tidally influenced river reaches subjected to pronounced wet/dry seasons seem to follow most of the same generic pathways of non-tidal abandoned channel fills. Fluvial units from Ropers Slough abandoned channel fill sequences appear to have been derived primarily from suspended sediment. However, higher connectivity with the main northern channel (RSC complex) during the first abandonment sequence appears to have allowed for coarser material, perhaps bed or highly stratified coarse suspended sediment, to enter the slough during larger discharge events. Further evidence was found for the control of channel meander bend morphology relative to abandoned channel entrance position on plug bar formation. Inner bend position of the channel entrance seems to have resulted in rapid plug bar formation during the latest abandonment sequence of Ropers Slough. This resulted in a slower progression of channel narrowing, and thinner fluvial strata that did not respond to discharge magnitude in terms of deposition thickness or coarseness. Decreasing sediment load in the Eel River over the time period of accretion may also have influenced this difference, but this issue remains unclear.

Tidally influenced abandoned channel fills in dry summer climates diverge from the generic model developed for rivers experiencing only unidirectional flow by generating the following structures:

1. Fine/coarse textured unit couplets that correspond to dry season tidal deposition and wet season fluvial deposition, respectively.
2. Differences between tidal and fluvial deposits include marine and dry season signatures, such as increased carbonate levels, and presumably other proxies for salinity such as diatoms, algae and invertebrates.
3. Fine textured units will often possess fine scale laminations due to sub-seasonal cycles (tidal, wind, etc.).
4. Speculatively: bi-direction tidal flow through the downstream abandoned channel 'exit' may lead to scour that maintains abandoned channel bed slope may increase the probability of eventual reoccupation as a main fluvial channel. The authors have observed persistent downstream abandoned channel mouth maintenance over the time series of aerial images for the Eel River Estuary. This relationship remains to be tested.

Additional large scale planform investigations of numerous abandoned channels experiencing wet/dry seasonality along a continuum of tidal influence is required to address the role of tidal pumping on channel reoccupation behavior. In depth reductive studies on the hydraulics, sediment transport and erosional dynamics of tidal rivers are also critical to understanding the relative roles of the forcing factors speculated upon here. Tidal channel fills are a widespread and important geomorphic phenomena, and it is critical that their functionality and depositional characteristics are more fully understood. Most of these environments in developed nations such as the U.S. are severely impacted by human activity, and will increasingly be the target of restoration activities, which will require generic and reductionist understanding in order to be successful. Furthermore, the deposits within the abandoned channels have much to offer communities interested in historical characterization of coastal, estuarine and integrated watershed environmental signals, as they can potentially capture high resolution records of fluvial and tidal activity. There is currently great interest in mapping tsunami and rapid subsidence deposits related to large ground shaking events along active margins (Atwater, 1992; Shennan et al., 1996; Dawson and Shi, 2000; Vott et al., 2014). Accurate identification of such deposits in fluvial estuaries can be

complicated by their similarity to abandoned channel fills, particularly when an intensive characterization of the estuary fill architecture at large is not available. Thus, developing a clear stratigraphic framework that unites abandoned channel fills with the tidal environment would be an important step toward increasing the understanding and utility of these widespread features of coastal sedimentary deposits.

## 5.8 References

- Aalto R, Lauer JW, Dietrich WE. 2008. Spatial and temporal dynamics of sediment accumulation and exchange along Strickland River floodplains (Papua New Guinea) over decadal-to-centennial timescales. *Journal of Geophysical Research: Earth Surface* **113**: F01S04. DOI: 10.1029/2006JF000627
- Allen JRL. 1965. A REVIEW OF THE ORIGIN AND CHARACTERISTICS OF RECENT ALLUVIAL SEDIMENTS. *Sedimentology* **5**: 89-191. DOI: 10.1111/j.1365-3091.1965.tb01561.x
- Andrews ED, Antweiler RC, Neiman PJ, Ralph FM. 2004. Influence of ENSO on flood frequency along the California coast. *Journal of Climate* **17**: 337-348
- Atwater BF. 1992. GEOLOGIC EVIDENCE FOR EARTHQUAKES DURING THE PAST 2000 YEARS ALONG THE COPALIS RIVER, SOUTHERN COASTAL WASHINGTON. *Journal of Geophysical Research-Solid Earth* **97**: 1901-1919. DOI: 10.1029/91jb02346
- Blair NE, Leithold EL, Aller RC. 2004. From bedrock to burial: the evolution of particulate organic carbon across coupled watershed-continental margin systems. *Marine Chemistry* **92**: 141-156. DOI: 10.1016/j.marchem.2004.06.023
- Boles GL, Clawson RF, Lallatin RD. 1977. Some physical, chemical, and biological characteristics of the Eel River Estuary. California Department of Water Resources. Memorandum. 100 pp.
- Blott SJ, Pye K. 2001. GRADISTAT: A grain size distribution and statistics package for the analysis of unconsolidated sediments. *Earth Surface Processes and Landforms* **26**: 1237-1248. DOI: 10.1002/esp.261
- Buchholz BA. 2009. Bomb-Pulse Dating. In Wiley Encyclopedia of Forensic Science. John Wiley & Sons, Ltd.

- Citterio A, Piégay H. 2009. Overbank sedimentation rates in former channel lakes: characterization and control factors. *Sedimentology* **56**: 461–482
- Constantine JA, Dunne T, Piégay H, Mathias Kondolf G. 2010. Controls on the alluviation of oxbow lakes by bed-material load along the Sacramento River, California. *Sedimentology* **57**: 389-407. DOI: 10.1111/j.1365-3091.2009.01084.x
- Constantine JA, Pasternack GB, Johnson ML. 2005. Logging effects on sediment flux observed in a pollen-based record of overbank deposition in a northern California catchment. *Earth Surface Processes and Landforms* **30**: 813-821. DOI: 10.1002/esp.1190
- Dawson AG, Shi SZ. 2000. Tsunami deposits. *Pure Appl. Geophys.* **157**: 875-897
- Downie ST, Lucey KP. 2005. Salt River watershed assessment. California Department of Fish and Game, Coastal Watershed Planning and Assessment Program, Fortuna, CA.
- Fisk HN. 1947. Fine grained alluvial deposits and their effects on Mississippi River activity, Vols 1 & 2. Mississippi River Commission, Vicksburg, MS.
- Folk RL. 1974. Petrology of Sedimentary Rocks. Hemphill, Austin, TX, 184 pp.
- Fry B, Brand W, Mersch F, Tholke K, Garritt R. 1992. Automated analysis system for coupled delta-C-13 and delta N-15 measurements. *Analytical Chemistry* **64**: 288–291
- Goni MA, Yunker MB, Macdonald RW, Eglinton TI. 2000. Distribution and sources of organic biomarkers in arctic sediments from the Mackenzie River and Beaufort Shelf. *Marine Chemistry* **71**: 23-51. DOI: 10.1016/s0304-4203(00)00037-2
- Goni MA, Yunker MB, Macdonald RW, Eglinton TI. 2005. The supply and preservation of ancient and modern components of organic carbon in the Canadian Beaufort Shelf of the Arctic Ocean. *Marine Chemistry* **93**: 53-73. DOI: 10.1016/j.marchem.2004.08.001
- Gray AB, Pasternack GB, Watson EB. 2010. Hydrogen peroxide treatment effects on the particle size distribution of alluvial and marsh sediments. *Holocene* **20**: 293-301.
- Haley R. 1970. Changes in the Eel River Estuary and its Fisheries. California Department of Fish and Game, Memorandum. 7 pp.
- Helsel DR, Hirsch RM. 2002. Statistical methods in water resources—hydrologic analysis and interpretation: U.S. Geological Survey Techniques of Water-Resources Investigations. 510 pp.

- Hoek WZ, Minderhoud PSJ, Cohen KM, Erkens G, Toonen WHJ. 2011. Towards a decadal flood record of the River Rhine over the last 7000 years, Abstract volume: *Quaternary Research Association*, Annual Discussion Meeting.
- Hooke JM. 1995. River channel adjustment to meander cutoffs on the River Bollin and River Dane, northwest England. *Geomorphology* **14**: 235-253. DOI: [http://dx.doi.org/10.1016/0169-555X\(95\)00110-Q](http://dx.doi.org/10.1016/0169-555X(95)00110-Q)
- Hughes ML, McDowell PF, Marcus WA. 2006. Accuracy assessment of georectified aerial photographs: Implications for measuring lateral channel movement in a GIS. *Geomorphology* **74**: 1-16. DOI: [10.1016/j.geomorph.2005.07.001](http://dx.doi.org/10.1016/j.geomorph.2005.07.001)
- Kelsey HM. 1980. A sediment budget and an analysis of geomorphic process in the Van-Duzen river basin, north coastal California, 1941-1975 - summary. *Geological Society of America Bulletin* **91**: 190-195.
- Kleinhans MG, Cohen KM, Hoekstra J, Ijmker JM. 2011. Evolution of a bifurcation in a meandering river with adjustable channel widths, Rhine delta apex, The Netherlands. *Earth Surface Processes and Landforms* **36**: 2011-2027. DOI: [10.1002/esp.2222](http://dx.doi.org/10.1002/esp.2222)
- Kleinhans MG, Jagers HRA, Mosselman E, Sloff CJ. 2008. Bifurcation dynamics and avulsion duration in meandering rivers by one-dimensional and three-dimensional models. *Water Resources Research* **44**. DOI: [10.1029/2007wr005912](http://dx.doi.org/10.1029/2007wr005912)
- Kleinhans MG, Schuurman F, Bakx W, Markies H. 2009. Meandering channel dynamics in highly cohesive sediment on an intertidal mud flat in the Westerschelde estuary, the Netherlands. *Geomorphology* **105**: 261-276. DOI: [10.1016/j.geomorph.2008.10.005](http://dx.doi.org/10.1016/j.geomorph.2008.10.005)
- Lario J, Spencer C, Plater AJ, Zazo C, Goy JL, Dabrio CJ. 2002. Particle size characterisation of Holocene back-barrier sequences from North Atlantic coasts (SW Spain and SE England). *Geomorphology* **42**: 25-42. DOI: [10.1016/S0169-555X\(01\)00071-X](http://dx.doi.org/10.1016/S0169-555X(01)00071-X)
- Li WH. 1992. The late Holocene stratigraphy of the Eel River delta. In: *Field guide to the late Cenozoic subduction tectonics and sedimentation of northern coastal California* (Eds G.A. Carver and K.R. Aalto). GB-71. Pacific section. *American Association of Petroleum Geologists*. 55-57.

- Mackey BH, Roering JJ. 2011. Sediment yield, spatial characteristics, and the long-term evolution of active earthflows determined from airborne LiDAR and historical aerial photographs, Eel River, California. *Geological Society of America Bulletin* **123**: 1560-1576. DOI: 10.1130/b30306.1
- Madej MA, Bundros G, Klein R. 2012. Assessing effects of changing land use practices on sediment loads in Panther Creek, North Coastal California. In: Proceedings of Coast Redwood Forests in a Changing California: A Symposium for Scientists and Managers (Eds R.B. Standiford, T.J. Weller, D.D. Piirto, J.D. Stuart). Gen. Tech. Rep. PSW-GTR-238. Pacific Southwest Research Station, Forest Service, U.S. Department of Agriculture, Albany, CA.
- McLaughlin RJ, Blake MCJ, Griscom A. 1988. Tectonics of Formation, Translation, and Dispersal of the Coast Range Ophiolite of California. *Tectonics* **7**: 24
- Mount NJ, Louis J, Teeuw RM, Zukowskyj PM, Stott T. 2003. Estimation of error in bankfull width comparisons from temporally sequenced raw and corrected aerial photographs. *Geomorphology* **56**: 65-77. DOI: 10.1016/s0169-555x(03)00046-1
- Nittrouer CA. 1999. STRATAFORM: overview of its design and synthesis of its results. *Marine Geology* **154**: 3-12
- Ostermann DR, Karbott D, Curry WB. 1990. Automated system to measure the carbonate concentration of sediments. WHOI Tech. Rept., 90-03, 17 pp.
- Puckett LK. 1977. The Eel River Estuary – Observations on morphometry, fishes, water quality, and invertebrates. California Department of Fish and Game. Memorandum Report. 27 pp.
- Puckridge JT, Walker KF, Costelloe JF. 2000. Hydrological persistence and the ecology of dryland rivers. *Regulated Rivers-Research & Management* **16**: 385-402. DOI: 10.1002/1099-1646(200009/10)16:5<385::aid-rrr592>3.3.co;2-n
- Rafter TA, Fergusson GJ. 1957. The atom bomb effect. Recent increase in the <sup>14</sup>C content of the atmosphere, biosphere, and surface waters of the oceans. *New Zealand Jour Sci and Technol Ser B* **38**: 871-883
- Reimer PJ, Bard E, Bayliss A, Beck JW, Blackwell PG, Ramsey CB, Buck CE, Cheng H, Edwards RL, Friedrich M, Grootes PM, Guilderson TP, Hafliðason H, Hajdas I, Hatte C, Heaton TJ, Hoffmann DL, Hogg AG, Hughen KA, Kaiser KF, Kromer B, Manning SW, Niu M, Reimer RW, Richards DA, Scott

- EM, Southon JR, Staff RA, Turney CSM, van der Plicht J. 2013. INTCAL13 and MARINE13 Radiocarbon age calibration curves 0-50,000 Years cal BP. *Radiocarbon* **55**: 1869-1887
- Schlösser S, Eicher A. 2012. The Humboldt Bay and Eel River Estuary Benthic Habitat Project. California Sea Grant Publication T-075. 246 pp.
- SCS. 1989. Salt River Watershed Workplan, including the Lower Eel River, Delta, and Estuary Workplan. US Department of Agriculture, Soil Conservation Service, Eureka, CA.
- Seminara G, Zolezzi G, Tubino M, Zardi D. 2001. Downstream and upstream influence in river meandering. Part 2. Planimetric development. *Journal of Fluid Mechanics* **438**: 213-230
- Shennan I, Long AJ, Rutherford MM, Green FM, Innes JB, Lloyd JM, Zong Y, Walker KJ. 1996. Tidal marsh stratigraphy, sea-level change and large earthquakes .1. A 5000 year record in Washington, USA. *Quaternary Science Reviews* **15**: 1023-1059. DOI: 10.1016/s0277-3791(96)00007-8
- Shields FDJ, Abt SR. 1989. Sediment deposition in cutoff meander bends and implications for effective management. *Regulated Rivers Research and Management* **4**: 381-396
- Sloan J, Miller JR, Lancaster N. 2001. Response and recovery of the Eel River, California, and its tributaries to floods in 1955, 1964, and 1997. *Geomorphology* **36**: 129-154. DOI: 10.1016/s0169-555x(00)00037-4
- Smith ND, Slingerland RL, Perez-Arlucea M, Morozova GS. 1998. The 1870s avulsion of the Saskatchewan River. *Canadian Journal of Earth Sciences* **35**: 453-466. DOI: 10.1139/e97-113
- Sommerfield CK, Drake DE, Wheatcroft RA. 2002. Shelf record of climatic changes in flood magnitude and frequency, north-coastal California. *Geology* **30**: 395-398
- Sommerfield CK, Wheatcroft RA. 2007. Late Holocene sediment accumulation on the northern California shelf: Oceanic, fluvial, and anthropogenic influences. *Geological Society of America Bulletin* **119**: 1120-1134. DOI: 10.1130/b26019.1
- Sun T, Meakin P, Jossang T, Schwarz K. 1996. A simulation model for meandering rivers. *Water Resources Research* **32**: 2937-2954. DOI: 10.1029/96wr00998
- Stouthamer E. 2005. Reoccupation of channel belts and its influence on alluvial architecture in the Holocene Rhine-Meuse delta, the Netherlands. In *River Deltas: Concepts, Models, and Examples*

- (Eds L. Giosan, J.P. Bhattacharya), SEPM, Special Publication 83. SEPM (*Society for Sedimentary Geology*): Tulsa, OK; 319–339.
- Stuiver M, Polach HA. 1977. Reporting of C-14 data - discussion. *Radiocarbon* **19**: 355-363
- Tanner WF. 1991. Suite statistics: the hydrodynamic evolution of the sediment pool. In: Principles, Methods and Applications of Particle Size Analysis (Ed J.P.M. Syvitski). Cambridge University Press, Cambridge, UK. 225-236.
- Tanner WF. 1995. William F. Tanner on environmental clastic granulometry. Florida Geological Survey Special Publication No. 40, 163 pp. ISSN 0085-0640.
- Toonen WHJ, Kleinhans MG, Cohen KM. 2012. Sedimentary architecture of abandoned channel fills. *Earth Surface Processes and Landforms* **37**: 459-472. DOI: 10.1002/esp.3189
- U.S. Geological Survey Earth Explorer (USGS EarthExplorer). 2014. <http://earthexplorer.usgs.gov/> (last accessed: 3/2014)
- U.S. Geological Survey National Water Information System (USGS NWIS). 2014. <http://waterdata.usgs.gov/nwis/sw> (last accessed: 03/2014)
- Van Kirk S. 1996. Historical accounts of the Lower Eel (Wiyot) River navigation, fisheries, “angry waters”, land use, and the river environment 1850–1995. Prepared by Trinity Associates, Arcata, CA.
- Vott A, Reicherter K, Papanikolaou I. 2013. Reconstructing and modeling palaeotsunami events by multi-proxy geoscientific analyses. *Zeitschrift Fur Geomorphologie* **57**: 1-4. DOI: 10.1127/0372-8854/2013/s-00148
- Warrick JA, Madej MA, Goni MA, Wheatcroft RA. 2013. Trends in the suspended-sediment yields of coastal rivers of northern California, 1955-2010. *Journal of Hydrology* **489**: 108-123. DOI: 10.1016/j.jhydrol.2013.02.041
- Warrick JA. 2014. Eel River margin source-to-sink sediment budgets: Revisited. *Marine Geology* **351**: 25-37
- Wentworth CK. 1922. A scale of grade and class terms for clastic sediments. *Journal of Geology* **30**: 377-392

Werritty A, Paine JL, Macdonald N, Rowan JS, McEwen LJ. 2006. Use of multi-proxy flood records to improve estimates of flood risk: Lower River Tay, Scotland. *Catena* **66**: 107-119. DOI: 10.1016/j.catena.2005.07.012

Watson EB, Pasternack GB, Gray AB, Goni M, Woolfolk AM. 2013. Particle size characterization of historic sediment deposition from a closed estuarine lagoon, Central California. *Estuarine Coastal and Shelf Science* **126**: 23-33. DOI: 10.1016/j.ecss.2013.04.006

Wheatcroft RA, Sommerfield CK, Drake DE, Borgeld JC, Nittrouer CA. 1997. Rapid and widespread dispersal of flood sediment on the northern California margin. *Geology* **25**: 163-166

## Acknowledgements

I am profoundly grateful for the mentors that have guided me along the path toward a career in the sciences. First and foremost, I thank my adviser Greg Pasternack. From an erstwhile field bum's first tentative emails, to the final touches on this dissertation, and the long journey between – you were always there with enthusiasm, insight and wisdom. Over the years I have only grown to appreciate more my good fortune in having found a true adviser. Thank you for showing me the wilderness of scientific inquiry, and for allowing me to explore it with the patience to let me get lost, yet the attentiveness to provide much needed oases. And most of all, thank you for believing that I would find my way through.

I was also lucky enough to have another key mentor from the very beginning of my time at Davis. Elizabeth Watson – thank you for introducing me to the world of paleoenvironmental analysis, from the canon of literature, to the field and laboratory. But more importantly, thank you for showing me what it takes to be an independent scientist and an exemplary collaborator. You are an inspiration.

Perhaps the most important factor for science to flourish is collaboration, as two additional mentors have shown me over the course of developing the works herein. When I first staggered out of the 'suspended sediment forest,' Jon Warrick was there. Thank you Jon for helping to make sense of my initial scrawls, for leading me back in with more robust tools, and patiently prodding me along toward effectively communicating the journey. Miguel Goñi, who was kind enough to take this sea dog back to the ocean, provided many valuable insights into the process of crafting scientific works and being a scientist. Thank you Miguel for lifting me up with encouragement and brightening the way.

Of the many graduate students I have had the pleasure to meet, learn beside, work with and live with during my time at Davis, the following must be named: Many thanks to my dearest cohort companions Darren Ficklin and Sarah Gatzke. Thank you Anne Senter, particularly for guidance during my first year. Also, thanks to the whole rotating cast of the Pasternack lab over the years, including: Scott Morford, Aaron Fulton, Jason White, Bobby Gonzales, Josh Wyrick, Matt Vaughn, Leah Kammel, Michael Strom and Marisa Escobar Arias. And special thanks to Rocko Brown, for joining me in the sediment lab, showing me how to press forward through example, and elevating these last years of work out of isolation and into good times.

The foundation of my dissertation benefitted from the contributions of several hard working undergraduate students. I thank Peter Barnes, Sarah Greve, Duyen Ho, Olivia Oseguera, Larissa Salaki, for laboratory and field assistance. I wish you all the best in your future endeavors. Additional field support from Sonja Gray, Drisanna Watson, the Pirate, and the Elkhorn Slough National Estuarine Research Reserve were also much appreciated. Kind and helpful access to instrumentation was provided by Michael J. Singer, Ivano Aiello, Ben Houlton, and Sanjai Parikh. I thank Dr. Erik Wisner and the University of California at Davis Veterinary Medical Center Small Animal Clinic staff for assistance and support with x-radiography of sediment cores. I would also like to acknowledge all of the hard work from the UC Davis Metro staff over the years, particularly the graduate student advisers Merlyn Potter and Angie Nguyen for helping me through the beginning, and the end.

The final form of this dissertation was greatly improved on the basis of numerous suggestions, challenges and edits by Michael Church, Fiona Kirkby, Richard Marston, Dawn Sumner, Zicheng Yu and five anonymous reviewers. Valuable conversations were had with my qualifying examination committee: Carlos Puente, Randy Southard, Peter Hernes, and Dawn Sumner, as well as Jeff Hatten, Bill Dietrich, Liam Reidy, Roger Byrne, Louise Slater, Susan Zimmerman, Doug George, Tripti Bhattacharya, and Alicia Cowart, Wes Christensen, Keith Wohlwend, Dave Bosworth, and Sandrine Matiasek, Sarah Hotton and Brendan White. To one anonymous reviewer of a long forgotten grant proposal – you were right, the spirit has moved me.

I am forever grateful to Paul Sereno for inviting me into the life of adventure and science, and being my first mentor in the field. Those early adventures were full of mentors and young compatriots who indelibly shaped my life, including Zhao Xijin, Dave Varricchio, Jeff Wilson, Jeff Stivers, Sterling Roop, Nels Peterson, Shiao Li, Bob Masek and Didier Duthiel. Among these luminaries, I place particular blame on D. Luke Mahler and Josh Miller for aiding and abetting my way out of the life and into graduate school.

I have cherished my friends beyond the scientific community throughout this process. A huge debt of gratitude is owed to all of my climbing partners over the years, without whom my stay in graduate school would have been woefully foreshortened. The same sentiment is reserved for the Merry Growlers and all the scions thereof. And to all of my friends who have shared the good life with me over the years,

I know who you are, and I am so thankful for you.

Finally, to my family: Sonja, my wife, my fellow traveler, my partner in life and all of its adventures – I thank you with all of my heart for everything that you are, have been, and will be. I see our future in you, in me. To my parents, Brenda and Daniel Gray, I owe so much of who I am. Thank you for showing me how to be a human and how to love. Especially, I thank you Mom, for teaching me how to read, which opened the world. And thank you Dad for showing me what work ethic really means, and how to critically encounter that world. Many thanks to my brothers Eric and Matthew and my sister Audrey – forever siblings and friends, for cheering me on and showing me what hard work our blood has in it. And to Lobo Kysolit Gray – yours is the sweetest soul I have found in this universe.

This research was funded by the National Science Foundation under award No. 0628385, and by the following competitive grants for graduate research from the University of California at Davis: three Henry A. Jastro Awards, the Ernest E. Hill Fellowship, and a summer stipend for computational research in engineering and environmental science. The Hydrologic Sciences Graduate Group at the University of California at Davis also provided critical stipend and student fee support during the early and late stages of my graduate career. This project was also supported tangentially by the USDA National Institute of Food and Agriculture, Hatch project number #CA-D-LAW-7034-H. The radiocarbon work at NOSAMS was supported in part by the NSF Cooperative Agreement number, OCE-0753487. Communication of the findings presented here was aided by conference travel awards from the International Association of Sedimentologists, and the University of California at Davis Graduate Student Association and Hydrologic Sciences Graduate Group. Any opinions, findings, and conclusions or recommendations expressed in this material are those of the author and do not necessarily reflect the views of the funding institutions.